Floquet-based perturbative treatment of finite-pulse effects in quadrupolar spins: Challenges and Perspectives

A Thesis

submitted by

Vinay Ganapathy

(PH12124, PhD Student)

for the partial fulfilment of the degree

of

Doctor of Philosophy

Department of Chemical Sciences
Indian Institute of Science Education and Research (IISER) Mohali
Knowledge city, Mohali, Punjab - 140306, INDIA.
February, 2019

Declaration

The work presented in this thesis entitled "**Floquet-based perturbative treatment of finite-pulse effects in quadrupolar spins: Challenges and Perspectives**" has been carried out by me under the supervision of **Dr. Ramesh Ramachandran** in the Department of Chemical Sciences, Indian Institute of Science Education and Research (IISER) Mohali.

This work has not been submitted in part or in full for a degree, a diploma, or a fellowship to any other university or institute. Whenever contributions of others are involved, every effort is made to indicate this clearly, with due acknowledgement of collaborative research and discussions. This thesis is a bonafide record of original work done by me and all sources listed within have been detailed in the bibliography.

Date: **Vinay Ganapathy**
Place: Mohali (PH12124)

In my capacity as the supervisor of the candidate's thesis work, I certify that the above statements by the candidate are true to the best of my knowledge.

Date: **Dr. Ramesh Ramachandran**
Place: Mohali (Supervisor)

Acknowledgements

My PhD journey is a democratic process where lot of people invested their time and efforts. I am greatly thankful to all of them.

Let me begin by thanking my supervisor **Dr. Ramesh Ramachandran** for being very cooperative and professional. I am greatly surprised by his enthusiasm, patience and commitment towards his work and I would like to replicate the same in my life too. I can proudly say that I have completed my PhD with my self-respect and self-confidence intact.

I thank my Doctoral committee members **Prof. K. S. Viswanathan** and **Dr. Varadharaj Ravi Srinivasan** for taking out time from their busy schedule, monitoring my progress at regular intervals and providing their valuable suggestions.

I am greatly indebted to all the faculty members of the **Department of Chemical Sciences** for their guidance and encouragement. The **Curie Club** talks has taught me the appropriate way of presenting my research work to the more general audience.

My stay at IISER Mohali, was greatly enhanced with the company of **Dr. P. Bapaiah** and family. I will greatly miss the festival invitations and the time spent in badminton courts.

The library services of IISER Mohali should be specially appreciated and I thank **Dr. P. Visakhi** for maintaining it so well.

I am thankful to **Dr. Manoj kumar Pandey** for helping me when I was writing my first review on Multi-Quantum experiments by lending his experimental expertise.

I am very fortunate to find myself in a group where a healthy working atmosphere has been established and maintained very religiously. I am thankful to all my seniors **Dr. Subba Rao, Dr. Zeba Qadri, Dr. Sivaranjan Uppala,** and juniors **Mr. Rajat Garg, Mr. Shreyan Ganguly, Ms. Nisha Bamola, Mr. Mohit Bansal, Mr. Kuntal Mukherjee** for their open-minded and straight forward approach.

There is a big list of BS-MS, Integrated PhD and PhD friends that I cannot mention here individually. They are the support system who kept me motivated and has witnessed both my good and bad times.

I am thankful to **IISER Mohali**, and **MHRD India** for providing me the opportunity and fellowship to pursue my Doctoral studies.
I am blessed to have encouraging parents and I thank my family members, especially my sister **G. Vijayalakshmi** and brother-in-law **G. Venkataramanan**. They gladly took my responsibilities and allowed me to pursue my passion. It would be impossible for me to graduate without their co-operation and support.
Above all, I thank the **Almighty** for making this happen and including the chapter of Doctoral studies in my life.

Abbreviations

ZQ	Zero Quantum
SQ	Single Quantum
DQ	Double Quantum
TQ	Triple Quantum
MQ	Multiple Quantum
RF	Radio Frequency
AHT	Average Hamiltonian Theory
CT	Central Transition
PAS	Principal Axis System
MolAs	Molecular Axis System
RAS	Rotor Axis System
LAS	Lab Axis System
BCH	Baker-Campbell-Hausdorff
FID	Free Induction Decay
FT	Fourier Transform
kHz	kilo Hertz
MHz	Mega Hertz
EFG	Electric Field Gredient

Notations

(α, β, γ)	Euler angles
$D_{q',q}(\alpha, \beta, \gamma)$	Wigner Rotation matrix
ω_0	Excitation frequency
ω_1	amplitude of RF pulse
ω_Q	quadrupolar frequency (rad/sec)
C_Q	quadrupolar coupling constant (Hz)
H_z	Zeeman Hamiltonian
H_{RF}	Hamiltonian of RF pulse
H_Q	Quadrupolar Hamiltonian
$T^{(k)q}$	Spherical (spin) Tensor of rank 'k' and coherence 'q'
ϕ	phase of the pulse
Φ_1	Phase factor of the pulse
Φ_R	Phase factor of the receiver
H_1	Perturbing Hamiltonian
H_F	Floquet Hamiltonian
$\rho(0)$	Initial density matrix (at time '$t = 0$')
$\rho(t_p)$	density matrix after time '$t = t_p$'
γ	Nuclear gyromagnetic ratio
$R^{(k)q}$	Spatial tensor of rank 'k' and coherence 'q'
I_F	Floquet diagonal matrix
H_{eff}	Effective Hamiltonian
$H_{1,d}$	Diagonal component of perturbing Hamiltonian
$H_{1,od}$	Off-diagonal component of perturbing Hamiltonian
$H_n^{(m)}$	n^{th} order Hamiltonian after m^{th} transformation

$G_{coe}^{(n)}$	Hamiltonian (G) coefficients of n^{th} transformation
$C_{coe}^{(n)}$	S_n coefficients (C) coefficient of n^{th} transformation
$R_{coe}^{(n)}$	Density matrix (R) coefficients of n^{th} transformation
$P_{coe}^{(n)}$	Detection operator (P) coefficients of n^{th} transformation

List of Figures

List of Tables

Contents

Abstract

Understanding the response of nuclear spins subjected to an oscillating field has remained an active pursuit in methodology development in NMR spectroscopy. In particular, the response of a quadrupolar nuclear spin (spins with $I > {}^1/_2$) is delicately dependent on the ratio of the quadrupolar coupling constant to the amplitude of the oscillating pulse. In addition to its duration and oscillating frequency. In contrast spin to $I = {}^1/_2$ systems, the time-evolution of the quadrupolar spins during an RF pulse is less understood owing to the dominant presence of the quadrupolar interactions. Consequently, analytic description of the excitation process has remained less transparent within existing theoretical frameworks. As an alternative, the concept of "Effective Floquet Hamiltonians" is explored in the present thesis to explain the nuances of the excitation process in multi-level systems. Employing spin $I = 1$ and ${}^3/_2$ as model systems, a unified theoretical framework for describing the excitation of multiple-quantum transitions in static isotropic and anisotropic solids is proposed within the framework of perturbation theory. The challenges resulting from the anisotropic nature of the quadrupolar interactions are addressed within the effective Hamiltonian framework. The possible role of the various interaction frames on the convergence of the perturbation corrections is discussed along with a proposal for a "hybrid method" for describing the excitation process in anisotropic solids. Employing suitable model systems, the validity of the proposed hybrid method is substantiated through a rigorous comparison between simulations emerging from exact numerical and analytic methods.

CHAPTER-1

INTRODUCTION

Chapter 1

Introduction

1.1 Basics of NMR

The phenomenon of Nuclear Magnetic Resonance (NMR)[1–3] exhibited by a nucleus arises from a quantum mechanical property called 'spin'. Being quantum mechanical in nature, the spin of a nucleus is described in-terms of a label commonly referred to as the spin quantum number 'I'. Unlike the spin of an electron (always restricted to spin $S = {}^1/_2$), a nucleus possess both integral (referred to as bosons) and half-integral (fermions) values of spin. Along with spin, a nucleus is associated with a magnetic moment (due to spin) and an angular momentum '$\hbar I$', related by,

$$\mu = \gamma \hbar I \tag{1.1}$$

where 'γ' is the nuclear gyromagnetic ratio and is an intrinsic property of a nucleus. When a nucleus (with spin I) is placed in a strong static magnetic field, the degeneracy associated with the $(2I + 1)$ nuclear spin states, 'm' ($m = -I \rightarrow I$) is lifted. This interaction between the nuclear spin magnetic moment (μ) and the external magnetic field (B_0) is referred to as the Zeeman interaction and is quantum mechanically represented through the Zeeman Hamiltonian[4–10],

$$H_z = -\mu.B_0 = -\hbar\omega_0 I_z \tag{1.2}$$

where, '$\omega_0 = \gamma B_0$' is the Larmor frequency and the external magnetic field direction is chosen along the z-direction. Here in this thesis, we confine our discussion to isolated single spin systems involving quadrupolar nucleus (say $I = 1$ and $^3/_2$). In addition to the interaction with the applied magnetic field, nuclei with asymmetric charge distribution (usually exhibited by nucleus with $I > {}^1/_2$) are associated with a non-zero nuclear quadrupole moment. The resulting interaction of the nuclear quadrupole moment with the electric field gradient surrounding the nuclei is commonly referred to as the nuclear quadrupole interaction[10–13]. A brief description of the quadrupolar interaction is presented in Appendix-A. To first order, the quadrupolar interactions are approximated by the quadrupolar Hamiltonian given below.

$$H_Q = \frac{e^2qQ}{4I(2I-1)}(3I_z^2 - I^2) = \frac{\hbar\omega_Q}{6}\ \left(3I_z^2 - I^2\right) \tag{1.3}$$

where 'ω_Q' represents the quadrupolar frequency and 'C_Q' the quadrupolar coupling constant. In the absence of the quadrupolar interaction, the energy eigen values associated with the nuclear spin states in a multi-level system are degenerate[4]. A detailed description of the energy level splitting in the presence of quadrupolar interaction for spin $I = 1$ (chapter-2) and spin $I = {}^3/_2$ (chapter-3) is presented in the forthcoming chapters. Subsequently, to induce transitions between the nuclear spin states, an oscillating field with appropriate frequency perpendicular to the static field is employed in NMR spectroscopy[14]. Quantum mechanically, the interaction of the nuclear magnetic moment with the oscillating field is represented by,

$$H_{RF}(t) = \sum_{i=1} -2\hbar\omega_{i,1}\cos(\omega_i t - \phi_i)\ I_{i,\alpha} \tag{1.4}$$

where, '$\omega_{i,1}$' is the amplitude, 'ω_i' is the frequency, 'ϕ_i' is the phase of the 'i^{th}' pulse. '$I_{i,\alpha}$' is the spin angular momentum operator defined along 'α'($\alpha = x$ or y) axis.

From the theoretical prespective, the time-domain signal observed in typical NMR experiments is obtained through the solution obtained from the quantum-Liouville

equation[15],

$$i\hbar\frac{\mathrm{d}\rho(t)}{\mathrm{d}t} = [H(t), \rho(t)] \tag{1.5}$$

When the Hamiltonian is time-independent, the formal solution to the above equation reduces to a much simpler form.

$$\rho(t) = exp\left(\frac{-iHt}{\hbar}\right)\rho(0)\ exp\left(\frac{iHt}{\hbar}\right) \tag{1.6}$$

In the above equation, '$\rho(0)$' represents to the state of the system at time '$t = 0$', $\rho(t)$ the state at any later instant of time, 't'. The quantity $\rho(t)$ is often termed the density operator and is the quantum equivalent of the 'density of states' employed in the classical statistical mechanics[15,16]. Interestingly, in most NMR experiments, the spin Hamiltonians are explicitly time-dependent. In such cases, the formal solution to the above equation has a complicated form.

$$\rho(t) = U(t,0)\ \rho(0)\ U^{\dagger}(t,0) = e^{-\left(i/\hbar\right)\int_0^t H(t')dt'}\ \rho(0)\ e^{\left(i/\hbar\right)\int_0^t H(t')dt'} \tag{1.7}$$

From an experimental perspective, analytic expressions are desirable both for deducing optimal conditions and quantifying the resulting NMR experimental data. Below, a schematic of the single pulse experiment routinely employed in the NMR spectroscopy is depicted.
From a theoretical perspective, analytic description of the evolution operator is essential for optimizing NMR experiments, '$U(t,0)$'. From an operational view point, analytic description of the evolution operator in NMR experiments is confronted with

- Time-dependent nature of spin Hamiltonians
- Non-commuting nature of the Hamiltonians.

In the present study, the Hamiltonian for the isolated single spin comprises of the Zeeman, quadrupolar and the RF interactions.

$$H = H_z + H_Q + H_{RF} \tag{1.8}$$

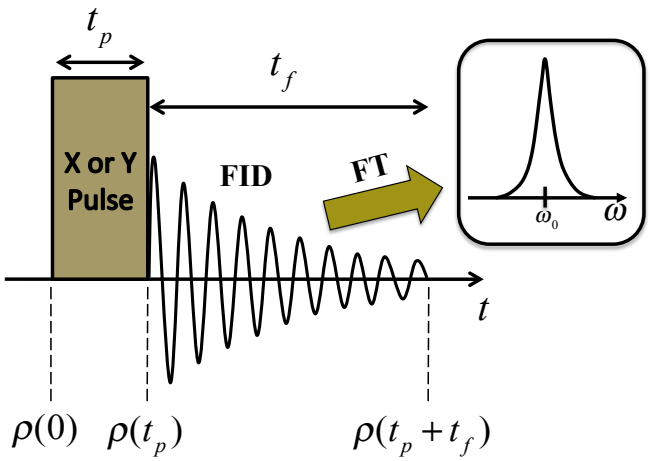

Figure 1.1: A single-pulse NMR experiment portraying the RF pulse employed, the Free Induction Decay (FID) and its Fourier transformed (FT) signal. The density operators used to track the time evolution of the system is also shown.

As indicated above, the complication arises from both the presence of non-commuting terms and interactions of differing magnitudes. For example, the Zeeman interaction/Hamiltonian in the above case is of no relevance in the actual design/optimization of experiments. Since, the desired information on the molecular constraints is contained in the internal Hamiltonians (say Quadrupolar Hamiltonian in the present case), the description in the laboratory frame is transformed into the rotating frame through a unitary transformation described below,

$$\tilde{\rho}(t) = e^{-i\omega_0 t I_z} \rho(t)\ e^{i\omega_0 t I_z} \tag{1.9}$$

$$i\hbar \frac{\mathrm{d}\tilde{\rho}(t)}{\mathrm{d}t} = \left[\tilde{H}(t), \tilde{\rho}(t)\right] \tag{1.10}$$

where, $\tilde{H} = \tilde{H}_z + \tilde{H}_Q + \tilde{H}_{RF}$, employing secular approximation and dropping non-commuting terms (w.r.t to the I_z operator) the Hamiltonian in the rotating frame reduces to a much simpler form.

$$\tilde{H}_Q = \frac{\hbar\omega_Q}{6}\ \left(3I_z^2 - I^2\right) \tag{1.11}$$

$$\tilde{H}_z = -\hbar\Delta\omega I_z \tag{1.12}$$

$$\tilde{H}_{RF} = -\hbar\omega_1 I_x \tag{1.13}$$

when the frequency of the oscillating field is matched to the Larmor frequency (ω_0), '$\Delta\omega$' tends to zero. Under the above resonance condition, the Hamiltonian in the rotating frame has only two terms, namely,

$$\tilde{H} = \tilde{H}_Q + \tilde{H}_{RF} \tag{1.14}$$

In the case of spin $I = {}^1/_2$ systems, the magnitude of the RF amplitude of the pulse often exceeds the other internal spin interactions present in the system. Consequently, the evolution of the system during the RF pulse is approximated through the 'RF Hamiltonians' only, i.e. for the time period from $t = 0$ to $t = t_p$, the system is governed only by the RF Hamiltonian.

$$\tilde{\rho}(t) = e^{-i/\hbar \tilde{H}_{RF} t_p} \tilde{\rho}(0)\ e^{i/\hbar \tilde{H}_{RF} t_p} \tag{1.15}$$

However, in the case of quadrupolar spins, the magnitude of the quadrupolar interaction largely exceeds the amplitude of the RF pulse employed in NMR experiments. In such cases, the spin Hamiltonian during the pulse comprises of two non-commuting terms ($H_{RF} + H_Q$). To circumvent this problem, the spin Hamiltonian is further transferred into the quadrupolar interaction frame, such that the quadrupolar interaction is eliminated in the evolution.

$$\tilde{\tilde{\rho}}(t) = e^{-i/\hbar H_Q t}\ \tilde{\rho}(t) e^{i/\hbar H_Q t} \tag{1.16}$$

$$i\hbar \frac{\mathrm{d}\tilde{\tilde{\rho}}(t)}{\mathrm{d}t} = \left[\tilde{\tilde{H}}(t), \tilde{\tilde{\rho}}(t)\right] \tag{1.17}$$

where, $\tilde{\tilde{H}} = \tilde{\tilde{H}}_{RF}$ and $\tilde{\tilde{H}}_{RF} = \ e^{-i/\hbar H_Q t}\ \tilde{H}_{RF}\ e^{i/\hbar H_Q t}$
In the quadrupolar interaction frame, the evolution during the pulse is governed by a time-dependent form of the RF Hamiltonian (see Eq. 1.7)

$$\tilde{\tilde{\rho}}(t) e^{-\left(i/\hbar\right) \int_0^t \tilde{\tilde{H}}_{RF}(t')dt'}\ \rho(0)\ e^{\left(i/\hbar\right) \int_0^t \tilde{\tilde{H}}_{RF}(t')dt'} \tag{1.18}$$

Although, the spin system during the pulse (in the quadrupolar interaction frame) is modulated only by the RF Hamiltonian, the RF Hamiltonian in Eq. 1.18 is time-dependent (modulated by the quadrupolar interaction). This defines the problem addressed in this thesis.

To facilitate analytic description, the concept of effective Hamiltonians[17–22]/ time-averaged Hamiltonians[23–25] have been employed in the past. In the approach introduced by Waugh and co-workers[23–25], a time-averaged Hamiltonian (defined for certain duration) is proposed to describe the evolution operator. A brief description of the Average Hamiltonian theory (AHT) formalism is presented in Appendix-C. Accordingly, the evolution operator during the pulse is approximated by a time-averaged Hamiltonian facilitating in the analytic evaluation of the density operator during a pulse.

$$U(t_p, 0) = e^{-i/\hbar H_{eff} t_p} \tag{1.19}$$

$$\tilde{\tilde{\rho}}(t_p) = U(t_p, 0)\ \tilde{\tilde{\rho}}(0)\ U^{\dagger}(t_p, 0) \tag{1.20}$$

In an alternate approach, the time-dependent RF Hamiltonian in the quadrupolar interaction frame is transformed into a time-independent Hamiltonian using Floquet formalism. In the Floquet formalism[22,26–29], a time-dependent Hamiltonian (described in finite dimension vector space) is transformed into a time-independent Hamiltonian defined in an infinite dimensional vector space (Floquet Hamiltonian H_F) via Fourier series expansion.

To overcome the complexity introduced by the infinite dimensionality in the Floquet framework, we proposed the derivation of effective Floquet Hamiltonians based on the method of contact transformation[30–33]. The contact transformation method is an operator equivalent of the standard Rayleigh perturbation theory, wherein the perturbation corrections are obtained in terms of operators resulting in an effective Hamiltonian as opposed to the evaluation of the matrix elements commonly encountered in perturbative treatments. Although, the method has found utility in the description of spin $I = {}^1/_2$[34,35], the method has not been extended to quadrupolar spins. In this thesis an analytic framework based on the concept of effective Floquet Hamiltonians is proposed to describe finite-pulse effects[36–38] involving quadrupolar spins. The simulations emerging from the proposed ana-

lytic theory are well corroborated using exact numerical methods (obtained using SIMPSON[39–41] software). In Chapter-2, effective Floquet Hamiltonians are derived for describing DQ excitation in spin $I = 1$ system, while TQ excitation in spin $I = {}^{3}/_{2}$ systems is presented in Chapter-3. A brief summary of the results obtained in this thesis, are summarized in Chapter-4.

References

[1] F. Bloch, *Phys. Rev.*, 1946, **70**, 460–474.

[2] F. Bloch, A. C. Graves, M. Packard and R. W. Spence, *Phys. Rev.*, 1947, **71**, 551–551.

[3] E. M. Purcell, H. C. Torrey and R. V. Pound, *Phys. Rev.*, 1946, **69**, 37–38.

[4] C. Dean, *Phys. Rev.*, 1954, **96**, 1053–1059.

[5] J. Keeler, *Understanding NMR spectroscopy*, John Wiley & Sons, 2011.

[6] M. H. Levitt, *Spin dynamics: basics of nuclear magnetic resonance*, John Wiley & Sons, 2001.

[7] M. Mehring, *Principles of High Resolution NMR in solids*, (Springer, Berlin, 1983), Berlin, 2nd edn, 1999.

[8] U. Haeberlen, *High Resolution NMR in solids selective averaging: supplement 1 advances in magnetic resonance*, Elsevier, 2012, vol. 1.

[9] A. Abragam, *The Principles of Nuclear Magnetism*, Clarendon Press, 1961.

[10] C. P. Slichter, *Principles of Magnetic Resonance*, Springer Science & Business Media, 2013, vol. 1.

[11] M. Cohen and F. Reif, *Quadrupole Effects in Nuclear Magnetic Resonance Studies of Solids*, Academic Press, 1957, vol. 5, pp. 321 – 438.

[12] P. P. Man, *Encycl. Nucl. Magn. Reson.*, 1996, **6**, 3838–3848.

[13] P. P. Man, in *Quadrupole Couplings in Nuclear Magnetic Resonance, General*, John Wiley & Sons, Ltd, 2006, p. 12224 12265.

[14] I. I. Rabi, *Phys. Rev.*, 1937, **51**, 652–654.

[15] K. Blum, *Density matrix theory and applications*, Springer Science & Business Media, 2012, vol. 64.

[16] U. Fano, *Rev. Mod. Phys.*, 1957, **29**, 74–93.

[17] R. Ramesh and M. S. Krishnan, *J. Chem. Phys.*, 2001, **114**, 5967–5973.

[18] G. Vinay and R. Ramachandran, *Annu. Rep. NMR Spectrosc.*, Elsevier, 2016, vol. 89, pp. 123–184.

[19] D. Srivastava and R. Ramachandran, *RSC Adv.*, 2013, **3**, 25231–25236.

[20] R. Venkata SubbaRao, D. Srivastava and R. Ramachandran, *Phys. Chem. Chem. Phys.*, 2013, **15**, 2081–2104.

[21] D. Srivastava, R. Venkata SubbaRao and R. Ramachandran, *Phys. Chem. Chem. Phys.*, 2013, **15**, 6699–6713.

[22] R. Ramachandran and R. G. Griffin, *J. Chem. Phys.*, 2005, **122**, 164502.

[23] U. Haeberlen and J. S. Waugh, *Phys. Rev.*, 1968, **175**, 453–467.

[24] M. M. Maricq, *Phys. Rev. B*, 1982, **25**, 6622–6632.

[25] J. S. Waugh, in *eMagRes (eds R. K. Harris and R. L. Wasylishen)*, American Cancer Society, 2007.

[26] G. Floquet, *Ann. Sci. Ecole Norm. Sup.*, 1883, **12**, 47–88.

[27] J. H. Shirley, *Phys. Rev.*, 1965, **138**, B979–B987.

[28] I. Scholz, J. D. van Beek and M. Ernst, *Solid State Nucl. Magn. Reson.*, 2010, **37**, 39 – 59.

[29] M. Leskes, P. Madhu and S. Vega, *Prog. Nucl. Magn. Reson. Spectrosc.*, 2010, **57**, 345380.

[30] J. H. Van Vleck, *Phys. Rev.*, 1929, **33**, 467–506.

[31] D. Papousek and M. Aliev, *Molecular Vibrational-rotational Spectra: Theory and Applications of High Resolution Infrared*, Elsevier, 1982.

[32] V. Aliev, M.R. Aleksanyan, *Optika Spectroscopia*, 1968, **24**, 520.

[33] V. Aliev, M.R. Aleksanyan, *Optika Spectroscopia*, 1968, **24**, 695.

[34] U. SivaRanjan and R. Ramachandran, *J. Chem. Phys.*, 2014, **140**, 054101.

[35] M. K. Pandey, Z. Qadri and R. Ramachandran, *J. Chem. Phys.*, 2013, **138**, 114108.

[36] M. Bloom, J. H. Davis and M. I. Valic, *Cana. J. Phys.*, 1980, **58**, 1510–1517.

[37] F. H. Larsen and N. C. Nielsen, *J. Phys. Chem. A*, 1999, **103**, 10825–10832.

[38] N. C. Nielsen, H. Bildsøe and H. J. Jakobsen, *Chem. Phys. Lett.*, 1992, **191**, 205 – 212.

[39] M. Bak, J. T. Rasmussen and N. C. Nielsen, *J. Magn. Reson.*, 2011, **213**, 401 – 403.

[40] M. Bak, J. T. Rasmussen and N. C. Nielsen, *J. Magn. Reson.*, 2011, **213**, 366 – 400.

[41] Z. Tosner, R. Andersen, B. Stevensson, M. Edén, N. C. Nielsen and T. Vosegaard, *J. Magn. Reson.*, 2014, **246**, 79 – 93.

[42] R. V. Pound, *Phys. Rev.*, 1950, **79**, 685–702.

[43] H. B. G. Casimir, in *On the Interaction between Atomic Nuclei and Electrons*, Springer Netherlands, Dordrecht, 1936, pp. 201–283.

[44] A. R. Edmonds, *Angular momentum in quantum mechanics*, Princeton university press, 1996, vol. 4.

[45] W. Magnus, *Commun. Pure Appl. Math.*, 1954, **7**, 649–673.

[46] R. M. Wilcox, *J. Math. Phys.*, 1967, **8**, 962–982.

[47] S. Klarsfeld and J. A. Oteo, *Phys. Rev. A*, 1989, **39**, 3270–3273.

[48] R. Kubo, *J. Phys. Soc. Jap.*, 1962, **17**, 1100–1120.

Appendix

A Quadrupolar Interactions/Hamiltonian

A nucleus with charge 'Ze' is distributed over the nuclear volume '$d^3\mathbf{x}$' with charge density '$\rho(\mathbf{x})$' and '$V(\mathbf{x})$' is the potential arising due to the surrounding electrons onto the nucleus under consideration, then the Hamiltonian of the system is given by[10,11],

$$H = \int \rho(\mathbf{x}) V(\mathbf{x}) d^3\mathbf{x} \tag{A.1}$$

Expanding '$V(\mathbf{x})$' under power series about the nuclear centre of mass, where cartesian components of '$\mathbf{x}$' are denoted by $x_1 = x$, $x_2 = y$, and $x_3 = z$.

$$H = \int d^3\mathbf{x}\ \rho(\mathbf{x}) \left\{ V_0 + \sum_j \left(\frac{\partial V}{\partial x_j} \right)_0 x_j + \frac{1}{2} \sum_{j,k} \left(\frac{\partial^2 V}{\partial x_j \partial x_k} \right)_0 x_j x_k + \dots \right\} \tag{A.2}$$

$$H = ZeV_0 + \sum_j P_j \left(\frac{\partial V}{\partial x_j} \right)_0 + \frac{1}{2} \sum_{j,k} Q'_{jk} \left(\frac{\partial^2 V}{\partial x_j \partial x_k} \right)_0 \tag{A.3}$$

where,

$$\int d^3\mathbf{x}\ \rho(\mathbf{x}) = Ze \tag{A.4}$$

$$\int d^3\mathbf{x}\ \rho(\mathbf{x})\ x_j = P_j = \text{electric dipole moment} \tag{A.5}$$

$$\int d^3\mathbf{x}\ \rho(\mathbf{x})\ x_j x_k = Q'_{jk} = \text{electric quadrupole moment tensor} \tag{A.6}$$

As we are interested in understanding the quadrupolar Hamiltonian, we look more closely into the third term of Eq.A.3. Also,

$$V_{jk} = \frac{\partial^2 V}{\partial x_j \partial x_k} = -\frac{\partial E_j}{\partial x_k} \tag{A.7}$$

where, 'E_j' is the electric field at the nuclear position. Hence, quadrupolar Hamiltonian is defined as the interaction between the quadrupole moment with the gradient of the electric field at the nucleus[42].
For the sake of mathematical convenience and to make the quadrupolar Hamiltonian traceless, 'Q_{jk}' is defined as

$$Q_{jk} = 3Q'_{jk} - \delta_{jk} \sum_{e} Q'_{ee} \tag{A.8}$$

Substituting the above equation in the third term of the Eq.A.3, we get

$$H = \frac{1}{6} \sum_{j,k} Q_{jk} V_{jk} + \frac{1}{2} \left(\sum_{e} Q_{ee} \right) \left(\sum_{j} V_{jj} \right) \tag{A.9}$$

The second term in the above equation can be neglected for all the practical purposes giving rise to the quadrupolar Hamiltonian 'H_Q'.

$$H_Q = \frac{1}{6} \sum_{j,k} Q_{jk} V_{jk} \tag{A.10}$$

According to the quantum-mechanical treatment of the quadrupolar Hamiltonian given by Casimir[43,44], the matrix elements of 'Q_{jk}' may be written as,

$$\langle Im' | \, Q_{jk} \, | Im \rangle = \frac{eQ}{I(2I-1)} \langle Im' | \, {}^{3}/_{2} \left(I_j I_k + I_k I_j \right) - \delta_{jk} I^2 \, | Im \rangle \tag{A.11}$$

where 'Q' is electric quadrupole moment. Substituting Eq. A.11 in Eq. A.10, we get

$$\langle Im' | \, H_Q \, | Im \rangle = \frac{eQ}{6I(2I-1)} \sum_{j,k} \langle Im' | \, {}^{3}/_{2} \left(I_j I_k + I_k I_j \right) - \delta_{jk} I^2 \, | Im \rangle \, V_{jk} \tag{A.12}$$

Let us define,

$$V_0 = \sqrt{\frac{3}{2}} V_{zz} \quad ; \quad V_{\pm 1} = \mp V_{xz} - i V_{yz} \quad ; \quad V_{\pm 2} = \frac{1}{2} \left(V_{xx} - V_{yy} \right) \pm i V_{xy}$$

$$eq = V_{zz} \quad ; \quad \eta = \frac{V_{xx} - V_{yy}}{V_{zz}} \quad ; \quad I_{\pm} = I_x \pm i I_y$$

Substituting the above relations in Eq. A.12, we get

$$\begin{aligned}\langle Im'|\, H_Q\, |Im\rangle = \frac{eQ}{4I(2I-1)} \langle Im'|\, \sqrt{2/3}(3I_z^2 - I^2)V_0 + (I_zI_+ + I_+I_z)V_{-1} \\ -(I_zI_- + I_-I_z)V_1 + I_+^2V_{-2} + I_-^2V_2 \;\; |Im\rangle \\ H_Q = \sqrt{2/3}(3I_z^2 - I^2)V_0 + (I_zI_+ + I_+I_z)V_{-1} - (I_zI_- + I_-I_z)V_1 + I_+^2V_{-2} + I_-^2V_2\end{aligned} \tag{A.13}$$

Eq. A.13 represents the quadrupolar Hamiltonian for any arbitrary set of axes. In the Zeeman interaction frame, the quadrupolar Hamiltonian reduces to the following form

$$\tilde{H}_Q = exp\left(\frac{-iH_zt}{\hbar}\right) H_Q \; exp\left(\frac{iH_zt}{\hbar}\right) \tag{A.14}$$

$$\begin{aligned}\tilde{H}_Q(t) = \frac{eQ}{4I(2I-1)} \Big(\sqrt{2/3}(3I_z^2 - I^2)V_0 + (I_zI_+ + I_+I_z)V_{-1}\; e^{-i\omega_0 t} \\ -(I_zI_- + I_-I_z)V_1\; e^{i\omega_0 t} + I_+^2V_{-2}\; e^{-2i\omega_0 t} + I_-^2V_2\; e^{2i\omega_0 t}\Big)\end{aligned} \tag{A.15}$$

Employing the time averaging over the larmor period '$2\pi/\omega_0$'. the quadrupolar Hamiltonian is redefined based on Magnus formula[45–48],

$$H_Q^{(1)} = \frac{\omega_0}{2\pi}\int_0^{2\pi/\omega_0} \tilde{H}_Q(t)dt = \frac{eQ}{4I(2I-1)}\left(\sqrt{2/3}(3I_z^2 - I^2)V_0\right) \tag{A.16}$$

$$\begin{aligned}H_Q^{(2)} &= \frac{-i\omega_0}{4\pi}\int_0^{2\pi/\omega_0} dt_2 \int_0^{t_2} dt_1 \left[\tilde{H}_Q(t_2), \tilde{H}_Q(t_1)\right] \\ &= -\frac{1}{\hbar\omega_0}\left(\frac{eQ}{4I(2I-1)}\right)^2 \Big\{\sqrt{6}V_0V_{-1}I_+(2I_z + I)^2 - \sqrt{6}V_0V_1I_-(2I_z - I)^2 \\ &\qquad +\sqrt{6}V_0V_{-2}I_+^2(I_z + I) + \sqrt{6}V_0V_2I_-^2(I_z - I) \\ &\qquad +2V_{-1}V_1I_z\left(4I^2 - 8I_z^2 - I\right) + 2V_{-2}V_2I_z\left(2I^2 - 2I_z^2 - I\right)\Big\}\end{aligned} \tag{A.17}$$

where 'I' is the identity operator.
In Principal Axis System (PAS), all the off-diagonal terms of the spatial tensor

are zero without any change in the diagonal terms (i.e. $\forall\ i,j \in x,y,z\ \ V_{ii} \neq 0$ and $V_{ij} = 0$)

$$\mathbf{V^{PAS}} = \begin{bmatrix} V_{xx} & 0 & 0 \\ 0 & V_{yy} & 0 \\ 0 & 0 & V_{zz} \end{bmatrix}$$

with the conventions $|V_{zz}| \geq |V_{yy}| \geq |V_{xx}|$. Also, $\mathbf{V^{PAS}}$ is traceless. Therefore,

$$V_{xx}^{PAS} + V_{yy}^{PAS} + V_{zz}^{PAS} = 0$$
$$\text{Also, } V_0^{PAS} = \sqrt{\frac{3}{2}}eq \quad ; \quad V_{\pm 1}^{PAS} = 0 \quad ; \quad V_{\pm 2}^{PAS} = \frac{1}{2}eq\eta \tag{A.18}$$

In PAS, the quadrupolar interaction is rewritten as[12,13],

$$H_Q^{PAS} = \frac{e^2qQ}{4I(2I-1)}\left\{(3\hat{I}_z^2 - I^2) + \frac{\eta}{2}(\hat{I}_+^2 - \hat{I}_-^2)\right\}$$

To first order, the quadrupolar interaction is represented by,

$$H_Q^{(1)} = \frac{e^2qQ}{4I(2I-1)}(3I_z^2 - I^2) = \frac{\hbar\omega_Q}{6}\ \left(3I_z^2 - I^2\right) \tag{A.19}$$

where,

$$\omega_Q = \frac{3C_Q}{2I(2I-1)} \quad ; \quad C_Q = \frac{e^2Qq}{\hbar}$$

B Concept of Effective Hamiltonians

B.1 Floquet Theory

Let us consider the time dependent Schrödinger equation is given by,

$$i\hbar\frac{\mathrm{d}\,|\psi(t)\rangle}{\mathrm{d}t} = H(t)\,|\psi(t)\rangle \tag{B.1.1}$$

where '$\psi(t)$' is the state of the system defined by $N \times 1$ matrix and '$H(t)$' is a time-dependent periodic Hamiltonian (with time period 'T' and frequency 'ω') denoted by $N \times N$ matrix .

Since the above equation is a first order differential equation with 'N' linearly independent solutions, the 'N' eigenvectors thus obtained can be used to form columns for a square $(N \times N)$ matrix '$F(t)$' that satisfies the Schrödinger equation.

$$i\hbar \frac{\mathrm{d}F(t)}{\mathrm{d}t} = H(t)F(t) \tag{B.1.2}$$

Since, the Hamiltonian '$H(t)$' is time-dependent the evolution of '$F(t)$' is given by,

$$F(t) = \left(e^{-\left(i/\hbar\right)\int_0^t H(t')dt'}\right) F(0) \tag{B.1.3}$$

The above equation is very complicated and has to be solved numerically. To solve Eq. B.1.2 analytically, we use Floquet theory[22,26–29], where '$F(t)$' is defined as,

$$F(t) = X(t)e^{-iQt} \tag{B.1.4}$$

In the above equation, '$X(t)$' is a periodic time-dependent $N \times N$ matrix with time period 'T' and 'Q' is a $N \times N$ diagonal matrix with eigenvalues 'λ_i' corresponding to '$|i\rangle$'

Since, '$X(t)$' is a periodic function, we can expand this function in Fourier series with coefficients 'F^n'

$$X(t) = \sum_n F^n e^{in\omega t} \tag{B.1.5}$$

Writing Eq. B.1.4 in the Dirac notation and substituting Eq. B.1.5, we get

$$\langle\alpha| F(t) |\beta\rangle = F_{\alpha\beta}(t) = \langle\alpha| \sum_n F^n e^{in\omega t} e^{-iQt} |\beta\rangle \tag{B.1.6}$$

Since, '$Q\left|\beta\right\rangle = \lambda_\beta \left|\beta\right\rangle$', we have

$$e^{-iQt}\left|\beta\right\rangle = e^{-i\lambda_\beta t}\left|\beta\right\rangle \tag{B.1.7}$$

Eq. B.1.6 can be compactly written as,

$$F_{\alpha\beta}(t) = \sum_n F^n_{\alpha\beta} e^{in\omega t} e^{-i\lambda_\beta t} \tag{B.1.8}$$

Since, '$H(t)$' is also periodic function it can also be written in Fourier series as,

$$H_{\alpha\beta}(t) = \sum_n H^n_{\alpha\beta} e^{in\omega t} \tag{B.1.9}$$

Writing Eq. B.1.2 in Dirac notation,

$$i\hbar \left\langle\alpha\right| \frac{\mathrm{d}F(t)}{\mathrm{d}t}\left|\beta\right\rangle = \left\langle\alpha\right| H(t)F(t)\left|\beta\right\rangle \tag{B.1.10}$$

and substituting Eqs. B.1.8 and B.1.9, we get (put '$\hbar = 1$')

$$\begin{aligned} i\,\frac{\mathrm{d}F_{\alpha\beta}(t)}{\mathrm{d}t} &= \sum_\gamma \left\langle\alpha\right| H(t)\left|\gamma\right\rangle \;\; \left\langle\gamma\right| F(t)\left|\beta\right\rangle \\ &= \sum_\gamma \sum_n H^n_{\alpha\gamma} e^{in\omega t} \sum_m F^m_{\gamma\beta} e^{im\omega t} e^{-i\lambda_\beta t} \end{aligned} \tag{B.1.11}$$

differentiating Eq. B.1.8 w.r.t 't'

$$i\,\frac{\mathrm{d}F_{\alpha\beta}(t)}{\mathrm{d}t} = \sum_n F^n_{\alpha\beta} e^{in\omega t} e^{-i\lambda_\beta t}\left(\lambda_\beta - n\omega\right) \tag{B.1.12}$$

Equating Eqs: B.1.11 and B.1.12, and solving

$$\sum_n F^n_{\alpha\beta} e^{in\omega t} e^{-i\lambda_\beta t}\left(\lambda_\beta - n\omega\right) = \sum_\gamma \sum_l H^l_{\alpha\gamma} e^{il\omega t} \sum_m F^m_{\gamma\beta} e^{im\omega t} e^{-i\lambda_\beta t} \tag{B.1.13}$$

$$\lambda_\beta \sum_n F^n_{\alpha\beta} = \sum_\gamma \sum_m H^{n-m}_{\alpha\gamma} F^m_{\gamma\beta} + n\omega \sum_n F^n_{\alpha\beta} \tag{B.1.14}$$

we get,

$$\lambda_\beta \; F^n_{\alpha\beta} = \sum_\gamma \left(\sum_m H^{n-m}_{\alpha\gamma} + n\omega\delta_{\alpha\gamma}\delta_{nm} \right) F^m_{\gamma\beta} \tag{B.1.15}$$

In the above equation, 'λ_β' is the eigen value corresponding to eigen vector '$F^n_{\alpha\beta}$' denoted by the pair of indices 'α, n'. The above equation resembles to the well known equation,

$$H\psi = E\psi \tag{B.1.16}$$

where the Hamiltonian is time-independent infinite dimensional matrix commonly referred to as the 'Floquet Hamiltonian' denoted by 'H_F'.
The Floquet Hamiltonian in Dirac notation is written as[27],

$$\langle \alpha, n | H_F | \beta, m \rangle = H^{n-m}_{\alpha\beta} + n\omega\delta_{\alpha\beta}\delta_{nm} \tag{B.1.17}$$

Now, the problem is redefined as,

$$i\hbar \frac{\mathrm{d}\psi_F(t)}{\mathrm{d}t} = H_F \; \psi_F(t) \tag{B.1.18}$$

where '$\psi_F(t)$' is the Floquet wavefunction defined as the linear combination of Floquet basis '$\phi_{i,n}$',

$$|\psi_F(t)\rangle = \sum_{n=-\infty}^{+\infty} \sum_{i=1} C_{n,i}(t) \, |\phi_{n,i}\rangle \tag{B.1.19}$$

$$|\phi_{n,i}\rangle = |n\rangle \otimes |\phi_i\rangle \tag{B.1.20}$$

Hence, the solution of the Eq. B.1.18 is given by,

$$\psi_F(t) = e^{-iH_F t}\psi_F(0) \tag{B.1.21}$$

B.2 Contact Transformations

Contact transformation [30–33] is an operator equivalent of perturbation theory, where in the perturbation corrections are obtained in the form of operators leading to Effective Hamiltonians. In the method of contact transformation, a series of unitary transformations are employed to fold the off-diagonality in the original Hamiltonian. The transformation functions/operators employed in the unitary transformations are carefully chosen to compensate the off-diagonality to the desired order. The accuracy of the solutions depend on the order of the corrections included in the Effective Hamiltonians, thus providing a deeper insight into the different processes arising due to the interaction of Effective Hamiltonians with the spin system.

Let us suppose, the Hamiltonian of the system 'H' us expressed as

$$H = H_0 + \lambda H_1 \tag{B.2.1}$$

where 'H_0' is the diagonal term and 'H_1' is the off-diagonal correction that needs to be folded.
The above Hamiltonian is transformed by a Unitary transformation ($X_1 = e^{i\lambda S_1}$),

$$H' = e^{i\lambda S_1}\ H\ e^{-i\lambda S_1} \tag{B.2.2}$$

Expanding the above equation using Baker-Campbell-Hausdorff (BCH) expansion and equating the like powers of 'λ' on both sides, we get

Table B.2.1: Different orders of corrections obtained by Contact Transformation

n^{th} **order Hamiltonian**	**Expression for the** n^{th} **order Hamiltonian**
Zero order (λ^0)	$H_0^{(1)} = H_0$
I order (λ^1)	$H_1^{(1)} = i[S_1, H_0] + H_1$
II order (λ^2)	$H_2^{(1)} = -\frac{1}{2!}[S_1, [S_1, H_0]] + i[S_1, H_1]$
III order (λ^3)	$H_3^{(1)} = -\frac{i}{3!}[S_1, [S_1, [S_1, H_0]]] - \frac{1}{2!}[S_1, [S_1, H_1]]$
$\vdots$	$\vdots$

The Effective Hamiltonians (to the third order) comprises of diagonal contributions from different orders, while the off-diagonal contributions are treated as perturbations.

$$H_{eff} = H_0^{(1)}(d) + H_1^{(1)}(d) + H_2^{(1)}(d) + H_3^{(1)}(d) + \dots \tag{B.2.3}$$

$$H_1 = H_2^{(1)}(od) + H_3^{(1)}(od) + \dots \tag{B.2.4}$$

The important aspect of the method lies in the selection of 'S_1'. 'S_1' is selected such that the first order correction is free from off-diagonal contributions. Once 'S_1' is selected, higher order corrections are computed using simple commutator relations. The diagonal and off-diagonal contributions from different orders are grouped together and the off-diagonal contributions arising from X_1 are again folded using a second contact transformation ($X_2 = e^{i\lambda^2 S_2}$). Thus the off-diagonal contributions arising from different transformations are folded iteratively till their contributions become insignificant. This is explained in detail in the following chapters.

C Effective Hamiltonians based on AHT

In the Average Hamiltonian (AHT) framework[23–25], a time averaged Hamiltonian is proposed over a cycle time 'τ_c' based on the formula provided by Magnus[45–48]. In a typical Multi-pulse NMR experiment, the evolution operator during different stages is represented by,

$$U(t) = exp\,(-iH_n t_n) \dots exp\,(-iH_2 t_2)\, exp\,(-iH_1 t_1) \tag{C.1}$$

where '$t = t_1 + t_2 + \dots + t_n$' and '$H_1$' is the Hamiltonian acting on the system for the time interval 't_1' and so-on.

To simplify the description, the series of exponential operators are replaced by a single time propagator governed by an *Average Hamiltonian* '$\bar{H}$' valid over the

cycle time 'τ_c'.

$$U(\tau_c) = exp\left(-iH_n t_n\right) \ldots exp\left(-iH_2 t_2\right) exp\left(-iH_1 t_1\right) = exp\left(-i\bar{H}\tau_c\right) \tag{C.2}$$

Employing the Magnus formula, the Average Hamiltonian over a cycle time τ_c is derived as given below.

$$\bar{H}(\tau_c) = H^{(1)} + H^{(2)} + H^{(3)} + \ldots \tag{C.3}$$

where, '$H^{(n)}$' represents the 'n^{th}' order correction given by,

$$H^{(1)} = \frac{1}{\tau_c} \int_0^{\tau_c} \tilde{\tilde{H}}(t) dt \tag{C.4}$$

$$H^{(2)} = \frac{(-i)}{2\tau_c} \int_0^{\tau_c} dt_2 \int_0^{t_2} dt_1 \left[\tilde{\tilde{H}}(t_2), \tilde{\tilde{H}}(t_1)\right] \tag{C.5}$$

$$H^{(3)} = \frac{1}{6\tau_c} \int_0^{\tau_c} dt_3 \int_0^{t_3} dt_2 \int_0^{t_2} dt_1 \left\{ \left[\tilde{\tilde{H}}(t_3), \left[\tilde{\tilde{H}}(t_2), \tilde{\tilde{H}}(t_1)\right]\right] + \left[\tilde{\tilde{H}}(t_1), \left[\tilde{\tilde{H}}(t_2), \tilde{\tilde{H}}(t_3)\right]\right]\right\} \tag{C.6}$$

CHAPTER-2

EFFECTIVE HAMILTONIANS FOR DOUBLE–QUANTUM (DQ) EXCITATION IN SPIN I=1

Chapter 2

Effective Hamiltonians for Double Quantum excitation in spin $I = 1$

2.1 Introduction

As discussed in Chapter-1, nuclei with spin '$I > {}^1/_2$' have an additional interaction between the non-zero electric quadrupole moment and the inhomogeneous electric fields around the nucleus (generated by surroundings). The resulting quadrupolar interactions often dominate other internal spin interactions (such as chemical shift, dipolar interactions etc.) present in the system. While the inherent rapid molecular tumbling motion in liquids diminishes the effects of quadrupolar interaction, the spectra of quadrupolar nuclei in solids are broadened over Mega Hertz (MHz). Since 70 % of the elements in the periodic table are quadrupolar in nature, NMR of quadrupolar nuclei is essential for expanding the repositoire of NMR spectroscopy in structural characterization of inorganic materials and clusters. Here in this chapter, we confine our discussion to spin '$I = 1$' system. Although, '^2H' and '^{14}N' are the most commonly studied nuclei with spin $I = 1$, the disparate order of magnitudes in their quadrupolar coupling constants necessitates different experimental strategies for detecting them. For example, the quadrupolar coupling constant in solids for ^{14}N nucleus ranges from 1 to 5 MHz, while, for ^2H it ranges from 100 to 300 kHz[1]. Since, the amplitude of the RF pulse employed in experiments varies from $10 - 200$ kHz, the optimum conditions for the excitation

may vary and deserves a formal theoretical discussion. Here in this chapter, we confine our discussion to the excitation of DQ transitions in spin $I = 1$ systems both in isotropic and anisotropic solids.

To begin with, in the presence of the static magnetic field (of strength 'B_0'), the degeneracy associated with the $(2I+1)$ spin states is lifted. In the absence of other internal interactions, the two single-quantum (SQ) transition frequencies (corresponding to $|1\rangle \rightarrow |0\rangle, |0\rangle \rightarrow |-1\rangle$) are degenerate and result in a single peak as depicted in Fig. 2.1. In the presence of quadrupolar interactions (to first-order) the degeneracy associated with the two SQ transitions is lifted resulting in two peaks (see Fig. 2.1).

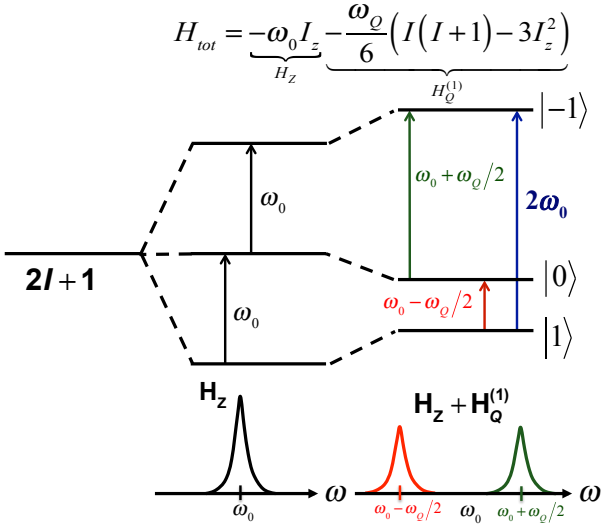

Figure 2.1: Energy level diagram of Spin I=1 depicting the energy shifts due to Zeeman Hamiltonian and the first order quadrupolar Hamiltonian is presented. In the equation of the Hamiltonain ($\hbar = 1$). It is to be noted that the degeneracy of Zeeman NMR signal is lifted due to the presence of electric field gradient due to the quadrupolar Hamiltonian. The Double Quantum (DQ) transition independent of first order quadrupolar coupling constant is also shown.

In a powder sample, the spatial anisotropy due to restricted mobility results in a distribution of quadrupolar coupling constants. Consequently, the NMR peaks corresponding to the two SQ transitions are broadened compromising the spectral resolution. Hence, direct detection of ^{14}N transitions in powder samples is

abandoned and indirect detection is favoured.[2–6] As an alternative, detection of Double Quantum (DQ) transitions is preferred in the study of systems with larger quadrupolar coupling constants. In contrast to the SQ transitions, the DQ transitions in spin I=1 ($|-1\rangle \rightarrow |1\rangle$) are independent of first-order quadrupolar interactions and seem to be an attractive option[7]. Since DQ transitions are forbidden, a formal understanding of the excitation process is essential for developing new experimental strategies and quantifying experimental data involving spin $I = 1$ nuclei.

To this end, Vega and Pines[8,9] developed a theoretical framework for describing DQ transitions in spin I=1 system. Employing the fictitious spin operator algebra[10,11], an analytic expression describing the excitation of double-quantum (DQ) transitions in single crystal was proposed in 1976. A brief illustration of the dependence of the excitation profile on the quadrupolar coupling constants (C_Q) is presented in Figure. 2.2 along with a comparison of their analytic results with exact numerical simulations emerging from SIMPSON[12]. As depicted, the simulations emerging from their analytic results agree only in the strong coupling regime ($C_Q > ({}^{\omega_1}/_{2\pi})$) and deviate significantly when the magnitude of the quadrupolar constant approaches to that of the amplitude of the RF pulse.

Since the magnitude of the quadrupolar frequency (ω_Q) is always greater than both the RF amplitude and the internal spin interactions, the deviations reported above have often been ignored and remain unexplained. Interestingly, in the case of studies involving ${}^2H$, the quadrupolar coupling constant ranges from $100 - 300$ kHz. Hence, a more general framework suitable for describing the excitation process in systems with wide range of quadrupolar coupling constants ($0.1 \rightarrow 4$ MHz) is essential. Additionally, the extension of their approach for describing the excitation of MQ transitions in a powder (anisotropic) sample is less straightforward and has remained elusive[13].

In an alternate formulation, Nielsen and coworkers[14] proposed an approach based on numerical methods for understanding the excitation process in isotropic and anisotropic solids. In their approach, the evolution of the spin system during the pulse was evaluated numerically using time-ordered integration of the evolution operator comprising of the quadrupolar and the RF Hamiltonians. Although, their approach yields results in agreement with exact numerical methods, the method-

ology employed involves numerical diagonalization of matrices and is computationally less efficient when integrated with iterative fitting routines for extracting molecular constraints from experimental data. Additionally, lack of physical insights into the excitation process limits the utility of such methods.

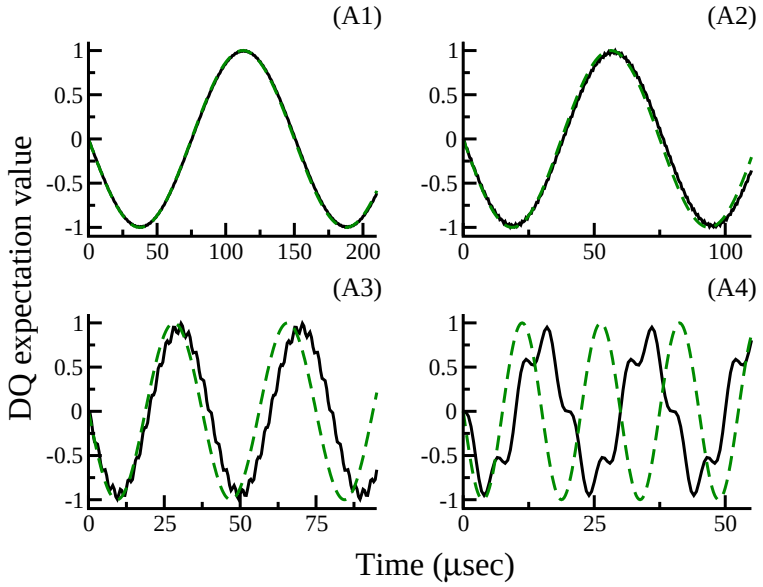

Figure 2.2: Simulations depicting the efficiency of double quantum (DQ) excitation in static I=1 system (single crystal) derived from analytic[8,9,15] (green dotted lines) and numerical (black thick lines) methods. In the simulations depicted, the quadrupole coupling constant ($C_Q = {}^{\omega_Q}/_{3\pi}$) is varied A1) $C_Q = 2$ MHz, A2) $C_Q = 1$ MHz, A3) $C_Q = 500$ kHz, A4) $C_Q = 200$ kHz, employing an excitation pulse of constant RF amplitude, $({}^{\omega_1}/_{2\pi}) = 100$ kHz.

As an alternative to these existing frameworks, an analytic method based on the concept of effective Floquet Hamiltonians[15–18] is proposed to explain the nuances of the excitation of DQ transitions in both isotropic and anisotropic solids. The proposed effective Floquet Hamiltonians are derived systematically from the contact transformation procedure[19–22]. Although, effective Floquet Hamiltonians have found their importance in the description of solid-state NMR experiments involving spin I=$^1/_2$ nuclei,[23–26] their utility in the description of the excitation profile in quadrupolar systems is less realized[15,17,18]. To this end, a unified approach suitable

for describing both isotropic and anisotropic systems is presented in this chapter. The importance of the interaction frames and their role in the convergence of the perturbation corrections employed in the derivation of effective Floquet Hamiltonians is discussed extensively through comparisons with analytic and numerical simulations. Additionally, a new hybrid method based on the concept of effective Floquet Hamiltonians derived from different interaction frames is proposed to quantify the excitation profiles observed in anisotropic solids.

2.2 Theory and Simulations

To understand the response of the $I = 1$ spin system under RF pulses, the Hamiltonians defined in the laboratory frame (see Eq. 2.1) are transformed into the Zeeman-interaction frame using the transformation operator, $U_1 = e^{-(i\omega_0 t)I_z}$.

$$\begin{aligned} H_{lab}(t) &= H_z + H_{RF}(t) + H_Q \\ &= \underbrace{-\hbar\omega_0 I_z}_{H_z} \underbrace{-2\hbar\omega_1 \cos(\omega t - \phi_1)\ I_x}_{H_{RF}(t)} \underbrace{+ \sum R^{(2)q} T^{(2)q}}_{H_Q} \end{aligned} \tag{2.1}$$

Here, '$H_{lab}(t)$' denotes the Hamiltonian in the laboratory frame. The RF pulse is characterized in-terms of the amplitude (ω_1), frequency (ω) and phase (ϕ_1). The quadrupolar interaction is expressed as a product in-terms of the spatial and spin tensor operators[27–36]. A detailed description of these operators is discussed was chapter-1.

$$\tilde{H}(t) = U_1\ H_{lab}(t)\ U_1^{-1} = e^{-(i\omega_0 t)I_z}\ H_{lab}(t)\ e^{(i\omega_0 t)I_z}$$

$$\begin{aligned} \tilde{H}(t) = -\hbar\omega_1 \Big\{ &\left(e^{i(\omega-\omega_0)t} + e^{-i(\omega+\omega_0)t}\right) \Phi_1 \left(iT^{(1)1}\right) \\ &- \left(e^{i(\omega+\omega_0)t} + e^{-i(\omega-\omega_0)t}\right) \Phi_1^{-1} \left(iT^{(1)-1}\right) \Big\} + \sum_{q=-2}^{+2} R^{(2)q}\ T^{(2)q}\ e^{-iq\omega_0 t} \end{aligned} \tag{2.2}$$

In the above eq, $\Phi_1^n = e^{-in\phi_1}$ denotes the phase factor of the pulse. When the frequency of the RF pulse is adjusted to the Larmor frequency, 'ω_0' (i.e., $\omega = \omega_0$), the RF Hamiltonian reduces to a much simpler form under secular approximation.

$$\tilde{H}_{RF} = -\hbar\omega_1 \left\{ \Phi_1 i T^{(1)1} - \Phi_1^{-1} i T^{(1)-1} \right\} \tag{2.3}$$

In a similar vein, under secular approximation, the time-dependent terms in the quadrupolar Hamiltonian are ignored, resulting in a much simpler form (commonly referred to as first-order quadrupolar interaction)

$$\tilde{H}_Q = -\frac{\hbar\Omega_Q}{\sqrt{6}} T^{(2)0} \tag{2.4}$$

Subsequently, the Hamiltonian in the Zeeman interaction frame reduces to a simple form given below.

$$\tilde{H} = -\hbar\omega_1 \left\{ \Phi_1 i T^{(1)1} - \Phi_1^{-1} i T^{(1)-1} \right\} - \frac{\hbar\Omega_Q}{\sqrt{6}} T^{(2)0} \tag{2.5}$$

Depending on the nature of the sample, the form of 'Ω_Q' varies. For example, in the case of a single crystal, $\Omega_Q = \omega_Q$, ('ω_Q'(rad/s) represents the quadrupolar frequency and is related to the quadrupolar coupling constant 'C_Q'(Hz), (i.e., $\omega_Q = {}^{3(2\pi)C_Q}/_{2I(2I-1)}$; $C_Q = {}^{e^2Qq}/_{h}$); while, in a powder sample, the quadrupolar interaction is anisotropic and is represented by, $\Omega_Q = \omega_Q^{(\alpha\beta\gamma)}$. The orientation dependence of the quadrupolar interaction is evaluated using the following expression.

$$\omega_Q^{(\alpha\beta\gamma)} = \omega_Q \left\{ D_{0,0}(\Omega_{PL}) + \frac{\eta}{\sqrt{6}} \left(D_{-2,0}(\Omega_{PL}) + D_{2,0}(\Omega_{PL}) \right) \right\} \tag{2.6}$$

The term, '$D(\Omega_{PL})$' represents the Wigner rotation matrix[37,38] and essentially describes the transformation from the principal axis (PAS) to the laboratory axis (LAS). In the case of a static powder sample, the transformation from the PAS to laboratory frame is derived through two sets of Euler angles $\Omega_{PM} =$

$(\alpha_{PM}, \beta_{PM}, \gamma_{PM})$ and $\Omega_{ML} = (\alpha_{ML}, \beta_{ML}, \gamma_{ML})$.

$$D_{q,0}(\Omega_{PL}) = \sum_{q_1=-2}^{2} D_{q,q_1}(\Omega_{PM})\ D_{q_1,0}(\Omega_{ML}) \tag{2.7}$$

The Euler angles (Ω_{PM}) relating the PAS to the molecular axis (MolAS) are unique and identical for all the crystallites present in a powder sample. The transformation from the molecular axis to the laboratory axis is orientation dependent (varies for each crystallite and is represented by Ω_{ML}). In the case of a spinning sample, an additional transformation defining the orientation of the rotor axis (RAS) with respect to lab axis (LAS) is defined and the Hamiltonian becomes periodically time-dependent.

$$D_{q,0}(\Omega_{PL}) = \sum_{q_1,q_2=-2}^{2} D_{q,q_1}(\Omega_{PM})\ D_{q_1,q_2}(\Omega_{MR})\ D_{q_2,0}(\Omega_{RL}) \tag{2.8}$$

The term, '$D(\Omega_{RL}) = (\omega_r t, \beta_m, 0)$' represents the time-dependent transformation from the rotor axis to the lab-frame (where ω_r denotes the sample spinning frequency and β_m the magic angle).
A special set (*in-situ and operando*) of experiments are performed under Magic angle, without spinning. For such systems '$D(\Omega_{RL}) = (0, \beta_m, 0)$' and this conditions is called as 'Static MAS' condition throughout this thesis.
As described in Eq. 2.5, the Hamiltonian comprises of non-commuting operators and in its present form is less suitable for analytic description of the time-evolution. Depending on the magnitude of the quadrupolar interaction (ω_Q) relative to the amplitude of the RF pulse (ω_1), the Hamiltonian in the Zeeman interaction frame is further transformed. Based on the above criterion, the following regimes are identified and discussed for both single crystal and powder samples under static conditions.

2.2.1 DQ excitation in Single Crystal ($\Omega_Q = \omega_Q$)

Regime-I: Strong coupling ($\omega_Q >> \omega_1$)

When the magnitude of the quadrupolar frequency exceeds the amplitude of the pulse, 'ω_1', the Hamiltonian in the Zeeman interaction frame[18] (Eq. 2.2) is further transformed into the quadrupolar interaction frame, defined by the transformation operator, $U_2 = e^{-\left(i\omega_Q t/\sqrt{6}\right)T^{(2)0}}$

$$\tilde{\tilde{H}}(t) = U_2 \; \tilde{H} \; U_2^{-1} = \tilde{\tilde{H}}_Q + \tilde{\tilde{H}}_{RF}(t) \tag{2.9}$$

In the combined Zeeman-Quadrupolar interaction frame, the quadrupolar interaction is time-independent and is described by an offset term 'Δ', (i.e., $\Delta = \frac{1}{\sqrt{6}}(\omega_Q - \Omega_Q)$)

$$\tilde{\tilde{H}}_Q = \hbar \Delta T^{(2)0} \tag{2.10}$$

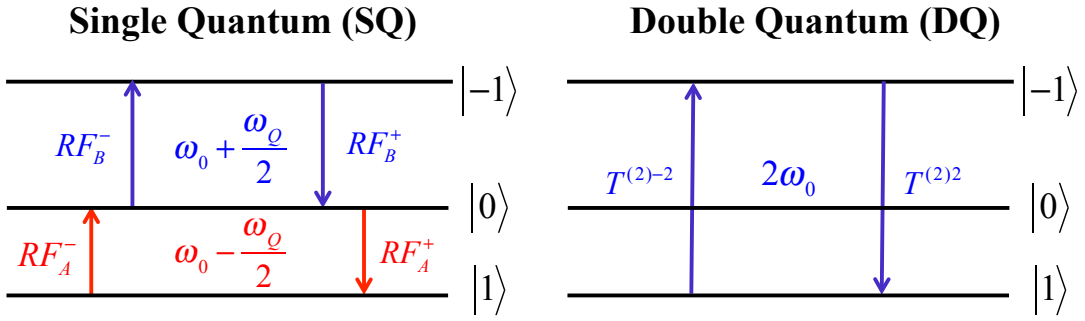

Figure 2.3: Schematic depiction of transitions along with operators for a spin I=1 system

Accordingly, the offset is zero for a single crystal ($\Delta = \frac{1}{\sqrt{6}}(\omega_Q - \omega_Q) = 0$) and orientation dependent for a powder sample ($\Delta = \frac{1}{\sqrt{6}}\left(\omega_Q - \omega_Q^{(\alpha\beta\gamma)}\right)$).

The RF Hamiltonian in the Zeeman-Quadrupolar interaction is time-dependent.

$$\begin{aligned}\tilde{\tilde{H}}_{RF}(t) = -\frac{\hbar\omega_1}{2}\Big\{\Big(&\Phi_1\left(i\,T^{(1)1} + \;T^{(2)1}\right)\; e^{i\omega_Q t/2}\\ &+\Phi_1^{-1}\left(-i\,T^{(1)-1} + \;T^{(2)-1}\right)\; e^{i\omega_Q t/2}\Big)\\ +\Big(&\Phi_1^{-1}\left(-i\,T^{(1)-1} - \;T^{(2)-1}\right)\; e^{-i\omega_Q t/2}\\ &+\Phi_1\left(i\,T^{(1)1} - \;T^{(2)1}\right)\; e^{-i\omega_Q t/2}\Big)\Big\}\end{aligned} \tag{2.11}$$

To understand the effects of the RF pulse, the RF Hamiltonian ($\tilde{\tilde{H}}_{RF}$) in the Zeeman-Quadrupolar interaction frame is grouped in terms of operators depicting the possible transitions specific to a given spin system[39]. A schematic depiction of the possible transitions along with their frequencies and operators is illustrated in Figure. 2.3. A detailed description of the operators along with their relationship to the spherical tensor operators[39] is tabulated in Table. 2.1.

Table 2.1: Definition of the spin operators corresponding to the possible transitions in a spin $I = 1$ system

Operator	Tensoral Operators	Frequency
+1 Coherence Operators		
RF_A^+	$i\,T^{(1)1} + \;T^{(2)1}$	$\omega = \omega_0 - {}^{\omega_Q}/_2$
RF_B^+	$i\,T^{(1)1} - \;T^{(2)1}$	$\omega = \omega_0 + {}^{\omega_Q}/_2$
-1 Coherence Operators		
RF_A^-	$-i\,T^{(1)-1} - \;T^{(2)-1}$	$\omega = \omega_0 - {}^{\omega_Q}/_2$
RF_B^-	$-i\,T^{(1)-1} + \;T^{(2)-1}$	$\omega = \omega_0 + {}^{\omega_Q}/_2$
+2 Coherence Operators		
D^+	$T^{(2)2}$	$\omega = 2\omega_0$
-2 Coherence Operators		
D^-	$T^{(2)-2}$	$\omega = 2\omega_0$

Employing the operators described in Table. 2.1, the RF Hamiltonian (Eq. 2.11) is represented as follows,

$$\tilde{\tilde{H}}_{RF}(t) = -\frac{\hbar\omega_1}{2}\left\{\left(\Phi_1 RF_A^+ + \Phi_1^{-1} RF_B^-\right) e^{\left(i\omega_Q t/2\right)} + \left(\Phi_1^{-1} RF_A^- + \Phi_1 RF_B^+\right) e^{-\left(i\omega_Q t/2\right)}\right\} \tag{2.12}$$

Table 2.2: Symmetric and Anti-symmetric combination of spin operators employed in spin $I = 1$ system

Operator	Combination	Operator	Combination
$\hat{SQ}_S^{(r)}$	$\left(\Phi_1^{-1} RF_A^- + \Phi_1 RF_B^+\right)$	$\hat{SQ}_{AS}^{(r)}$	$\left(\Phi_1^{-1} RF_A^- - \Phi_1 RF_B^+\right)$
$\hat{SQ}_S^{(cr)}$	$\left(\Phi_1 RF_A^+ + \Phi_1^{-1} RF_B^-\right)$	$\hat{SQ}_{AS}^{(cr)}$	$\left(\Phi_1 RF_A^+ - \Phi_1^{-1} RF_B^-\right)$
$\hat{D}_S$	$\left(\Phi_1^2 D^+ + \Phi_1^{-2} D^-\right)$	$\hat{D}_{AS}$	$\left(\Phi_1^2 D^+ - \Phi_1^{-2} D^-\right)$

To further simplify the description, the time-dependent phase factor due to '$e^{\pm i\omega_Q t/2}$' is further classified into rotating ($e^{-i\omega_Q t/2}$) and counter rotating terms ($e^{+i\omega_Q t/2}$) and the Hamiltonian (Eq. 2.12) is re-expressed in terms of the symmetric and anti-symmetric combination of spin operators (see Table. 2.2). The final form of the Hamiltonian in the Zeeman-Quadrupolar interaction frame is represented by,

$$\tilde{\tilde{H}}(t) = \hbar\Delta T^{(2)0} - \frac{\hbar\omega_1}{2}\left\{\left(\hat{SQ}_S^{(cr)}\right) e^{\left(i\omega_Q t/2\right)} + \left(\hat{SQ}_S^{(r)}\right) e^{-\left(i\omega_Q t/2\right)}\right\} \tag{2.13}$$

Since, understanding of spectroscopic phenomena under time-dependent Hamiltonians is important and less straightfarward, analytic methods based on Average Hamiltonian Theory (AHT)[40–42] and Floquet theory[23,43–46] have become important. A brief description of the spin dynamics based on AHT along with its limitations is discussed in Appendix.B. Here in this thesis, we employ Floquet theory to explicate the nuances of the excitation of MQ transitions. In contrast to AHT, Floquet theory presents a more general framework for describing the time evolution (non-stroboscopic detection) of the system in solid-state NMR experiments. Employing Floquet theorem, the time-dependent Hamiltonian (Eq. 2.13) is trans-

formed into a time-independent Floquet Hamiltonian and is represented through a set of operators (Floquet operators) defined in an infinite-dimensional vector space. Accordingly, in the Floquet framework, the Hamiltonian depicting an RF pulse is represented by,

$$H_F = \frac{\omega_Q}{2} I_F + \hbar\Delta \left(T^{(2)0}\right)_0 - \frac{\hbar\omega_1}{2} \left\{ \left(\hat{SQ}_S^{(cr)}\right)_{-1} + \left(\hat{SQ}_S^{(r)}\right)_{+1} \right\} \tag{2.14}$$

In the above equation 'I_F' represents the identity operator defined in the Floquet space,

$$I_F = N \otimes I \quad ; \quad N = \sum_{n=-\infty}^{\infty} n \left|n\right\rangle \left\langle n\right| \tag{2.15}$$

where, 'I' is the identity operator. The Floquet spin operators '$(I_\alpha)_m$' are constructed from a direct product between the Fourier 'F_m' and spin 'I_α' operators

$$(I_\alpha)_m = F_m \otimes I_\alpha \quad ; \quad F_m = \sum_{n=-\infty}^{\infty} \left|n\right\rangle \left\langle n+m\right| \tag{2.16}$$

The subscript 'm' denotes the off-diagonality in the Fourier dimension and connects states that differ by 'm'. A detailed description of the Floquet operators is described in Appendix.C. It is important to realize here that the Floquet Hamiltonian derived above (Eq. 2.14) is defined in an infinite-dimensional vector space and only the non-zero terms associated with the Floquet operators are illustrated in Eq. 2.14 . Consequently, analytic descriptions have always remained difficult. To alleviate this problem, the concept of 'Effective Floquet Hamiltonians' based on the Contact tranformation method[19–22] is employed in the present study. Although,the utility of the effective Floquet Hamiltonians in the description of spin $I = {}^1/_2$ systems is known, the application of this approach has not been extended to the description of quadrupolar nuclei. This could largely be attributed to the presence of the dominant quadrupolar interaction and ambiguities in the definition of the zero-oreder and perturbing Hamiltonians. Since the contact transformation procedure is an operator equivalent of the standard Rayleigh-Schrodinger perturbation theory, the definition of the zero-order and perturbing Hamiltonians play an

important role in the overall convergence of the proposed effective Floquet Hamiltonian.

To begin with, Floquet operators that are diagonal '$(I_\alpha)_0$' are retained along the zero order Hamiltonian, while, the off-diagonal operators are included along 'H_1'.

$$H_F = H_0 + H_1 \tag{2.17}$$

$$H_0 = \frac{\omega_Q}{2} I_F + \hbar\Delta \left(T^{(2)0}\right)_0 \tag{2.18}$$

The perturbing Hamiltonian in the present study is chosen to contain only off-diagonal terms.

$$H_1 = -\frac{\omega_1}{2}\left\{\left(\hat{SQ}_S^{(r)}\right)_{+1} + \left(\hat{SQ}_S^{(cr)}\right)_{-1}\right\} \tag{2.19}$$

Employing the transformation function 'S_1', the original untransformed Floquet Hamiltonian (Eq. 2.14) is transformed through a unitary transformation as illustrated below.

$$H_{eff} = e^{i\lambda S_1}\ H_F\ e^{-i\lambda S_1} \tag{2.20}$$

$$S_1 = \ C_{SQ}^{(1)}\left\{\left(\hat{SQ}_S^{(r)}\right)_{+1} - \left(\hat{SQ}_S^{(cr)}\right)_{-1}\right\} \tag{2.21}$$

where,

$$C_{SQ}^{(1)} = -i\left(\frac{\omega_1}{\Omega_Q}\right) \tag{2.22}$$

The transformation function 'S_1' defined in Eq. 2.21 is carefully chosen to compensate the off-diagonal terms in 'H_1' and is derived through the procedure[16] given below,

$$H_1^{(1)} = H_1 + i[S_1, H_0] = 0$$

$$i[S_1, H_0] = -H_1$$

Subsequently, employing Baker-Campbell-Hausdorff (BCH) expansion[47], the higher-order corrections to the effective Hamiltonian are derived and described in detail

in Table. 2.3. In the description that follows, '$H_n^{(1)}$' represents the n^{th} order corrections obtained from the first transformation, 'S_1'.
In general, the higher order corrections to the effective Hamiltonian comprises of both diagonal and off-diagonal contributions. In the present problem, the higher order corrections mainly arise from commutator expressions involving the transformation function 'S_1' and the perturbing Hamiltonian 'H_1'. The commutator of the transformation function 'S_1' with 'H_1' to various orders could be derived through the expression.

$$H_n^{(1)} = \sum_{n=2}^{\infty} \frac{(i)^{n-1}}{n \times (n-2)!} \left[\underbrace{[S_1, \ldots\ldots\ldots\ldots [S_1}_{n-1}, H_1 \,] \ldots\ldots\ldots\ldots] \right] \tag{2.23}$$

A detailed description of the commutator relations involving the transformation function 'S_1' and 'H_1' to various orders of 'λ' are tabulated in Table 2.4.
As a standard procedure, the diagonal corrections are often retained, while neglecting the off-diagonal terms. Nevertheless, the validity of such approximations could only be verified through a rigorous comparison of simulations emerging from analytic (based on effective Hamiltonians) and numerical based exact methods.
To illustrate the importance of the various perturbation corrections (both diagonal and off-diagonal), a systematic study through comparison between simulations emerging from the effective Hamiltonians and exact numerical simulations based on SIMPSON (a numerical based software for simulating NMR experiments in solid state) is presented in the following sections.
As illustrated in Table. 2.4, the higher order contributions comprise of the diagonal (arising from ZQ ($T^{(2)0}$), and DQ $\left(\hat{D}_S\right)$) and off-diagonal (from SQ $\left(\hat{SQ}_S^{(r,cr)}\right)_{\pm 1}$) operators. Depending on the magnitude of the off-diagonal contributions, the convergence of the perturbation corrections could in principle, be accomplished through a single or a series of transformations (often termed as contact transformations) as discussed below.

$$H_{eff} = e^{i\lambda^n S_n} \ldots\ldots\ldots e^{i\lambda^2 S_2}\ e^{i\lambda S_1}\ H_F\ e^{-i\lambda S_1}\ e^{-i\lambda^2 S_2} \ldots\ldots\ldots e^{-i\lambda^n S_n} \tag{2.24}$$

Table 2.3: Description of higher-order corrections to the effective Hamiltonian derived from BCH expansion

n^{th} **order Correction**	**Expression for the** n^{th} **order Correction**
Zero order (λ^0)	$H_0^{(1)} = H_0$
I order (λ^1)	$H_1^{(1)} = i[S_1, H_0] + H_1$
II order (λ^2)	$H_2^{(1)} = -\frac{1}{2!}[S_1,[S_1,H_0]] + i[S_1,H_1]$
III order (λ^3)	$H_3^{(1)} = -\frac{i}{3!}[S_1,[S_1,[S_1,H_0]]] - \frac{1}{2!}[S_1,[S_1,H_1]]$
IV order (λ^4)	$H_4^{(1)} = \frac{1}{4!}[S_1,[S_1,[S_1,[S_1,H_0]]]] - \frac{i}{3!}[S_1,[S_1,[S_1,H_1]]]$
V order (λ^5)	$H_5^{(1)} = \frac{i}{5!}[S_1,[S_1,[S_1,[S_1,[S_1,H_0]]]]] + \frac{1}{4!}[S_1,[S_1,[S_1,[S_1,H_1]]]]$
VI order (λ^6)	$H_6^{(1)} = -\frac{1}{6!}[S_1,[S_1,[S_1,[S_1,[S_1,[S_1,H_0]]]]]] + \frac{i}{5!}[S_1,[S_1,[S_1,[S_1,[S_1,H_1]]]]]$
VII order (λ^7)	$H_7^{(1)} = -\frac{i}{7!}[S_1,[S_1,[S_1,[S_1,[S_1,[S_1,[S_1,H_0]]]]]]] - \frac{1}{6!}[S_1,[S_1,[S_1,[S_1,[S_1,[S_1,H_1]]]]]]$
VIII order (λ^8)	$H_8^{(1)} = \frac{1}{8!}[S_1,[S_1,[S_1,[S_1,[S_1,[S_1,[S_1,[S_1,H_0]]]]]]]] - \frac{i}{7!}[S_1,[S_1,[S_1,[S_1,[S_1,[S_1,[S_1,H_1]]]]]]]$
IX order (λ^9)	$H_9^{(1)} = \frac{i}{9!}[S_1,[S_1,[S_1,[S_1,[S_1,[S_1,[S_1,[S_1,[S_1,H_0]]]]]]]]] + \frac{1}{8!}[S_1,[S_1,[S_1,[S_1,[S_1,[S_1,[S_1,[S_1,H_1]]]]]]]]$
X order (λ^{10})	$H_{10}^{(1)} = -\frac{1}{10!}[S_1,[S_1,[S_1,[S_1,[S_1,[S_1,[S_1,[S_1,[S_1,[S_1,H_0]]]]]]]]]] + \frac{i}{9!}[S_1,[S_1,[S_1,[S_1,[S_1,[S_1,[S_1,[S_1,[S_1,H_1]]]]]]]]]$

Table 2.4: Description of the higher order (diagonal and off-diagonal) contributions to the effective Hamiltonian (Eq. 2.25) derived from first transformation

n^{th} **order** **Correction**	**Coefficients in the Effective Hamiltonian** $H_{eff} = H_0^{(1)} + H_2^{(1)} + H_4^{(1)} + H_6^{(1)} + \cdots = \frac{\omega_Q}{2} I_F + \sum_{i=0}^{N_1} G_{DQ,i}^{(1)} \left(\hat{D}_S\right)_0 + \sum_{i=0}^{N_1} G_{ZQ,i}^{(1)} \left(T^{(2)0}\right)_0$	
	Expression from the 'H_1' term	**Non-zero 'G' Coefficients**
Zero order (λ^0)	$H_0^{(1)} = \frac{\omega_Q}{2} I_F + \hbar\Delta \left(T^{(2)0}\right)_0$	$\frac{\omega_Q}{2} I_F + G_{ZQ,0}^{(1)} \left(T^{(2)0}\right)_0$
I order (λ^1)	$H_1^{(1)} = 0$	
II order (λ^2)	$H_2^{(1)} = \frac{i}{2 \times 0!}[S_1, H_1] = -\frac{1}{2 \times 0!} \left(\frac{\omega_1}{2}\right) (\theta) \left(\sqrt{6}\, T^{(2)0} + \hat{D}_S\right)_0$	$G_{ZQ,2}^{(1)} \left(T^{(2)0}\right)_0 + G_{DQ,2}^{(1)} \left(\hat{D}_S\right)_0$
III order (λ^3)	$H_3^{(1)} = -\frac{1}{3 \times 1!}[S_1, [S_1, H_1]] = \frac{1}{3 \times 1!} \left(\frac{\omega_1}{2}\right) (\theta)^2 \left\{ \left(S\hat{Q}_S^{(r)}\right)_{+1} + \left(S\hat{Q}_S^{(cr)}\right)_{-1} \right\}$	$G_{SQ,3}^{(1)} \left\{ \left(S\hat{Q}_S^{(r)}\right)_{+1} + \left(S\hat{Q}_S^{(cr)}\right)_{-1} \right\}$
IV order (λ^4)	$H_4^{(1)} = -\frac{i}{4 \times 2!}[S_1, [S_1, [S_1, H_1]]] = \frac{1}{4 \times 2!} \left(\frac{\omega_1}{2}\right) (\theta)^3 \left(\sqrt{6}\, T^{(2)0} + \hat{D}_S\right)_0$	$G_{ZQ,4}^{(1)} \left(T^{(2)0}\right)_0 + G_{DQ,4}^{(1)} \left(\hat{D}_S\right)_0$
V order (λ^5)	$H_5^{(1)} = \frac{1}{5 \times 3!}[S_1, [S_1, [S_1, [S_1, H_1]]]] = -\frac{1}{5 \times 3!} \left(\frac{\omega_1}{2}\right) (\theta)^4 \left\{ \left(S\hat{Q}_S^{(r)}\right)_{+1} + \left(S\hat{Q}_S^{(cr)}\right)_{-1} \right\}$	$G_{SQ,5}^{(1)} \left\{ \left(S\hat{Q}_S^{(r)}\right)_{+1} + \left(S\hat{Q}_S^{(cr)}\right)_{-1} \right\}$
VI order (λ^6)	$H_6^{(1)} = \frac{i}{6 \times 4!}[S_1, [S_1, [S_1, [S_1, [S_1, H_1]]]]] = -\frac{1}{6 \times 4!} \left(\frac{\omega_1}{2}\right) (\theta)^5 \left(\sqrt{6}\, T^{(2)0} + \hat{D}_S\right)_0$	$G_{ZQ,6}^{(1)} \left(T^{(2)0}\right)_0 + G_{DQ,6}^{(1)} \left(\hat{D}_S\right)_0$
VII order (λ^7)	$H_7^{(1)} = -\frac{1}{7 \times 5!}[S_1, [S_1, [S_1, [S_1, [S_1, [S_1, H_1]]]]]] = +\frac{1}{7 \times 5!} \left(\frac{\omega_1}{2}\right) (\theta)^6 \left\{ \left(S\hat{Q}_S^{(r)}\right)_{+1} + \left(S\hat{Q}_S^{(cr)}\right)_{-1} \right\}$	$G_{SQ,7}^{(1)} \left\{ \left(S\hat{Q}_S^{(r)}\right)_{+1} + \left(S\hat{Q}_S^{(cr)}\right)_{-1} \right\}$
$\theta = \left(\frac{4\omega_1}{\Omega_Q}\right) \quad ; \quad C_{(\theta)} = \cos(\theta)$		

For e.g., the first transformation function 'S_1' folds off-diagonal contributions to order 'λ' while, the off-diagonal contributions to order'λ^2' (arising from the residual terms from the first transformation) are folded by a second transformation function 'S_2'. In a similar vein, the third transformation folds off-diagonal corrections to order 'λ^3' present in the perturbing Hamiltonian, besides the residual off-diagonal contributions (to order λ^3) resulting from the first and second transformations. Nevertheless, it is important to realize here that the corrections obtained from successive transformations do not alter the results (coefficients) obtained from the previous transformations. A pedagogical description illustrating the role of higher order corrections in the excitation of DQ transitions in spin $I = 1$ is discussed below along with simulations.

I. Effective Hamiltonians from first transformation, 'S_1'

Based on Table. 2.4, let the general form of the effective Hamiltonian (comprising of diagonal corrections only) describing the excitation process (from a single pulse) be represented by,

$$H_{eff} = e^{i\lambda S_1}\ H_F\ e^{-i\lambda S_1}$$
$$H_{eff} = \frac{\omega_Q}{2} I_F + \ G^{(1)}_{DQ}\left(\hat{D}_S\right)_0 + G^{(1)}_{ZQ}\left(T^{(2)0}\right)_0 \tag{2.25}$$

where,

$$G^{(1)}_{DQ} = \sum_{i=0}^{N_1} G^{(1)}_{DQ,i} \quad ; \quad G^{(1)}_{ZQ} = \sum_{i=0}^{N_1} G^{(1)}_{ZQ,i} \quad ; \quad \theta = \left(\frac{4\omega_1}{\Omega_Q}\right) \tag{2.26}$$

$$G^{(1)}_{DQ} = \left(\frac{\omega_1}{2}\right)\left\{-\frac{1}{2\times 0!}(\theta) + \frac{1}{4\times 2!}(\theta)^3 - \frac{1}{6\times 4!}(\theta)^5 + \dots\right\} \tag{2.27}$$

$$G^{(1)}_{ZQ} = \Delta + \left(\frac{\omega_1}{2}\right)\sqrt{6}\left\{-\frac{1}{2\times 0!}(\theta) + \frac{1}{4\times 2!}(\theta)^3 - \frac{1}{6\times 4!}(\theta)^5 + \dots\right\} \tag{2.28}$$

In Eq. 2.25, '$G^{(1)}_{DQ}$' denotes the coefficients obtained from the first transformation (denoted by the superscript) corresponding to the double quantum operator and is expressed in-terms of contributions from the various orders (N_1 denotes the desired order, power of λ). In a similar vein, the coefficients corresponding to the ZQ

operator are denoted by $G^{(1)}_{DQ}$. A detailed description of the coefficients illustrating the contributions from various orders is listed in Appendix.E.1 (Table.E.1.1).
To have a consistent description, the initial density operator ($\rho_F(0) = (I_z)_0$) along with the detection operator '$T^{(2)-2}$,' (corresponding to DQ transition) is transformed by the transformation function 'S_1.'

$$\begin{aligned}\tilde{\rho}_F(0) &= e^{i\lambda S_1}\ \rho_F(0)\ e^{-i\lambda S_1} \\ &= R^{(1)}_{Iz}\ C_{(\alpha)}\,(I_z)_0 + R^{(1)}_{SQ}\ S_{(\alpha)}\left\{\left(\hat{SQ}^{(r)}_{AS}\right)_{+1} + \left(\hat{SQ}^{(cr)}_{AS}\right)_{-1}\right\} \qquad (2.29)\\ \tilde{T}^{(2)-2}_F &= e^{i\lambda S_1}\ T^{(2)-2}_F\ e^{-i\lambda S_1} \\ &= e^{2i\omega_0 t_2}\ \Phi_R\left\{P^{(1)}_{DQ}\ C_{(\alpha)}\left(T^{(2)-2}\right)_0 - P^{(1)}_{SQ}\ S_{(\alpha)}\left\{\left(\Phi_1 RF^{-}_{A}\right)_{+1} + \left(\Phi_1 RF^{-}_{B}\right)_{-1}\right\}\right\} \qquad (2.30)\end{aligned}$$

$$\alpha = 2i\ C^{(1)}_{SQ} = \frac{2\omega_1}{\Omega_Q} \quad ; \quad C_{(\alpha)} = \cos(\alpha) \quad ; \quad S_{(\alpha)} = \sin(\alpha) \quad ; \quad \Phi_R = e^{i\phi_r}$$

where, 'ϕ_r' is the phase of the receiver. A detailed description of the 'R' and 'P' coefficients is illustrated in Table. 2.5.

Table 2.5: Coefficients employed in the description of the density operator (Eqs. 2.29 and 2.32) and the detection operator Eq. 2.30

Operator	0 **coherence**	±1 **coherence**	±2 **coherence**
density matrix	$R^{(1)}_{Iz} = 1$	$R^{(1)}_{SQ} = \frac{1}{2}$	$R^{(1)}_{DQ} = 0$
Operator	0 **coherence**	±1 **coherence**	±2 **coherence**
detection operator	0	$P^{(1)}_{SQ} = \frac{1}{2}$	$P^{(1)}_{DQ} = 1$
$\alpha = 2i\ C^{(1)}_{SQ} \quad ; \quad \beta = \left(\sqrt{\frac{3}{2}}\ G^{(1)}_{ZQ} - \ G^{(1)}_{DQ} - \frac{\omega_Q}{2}\right) t_{p1}$ $\theta_{DQ} = 2\ G^{(1)}_{DQ} t_{p1} \quad ; \quad C_{(\alpha)} = \cos(\alpha) \quad ; \quad S_{(\alpha)} = \sin(\alpha)$			

Based on Eqs. 2.29 and 2.30, it may be verified that at time, $t = 0$, the

DQ signal is zero. (i.e., $\left\langle T^{(2)-2}(0)\right\rangle = Tr\left[\tilde{\rho}_F(0).\tilde{T}_F^{(2)-2}\right] = 0$). Subsequently, to induce DQ transitions, the initial density operator (Eq. 2.29) is transformed by the effective pulse Hamiltonian (Eq. 2.25). Employing Eq. 2.31, the density operator during the pulse is evaluated,

$$\tilde{\rho}_F(t_{p1}) = \ exp\left(\frac{-iH_{eff}t_{p1}}{\hbar}\right)\ \tilde{\rho}_F(0)\ exp\left(\frac{iH_{eff}t_{p1}}{\hbar}\right) \tag{2.31}$$

(where, 't_{p1}' denotes the duration of the pulse). To simplify the description and illustrate the development of coherences, the density operator is expressed in terms of the different coherences present in the system.

$$\tilde{\rho}_F(t_{p1}) = \tilde{\rho}_F(t_{p1})_{ZQ} + \tilde{\rho}_F(t_{p1})_{SQ} + \tilde{\rho}_F(t_{p1})_{DQ} \tag{2.32}$$

The Zero-Quantum (ZQ) coherence or the populations is represented by,

$$\tilde{\rho}_F(t_{p1})_{ZQ} = R_{Iz}\ C_{(\alpha)}\ C_{(\theta_{DQ})}\,(I_z)_0 \tag{2.33}$$

The Single-Quantum (SQ) coherence comprises of

$$\tilde{\rho}_F(t_{p1})_{SQ} = R_{SQ}\ S_{(\alpha)}\left\{\left(\hat{SQ}_{AS}^{(cr)}\right)_{-1} e^{i\beta} + \left(\hat{SQ}_{AS}^{(r)}\right)_{+1} e^{-i\beta}\right\} \tag{2.34}$$

where,

$$\theta_{DQ} = 2\ G_{DQ}^{(1)}t_{p1} \quad ; \quad \alpha = 2i\ C_{SQ}^{(1)} \quad ; \quad \beta = \left(\sqrt{\frac{3}{2}}\ G_{ZQ}^{(1)} - \ G_{DQ}^{(1)} - \frac{\omega_Q}{2}\right)t_{p1}$$

The coherences corresponding to the Double-Quantum (DQ) transitions is represented through ,

$$\tilde{\rho}_F(t_{p1})_{DQ} = iR_{Iz}\ C_{(\alpha)}\ S_{(\theta_{DQ})}\left(\hat{D}_{AS}\right)_0 \tag{2.35}$$

As represented above, the coherences corresponding to the ZQ and DQ transitions are expressed in terms of diagonal operators, while, the coherences corresponding to the SQ transitions are represented in terms of off-diagonal operators in the

Floquet framework. Although, from an experimental perspective, DQ transitions cannot be detected through direct means (they need to be reconverted back to detectable SQ(-1) transitions), the DQ excitation is evaluated through the standard procedure illustrated below.

$$\begin{aligned}&\left\langle T^{(2)-2}(t_{p1})\right\rangle = Tr\left[\tilde{\rho}_F(t_{p1}).\tilde{T}_F^{(2)-2}\right]\\&= e^{2i\omega_0 t_2}\ \Phi_1^2\ \Phi_R\left\{-2\ R_{SQ}^{(1)}.P_{SQ}^{(1)}\ \left(S_{(\alpha)}\right)^2\left(e^{i\beta}-e^{-i\beta}\right)+iR_{Iz}^{(1)}.P_{DQ}^{(1)}\ \left(C_{(\alpha)}\right)^2\ S_{(\theta_{DQ})}\right\}\end{aligned} \tag{2.36}$$

Substituting the coefficients in the above equation, the expression for calculating DQ signal reduces to the form

$$\left\langle T^{(2)-2}(t_{p1})\right\rangle = ie^{2i\omega_0 t_2}\ \Phi_1^2\ \Phi_R\left\{(\cos(\alpha))^2\ \sin(\theta_{DQ})-(\sin(\alpha))^2\sin(\beta)\right\} \tag{2.37}$$

To illustrate the importance of the higher-order corrections in the exactness of the effective Hamiltonians, a systematic study incorporating diagonal corrections to second order (i.e. $G_{DQ}^{(1)}=\sum_{i=0}^{2}G_{DQ,i}^{(1)}\quad;\quad G_{ZQ}^{(1)}=\sum_{i=0}^{2}G_{ZQ,i}^{(1)}$), and n^{th} order (i.e. $G_{DQ}^{(1)}=\sum_{i=0}^{N_1}G_{DQ,i}^{(1)}\quad;\quad G_{ZQ}^{(1)}=\sum_{i=0}^{N_1}G_{ZQ,i}^{(1)}$) were performed. A detailed description of coefficients employed in the effective Hamiltonians for the above two cases are given in Appendix.E.1 (Table. E.1.2).

In Figure. 2.4, simulations depicting the efficiency of DQ excitation are plotted as a function of the pulse duration (t_{p1}). In these simulations, the diagonal corrections to second order 'λ^2' are only incorporated (representing Case:I). As depicted, when the magnitude of the quadrupolar frequency (ω_Q) largely exceeds the amplitude of the RF pulse, the analytic simulations are in excellent agreement with those obtained from SIMPSON. In the strong coupling limit, the DQ signal in Eq. 2.37 reduces to the familiar form proposed by Vega and Pines[8,9].

$$\left\langle T^{(2)-2}(t_{p1})\right\rangle = ie^{2i\omega_0 t_2}\ \Phi_1^2\ \Phi_R\left\{\sin\frac{2\omega_1^2 t_p}{\omega_Q}\right\} \tag{2.38}$$

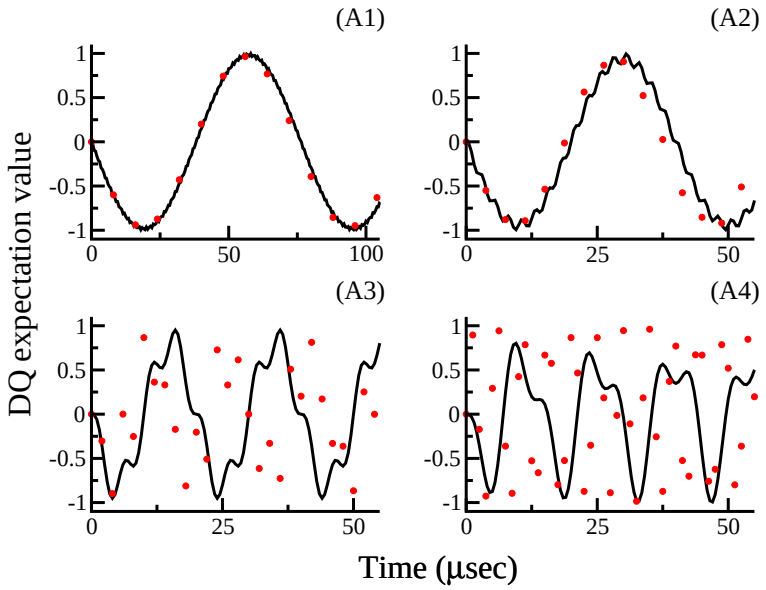

Figure 2.4: Comparison of numerical (black thick line) and analytic simulations (red dots) based on effective Hamiltonians derived from a single transformation comprising of diagonal corrections to order $\lambda^2(N_1 = 2)$. In the simulations depicted, the quadrupole coupling constant ($C_Q = {}^{\omega_Q}/_{3\pi}$) is varied A1) $C_Q = 1$ MHz, A2) $C_Q = 500$ kHz, A3) $C_Q = 200$ kHz, A4) $C_Q = 100$ kHz, employing an excitation pulse of constant RF amplitude, $({}^{\omega_1}/_{2\pi}) = 100$ kHz. The simulations correspond to a single crystal.

However, with decreasing magnitudes of the quadrupolar coupling constant, the discrepancy between the analytic and numerical simulations increases. To address this aspect, effective Hamiltonians comprising of diagonal contributions to (n^{th} order, $N_1 > 2$) were employed in the simulations depicted in Figure. 2.5. As depicted, the discrepancy still prevails in panels A3 and A4, despite the inclusion of diagonal corrections to n^{th} order. Hence, the residual off-diagonal terms ignored from the first transformation could play an important role in the excitation process. Interestingly, the AHT formalism (see Appendix.B) does not provide such a framework in the derivation of effective Hamiltonians.

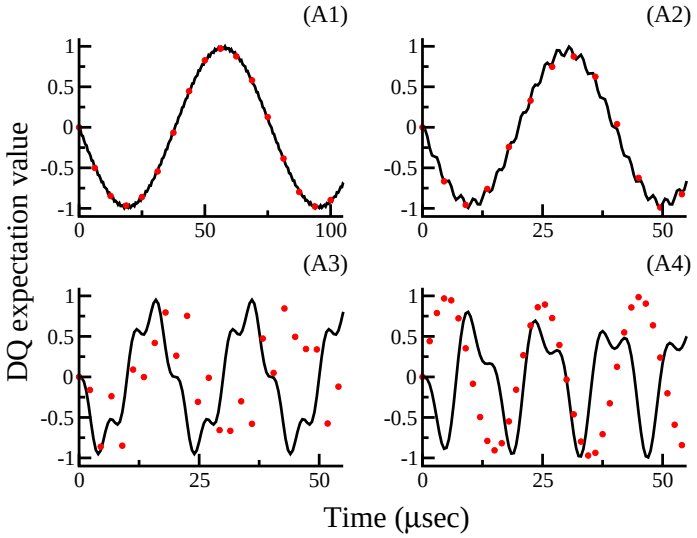

Figure 2.5: Comparison of numerical (black thick line) and analytic simulations (red dots) based on effective Hamiltonians derived from a single transformation comprising of diagonal corrections to n^{th} - order $\lambda^2(N_1 > 2)$. In the simulations depicted, the quadrupole coupling constant ($C_Q = {}^{\omega_Q}/_{3\pi}$) is varied A1) $C_Q = 1$ MHz, A2) $C_Q = 500$ kHz, A3) $C_Q = 200$ kHz, A4) $C_Q = 100$ kHz, employing an excitation pulse of constant RF amplitude, $({}^{\omega_1}/_{2\pi}) = 100$ kHz. The simulations correspond to a single crystal.

II. Effective Hamiltonians from second transformation, 'S_2'

To resolve the discrepancy observed in the analytic simulations, the residual off-diagonal terms neglected in the first transformation were considered in the calculations. As depicted in Table. 2.4, the off-diagonal contributions comprises of the single-quantum (SQ) operators. To fold the above off-diagonal contributions, a second transformation function 'S_2' was employed. A brief description of the procedure employed in the derivation of effective Floquet Hamiltonians from the second transformation 'S_2' is outlined below. The diagonal corrections from the first transformation are included along 'H_0' and the off-diagonal operators $\left(\left(\hat{SQ}\right)_{\pm 1}\right)$ resulting from the first transformation forms the perturbing Hamiltonian.

$$H_0 = \frac{\omega_Q}{2} I_F + \; G^{(1)}_{DQ}\left(\hat{D}_S\right)_0 + G^{(1)}_{ZQ}\left(T^{(2)0}\right)_0 \tag{2.39}$$

$$H_1 = G^{(1)}_{SQ}\left\{\left(\hat{SQ}^{(r)}_{S}\right)_{+1} + \left(\hat{SQ}^{(cr)}_{S}\right)_{-1}\right\} \tag{2.40}$$

$$G^{(1)}_{SQ} = \sum_{i=0}^{N_1} G^{(1)}_{SQ,i} = \left(\frac{\omega_1}{2}\right)\left\{\frac{1}{3\times 1!}(\theta)^2 - \frac{1}{5\times 3!}(\theta)^4 + \frac{1}{7\times 5!}(\theta)^6 - \dots\right\} \tag{2.41}$$

In the above equation, the coefficients '$G^{(1)}_{SQ} = \sum_{i=0}^{N_1} G^{(1)}_{SQ,i}$' denotes the off-diagonal coefficients resulting from the first-transformation and are described in Appendix.E.2 (Table.E.2.1). Depending on the desired level of accuracy, the off-diagonal contributions (denoted by value of N_1) from the first-transformation are incorporated accordingly. Employing the transformation function 'S_2', the off-diagonal contributions from H_1 are folded.

$$S_2 = \; C^{(2)}_{SQ'}\left\{\left(\hat{SQ}^{(r)}_{S}\right)_{+1} - \left(\hat{SQ}^{(cr)}_{S}\right)_{-1}\right\} \tag{2.42}$$

where,

$$C^{(2)}_{SQ'} = -i\left(\frac{G^{(1)}_{SQ}}{G^{(1)}_{DQ} + \sqrt{\frac{3}{2}}\,G^{(1)}_{ZQ} - \frac{\Omega_Q}{2}}\right) \tag{2.43}$$

$$C^{(i+1)}_{SQ} = \sum_{j=1}^{n-1} C^{(j+1)}_{SQ'} \tag{2.44}$$

where 'j' takes values from 1 to '$n-1$', where 'n' is the number of 'S' transformations applied (Here $n = 2$).
A detailed description of the corrections (both diagonal and off-diagonal) emerging from the second transformation are tabulated in Table. 2.6.
Accordingly, following the procedure described in the previous section, the effective Hamiltonians after the second transformation is evaluated and represented by,

$$H_0 = \frac{\omega_Q}{2}I_F + \; G^{(2)}_{DQ}\left(\hat{D}_S\right)_0 + G^{(2)}_{ZQ}\left(T^{(2)0}\right)_0 \tag{2.45}$$

Table 2.6: Description of the higher order (diagonal and off-diagonal) contributions to the effective Hamiltonian (Eq. 2.39) derived from second transformation

n^{th} **order** **Correction**	**Coefficients in the Effective Hamiltonian** $H_{eff} = H_0^{(2)} + H_2^{(2)} + H_4^{(2)} + H_6^{(2)} + \cdots = \frac{\omega_Q}{2} I_F + \left(G_{DQ}^{(1)} + \sum_{i=0}^{N_1} G_{DQ,i}^{(2)}\right)\left(\hat{D}_S\right)_0 + \left(G_{ZQ}^{(1)} + \sum_{i=0}^{N_1} G_{ZQ,i}^{(1)}\right)\left(T^{(2)0}\right)_0$	
	Expression from the 'H_1' term	**Non-zero 'G' Coefficients**
Zero order (λ^0)	$H_0^{(2)} = \frac{\omega_Q}{2} I_F + G_{ZQ}^{(1)}\left(T^{(2)0}\right)_0 + G_{DQ}^{(1)}\left(\hat{D}_S\right)_0$	$\frac{\omega_Q}{2} I_F + G_{ZQ,0}^{(2)}\left(T^{(2)0}\right)_0 + G_{DQ,0}^{(2)}\left(\hat{D}_S\right)_0$
I order (λ^1)	$H_1^{(2)} = 0$	
II order (λ^2)	$H_2^{(2)} = \frac{i}{2\times 0!}[S_2, H_1] = +\left(\frac{1}{2\times 0!}\right)\underbrace{-4i\left(C_{SQ}^{(2)}\, G_{SQ}^{(1)}\right)}_{G_{DQ,A}^{(2)}}\left\{\left(\sqrt{6}\, T^{(2)0}\right)_0 + \left(\hat{D}_S\right)_0\right\}$	$G_{ZQ,2}^{(2)}\left(T^{(2)0}\right)_0 + G_{DQ,2}^{(2)}\left(\hat{D}_S\right)_0$
III order (λ^3)	$H_3^{(2)} = -\frac{1}{3\times 1!}[S_2, [S_2, H_1]] = +\left(\frac{1}{3\times 1!}\right)\underbrace{-4\left(C_{SQ}^{(2)}\, G_{DQ,A}^{(2)}\right)}_{G_{SQ,A}^{(2)}}\left\{\left(\hat{SQ}_S^{(r)}\right)_{+1} + \left(\hat{SQ}_S^{(cr)}\right)_{-1}\right\}$	$G_{SQ,3}^{(2)}\left\{\left(\hat{SQ}_S^{(r)}\right)_{+1} + \left(\hat{SQ}_S^{(cr)}\right)_{-1}\right\}$
IV order (λ^4)	$H_4^{(2)} = -\frac{i}{4\times 2!}[S_2, [S_2, [S_2, H_1]]] = -\left(\frac{1}{4\times 2!}\right)\underbrace{-4i\left(C_{SQ}^{(2)}\, G_{SQ,A}^{(2)}\right)}_{G_{DQ,B}^{(2)}}\left\{\left(\sqrt{6}\, T^{(2)0}\right)_0 + \left(\hat{D}_S\right)_0\right\}$	$G_{ZQ,4}^{(2)}\left(T^{(2)0}\right)_0 + G_{DQ,4}^{(2)}\left(\hat{D}_S\right)_0$
V order (λ^5)	$H_5^{(2)} = \frac{1}{5\times 3!}[S_2, [S_2, [S_2, [S_2, H_1]]]] = -\left(\frac{1}{5\times 3!}\right)\underbrace{-4\left(C_{SQ}^{(2)}\, G_{DQ,B}^{(2)}\right)}_{G_{SQ,B}^{(2)}}\left\{\left(\hat{SQ}_S^{(r)}\right)_{+1} + \left(\hat{SQ}_S^{(cr)}\right)_{-1}\right\}$	$G_{SQ,5}^{(2)}\left\{\left(\hat{SQ}_S^{(r)}\right)_{+1} + \left(\hat{SQ}_S^{(cr)}\right)_{-1}\right\}$
VI order (λ^6)	$H_6^{(2)} = \frac{i}{6\times 4!}[S_2, [S_2, [S_2, [S_2, [S_2, H_1]]]]] = +\left(\frac{1}{6\times 4!}\right)\underbrace{-4i\left(C_{SQ}^{(2)}\, G_{SQ,B}^{(2)}\right)}_{G_{DQ,C}^{(2)}}\left\{\left(\sqrt{6}\, T^{(2)0}\right)_0 + \left(\hat{D}_S\right)_0\right\}$	$G_{ZQ,6}^{(2)}\left(T^{(2)0}\right)_0 + G_{DQ,6}^{(2)}\left(\hat{D}_S\right)_0$
VII order (λ^7)	$H_7^{(2)} = -\frac{1}{7\times 5!}[S_2, [S_2, [S_2, [S_2, [S_2, [S_2, H_1]]]]]] = +\left(\frac{1}{7\times 5!}\right)\underbrace{-4\left(C_{SQ}^{(2)}\, G_{DQ,C}^{(2)}\right)}_{G_{SQ,C}^{(2)}}\left\{\left(\hat{SQ}_S^{(r)}\right)_{+1} + \left(\hat{SQ}_S^{(cr)}\right)_{-1}\right\}$	$G_{SQ,7}^{(2)}\left\{\left(\hat{SQ}_S^{(r)}\right)_{+1} + \left(\hat{SQ}_S^{(cr)}\right)_{-1}\right\}$

$$G^{(2)}_{DQ} = G^{(1)}_{DQ} + \left\{ \frac{1}{2 \times 0!}\, G^{(2)}_{DQ,A} - \frac{1}{4 \times 2!}\, G^{(2)}_{DQ,B} + \frac{1}{6 \times 4!}\, G^{(2)}_{DQ,C} + \dots \right\}$$

$$G^{(2)}_{ZQ} = G^{(1)}_{ZQ} + \sqrt{6} \left\{ \frac{1}{2 \times 0!}\, G^{(2)}_{DQ,A} - \frac{1}{4 \times 2!}\, G^{(2)}_{DQ,B} + \frac{1}{6 \times 4!}\, G^{(2)}_{DQ,C} + \dots \right\}$$

The coefficients '$G^{(2)}_{DQ,A}$', '$G^{(2)}_{DQ,B}$' are described in detail in Table. 2.6. The off-diagonal contributions emerging from the second transformation forms the perturbation for the third transformation.

$$H_1 = G^{(2)}_{SQ} \left\{ \left(\hat{SQ}^{(r)}_{S} \right)_{+1} + \left(\hat{SQ}^{(cr)}_{S} \right)_{-1} \right\} \tag{2.46}$$

where,

$$G^{(2)}_{SQ} = \left\{ \frac{1}{3 \times 1!}\, G^{(2)}_{SQ,A} - \frac{1}{5 \times 3!}\, G^{(2)}_{SQ,B} + \frac{1}{7 \times 5!}\, G^{(2)}_{SQ,C} + \dots \right\}$$

In general, the magnitude of '$G^{(n)}_{SQ}$' coefficients decreases with increasing'n' and its utility is decided by comparisons with the exact numerical simulations. After 'n' transformations the magnitude of '$G^{(n)}_{SQ}$' decreases significantly and the effective Hamiltonian reduces to the form given below,

$$H_{eff} = \frac{\omega_Q}{2} I_F + \; G^{(n)}_{DQ} \left(\hat{D}_S \right)_0 + G^{(n)}_{ZQ} \left(T^{(2)0} \right)_0 \tag{2.47}$$

The final equation depicting the DQ excitation after 'n' transformations is represented by,

$$\left\langle T^{(2)-2}(t_{p1}) \right\rangle = i e^{2i\omega_0 t_2}\; \Phi_1^2\; \Phi_R \left\{ \left(\cos(\alpha) \right)^2\; \sin(\theta_{DQ}) - \left(\sin(\alpha) \right)^2 \sin(\beta) \right\} \tag{2.48}$$

where,

$$\alpha = 2i\ C_{SQ}^{(n)} \quad ; \quad \beta = \left(\sqrt{\frac{3}{2}}\ G_{ZQ}^{(n)} - \ G_{DQ}^{(n)} - \frac{\omega_Q}{2}\right) t_{p1} \quad ; \quad \theta_{DQ} = 2\ G_{DQ}^{(n)} t_{p1}$$

Table 2.7: Definition of coefficients employed in the perturbing Hamiltonians for Case-III and Case-IV

	$G_{SQ}^{(1)}$
Case-III $(N_1 = 2)$	$-\frac{1}{3 \times 1!}\left(\frac{\omega_1}{2}\right)(\theta)^2$
Case-IV $(N_1 > 2)$	$G_{SQ}^{(1)} = -\left(\frac{\omega_1}{2}\right)\left\{\frac{1}{3 \times 1!}(\theta)^2 - \frac{1}{5 \times 3!}(\theta)^4 + \frac{1}{7 \times 5!}(\theta)^6 - ....\right\}$

	$G_{DQ}^{(2)}$	$G_{ZQ}^{(2)}$
Case-III	$\sum_{i=0}^{N_1} G_{DQ,i}^{(1)} + \sum_{j=1}^{2} G_{DQ,j}^{(2)}$	$\sum_{i=0}^{N_1} G_{ZQ,i}^{(1)} + \sum_{j=1}^{2} G_{ZQ,j}^{(2)}$
Case-IV	$\sum_{i=0}^{N_1} G_{DQ,i}^{(1)} + \sum_{j=1}^{N_2} G_{DQ,j}^{(2)}$	$\sum_{i=0}^{N_1} G_{ZQ,i}^{(1)} + \sum_{j=1}^{N_2} G_{ZQ,j}^{(2)}$

$$\theta = \left(\frac{4\omega_1}{\Omega_Q}\right) \quad ; \quad C_{(\theta)} = \cos(\theta) \quad ; \quad S_{(\theta)} = \sin(\theta)$$

To illustrate the importance of the second transformation, diagonal corrections to second order (Figure. 2.6) and 'n^{th}' order (Figure. 2.7) were included in the analytic simulations. As depicted, in contrast to the simulations in panel A3 (Figure. 2.4 and 2.5) resulting from the first transformation, the agreement is much better in the analytic simulations resulting from the second transformation. Nevertheless, the simulations presented in panel A4 highlights the inadequacy of the corrections deduced from the present approach.

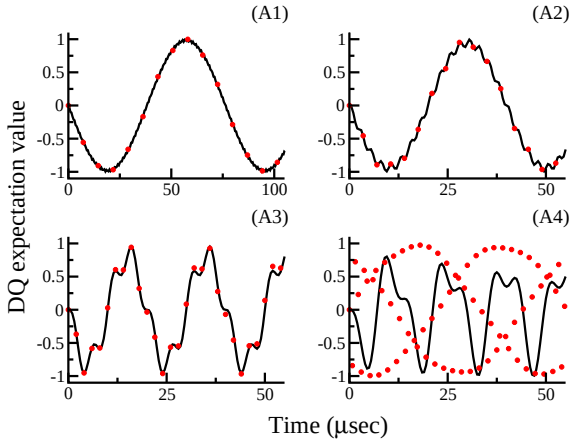

Figure 2.6: Comparison of numerical (black thick line) and analytic simulations (red dots) based on effective Hamiltonians derived from the second transformation. The off-diagonal contributions to order λ^n from the first transformation ($N_1 > 2$) and diagonal corrections to order λ^2 from the second transformation ($N_2 = 2$) were included in the derivation of the effective Hamiltonians. In the simulations depicted, the quadrupole coupling constant ($C_Q = {}^{\omega_Q}/_{3\pi}$) is varied A1) $C_Q = 1$ MHz, A2) $C_Q = 500$ kHz, A3) $C_Q = 200$ kHz, A4) $C_Q = 100$ kHz, employing an excitation pulse of constant RF amplitude, $({}^{\omega_1}/_{2\pi}) = 100$ kHz. The simulations correspond to a single crystal.

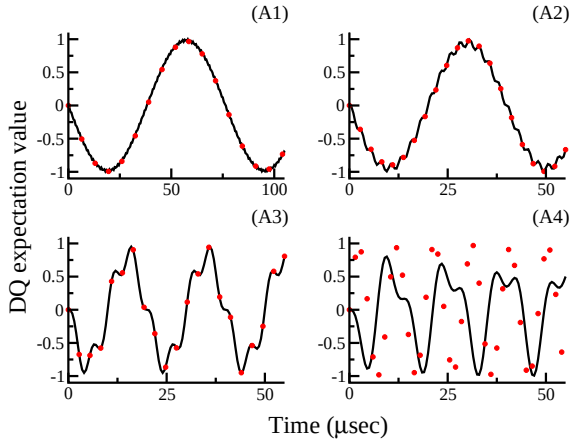

Figure 2.7: Comparison of numerical (black thick line) and analytic simulations (red dots) based on effective Hamiltonians derived from the second transformation. The off-diagonal contributions to order λ^n from the first transformation ($N_1 > 2$) and diagonal corrections to order λ^n from the second transformation ($N_2 > 2$) were included in the derivation of the effective Hamiltonians. In the simulations depicted, the quadrupole coupling constant ($C_Q = {}^{\omega_Q}/_{3\pi}$) is varied A1) $C_Q = 1$ MHz, A2) $C_Q = 500$ kHz, A3) $C_Q = 200$ kHz, A4) $C_Q = 100$ kHz, employing an excitation pulse of constant RF amplitude, $({}^{\omega_1}/_{2\pi}) = 100$ kHz. The simulations correspond to a single crystal.

To explain the observed discrepancy (in Panel A4) in the analytic simulations, an alternate method is proposed in the following section.

Regime-II: Weak coupling ($\omega_Q \approx \omega_1$)

In cases where the amplitude of the RF pulse exceeds the magnitude of the quadrupolar frequency ($\omega_Q = {}^3/_2 C_Q$), the Hamiltonian in the zeeman interaction frame (Eq. 2.49) is tilted such that the RF part of the Hamiltonian is quantized along the z-axis (employing the transformation function 'U_2' ($U_2 = e^{i\pi/2 I_y}$)).

$$\tilde{H} = -i\hbar\omega_1 \left\{ \Phi_1 T^{(1)1} - \Phi_1^{-1} T^{(1)-1} \right\} - \frac{\hbar\Omega_Q}{\sqrt{6}} T^{(2)0} \tag{2.49}$$

$$\begin{aligned} \tilde{\tilde{H}} =& U_2 \; \tilde{H} \; U_2^{-1} \\ =& -\hbar\omega_1 I_z + \left(\frac{\hbar\Omega_Q}{2\sqrt{6}}\right) T^{(2)0} - \left(\frac{\hbar\Omega_Q}{4}\right) \left(\Phi_1^2 T^{(2)2} + \Phi_1^{-2} T^{(2)-2} \right) \end{aligned} \tag{2.50}$$

To further simplify the description, the above Hamiltonian is transformed into the RF interaction frame defined by the transformation function, 'U_3' ($U_3 = exp\left(-i\omega_1 t I_z\right)$)

$$\begin{aligned} \tilde{\tilde{H}}(t) =& U_3 \; \tilde{\tilde{H}} \; U_3^{-1} \\ =& \left(\frac{\hbar\Omega_Q}{2\sqrt{6}}\right) T^{(2)0} - \left(\frac{\hbar\Omega_Q}{4}\right) \left(\Phi_1^2 T^{(2)2} e^{-2i\omega_1 t} + \Phi_1^{-2} T^{(2)-2} e^{2i\omega_1 t} \right) \end{aligned} \tag{2.51}$$

As illustrated above, the Hamiltonian in the tilted RF interaction frame is periodically time-dependent. In accord with the description presented in the previous section, the above time-dependent Hamiltonian is transformed into a time-independent Floquet Hamiltonian.

$$H_F = \omega_1 I_F + \left(\frac{\hbar\Omega_Q}{2\sqrt{6}}\right) \left(T^{(2)0}\right)_0 - \left(\frac{\hbar\Omega_Q}{4}\right) \left\{ \left(\Phi_1^2 T^{(2)2}\right)_2 + \left(\Phi_1^{-2} T^{(2)-2}\right)_{-2} \right\} \tag{2.52}$$

To facilitate analytic description, the above untransformed Floquet Hamiltonian is re-expressed as a sum of zero-order (H_0) and perturbing Hamiltonian (H_1).

$$H_0 = \omega_1 I_F + \left(\frac{\hbar\Omega_Q}{2\sqrt{6}}\right)\left(T^{(2)0}\right)_0$$
$$H_1 = -\left(\frac{\hbar\Omega_Q}{4}\right)\left\{\left(\Phi_1^2 T^{(2)2}\right)_2 + \left(\Phi_1^{-2} T^{(2)-2}\right)_{-2}\right\} \tag{2.53}$$

Employing the transformation function, 'S_1'.

$$S_1 = C_{DR}^{(1)}\left\{\left(\Phi_1^2 T^{(2)2}\right)_2 - \left(\Phi_1^{-2} T^{(2)-2}\right)_{-2}\right\} \tag{2.54}$$

where,

$$C_{DR}^{(1)} = -i\left(\frac{\Omega_Q}{8\omega_1}\right) \tag{2.55}$$

the off-diagonal contributions due to H_1 are folded resulting in an effective Hamiltonian. The higher order corrections to the effective Floquet Hamiltonian are derived using the relations described in Table. 2.9.

$$H_{eff} = H_0^{(1)} = \omega_1 I_F + \frac{\Omega_Q}{2\sqrt{6}}\left(T^{(2)0}\right)_0 \tag{2.56}$$

A detailed derivation of the commutator relations involving the transformation 'S_1' and 'H_1' to various orders of 'λ' is tabulated in Table 2.9. As illustrated (in Table. 2.9), the diagonal corrections mainly comprise of ZQ operators $\left(\left(T^{(k)0}\right)_0 ; k = 1\right)$, while, the off-diagonal contributions are represented through the DQ operators $\left(\left(T^{(2)\pm 2}\right)_{\pm 2}\right)$. A pedagogical description analogous to Regime-I is presented below to explicate the role of the higher-order contributions in the excitation process.

I. Effective Hamiltonians from first transformation, 'S_1'

Based on Table. 2.9, let the effective Hamiltonian (comprising of diagonal correc-

tions only) describing the excitation process in Regime-II be represented by,

$$\begin{aligned} H_{eff} &= e^{i\lambda S_1}\ H_F\ e^{-i\lambda S_1} \\ &= \omega_1 I_F + G_{1R}^{(1)}\,(I_z)_0 + \ G_{2R}^{(1)}\left(T^{(2)0}\right)_0 \end{aligned} \tag{2.57}$$

$$G_{1R}^{(1)} = \sum_{i=1}^{N_1} G_{1R,i}^{(1)} \quad ; \quad G_{2R}^{(1)} = G_{2R,0}^{(1)} = \frac{\Omega_Q}{2\sqrt{6}} \quad ; \tag{2.58}$$

$$G_{1R}^{(1)} = \left(\frac{-\Omega_Q}{4}\right)\left\{+\frac{1}{2\times 0!}\,(\xi) - \frac{1}{4\times 2!}\,(\xi)^3 + \frac{1}{6\times 4!}\,(\xi)^5 + \ldots\right\} \tag{2.59}$$

and N_1 represents the order of the corrections from the first transformation.
To have a consistent description, the initial density operator ($\rho_F(0) = (I_z)_0$) along with the detection operator '$T^{(2)-2}$', is transformed by the transformation function 'S_1.' The transformed initial density operator and the detection operators are illustrated below.

$$\begin{aligned} \tilde{\rho}_F(0) &= e^{i\lambda S_1}\ \rho_F(0)\ e^{-i\lambda S_1} \\ &= R_{SQA}^{(1)}\ C_{(\xi_{DR})}\left\{\left(\Phi_1 T^{(1)1}\right)_{+1} - \left(\Phi_1^{-1} T^{(1)-1}\right)_{-1}\right\} \\ &\quad + R_{SQB}^{(1)}\ S_{(\xi_{DR})}\left\{\left(\Phi_1 T^{(2)1}\right)_{+1} - \left(\Phi_1^{-1} T^{(2)-1}\right)_{-1}\right\} \end{aligned} \tag{2.60}$$

$$\begin{aligned} \tilde{T}_F^{(2)-2} &= e^{i\lambda S_1}\ T_F^{(2)-2}\ e^{-i\lambda S_1} \\ &= e^{2i\omega_0 t_2}\ \Phi_R\left\{P_{ZQ}^{(1)}\left(T^{(2)0}\right)_0 - P_{SQA}^{(1)}\ S_{(\xi_{DR})}\left(\Phi_1^3 T^{(1)1}\right)_{+1}\right. \\ &\quad \left. + P_{SQB}^{(1)}\ C_{(\xi_{DR})}\left(\Phi_1 T^{(2)-1}\right)_{-1}\right\} \end{aligned} \tag{2.61}$$

where,

$$\xi_{DR} = i\ C_{DR}^{(1)} = \quad ; \quad C_{(\xi)} = \cos(\xi) \quad ; \quad S_{(\xi)} = \sin(\xi)$$

A detailed description of the 'R' and 'P' coefficients employed in the initial density operator and detection operator is illustrated in Table. 2.8.
Employing the effective pulse Hamiltonian (Eq. 2.57), the density operator during

the pulse is evaluated,

$$\tilde{\rho}_F(t_{p1}) = \; exp\left(\frac{-iH_{eff}t_{p1}}{\hbar}\right)\; \tilde{\rho}_F(0)\; exp\left(\frac{iH_{eff}t_{p1}}{\hbar}\right) \tag{2.62}$$

Table 2.8: Coefficients employed in the description of the density operator (Eqs. 2.60 and 2.64) and the detection operator Eq. 2.61

Operator	0 **coherence**	± 1 **coherence**
density matrix	0	$R^{(1)}_{SQA} = -i$ $R^{(1)}_{SQB} = 1$
Operator	0 **coherence**	± 1 **coherence**
detection operator	$P^{(1)}_{ZQ} = \dfrac{\sqrt{3}}{2\sqrt{2}}$	$P^{(1)}_{SQA} = i$ $P^{(1)}_{SQB} = 1$
$\xi_{DR} = i\; C^{(1)}_{DR} \quad ; \quad \xi_{1R} = \left(G^{(1)}_{1R} - \omega_1\right) t_{p1} \quad ; \quad \xi_{2R} = \sqrt{\dfrac{3}{2}}\; G^{(1)}_{2R}\; t_{p1}$ $; \quad C_{(\xi)} = \cos(\xi) \quad ; \quad S_{(\xi)} = \sin(\xi)$		

To simplify the description and illustrate the development of coherences, the density operator is re-expressed in terms of the different coherences present in the system. The Single-Quantum (SQ) coherence comprises of

$$\begin{aligned}
\tilde{\rho}_F(t_{p1}) = & \left\{R^{(1)}_{SQA}\; C_{(\xi_{DR})}\; C_{(\xi_{2R})} - R^{(1)}_{SQB}\; S_{(\xi_{DR})}\; S_{(\xi_{2R})}\right\} e^{-i\xi_{1R}} \left(\Phi_1 T^{(1)1}\right)_{+1} \\
& - \left\{R^{(1)}_{SQA}\; C_{(\xi_{DR})}\; C_{(\xi_{2R})} + R^{(1)}_{SQB}\; S_{(\xi_{DR})}\; S_{(\xi_{2R})}\right\} e^{i\xi_{1R}} \left(\Phi_1^{-1} T^{(1)-1}\right)_{-1} \\
& + \left\{R^{(1)}_{SQA}\; C_{(\xi_{DR})}\; C_{(\xi_{2R})} + R^{(1)}_{SQB}\; S_{(\xi_{DR})}\; S_{(\xi_{2R})}\right\} e^{-i\xi_{1R}} \left(\Phi_1 T^{(2)1}\right)_{+1} \\
& + \left\{R^{(1)}_{SQA}\; C_{(\xi_{DR})}\; C_{(\xi_{2R})} - R^{(1)}_{SQB}\; S_{(\xi_{DR})}\; S_{(\xi_{2R})}\right\} e^{i\xi_{1R}} \left(\Phi_1^{-1} T^{(2)-1}\right)_{-1}
\end{aligned} \tag{2.63}$$

Here, $\xi_{DR} = i\; C^{(1)}_{DR} \quad ; \quad \xi_{1R} = \left(G^{(1)}_{1R} - \omega_1\right) t_{p1} \quad ; \quad \xi_{2R} = \sqrt{\dfrac{3}{2}}\; G^{(1)}_{2R}\; t_{p1}$

Table 2.9: Description of the higher order (diagonal and off-diagonal) contributions to the effective Hamiltonian (Eq. 2.56) derived from first transformation

n^{th} **order** **Correction**	**Coefficients in the Effective Hamiltonian** $H_{eff} = H_0^{(1)} + H_2^{(1)} + H_4^{(1)} + H_6^{(1)} + \cdots = \omega_1 I_F + \sum_{i=1}^{N_1} G_{1R,i}^{(1)} (I_z)_0 + \; G_{2R}^{(1)} \left(T^{(2)0}\right)_0$	
	Expression from the 'H_1' term	**Non-zero 'G' Coefficients**
Zero order (λ^0)	$H_0^{(1)} = \frac{\omega_Q}{2} I_F + \frac{\Omega_Q}{2\sqrt{6}} \left(T^{(2)0}\right)_0$	$\frac{\omega_Q}{2} I_F + G_{2R,0}^{(1)} \left(T^{(2)0}\right)_0$
I order (λ^1)	$H_1^{(1)} = 0$	
II order (λ^2)	$H_2^{(1)} = \frac{i}{2 \times 0!}[S_1, H_1] = -\frac{1}{2 \times 0!} \left(\frac{\Omega_Q}{4}\right) (\xi) (I_z)_0$	$G_{1R,2}^{(1)} (I_z)_0$
III order (λ^3)	$H_3^{(1)} = -\frac{1}{3 \times 1!}[S_1, [S_1, H_1]] = +\frac{1}{3 \times 1!} \left(\frac{\Omega_Q}{4}\right) (\xi)^2 \left\{ \left(\Phi_1^2 T^{(2)2}\right)_{+2} + \left(\Phi_1^{-2} T^{(2)-2}\right)_{-2} \right\}$	$G_{DR,3}^{(1)} \left\{ \left(\Phi_1^2 T^{(2)2}\right)_{+2} + \left(\Phi_1^{-2} T^{(2)-2}\right)_{-2} \right\}$
IV order (λ^4)	$H_4^{(1)} = -\frac{i}{4 \times 2!}[S_1, [S_1, [S_1, H_1]]] = \frac{1}{4 \times 2!} \left(\frac{\Omega_Q}{4}\right) (\xi)^3 (I_z)_0$	$G_{1R,4}^{(1)} (I_z)_0$
V order (λ^5)	$H_5^{(1)} = \frac{1}{5 \times 3!}[S_1, [S_1, [S_1, [S_1, H_1]]]] = -\frac{1}{5 \times 3!} \left(\frac{\Omega_Q}{4}\right) (\xi)^4 \left\{ \left(\Phi_1^2 T^{(2)2}\right)_{+2} + \left(\Phi_1^{-2} T^{(2)-2}\right)_{-2} \right\}$	$G_{DR,5}^{(1)} \left\{ \left(\Phi_1^2 T^{(2)2}\right)_{+2} + \left(\Phi_1^{-2} T^{(2)-2}\right)_{-2} \right\}$
VI order (λ^6)	$H_6^{(1)} = \frac{i}{6 \times 4!}[S_1, [S_1, [S_1, [S_1, [S_1, H_1]]]]] = -\frac{1}{6 \times 4!} \left(\frac{\Omega_Q}{4}\right) (\xi)^5 (I_z)_0$	$G_{1R,6}^{(1)} (I_z)_0$
VII order (λ^7)	$H_7^{(1)} = -\frac{1}{7 \times 5!}[S_1, [S_1, [S_1, [S_1, [S_1, [S_1, H_1]]]]]] = +\frac{1}{7 \times 5!} \left(\frac{\Omega_Q}{4}\right) (\xi)^6 \left\{ \left(\Phi_1^2 T^{(2)2}\right)_{+2} + \left(\Phi_1^{-2} T^{(2)-2}\right)_{-2} \right\}$	$G_{DR,7}^{(1)} \left\{ \left(\Phi_1^2 T^{(2)2}\right)_{+2} + \left(\Phi_1^{-2} T^{(2)-2}\right)_{-2} \right\}$
$\xi = \left(\frac{\Omega_Q}{4\omega_1}\right) \quad ; \quad C_{(\xi)} = \cos(\xi)$		

$$\tilde{\rho}_F(t_{p1}) = \left\{ R^{(1)}_{SQA}\ C_{(\xi_{DR})}\ C_{(\xi_{2R})} - R^{(1)}_{SQB}\ S_{(\xi_{DR})}\ S_{(\xi_{2R})} \right\} \left(e^{-i\xi_{1R}} \left(\Phi_1 T^{(1)1} \right)_{+1} + e^{i\xi_{1R}} \left(\Phi_1^{-1} T^{(2)-1} \right)_{-1} \right) + \left\{ R^{(1)}_{SQA}\ C_{(\xi_{DR})}\ C_{(\xi_{2R})} + R^{(1)}_{SQB}\ S_{(\xi_{DR})}\ S_{(\xi_{2R})} \right\} \left(e^{-i\xi_{1R}} \left(\Phi_1 T^{(2)1} \right)_{+1} - e^{i\xi_{1R}} \left(\Phi_1^{-1} T^{(1)-1} \right)_{-1} \right) \quad (2.64)$$

The coherences corresponding to the SQ transition are represented in terms of off-diagonal operators in the Floquet framework. Subsequently, the DQ excitation is evaluated through the standard procedure illustrated below.

$$\begin{aligned} \left\langle T^{(2)-2}(t_{p1}) \right\rangle &= Tr \left[\tilde{\rho}_F(t_{p1}).\tilde{T}^{(2)-2}_F \right] \\ &= -e^{2i\omega_0 t_2} \left(\Phi_R \Phi_1^2 \right) \left\{ P^{(1)}_{SQB}\ C_{(\xi_{DR})}\ \left\{ R^{(1)}_{SQA}\ C_{(\xi_{DR})}\ C_{(\xi_{2R})} + R^{(1)}_{SQB}\ S_{(\xi_{DR})}\ S_{(\xi_{2R})} \right\} \right. \\ &\quad \left. e^{-i\xi_{1R}} + P^{(1)}_{SQA}\ S_{(\xi_{DR})}\ \left\{ R^{(1)}_{SQA}\ C_{(\xi_{DR})}\ C_{(\xi_{2R})} + R^{(1)}_{SQB}\ S_{(\xi_{DR})}\ S_{(\xi_{2R})} \right\} e^{i\xi_{1R}} \right\} \end{aligned} \quad (2.65)$$

Substituting the coefficients in the above equation, the DQ excitation (expectation value) reduces to

$$\left\langle T^{(2)-2}(t_{p1}) \right\rangle = ie^{2i\omega_0 t_2}\ \Phi_1^2\ \Phi_R \left\{ \sin\left(\xi_{2R}\right) \cos\left(\xi_{1R}\right) + \cos\left(\xi_{2R}\right) \sin\left(\xi_{1R}\right) \sin\left(2\xi_{DR}\right) \right\} \quad (2.66)$$

To substantiate the validity of the effective Hamiltonian derived in regime-II, analytic simulations incorporating diagonal corrections to second order (i.e. $G^{(1)}_{1R} = \sum_{i=0}^{2} G^{(1)}_{1R,i}$; $G^{(1)}_{2R} = \sum_{i=0}^{2} G^{(1)}_{2R,i}$, Figure. 2.8) and n^{th} order (i.e. $G^{(1)}_{1R} = \sum_{i=0}^{N_1} G^{(1)}_{1R,i}$; $G^{(1)}_{2R} = \sum_{i=0}^{N_1} G^{(1)}_{2R,i}$, Figure. 2.9) resulting from the first transformation were compared with the exact numerical simulations. As depicted (see panel A3) the analytic simulations in Regime-II are in good agreement when compared to those depicted in Regime-I. The minor deviations that are observed in panel A4 are improved further with a second transformation (see Appendix.D).

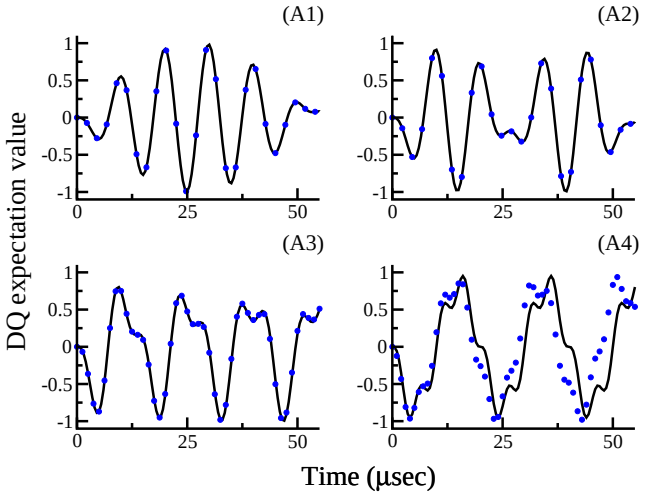

Figure 2.8: Comparison of numerical (black thick line) and analytic simulations (blue dots) based on effective Hamiltonians derived from a single transformation (in Regime-II) comprising of diagonal corrections to order λ^2 ($N_1 = 2$). In the simulations depicted, the quadrupole coupling constant ($C_Q = {}^{\omega_Q}/_{3\pi}$) is varied A1) $C_Q = 25$ kHz, A2) $C_Q = 50$ kHz, A3) $C_Q = 100$ kHz, A4) $C_Q = 200$ kHz, employing an excitation pulse of constant RF amplitude, $({}^{\omega_1}/_{2\pi}) = 100$ kHz. The simulations correspond to a single crystal.

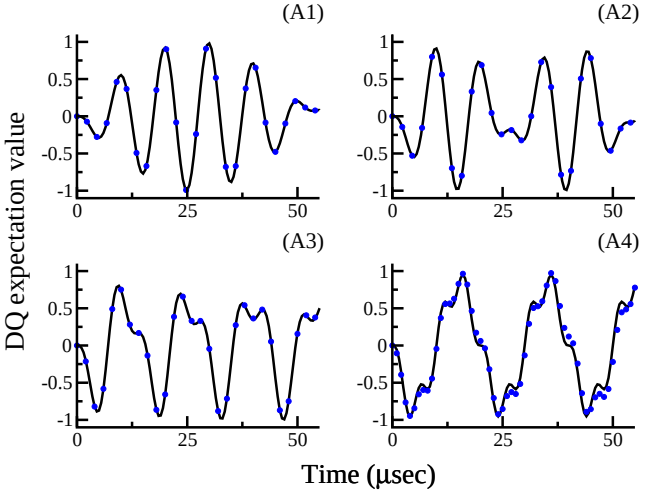

Figure 2.9: Comparison of numerical (black thick line) and analytic simulations (blue dots) based on effective Hamiltonians derived from a single transformation (in Regime-II) comprising of diagonal corrections to order λ^n ($N_1 > 2$). In the simulations depicted, the quadrupole coupling constant ($C_Q = {}^{\omega_Q}/_{3\pi}$) is varied A1) $C_Q = 25$ kHz, A2) $C_Q = 50$ kHz, A3) $C_Q = 100$ kHz, A4) $C_Q = 200$ kHz, employing an excitation pulse of constant RF amplitude, $({}^{\omega_1}/_{2\pi}) = 100$ kHz. The simulations correspond to a single crystal.

Hence, depending on the relative magnitudes of the quadrupolar frequency w.r.t. the amplitude of the pulse, the classification of regimes plays an important role in the accuracy of the derived effective Hamiltonians.

2.2.2 DQ excitation in Powder Sample

To further validate the effective Hamiltonian approach, the calculations described in the previous sections is extended to describe the excitation in a powder sample. In the past, analytic description of the excitation process have remained hindered due to the distribution of the quadrupolar coupling constant (spatial anisotropy) present in a powder sample. As described in the Appendix.B, the higher order corrections derived from the Magnus formula result in erroneous results and are ill-suited to describe the excitation in a powder sample. As an alternative, each crystallite could in principle be associated with a specific interaction frame corresponding to a particular quadrupolar frequency, $\omega_Q^{(\alpha\beta\gamma)}$. However, simultaneous obeservation of all the crystallites at a given single instant of time is untenable within the AHT framework.

To this end, the Floquet formalism presented in this thesis is tailor made to describe the excitation process both in isotropic and anisotropic solid samples. As described in the previous sections, the quadrupolar interaction represented through 'Ω_Q' becomes equal to '$\omega_Q^{(\alpha\beta\gamma)}$' for a powder sample$\left(\Omega_Q = \omega_Q^{(\alpha\beta\gamma)}\right)$. Consequently, an anisotropic offset term 'Δ',($\Delta = \Omega_Q - \omega_Q^{(\alpha\beta\gamma)}$) (corresponding to the $T^{(2)0}$ operator) is present along the zero-order Hamiltonian.

To investigate the exactness of the proposed effective Floquet Hamiltonians, DQ excitation in a powder sample is investigated in the following section. For comparative purposes, the quadrupolar parameters (say C_Q = 1MHz, 500kHz, 200kHz and 100kHz) employed in the single crystal calculations were retained in the powder simulations (Figure. 2.10-2.13). In the simulations presented below (Figure. 2.10-2.13), the effective Hamiltonians based on Regime-I were employed to simulate the DQ excitation in powder samples.

The analytic simulations depicted in panels A1 and A2 are based on effective Hamiltonians derived from the first transformation (A1, diagonal corrections to

II order, A2 diagonal corrections to n^{th} order), while, effective Hamiltonians from the second transformation were employed In panels A3 (diagonal corrections to II order) and A4 (diagonal corrections to n^{th} order).

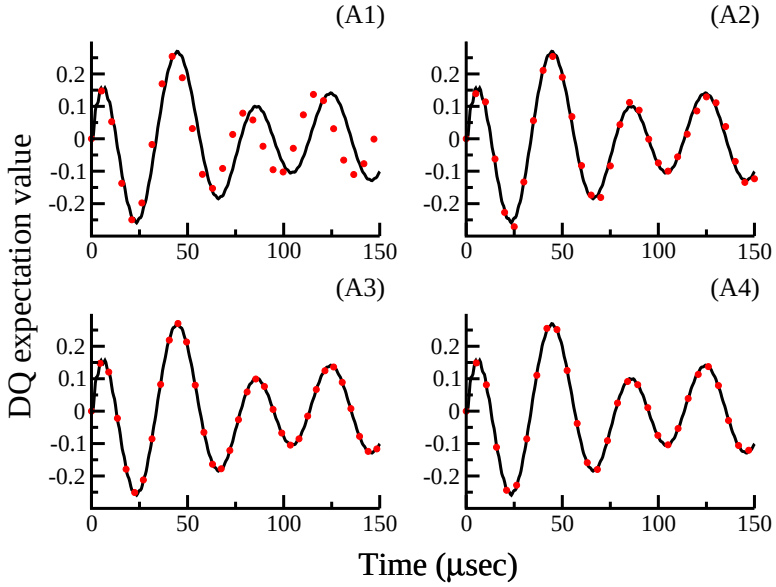

Figure 2.10: Comparison of numerical (black thick line) and analytic simulations (red dots) based on effective Hamiltonians derived from Regime-I corresponding to the quadrupole coupling constant ($C_Q = {}^{\omega_Q}/_{3\pi}$), $C_Q = 1$ MHz and RF amplitude, $({}^{\omega_1}/_{2\pi}) = 100$ kHz. In panel A1 (II order diagonal contributions from S_1), A2 (n^{th} order from S_1), A3 (II order from S_2 and n^{th} order diagonal contributions from S_1), A4 (n^{th} order from S_1 and S_2). The powder simulations were performed using a crystal file having 28656 orientations (α, β).

As depicted in Figures. 2.10 ($C_Q = 1$ MHz) and 2.11 ($C_Q = 500$ kHz) , a minimum of two transformations (S_1 and S_2) seem mandatory to improve the exactness of the proposed effective Hamiltonians. This is in stark contrast to the single crystal simulations based on similar parameters. In a typical powder sample, the effective quadrupolar frequency ($\omega_Q^{(\alpha\beta\gamma)}$) is always lower than or equal to the isotropic quadrupolar frequency (ω_Q). Hence, there could be crystallites with quadrupolar frequencies lower than the RF amplitude.

Consequently, the effective Hamiltonians based on Regime-I might not be strictly

valid for similar calculations (parameter) in powder samples. This could also be inferred from the simulations presented in Figures. 2.12 and 2.13.

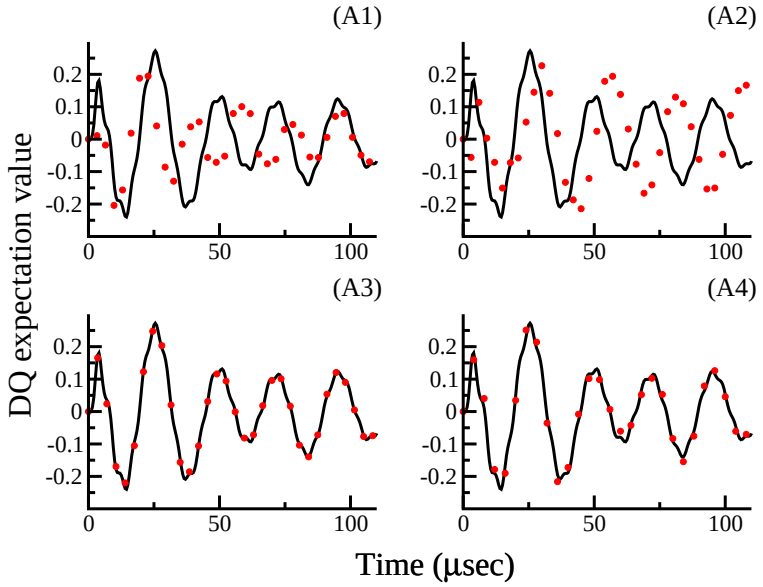

Figure 2.11: Comparison of numerical (black thick line) and analytic simulations (red dots) based on effective Hamiltonians derived from Regime-I corresponding to the quadrupole coupling constant ($C_Q = {}^{\omega_Q}/_{3\pi}$), $C_Q = 500$ kHz and RF amplitude, $({}^{\omega_1}/_{2\pi}) = 100$ kHz. In panel A1 (II order diagonal contributions from S_1), A2 (n^{th} order from S_1), A3 (II order from S_2 and n^{th} order diagonal contributions from S_1), A4 (n^{th} order from S_1 and S_2). The powder simulations were performed using a crystal file having 28656 orientations (α, β).

As depicted in Figures. 2.12 and 2.13, the effective Hamiltonians (Eq. D.13) in Regime-I do not accurately describe the excitation in powder sample.

To address this discrepancy, effective Hamiltonians based on Regime-II were employed to simulate the DQ excitation for quadrupolar parameters corresponding to $C_Q = 200$ kHz and 100 kHz. As depicted in Figures. 2.14 and 2.15, the analytic simulations based on effective Hamiltonians in Regime-II yield results in better agreement with exact numerical methods. Hence in a powder sample there exists no clear demarcation between two regimes.

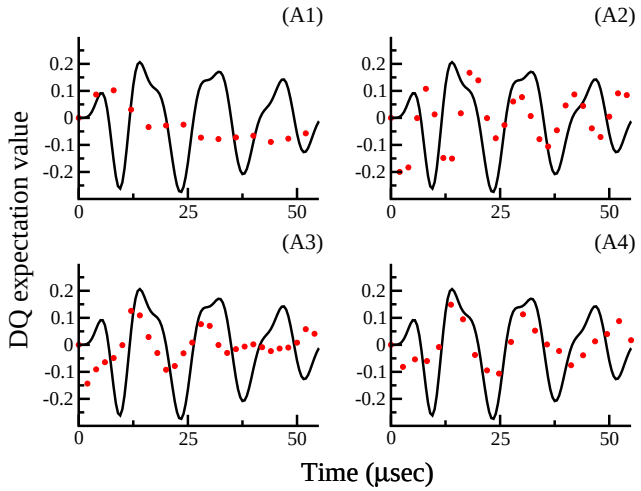

Figure 2.12: Comparison of numerical (black thick line) and analytic simulations (red dots) based on effective Hamiltonians derived from Regime-I corresponding to the quadrupole coupling constant ($C_Q = {}^{\omega_Q}/_{3\pi}$), C_Q = 200 kHz and RF amplitude, $({}^{\omega_1}/_{2\pi})$ = 100 kHz. In panel A1 (II order diagonal contributions from S_1), A2 (n^{th} order from S_1), A3 (II order from S_2 and n^{th} order diagonal contributions from S_1), A4 (n^{th} order from S_1 and S_2). The powder simulations were performed using a crystal file having 28656 orientations (α, β).

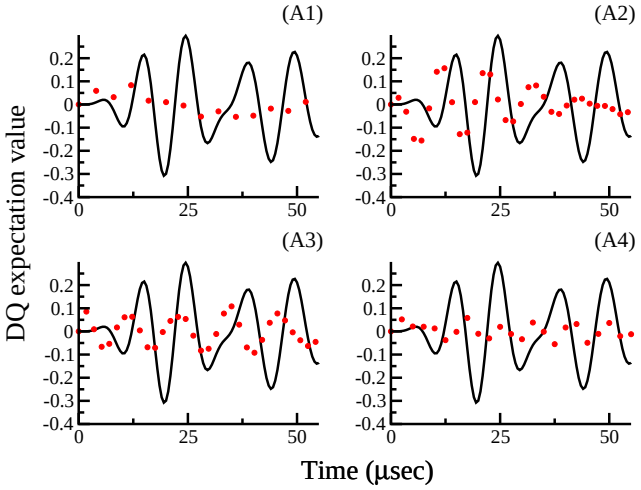

Figure 2.13: Comparison of numerical (black thick line) and analytic simulations (red dots) based on effective Hamiltonians derived from Regime-I corresponding to the quadrupole coupling constant ($C_Q = {}^{\omega_Q}/_{3\pi}$), C_Q = 100 kHz and RF amplitude, $({}^{\omega_1}/_{2\pi})$ = 100 kHz. In panel A1 (II order diagonal contributions from S_1), A2 (n^{th} order from S_1), A3 (II order from S_2 and n^{th} order diagonal contributions from S_1), A4 (n^{th} order from S_1 and S_2). The powder simulations were performed using a crystal file having 28656 orientations (α, β).

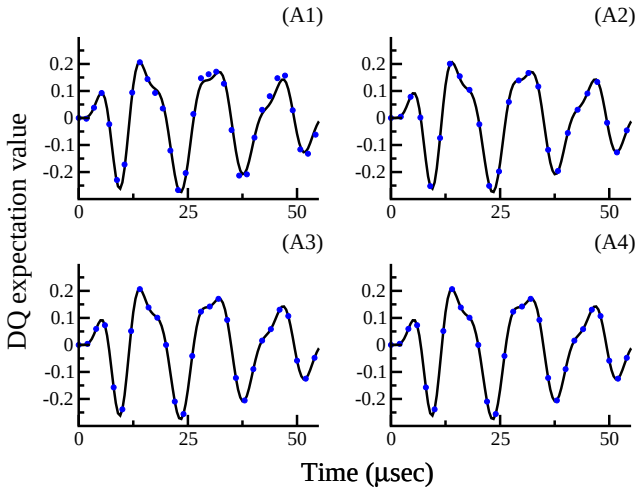

Figure 2.14: Comparison of numerical (black thick line) and analytic simulations (blue dots) based on effective Hamiltonians derived from Regime-II corresponding to the quadrupole coupling constant ($C_Q = {}^{\omega_Q}/_{3\pi}$), C_Q = 200 kHz and RF amplitude, $({}^{\omega_1}/_{2\pi})$ = 100 kHz. In panel A1 (II order diagonal contributions from S_1), A2 (n^{th} order from S_1), A3 (II order from S_2 and n^{th} order diagonal contributions from S_1), A4 (n^{th} order from S_1 and S_2). The powder simulations were performed using a crystal file having 28656 orientations (α, β).

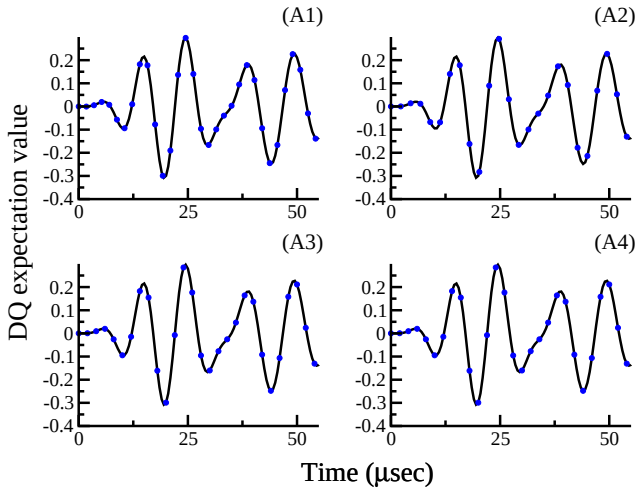

Figure 2.15: Comparison of numerical (black thick line) and analytic simulations (blue dots) based on effective Hamiltonians derived from Regime-II corresponding to the quadrupole coupling constant ($C_Q = {}^{\omega_Q}/_{3\pi}$), C_Q = 100 kHz and RF amplitude, $({}^{\omega_1}/_{2\pi})$ = 100 kHz. In panel A1 (II order diagonal contributions from S_1), A2 (n^{th} order from S_1), A3 (II order from S_2 and n^{th} order diagonal contributions from S_1), A4 (n^{th} order from S_1 and S_2). The powder simulations were performed using a crystal file having 28656 orientations (α, β).

To have a consistent description with exact numerical methods, we propose the '*Hybrid method*'[48] wherein the effective Hamiltonian derived from the two regimes are employed to describe the excitation profile. For crystallite orientations with '$\left|\omega_Q^{(\alpha\beta\gamma)}\right| < |\omega_1|$', the effective Hamiltonians based on Regime-II are suited (Eq. D.15, D.16), while for '$\left|\omega_Q^{(\alpha\beta\gamma)}\right| \geq |\omega_1|$', effective Hamiltonians based in Regime-I are suitable (Eq. D.13, D.14) in simulating the DQ excitation profile in the powder sample. A schematic depiction of the excitation profiles in the powder sample are illustrated in Figures. 2.16 - 2.18.

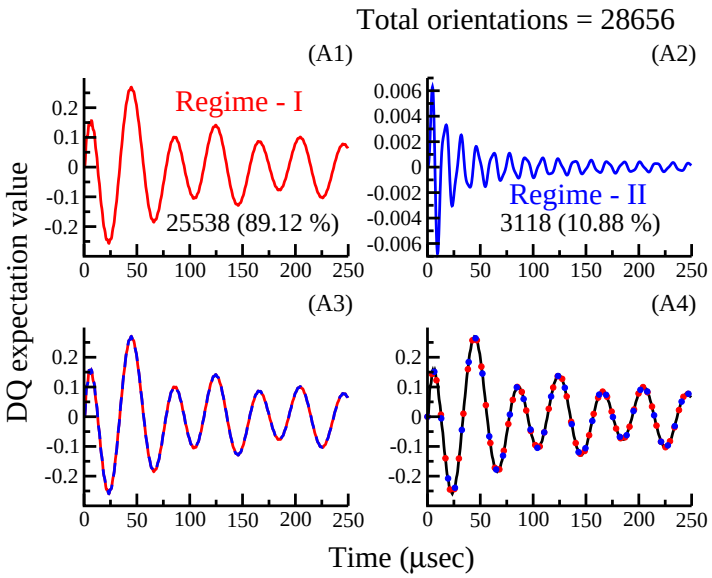

Figure 2.16: Comparison of numerical (black thick line) and analytic simulations (blue dots) based on effective Hamiltonians derived from both regimes corresponding to the quadrupole coupling constant ($C_Q = {}^{\omega_Q}/_{3\pi}$), $C_Q = 1$ MHz and RF amplitude, $({}^{\omega_1}/_{2\pi}) = 100$ kHz. The analytic simulations emerging from the effective Hamiltonians derived from Regime-I only (see panel A1), Regime-II only (see panel A2), hybrid method (combination of Regime-I and Regime-II) (in panel A3) are depicted. In panel A4, the analytic simulations from the hybrid method (combination of Regime-I (red) and Regime-II (blue)) are compared with exact numerical simulations (black line). The choice of Regime-I and Regime-II is purely dependent on the magnitude of $\omega_Q^{(\alpha\beta\gamma)}$ relative to the RF amplitude. When $\left|\omega_Q^{(\alpha\beta\gamma)}\right| < |\omega_1|$, Regime-II is employed, $\left|\omega_Q^{(\alpha\beta\gamma)}\right| \geq |\omega_1|$, Regime-I is employed. The powder simulations were performed using a crystal file having 28656 orientations (α, β).

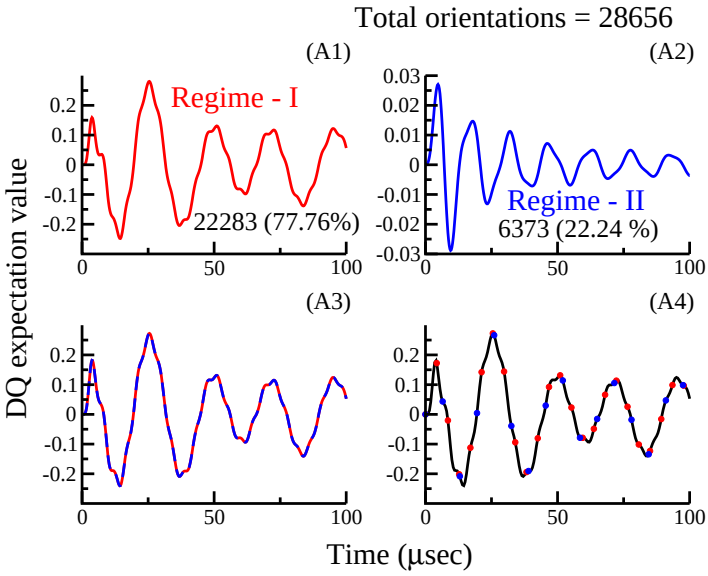

Figure 2.17: Comparison of numerical (black thick line) and analytic simulations (blue dots) based on effective Hamiltonians derived from both regimes corresponding to the quadrupole coupling constant ($C_Q = {}^{\omega_Q}/_{3\pi}$), $C_Q = 500$ kHz and RF amplitude, $({}^{\omega_1}/_{2\pi}) = 100$ kHz. The analytic simulations emerging from the effective Hamiltonians derived from Regime-I only (see panel A1), Regime-II only (see panel A2), hybrid method (combination of Regime-I and Regime-II) (in panel A3) are depicted. In panel A4, the analytic simulations from the hybrid method (combination of Regime-I (red) and Regime-II (blue)) are compared with exact numerical simulations (black line). The choice of Regime-I and Regime-II is purely dependent on the magnitude of $\omega_Q^{(\alpha\beta\gamma)}$ relative to the RF amplitude. When $\left|\omega_Q^{(\alpha\beta\gamma)}\right| < |\omega_1|$, Regime-II is employed, $\left|\omega_Q^{(\alpha\beta\gamma)}\right| \geq |\omega_1|$, Regime-I is employed. The powder simulations were performed using a crystal file having 28656 orientations (α, β).

In Figure. 2.16, the excitation profile for powder sample corresponding to the analytic simulations emerging from the effective Hamiltonians derived from the procedure described in Regime-I (panel A1) and Regime-II (panel A2) are depicted, respectively. In panel A3, analytic simulations emerging from the proposed hybrid method is depicted. In panel A4, the analytic simulations from the proposed hybrid method are compared with SIMPSON simulations. The powder simulations were performed using a crystal file comprising of 28656 orientations (α, β). Of the 28656 orientations that were employed, 89% of the crystallites had their

'$\left|\omega_Q^{(\alpha\beta\gamma)}\right| \geq |\omega_1|$' and 11% had '$\left|\omega_Q^{(\alpha\beta\gamma)}\right| < |\omega_1|$'. As depicted, the analytic simulations emerging from the proposed 'hybrid method' are in excellent agreement with the numerical simulations. To further substantiate this approach, additional set of simulations corresponding to ($C_Q = 500$ kHz; $C_Q = 200$ kHz) are depicted in Figures. 2.17, 2.18, respectively. As the magnitude of the quadrupolar coupling constant decreases, the percentage of crystallites that adhere to the dynamics governed by Regime-II should in-principle increase owing to the scaling introduced by the powder averaging. This reasoning is justified in the analytic simulations depicted in panel-A2 of Figures. 2.17 and 2.18.

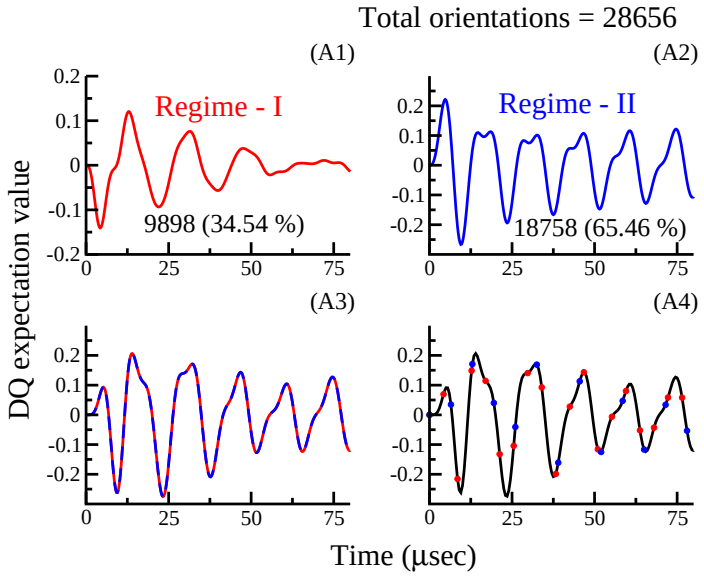

Figure 2.18: Comparison of numerical (black thick line) and analytic simulations (blue dots) based on effective Hamiltonians derived from both regimes corresponding to the quadrupole coupling constant ($C_Q = {}^{\omega_Q}/_{3\pi}$), $C_Q = 200$ kHz and RF amplitude, $({}^{\omega_1}/_{2\pi}) = 100$ kHz. The analytic simulations emerging from the effective Hamiltonians derived from Regime-I only (see panel A1), Regime-II only (see panel A2), hybrid method (combination of Regime-I and Regime-II) (in panel A3) are depicted. In panel A4, the analytic simulations from the hybrid method (combination of Regime-I (red) and Regime-II (blue)) are compared with exact numerical simulations (black line). The choice of Regime-I and Regime-II is purely dependent on the magnitude of $\omega_Q^{(\alpha\beta\gamma)}$ relative to the RF amplitude. When $\left|\omega_Q^{(\alpha\beta\gamma)}\right| < |\omega_1|$, Regime-II is employed, $\left|\omega_Q^{(\alpha\beta\gamma)}\right| \geq |\omega_1|$, Regime-I is employed. The powder simulations were performed using a crystal file having 28656 orientations (α, β).

Hence, the choice of the interaction frames (whether it is quadrupolar interaction frame or tilted RF interaction frame) play an important role in the exactness of the derived effective Hamiltonians. In contrast to the AHT framework, the effective Floquet Hamiltonian approach presents a unified description of the time-evolution for all the crystallites present in a powder sample. The proposed hybrid method is extremely beneficial in the analytic description of powder samples and could be employed to build theoretical models for quantifying experimental data involving powder samples.

References

[1] A. J. Vega, in *Quadrupolar Nuclei in Solids, eMagRes (eds R. K. Harris and R. L. Wasylishen)*, Am. Can. Soc., 2010.

[2] S. Cavadini, S. Antonijevic, A. Lupulescu and G. Bodenhausen, *Chem. Phys. Chem.*, 2007, **8**, 1363–1374.

[3] S. Cavadini, S. Antonijevic, A. Lupulescu and G. Bodenhausen, *J. Magn. Reson.*, 2006, **182**, 168 – 172.

[4] V. Vitzthum, M. A. Caporini, S. Ulzega and G. Bodenhausen, *J. Magn. Reson.*, 2011, **212**, 234 – 239.

[5] M. Shen, J. Trébosc, L. A. ODell, O. Lafon, F. Pourpoint, B. Hu, Q. Chen and J.-P. Amoureux, *J. Magn. Reson.*, 2015, **258**, 86 – 95.

[6] M. K. Pandey and Y. Nishiyama, *J. Magn. Reson.*, 2015, **258**, 96 – 101.

[7] N. Chandrakumar, *Spin-1 Nmr*, Springer Science & Business Media, 2012, vol. 34.

[8] S. Vega, T. W. Shattuck and A. Pines, *Phys. Rev. Lett.*, 1976, **37**, 43–46.

[9] S. Vega and A. Pines, *J. Chem. Phys.*, 1977, **66**, 5624–5644.

[10] S. Vega, *J. Chem. Phys.*, 1978, **68**, 5518–5527.

[11] A. Abragam, *The Principles of Nuclear Magnetism*, Clarendon Press, 1961.

[12] M. Bak, J. T. Rasmussen and N. C. Nielsen, *J. Magn. Reson.*, 2000, **147**, 296 – 330.

[13] H.-T. Kwak, S. Prasad, Z. Yao, P. Grandinetti, J. Sachleben and L. Emsley, *J. Magn. Reson.*, 2001, **150**, 71 – 80.

[14] N. C. Nielsen, H. Bildsøe and H. J. Jakobsen, *Chem. Phys. Lett.*, 1992, **191**, 205 – 212.

[15] D. Srivastava, R. Venkata SubbaRao and R. Ramachandran, *Phys. Chem. Chem. Phys.*, 2013, **15**, 6699–6713.

[16] R. Ramesh and M. S. Krishnan, *J. Chem. Phys.*, 2001, **114**, 5967–5973.

[17] D. Srivastava and R. Ramachandran, *RSC Adv.*, 2013, **3**, 25231–25236.

[18] R. Venkata SubbaRao, D. Srivastava and R. Ramachandran, *Phys. Chem. Chem. Phys.*, 2013, **15**, 2081–2104.

[19] V. Aliev, M.R. Aleksanyan, *Optika Spectroscopia*, 1968, **24**, 520.

[20] V. Aliev, M.R. Aleksanyan, *Optika Spectroscopia*, 1968, **24**, 695.

[21] D. Papousek and M. Aliev, *Molecular Vibrational-rotational Spectra: Theory and Applications of High Resolution Infrared*, Elsevier, 1982.

[22] J. H. Van Vleck, *Phys. Rev.*, 1929, **33**, 467–506.

[23] R. Ramachandran and R. G. Griffin, *J. Chem. Phys.*, 2005, **122**, 164502.

[24] R. Ramachandran and R. G. Griffin, *J. Chem. Phys.*, 2006, **125**, 044510.

[25] M. K. Pandey, Z. Qadri and R. Ramachandran, *J. Chem. Phys.*, 2013, **138**, 114108.

[26] M. K. Pandey and R. Ramachandran, *Mol. Phys.*, 2011, **109**, 1545–1565.

[27] H. A. Buckmaster, R. Chatterjee and Y. H. Shing, *Phys. Stat. Sol. (a)*, 1972, **13**, 9–50.

[28] B. Sanctuary and T. Halstead, *Adv. Magn. Opt. Reson.*, Academic Press, 1990, vol. 15, pp. 79 – 161.

[29] B. C. Sanctuary, *J. Chem. Phys.*, 1976, **64**, 4352–4361.

[30] G. Bowden and W. Hutchison, *J. Magn. Reson.*, 1986, **70**, 361 – 367.

[31] G. Bowden and W. Hutchison, *J. Magn. Reson.*, 1987, **72**, 61 – 74.

[32] G. Bowden, W. Hutchison and J. Khachan, *J. Magn. Reson.*, 1986, **67**, 415 – 437.

[33] G. Bowden and W. Hutchison, *J. Magn. Reson.*, 1986, **67**, 403 – 414.

[34] J. A. R. Coope, R. F. Snider and F. R. McCourt, *J. Chem. Phys.*, 1965, **43**, 2269–2275.

[35] J. A. R. Coope and R. F. Snider, *J. Math. Phys.*, 1970, **11**, 1003–1017.

[36] J. A. R. Coope, *J. Math. Phys.*, 1970, **11**, 1591–1612.

[37] M. Mehring, *Principles of High Resolution NMR in solids*, (Springer, Berlin, 1983), Berlin, 2nd edn, 1999.

[38] B. L. Silver, *Irreducible tensor methods: an introduction for chemists*, Academic Press, 2013, vol. 36.

[39] G. Vinay and R. Ramachandran, *Annu. Rep. NMR Spectrosc.*, Academic Press, 2016, vol. 89, pp. 123 – 184.

[40] U. Haeberlen and J. S. Waugh, *Phys. Rev.*, 1968, **175**, 453–467.

[41] M. M. Maricq, *Phys. Rev. B*, 1982, **25**, 6622–6632.

[42] J. S. Waugh, in *eMagRes (eds R. K. Harris and R. L. Wasylishen)*, American Cancer Society, 2007.

[43] G. Floquet, *Ann. Sci. Ecole Norm. Sup.*, 1883, **12**, 47–88.

[44] J. H. Shirley, *Phys. Rev.*, 1965, **138**, B979–B987.

[45] I. Scholz, J. D. van Beek and M. Ernst, *Solid State Nucl. Magn. Reson.*, 2010, **37**, 39 – 59.

[46] M. Leskes, P. Madhu and S. Vega, *Prog. Nucl. Magn. Reson. Spectrosc.*, 2010, **57**, 345380.

[47] C. P. Slichter, *Principles of Magnetic Resonance*, Springer Science & Business Media, 2013, vol. 1.

[48] V. Ganapathy and R. Ramachandran, *The Journal of Chemical Physics*, 2017, **147**, 144202.

Appendix

A Matrix Representation of Operators and Commutator Relations

A.1 Definition of Tensor Operators for Spin $I = 1$

Table A.1.1: **The Basis Tensor Operators for spin I=1**

Zero Coherence Operators	
$T^{(0)0} = \frac{1}{\sqrt{3}} \begin{bmatrix} 1 & 0 & 0 \\ 0 & 1 & 0 \\ 0 & 0 & 1 \end{bmatrix}$	$T^{(1)0} = \frac{i}{\sqrt{2}} \begin{bmatrix} 1 & 0 & 0 \\ 0 & 0 & 0 \\ 0 & 0 & -1 \end{bmatrix}$
$T^{(2)0} = \frac{-1}{\sqrt{6}} \begin{bmatrix} 1 & 0 & 0 \\ 0 & -2 & 0 \\ 0 & 0 & 1 \end{bmatrix}$	
$+1$ Coherence Operators	
$T^{(1)1} = \frac{-i}{\sqrt{2}} \begin{bmatrix} 0 & 1 & 0 \\ 0 & 0 & 1 \\ 0 & 0 & 0 \end{bmatrix}$	$T^{(2)1} = \frac{1}{\sqrt{2}} \begin{bmatrix} 0 & 1 & 0 \\ 0 & 0 & -1 \\ 0 & 0 & 0 \end{bmatrix}$
$RF_A^+ = \sqrt{2} \begin{bmatrix} 0 & 1 & 0 \\ 0 & 0 & 0 \\ 0 & 0 & 0 \end{bmatrix}$	$RF_B^+ = \sqrt{2} \begin{bmatrix} 0 & 0 & 0 \\ 0 & 0 & 1 \\ 0 & 0 & 0 \end{bmatrix}$
-1 Coherence Operators	
$T^{(1)-1} = \frac{i}{\sqrt{2}} \begin{bmatrix} 0 & 0 & 0 \\ 1 & 0 & 0 \\ 0 & 1 & 0 \end{bmatrix}$	$T^{(2)-1} = \frac{-1}{\sqrt{2}} \begin{bmatrix} 0 & 0 & 0 \\ 1 & 0 & 0 \\ 0 & -1 & 0 \end{bmatrix}$
$RF_A^- = \sqrt{2} \begin{bmatrix} 0 & 0 & 0 \\ 1 & 0 & 0 \\ 0 & 0 & 0 \end{bmatrix}$	$RF_B^- = \sqrt{2} \begin{bmatrix} 0 & 0 & 0 \\ 0 & 0 & 0 \\ 0 & 1 & 0 \end{bmatrix}$
± 2 Coherence Operators	
$T^{(2)2} = D^+ = \begin{bmatrix} 0 & 0 & -1 \\ 0 & 0 & 0 \\ 0 & 0 & 0 \end{bmatrix}$	$T^{(2)-2} = D^- = \begin{bmatrix} 0 & 0 & 0 \\ 0 & 0 & 0 \\ -1 & 0 & 0 \end{bmatrix}$

A.2 Commutation Relations for Spin $I = 1$

1. $\left[\left(\Phi^{-1} RF_A^- + \Phi RF_B^+\right), I_z\right] = \left(\Phi^{-1} RF_A^- - \Phi RF_B^+\right)$

2. $[\left(\Phi^{-1}RF_A^- - \Phi RF_B^+\right), I_z] = \left(\Phi^{-1}RF_A^- + \Phi RF_B^+\right)$
3. $[\left(\Phi RF_A^+ + \Phi^{-1}RF_B^-\right), I_z] = -\left(\Phi RF_A^+ - \Phi^{-1}RF_B^-\right)$
4. $[\left(\Phi RF_A^+ - \Phi^{-1}RF_B^-\right), I_z] = -\left(\Phi RF_A^+ + \Phi^{-1}RF_B^-\right)$

5. $[\left(\Phi^{-1}RF_A^- + \Phi RF_B^+\right), T^{(2)0}] = -\sqrt{\frac{3}{2}}\left(\Phi^{-1}RF_A^- + \Phi RF_B^+\right)$
6. $[\left(\Phi^{-1}RF_A^- - \Phi RF_B^+\right), T^{(2)0}] = -\sqrt{\frac{3}{2}}\left(\Phi^{-1}RF_A^- - \Phi RF_B^+\right)$
7. $[\left(\Phi RF_A^+ + \Phi^{-1}RF_B^-\right), T^{(2)0}] = \sqrt{\frac{3}{2}}\left(\Phi RF_A^+ + \Phi^{-1}RF_B^-\right)$
8. $[\left(\Phi RF_A^+ - \Phi^{-1}RF_B^-\right), T^{(2)0}] = \sqrt{\frac{3}{2}}\left(\Phi RF_A^+ - \Phi^{-1}RF_B^-\right)$

9. $[\left(\Phi^{-1}RF_A^- + \Phi RF_B^+\right), \left(\Phi^2\ T^{(2)2} + \Phi^{-2}\ T^{(2)-2}\right)] = -\left(\Phi^{-1}RF_A^- + \Phi RF_B^+\right)$
10. $[\left(\Phi^{-1}RF_A^- - \Phi RF_B^+\right), \left(\Phi^2\ T^{(2)2} + \Phi^{-2}\ T^{(2)-2}\right)] = \left(\Phi^{-1}RF_A^- - \Phi RF_B^+\right)$
11. $[\left(\Phi RF_A^+ + \Phi^{-1}RF_B^-\right), \left(\Phi^2\ T^{(2)2} + \Phi^{-2}\ T^{(2)-2}\right)] = \left(\Phi RF_A^+ + \Phi^{-1}RF_B^-\right)$
12. $[\left(\Phi RF_A^+ - \Phi^{-1}RF_B^-\right), \left(\Phi^2\ T^{(2)2} + \Phi^{-2}\ T^{(2)-2}\right)] = -\left(\Phi RF_A^+ - \Phi^{-1}RF_B^-\right)$

13. $[\left(\Phi^{-1}RF_A^- + \Phi RF_B^+\right), \left(\Phi^2\ T^{(2)2} - \Phi^{-2}\ T^{(2)-2}\right)] = \left(\Phi^{-1}RF_A^- + \Phi RF_B^+\right)$
14. $[\left(\Phi^{-1}RF_A^- - \Phi RF_B^+\right), \left(\Phi^2\ T^{(2)2} - \Phi^{-2}\ T^{(2)-2}\right)] = -\left(\Phi^{-1}RF_A^- - \Phi RF_B^+\right)$
15. $[\left(\Phi RF_A^+ + \Phi^{-1}RF_B^-\right), \left(\Phi^2\ T^{(2)2} - \Phi^{-2}\ T^{(2)-2}\right)] = -\left(\Phi RF_A^+ + \Phi^{-1}RF_B^-\right)$
16. $[\left(\Phi RF_A^+ - \Phi^{-1}RF_B^-\right), \left(\Phi^2\ T^{(2)2} - \Phi^{-2}\ T^{(2)-2}\right)] = \left(\Phi RF_A^+ - \Phi^{-1}RF_B^-\right)$

17. $[\left(\Phi^{-1}RF_A^- + \Phi RF_B^+\right), \left(T^{(2)2}\right)] = -\Phi^{-1}RF_B^+$
18. $[\left(\Phi^{-1}RF_A^- - \Phi RF_B^+\right), \left(T^{(2)2}\right)] = -\Phi^{-1}RF_B^+$
19. $[\left(\Phi RF_A^+ + \Phi^{-1}RF_B^-\right), \left(T^{(2)2}\right)] = \Phi^{-1}RF_A^+$

20. $[\left(\Phi RF_A^+ - \Phi^{-1}RF_B^-\right), \left(T^{(2)2}\right)] = -\Phi^{-1}RF_A^+$

21. $[\left(\Phi^{-1}RF_A^- + \Phi RF_B^+\right), \left(T^{(2)-2}\right)] = -\Phi RF_A^-$
22. $[\left(\Phi^{-1}RF_A^- - \Phi RF_B^+\right), \left(T^{(2)-2}\right)] = \Phi RF_A^-$
23. $[\left(\Phi RF_A^+ + \Phi^{-1}RF_B^-\right), \left(T^{(2)-2}\right)] = \Phi RF_B^-$
24. $[\left(\Phi RF_A^+ - \Phi^{-1}RF_B^-\right), \left(T^{(2)-2}\right)] = \Phi RF_B^-$

25. $[\left(\Phi^{-1}RF_A^- + \Phi RF_B^+\right), \left(\Phi^{-1}RF_B^+\right)] = 0$
26. $[\left(\Phi^{-1}RF_A^- - \Phi RF_B^+\right), \left(\Phi^{-1}RF_B^+\right)] = 0$
27. $[\left(\Phi RF_A^+ + \Phi^{-1}RF_B^-\right), \left(\Phi^{-1}RF_B^+\right)] = -2T^{(2)2} + \sqrt{2}\Phi^{-2}\left(iT^{(1)0} - \sqrt{3}T^{(2)0}\right)$
28. $[\left(\Phi RF_A^+ - \Phi^{-1}RF_B^-\right), \left(\Phi^{-1}RF_B^+\right)] = -2T^{(2)2} - \sqrt{2}\Phi^{-2}\left(iT^{(1)0} - \sqrt{3}T^{(2)0}\right)$

29. $[\left(\Phi^{-1}RF_A^- + \Phi RF_B^+\right), \left(\Phi^{-1}RF_A^+\right)] = 2T^{(2)2} + \sqrt{2}\Phi^{-2}\left(iT^{(1)0} + \sqrt{3}T^{(2)0}\right)$
30. $[\left(\Phi^{-1}RF_A^- - \Phi RF_B^+\right), \left(\Phi^{-1}RF_A^+\right)] = -2T^{(2)2} + \sqrt{2}\Phi^{-2}\left(iT^{(1)0} + \sqrt{3}T^{(2)0}\right)$
31. $[\left(\Phi RF_A^+ + \Phi^{-1}RF_B^-\right), \left(\Phi^{-1}RF_A^+\right)] = 0$
32. $[\left(\Phi RF_A^+ - \Phi^{-1}RF_B^-\right), \left(\Phi^{-1}RF_A^+\right)] = 0$

33. $[\left(\Phi^{-1}RF_A^- + \Phi RF_B^+\right), \left(\Phi RF_A^-\right)] = 0$
34. $[\left(\Phi^{-1}RF_A^- - \Phi RF_B^+\right), \left(\Phi RF_A^-\right)] = 0$
35. $[\left(\Phi RF_A^+ + \Phi^{-1}RF_B^-\right), \left(\Phi RF_A^-\right)] = -2T^{(2)-2} - \sqrt{2}\Phi^{2}\left(iT^{(1)0} + \sqrt{3}T^{(2)0}\right)$
36. $[\left(\Phi RF_A^+ - \Phi^{-1}RF_B^-\right), \left(\Phi RF_A^-\right)] = -2T^{(2)-2} - \sqrt{2}\Phi^{2}\left(iT^{(1)0} + \sqrt{3}T^{(2)0}\right)$

37. $[\left(\Phi^{-1}RF_A^- + \Phi RF_B^+\right), \left(\Phi RF_B^-\right)] = 2T^{(2)-2} - \sqrt{2}\Phi^{2}\left(iT^{(1)0} - \sqrt{3}T^{(2)0}\right)$

38. $[\left(\Phi^{-1}RF_A^- - \Phi RF_B^+\right), \left(\Phi RF_B^-\right)] = 2T^{(2)-2} + \sqrt{2}\Phi^2\left(iT^{(1)0} - \sqrt{3}T^{(2)0}\right)$
39. $[\left(\Phi RF_A^+ + \Phi^{-1}RF_B^-\right), \left(\Phi RF_B^-\right)] = 0$
40. $[\left(\Phi RF_A^+ - \Phi^{-1}RF_B^-\right), \left(\Phi RF_B^-\right)] = 0$

41. $[\left(\Phi^{-1}RF_A^- + \Phi RF_B^+\right), \left(\Phi^{-1}RF_A^- + \Phi RF_B^+\right)] = 0$
42. $[\left(\Phi^{-1}RF_A^- - \Phi RF_B^+\right), \left(\Phi^{-1}RF_A^- + \Phi RF_B^+\right)] = 0$
43. $[\left(\Phi RF_A^+ + \Phi^{-1}RF_B^-\right), \left(\Phi^{-1}RF_A^- + \Phi RF_B^+\right)] = -2\left(\sqrt{6}\ T^{(2)0} + \left(\hat{D}_S\right)\right)$
44. $[\left(\Phi RF_A^+ - \Phi^{-1}RF_B^-\right), \left(\Phi^{-1}RF_A^- + \Phi RF_B^+\right)] = 2\left(I_z - \left(\hat{D}_{AS}\right)\right)$

45. $[\left(\Phi^{-1}RF_A^- + \Phi RF_B^+\right), \left(\Phi^{-1}RF_A^- - \Phi RF_B^+\right)] = 0$
46. $[\left(\Phi^{-1}RF_A^- - \Phi RF_B^+\right), \left(\Phi^{-1}RF_A^- - \Phi RF_B^+\right)] = 0$
47. $[\left(\Phi RF_A^+ + \Phi^{-1}RF_B^-\right), \left(\Phi^{-1}RF_A^- - \Phi RF_B^+\right)] = 2\left(I_z + \left(\hat{D}_{AS}\right)\right)$
48. $[\left(\Phi RF_A^+ - \Phi^{-1}RF_B^-\right), \left(\Phi^{-1}RF_A^- - \Phi RF_B^+\right)] = -2\left(\sqrt{6}\ T^{(2)0} - \left(\hat{D}_S\right)\right)$

49. $[\left(\Phi^{-1}RF_A^- + \Phi RF_B^+\right), \left(\Phi RF_A^+ + \Phi^{-1}RF_B^-\right)] = 2\left(\sqrt{6}\ T^{(2)0} + \left(\hat{D}_S\right)\right)$
50. $[\left(\Phi^{-1}RF_A^- - \Phi RF_B^+\right), \left(\Phi RF_A^+ + \Phi^{-1}RF_B^-\right)] = -2\left(I_z + \left(\hat{D}_{AS}\right)\right)$
51. $[\left(\Phi RF_A^+ + \Phi^{-1}RF_B^-\right), \left(\Phi RF_A^+ + \Phi^{-1}RF_B^-\right)] = 0$
52. $[\left(\Phi RF_A^+ - \Phi^{-1}RF_B^-\right), \left(\Phi RF_A^+ + \Phi^{-1}RF_B^-\right)] = 0$

53. $[\left(\Phi^{-1}RF_A^- + \Phi RF_B^+\right), \left(\Phi RF_A^+ - \Phi^{-1}RF_B^-\right)] = -2\left(I_z - \left(\hat{D}_{AS}\right)\right)$
54. $[\left(\Phi^{-1}RF_A^- - \Phi RF_B^+\right), \left(\Phi RF_A^+ - \Phi^{-1}RF_B^-\right)] = 2\left(\sqrt{6}\ T^{(2)0} - \left(\hat{D}_S\right)\right)$
55. $[\left(\Phi RF_A^+ + \Phi^{-1}RF_B^-\right), \left(\Phi RF_A^+ - \Phi^{-1}RF_B^-\right)] = 0$
56. $[\left(\Phi RF_A^+ - \Phi^{-1}RF_B^-\right), \left(\Phi RF_A^+ - \Phi^{-1}RF_B^-\right)] = 0$

B Derivation of Effective Hamiltonians based on Average Hamiltonian Theory

To describe the effects of the pulse, the Hamiltonian employed in the Zeeman-quadrupolar interaction frame is employed.

$$\begin{aligned}\tilde{\tilde{H}}(t) &= \Delta T^{(2)0} \\ &- \frac{\omega_1}{2}\left\{\left(\Phi_1 R F_A^+ + \Phi_1^{-1} R F_B^-\right) e^{\left(i\omega_Q t/2\right)} + \left(\Phi_1^{-1} R F_A^- + \Phi_1 R F_B^+\right) e^{-\left(i\omega_Q t/2\right)}\right\}\end{aligned} \tag{B.1}$$

As described, the Hamiltonian in the Zeeman-quadrupolar frame is periodic with time period '$\tau_c = \frac{2\pi}{\left(\omega_Q/2\right)}$'. Employing the Magnus formula, a time-averaged effective Hamiltonian is derived to describe the excitation process.
To first order, the correction is evaluated using

$$H^{(1)} = \frac{1}{t_c}\int_0^{t_c} \tilde{\tilde{H}}(t)dt \tag{B.2}$$

In the case of single crystal

$$H^{(1)} = 0$$

while, for a powder sample

$$H^{(1)} = \Delta T^{(2)0}$$

The second order correction to the effective Hamiltonian is derived using Eq. B.3

$$H^{(2)} = \frac{(-i)}{2t_c}\int_0^{t_c} dt_2 \int_0^{t_2} dt_1 \left[\tilde{\tilde{H}}(t_2), \tilde{\tilde{H}}(t_1)\right] \tag{B.3}$$

In the case of single crystal the II order correction reduces to,

$$H^{(2)} = -\frac{\omega_1^2}{\omega_Q}\left(\sqrt{6}\ T^{(2)0} + \hat{D}_S\right)_0$$

while, in the powder sample, we have

$$H^{(2)} = -\sqrt{\frac{3}{2}}\Delta\omega_1\left(\Phi_1 R F_A^+ + \Phi_1^{-1} R F_B^-\right) - \frac{\omega_1^2}{\omega_Q}\left(\sqrt{6}\ T^{(2)0} + \hat{D}_S\right)_0$$

Based on the above calculations, it is clear that the AHT calculations are valid in the case of single crystal (only strong coupling regime) and deviate significantly in powder calculations.

C Matrix Representation of Floquet states and Operators

The spin states are defined as $|m\rangle$

$$|1\rangle = \begin{pmatrix}1\\0\\0\end{pmatrix} \quad ; \quad |0\rangle = \begin{pmatrix}0\\1\\0\end{pmatrix} \quad ; \quad |-1\rangle = \begin{pmatrix}0\\0\\1\end{pmatrix}$$

The Fourier states are defined as,

$$|-1\rangle = \begin{pmatrix}1\\0\\0\\\vdots\end{pmatrix} \quad ; \quad |0\rangle = \begin{pmatrix}0\\1\\0\\\vdots\end{pmatrix} \quad ; \quad |1\rangle = \begin{pmatrix}0\\0\\1\\\vdots\end{pmatrix}$$

$$F_m = \sum_{n=-\infty}^{+\infty} |n\rangle\langle n+m| \tag{C.1}$$

$$I_F = \sum_{n=-\infty}^{+\infty} n \left|n\right\rangle \left\langle n\right| \tag{C.2}$$

$$\begin{aligned}
F_1 &= \cdots + \left|-1\right\rangle \left\langle 0\right| + \left|0\right\rangle \left\langle 1\right| + \ldots \\
&= \cdots + \begin{pmatrix} \vdots \\ 1 \\ 0 \\ 0 \\ \vdots \end{pmatrix} \begin{pmatrix} \ldots & 0 & 1 & 0 & \ldots \end{pmatrix} + \begin{pmatrix} \vdots \\ 0 \\ 1 \\ 0 \\ \vdots \end{pmatrix} \begin{pmatrix} \ldots & 0 & 0 & 1 & \ldots \end{pmatrix} + \ldots \\
&= \cdots + \begin{pmatrix} \ddots & \ldots & \ldots & \ldots & \ldots \\ \ldots & 0 & 1 & 0 & \ldots \\ \ldots & 0 & 0 & 0 & \ldots \\ \ldots & 0 & 0 & 0 & \ldots \\ \ldots & \ldots & \ldots & \ldots & \ddots \end{pmatrix} + \begin{pmatrix} \ddots & \ldots & \ldots & \ldots & \ldots \\ \ldots & 0 & 0 & 0 & \ldots \\ \ldots & 0 & 0 & 1 & \ldots \\ \ldots & 0 & 0 & 0 & \ldots \\ \ldots & \ldots & \ldots & \ldots & \ddots \end{pmatrix} + \ldots \\
F_1 &= \begin{pmatrix} \ddots & \ldots & \ldots & \ldots & \ldots \\ \ldots & 0 & \mathbf{1} & 0 & \ldots \\ \ldots & 0 & 0 & \mathbf{1} & \ldots \\ \ldots & 0 & 0 & 0 & \ldots \\ \ldots & \ldots & \ldots & \ldots & \ddots \end{pmatrix}
\end{aligned}$$

$$\begin{aligned}
F_{-1} &= \cdots + \left|0\right\rangle \left\langle -1\right| + \left|1\right\rangle \left\langle 0\right| + \ldots \\
&= \cdots + \begin{pmatrix} \vdots \\ 0 \\ 1 \\ 0 \\ \vdots \end{pmatrix} \begin{pmatrix} \ldots & 1 & 0 & 0 & \ldots \end{pmatrix} + \begin{pmatrix} \vdots \\ 0 \\ 0 \\ 1 \\ \vdots \end{pmatrix} \begin{pmatrix} \ldots & 0 & 1 & 0 & \ldots \end{pmatrix} + \ldots \\
&= \cdots + \begin{pmatrix} \ddots & \ldots & \ldots & \ldots & \ldots \\ \ldots & 0 & 0 & 0 & \ldots \\ \ldots & 1 & 0 & 0 & \ldots \\ \ldots & 0 & 0 & 0 & \ldots \\ \ldots & \ldots & \ldots & \ldots & \ddots \end{pmatrix} + \begin{pmatrix} \ddots & \ldots & \ldots & \ldots & \ldots \\ \ldots & 0 & 0 & 0 & \ldots \\ \ldots & 0 & 0 & 0 & \ldots \\ \ldots & 0 & 1 & 0 & \ldots \\ \ldots & \ldots & \ldots & \ldots & \ddots \end{pmatrix} + \ldots \\
F_{-1} &= \begin{pmatrix} \ddots & \ldots & \ldots & \ldots & \ldots \\ \ldots & 0 & 0 & 0 & \ldots \\ \ldots & \mathbf{1} & 0 & 0 & \ldots \\ \ldots & 0 & \mathbf{1} & 0 & \ldots \\ \ldots & \ldots & \ldots & \ldots & \ddots \end{pmatrix}
\end{aligned}$$

$$
\begin{aligned}
F_0 &= \cdots + |-1\rangle\langle -1| + |0\rangle\langle 0| + |1\rangle\langle 1| + \dots \\
&= \cdots + \begin{pmatrix} \vdots \\ 1 \\ 0 \\ 0 \\ \vdots \end{pmatrix} \begin{pmatrix} \dots & 1 & 0 & 0 & \dots \end{pmatrix} + \begin{pmatrix} \vdots \\ 0 \\ 1 \\ 0 \\ \vdots \end{pmatrix} \begin{pmatrix} \dots & 0 & 1 & 0 & \dots \end{pmatrix} + \begin{pmatrix} \vdots \\ 0 \\ 0 \\ 1 \\ \vdots \end{pmatrix} \begin{pmatrix} \dots & 0 & 0 & 1 & \dots \end{pmatrix} + \dots \\
&= \cdots + \begin{pmatrix} \ddots & \dots & \dots & \dots & \dots \\ \dots & 1 & 0 & 0 & \dots \\ \dots & 0 & 0 & 0 & \dots \\ \dots & 0 & 0 & 0 & \dots \\ \dots & \dots & \dots & \dots & \ddots \end{pmatrix} + \begin{pmatrix} \ddots & \dots & \dots & \dots & \dots \\ \dots & 0 & 0 & 0 & \dots \\ \dots & 0 & 1 & 0 & \dots \\ \dots & 0 & 0 & 0 & \dots \\ \dots & \dots & \dots & \dots & \ddots \end{pmatrix} + \begin{pmatrix} \ddots & \dots & \dots & \dots & \dots \\ \dots & 0 & 0 & 0 & \dots \\ \dots & 0 & 0 & 0 & \dots \\ \dots & 0 & 0 & 1 & \dots \\ \dots & \dots & \dots & \dots & \ddots \end{pmatrix} + \dots \\
F_0 &= \begin{pmatrix} \ddots & \dots & \dots & \dots & \dots \\ \dots & \mathbf{1} & 0 & 0 & \dots \\ \dots & 0 & \mathbf{1} & 0 & \dots \\ \dots & 0 & 0 & \mathbf{1} & \dots \\ \dots & \dots & \dots & \dots & \ddots \end{pmatrix}
\end{aligned}
$$

$$
\begin{aligned}
I_F &= \cdots + (-1)\,|-1\rangle\langle -1| + (0)\,|0\rangle\langle 0| + (1)\,|1\rangle\langle 1| + \dots \\
&= \cdots + (-1) \begin{pmatrix} \vdots \\ 1 \\ 0 \\ 0 \\ \vdots \end{pmatrix} \begin{pmatrix} \dots & 1 & 0 & 0 & \dots \end{pmatrix} + (0) \begin{pmatrix} \vdots \\ 0 \\ 1 \\ 0 \\ \vdots \end{pmatrix} \begin{pmatrix} \dots & 0 & 1 & 0 & \dots \end{pmatrix} + (1) \begin{pmatrix} \vdots \\ 0 \\ 0 \\ 1 \\ \vdots \end{pmatrix} \begin{pmatrix} \dots & 0 & 0 & 1 & \dots \end{pmatrix} + \dots \\
&= \cdots + (-1) \begin{pmatrix} \ddots & \dots & \dots & \dots & \dots \\ \dots & 1 & 0 & 0 & \dots \\ \dots & 0 & 0 & 0 & \dots \\ \dots & 0 & 0 & 0 & \dots \\ \dots & \dots & \dots & \dots & \ddots \end{pmatrix} + (0) \begin{pmatrix} \ddots & \dots & \dots & \dots & \dots \\ \dots & 0 & 0 & 0 & \dots \\ \dots & 0 & 1 & 0 & \dots \\ \dots & 0 & 0 & 0 & \dots \\ \dots & \dots & \dots & \dots & \ddots \end{pmatrix} + (1) \begin{pmatrix} \ddots & \dots & \dots & \dots & \dots \\ \dots & 0 & 0 & 0 & \dots \\ \dots & 0 & 0 & 0 & \dots \\ \dots & 0 & 0 & 1 & \dots \\ \dots & \dots & \dots & \dots & \ddots \end{pmatrix} + \dots \\
I_F &= \begin{pmatrix} \ddots & \dots & \dots & \dots & \dots \\ \dots & -\mathbf{1} & 0 & 0 & \dots \\ \dots & 0 & \mathbf{0} & 0 & \dots \\ \dots & 0 & 0 & \mathbf{1} & \dots \\ \dots & \dots & \dots & \dots & \ddots \end{pmatrix}
\end{aligned}
$$

The Floquet states are defined as,

Floquet state = Fourier state $\otimes$ Spin state

$$(I_z)_n = F_n \otimes I_z$$

For e.g.,

$$(I_z)_1 = F_1 \otimes I_z = \begin{pmatrix} \ddots & \dots & \dots & \dots & \dots \\ \dots & 0 & 1 & 0 & \dots \\ \dots & 0 & 0 & 1 & \dots \\ \dots & 0 & 0 & 0 & \dots \\ \dots & \dots & \dots & \dots & \ddots \end{pmatrix} \otimes I_z = \begin{pmatrix} \ddots & \dots & \dots & \dots & \dots \\ \dots & 0 & (I_z) & 0 & \dots \\ \dots & 0 & 0 & (I_z) & \dots \\ \dots & 0 & 0 & 0 & \dots \\ \dots & \dots & \dots & \dots & \ddots \end{pmatrix}$$

$$= \begin{pmatrix} \ddots & \dots & \dots & \dots & \dots \\ \dots & 0 & 1 & 0 & \dots \\ \dots & 0 & 0 & 1 & \dots \\ \dots & 0 & 0 & 0 & \dots \\ \dots & \dots & \dots & \dots & \ddots \end{pmatrix} \otimes \begin{pmatrix} 1 & 0 & 0 \\ 0 & 0 & 0 \\ 0 & 0 & -1 \end{pmatrix}$$

The above matrix equals to

$\langle\alpha,n\vert$ \ $\vert\beta,m\rangle$	…	…	$\vert 1,-1\rangle$	$\vert 0,-1\rangle$	$\vert -1,-1\rangle$	$\vert 1,0\rangle$	$\vert 0,0\rangle$	$\vert -1,0\rangle$	$\vert 1,1\rangle$	$\vert 0,1\rangle$	$\vert -1,1\rangle$	…	…
⋮	⋱	…	…	…	…	…	…	…	…	…	…	…	…
⋮	…	⋱	…	…	…	…	…	…	…	…	…	…	…
$\langle 1,-1\vert$	…	…	0	0	0	**1**	0	0	0	0	0	…	…
$\langle 0,-1\vert$	…	…	0	0	0	0	0	0	0	0	0	…	…
$\langle -1,-1\vert$	…	…	0	0	0	0	0	**−1**	0	0	0	…	…
$\langle 1,0\vert$	…	…	0	0	0	0	0	0	**1**	0	0	…	…
$\langle 0,0\vert$	…	…	0	0	0	0	0	0	0	0	0	…	…
$\langle -1,0\vert$	…	…	0	0	0	0	0	0	0	0	**−1**	…	…
$\langle 1,1\vert$	…	…	0	0	0	0	0	0	0	0	0	…	…
$\langle 0,1\vert$	…	…	0	0	0	0	0	0	0	0	0	…	…
$\langle -1,1\vert$	…	…	0	0	0	0	0	0	0	0	0	…	…
⋮	…	…	…	…	…	…	…	…	…	…	…	⋱	…
⋮	…	…	…	…	…	…	…	…	…	…	…	…	⋱

The general form of the Hamiltonian is

$$H(t) = \sum_n H_{ij}^n \; e^{(in\omega t)} \tag{C.3}$$

where, 'n' is an integer, 'ω' is the base frequency and 'H_{ij}^n' is the Hamiltonian matrix element with 'i^{th}' row and 'j^{th}' column (in Hilbert space) of the corresponding integer 'n'.
The Floquet Hamiltonian is written as

$$\langle \alpha, n | H_F | \beta, m \rangle = H_{\alpha\beta}^{n-m} + n\omega\delta_{\alpha\beta}\delta_{nm} \tag{C.4}$$

The above equation represents a 'Floquet Hamiltonian' (H_F) with 'finite basis' (α, β) in Hilbert space and 'infinite coefficients' (n, m) in Fourier dimension. Also, '$\alpha, \beta \in \{-1, 0, 1\}$' and '$n, m \in \{-\infty, \infty\}$'.
The commutation relations used are

$$\left[(I_\alpha)_m \, , I_F \right] = m \, (I_\alpha)_m \quad ; \quad \left[(I_\alpha)_m \, , (I_\beta)_n \right] = i \, (I_\gamma)_{m+n} \tag{C.5}$$

where, '$\alpha, \beta, \gamma \in \{x, y, z\}$' defined by $[I_x, I_y] = iI_z$; $[I_y, I_z] = iI_x$; $[I_z, I_x] = iI_y$.
The Floquet Hamiltonian (H_F) of infinite dimension is elaborately written as

$\langle\alpha,n\vert$ \ $\vert\beta,m\rangle$	$\cdots$	$\cdots$	$\vert 1,-1\rangle$	$\vert 0,-1\rangle$	$\vert -1,-1\rangle$	$\vert 1,0\rangle$	$\vert 0,0\rangle$	$\vert -1,0\rangle$	$\vert 1,1\rangle$	$\vert 0,1\rangle$	$\vert -1,1\rangle$	$\cdots$	$\cdots$
$\vdots$	$\ddots$	$\cdots$	$\cdots$	$\cdots$	$\cdots$	$\cdots$	$\cdots$	$\cdots$	$\cdots$	$\cdots$	$\cdots$	$\cdots$	$\cdots$
$\vdots$	$\vdots$	$\ddots$	$\cdots$	$\cdots$	$\cdots$	$\cdots$	$\cdots$	$\cdots$	$\cdots$	$\cdots$	$\cdots$	$\cdots$	$\cdots$
$\vdots$	$\vdots$	$\cdots$	$\cdots$	$\cdots$	$\cdots$	$\cdots$	$\cdots$	$\cdots$	$\cdots$	$\cdots$	$\cdots$	$\cdots$	$\cdots$
$\langle 1,-1\vert$	$\cdots$	$\cdots$	$H^0_{11}-\omega$	H^0_{10}	H^0_{1-1}	H^{-1}_{11}	H^{-1}_{10}	H^{-1}_{1-1}	H^{-2}_{11}	H^{-2}_{10}	H^{-2}_{1-1}	$\cdots$	$\cdots$
$\langle 0,-1\vert$	$\cdots$	$\cdots$	H^0_{01}	$H^0_{00}-\omega$	H^0_{0-1}	H^{-1}_{01}	H^{-1}_{00}	H^{-1}_{0-1}	H^{-2}_{01}	H^{-2}_{00}	H^{-2}_{0-1}	$\cdots$	$\cdots$
$\langle -1,-1\vert$	$\cdots$	$\cdots$	H^0_{-11}	H^0_{-10}	$H^0_{-1-1}-\omega$	H^{-1}_{-11}	H^{-1}_{-10}	H^{-1}_{-1-1}	H^{-2}_{-11}	H^{-2}_{-10}	H^{-2}_{-1-1}	$\cdots$	$\cdots$
$\langle 1,0\vert$	$\cdots$	$\cdots$	H^1_{11}	H^1_{10}	H^1_{1-1}	H^0_{11}	H^0_{10}	H^0_{1-1}	H^{-1}_{11}	H^{-1}_{10}	H^{-1}_{1-1}	$\cdots$	$\cdots$
$\langle 0,0\vert$	$\cdots$	$\cdots$	H^1_{01}	H^1_{00}	H^1_{0-1}	H^0_{01}	H^0_{00}	H^0_{0-1}	H^{-1}_{01}	H^{-1}_{00}	H^{-1}_{0-1}	$\cdots$	$\cdots$
$\langle -1,0\vert$	$\cdots$	$\cdots$	H^1_{-11}	H^1_{-10}	H^1_{-1-1}	H^0_{11}	H^0_{-10}	H^0_{-1-1}	H^{-1}_{-11}	H^{-1}_{-10}	H^{-1}_{-1-1}	$\cdots$	$\cdots$
$\langle 1,1\vert$	$\cdots$	$\cdots$	H^2_{11}	H^2_{10}	H^2_{1-1}	H^1_{11}	H^1_{10}	H^1_{1-1}	$H^0_{11}+\omega$	H^0_{10}	H^0_{1-1}	$\cdots$	$\cdots$
$\langle 0,1\vert$	$\cdots$	$\cdots$	H^{-2}_{01}	H^{-2}_{00}	H^{-2}_{0-1}	H^1_{01}	H^1_{00}	H^1_{0-1}	H^0_{01}	$H^0_{00}+\omega$	H^0_{0-1}	$\cdots$	$\cdots$
$\langle -1,1\vert$	$\cdots$	$\cdots$	H^{-2}_{-11}	H^{-2}_{-10}	H^{-2}_{-1-1}	H^1_{-11}	H^1_{-10}	H^1_{-1-1}	H^0_{-1-1}	H^0_{-10}	$H^0_{-1-1}+\omega$	$\cdots$	$\cdots$
$\vdots$	$\vdots$	$\cdots$	$\cdots$	$\cdots$	$\cdots$	$\cdots$	$\cdots$	$\cdots$	$\cdots$	$\cdots$	$\cdots$	$\ddots$	$\cdots$
$\vdots$	$\vdots$	$\cdots$	$\cdots$	$\cdots$	$\cdots$	$\cdots$	$\cdots$	$\cdots$	$\cdots$	$\cdots$	$\cdots$	$\cdots$	$\ddots$

D Derivation of Effective Floquet Hamiltonians from 'S_2' transformation

To improve the accuracy of the effective Hamiltonians, the role of residual off-diagonal terms neglected in the first transformation is considered in the discussion presented below. As depicted in Table. 2.9, the off-diagonal contributions comprises of the double-quantum (DQ) operators. To fold the above off-diagonal contributions, a second transformation function 'S_2' was employed. A brief description of the procedure employed in the derivation of effective Floquet Hamiltonians from the second transformation 'S_2' is outlined below. The diagonal corrections from the first transformation are included along 'H_0' and the off-diagonal operators $\left(\Phi_1^{\pm 2}\ T^{(2)\pm 2}\right)_{\pm 2}$ form the perturbation.

$$H_0 = \omega_1 I_F + \ G_{1R}^{(1)}\left(\hat{D}_S\right)_0 + G_{2R}^{(1)}\left(T^{(2)0}\right)_0 \tag{D.1}$$

$$H_1 = G_{DR}^{(1)}\left\{\left(\Phi_1^2 T^{(2)2}\right)_{+2} + \left(\Phi_1^{-2} T^{(2)-2}\right)_{-2}\right\} \tag{D.2}$$

$$G_{DR}^{(1)} = +\left(\frac{\Omega_Q}{4}\right)\left\{\frac{1}{3\times 1!}(\xi)^2 - \frac{1}{5\times 3!}(\xi)^4 + \frac{1}{7\times 5!}(\xi)^6 - \dots\right\} \tag{D.3}$$

Employing the transformation function 'S_2',

$$S_2 = \ C_{DR'}^{(2)}\left\{\left(\Phi_1^2 T^{(2)2}\right)_{+2} - \left(\Phi_1^{-2} T^{(2)-2}\right)_{-2}\right\} \tag{D.4}$$

where,

$$C_{DR'}^{(2)} = -i\left(\frac{G_{DR}^{(1)}}{2\left(G_{1R}^{(1)} - \omega_1\right)}\right) \tag{D.5}$$

$$C_{DR}^{(i+1)} = \sum_{i=1}^{n-1} C_{DR'}^{(i+1)} \tag{D.6}$$

where 'i' takes values from 1 to '$n-1$', where 'n' is the number of 'S' transformations applied (Here $n = 2$).
In the above equation, the coefficients '$G^{(1)}_{DR} = \sum_{i=0}^{N_1} G^{(1)}_{DR,i}$' denote the off-diagonal coefficients resulting from the first-transformation. Depending on the desired level of accuracy, the off-diagonal contributions (denoted by value of N_1) from the first-transformation are incorporated accordingly.
The transformed Hamiltonian after second transformation is represented by,

$$H_0 = \omega_1 I_F + \ G^{(2)}_{1R} \left(I_z\right)_0 + G^{(1)}_{2R} \left(T^{(2)0}\right)_0 \tag{D.7}$$

where,

$$G^{(2)}_{1R} = G^{(1)}_{1R} + \left\{ \frac{1}{2 \times 0!} \ G^{(2)}_{1R,A} - \frac{1}{4 \times 2!} \ G^{(2)}_{1R,B} + \frac{1}{6 \times 4!} \ G^{(2)}_{1R,C} + \dots \right\} \tag{D.8}$$

The perturbed Hamiltonian after second transformation is represented by,

$$H_1 = G^{(2)}_{DR} \left\{ \left(\Phi_1^2 T^{(2)2}\right)_{+2} + \left(\Phi_1^{-2} T^{(2)-2}\right)_{-2} \right\} \tag{D.9}$$

$$G^{(2)}_{DR} = \left\{ -\frac{1}{3 \times 1!} G^{(2)}_{DR,A} + \frac{1}{5 \times 3!} \ G^{(2)}_{DR,B} - \frac{1}{7 \times 5!} \ G^{(2)}_{DR,C} + \dots \right\} \tag{D.10}$$

In the above equation, the magnitude of '$G^{(n)}_{DR}$' keeps on decreasing as 'n' increases. The choice of 'n' is problem specific and is decided by comparing with the exact numerical simulations. After 'n' transformations the magnitude of '$G^{(n)}_{DR}$' becomes small enough such that 'H_1' can be neglected and the effective Hamiltonian reduces to the form given below,

$$H_0 = \omega_1 I_F + \ G^{(n)}_{1R} \left(I_z\right)_0 + G^{(1)}_{2R} \left(T^{(2)0}\right)_0 \tag{D.11}$$

The final equation depicting the DQ excitation efficiency is

$$\left\langle T^{(2)-2}(t_{p1}) \right\rangle = i e^{2i\omega_0 t_2} \ \Phi_1^2 \ \Phi_R \left\{ \sin\left(\xi_{2R}\right) \cos\left(\xi_{1R}\right) + \cos\left(\xi_{2R}\right) \sin\left(\xi_{1R}\right) \sin\left(2\xi_{DR}\right) \right\} \tag{D.12}$$

where,

$$\xi_{DR} = i\ C_{DR}^{(n)} \quad ; \quad \xi_{1R} = \left(G_{1R}^{(n)} - \omega_1\right) t_{p1} \quad ; \quad \xi_{2R} = \sqrt{\frac{3}{2}}\ G_{2R}^{(1)}\ t_{p1}$$

Table D.1: Definition of coefficients employed in the perturbing Hamiltonians for Case-III and Case-IV

	$G_{DR}^{(1)}$
Case-III $(N_1 = 3)$ **Case-IV** $(N_1 > 3)$	$+\frac{1}{3\times 1!}\left(\frac{\Omega_Q}{4}\right)(\xi)^2$ $+\left(\frac{\Omega_Q}{4}\right)\left\{\frac{1}{3\times 1!}(\xi)^2 - \frac{1}{5\times 3!}(\xi)^4 + \frac{1}{7\times 5!}(\xi)^6 - ....\right\}$

	$G_{1R}^{(2)}$	$G_{2R}^{(2)}$
Case-III	$\sum_{i=0}^{N_1} G_{1R,i}^{(1)} + \sum_{j=1}^{2} G_{1R,j}^{(2)}$	$G_{2R}^{(1)} = \frac{\Omega_Q}{2\sqrt{6}}$
Case-IV	$\sum_{i=0}^{N_1} G_{1R,i}^{(1)} + \sum_{j=1}^{N_2} G_{1R,j}^{(2)}$	$G_{2R}^{(1)}$

$$\xi = \left(\frac{\Omega_Q}{4\omega_1}\right) \quad ; \quad C_{(\theta)} = \cos(\theta) \quad ; \quad S_{(\theta)} = \sin(\theta)$$

In the simulations, presented in Figure. 2.19, diagonal corrections to

- second order (Panels A1 $\rightarrow$ A4) resulting from the second transformation 'S_2'
- n^{th} order (Panels B1 $\rightarrow$ B4) resulting from the second transformation 'S_2'

are compared with the exact numerical simulations. In all the simulations, off-diagonal contributions (to n^{th} order) resulting from the first transformation 'S_1' is incorporated.

Table D.2: Description of the higher order (diagonal and off-diagonal) contributions to the effective Hamiltonian (Eq. D.1) derived from second transformation

n^{th} **order** **Correction**	**Coefficients in the Effective Hamiltonian** $H_{eff} = H_0^{(2)} + H_2^{(2)} + H_4^{(2)} + H_6^{(2)} + \cdots = \omega_1 I_F + \left(G_{1R}^{(1)} + \sum_{i=1}^{N_1} G_{1R,i}^{(2)}\right)(I_z)_0 + G_{2R}^{(1)}\left(T^{(2)0}\right)_0$	
	Expression from the 'H_1' term	**Non-zero 'G' Coefficients**
Zero order (λ^0)	$H_0^{(2)} = \omega_1 I_F + G_{1R}^{(1)}(I_z)_0 + G_{2R}^{(1)}\left(T^{(2)0}\right)_0$	$\frac{\omega_Q}{2} I_F + G_{1R,0}^{(2)}(I_z)_0 + G_{2R,0}^{(1)}\left(T^{(2)0}\right)_0$
I order (λ^1)	$H_1^{(2)} = 0$	
II order (λ^2)	$H_2^{(2)} = \frac{i}{2\times 0!}[S_2, H_1] = +\left(\frac{1}{2\times 0!}\right)\underbrace{\left(-2i\, C_{DR}^{(2)}\, G_{DR}^{(1)}\right)}_{G_{1R,A}^{(2)}}(I_z)_0$	$G_{1R,2}^{(2)}(I_z)_0$
III order (λ^3)	$H_3^{(2)} = -\frac{1}{3\times 1!}[S_2,[S_2,H_1]] = +\left(\frac{1}{3\times 1!}\right)\underbrace{-2\left(C_{DR}^{(2)}\, G_{1R,A}^{(2)}\right)}_{G_{DR,A}^{(2)}}\left\{\left(\Phi_1^2 T^{(2)2}\right)_{+2} + \left(\Phi_1^{-2} T^{(2)-2}\right)_{-2}\right\}$	$G_{2R,3}^{(2)}\left\{\left(\Phi_1^2 T^{(2)2}\right)_{+2} + \left(\Phi_1^{-2} T^{(2)-2}\right)_{-2}\right\}$
IV order (λ^4)	$H_4^{(2)} = -\frac{i}{4\times 2!}[S_2,[S_2,[S_2,H_1]]] = -\left(\frac{1}{4\times 2!}\right)\underbrace{\left(-2i\, C_{DR}^{(2)}\, G_{DR,A}^{(2)}\right)}_{G_{1R,B}^{(2)}}(I_z)_0$	$G_{1R,4}^{(2)}(I_z)_0$
V order (λ^5)	$H_5^{(2)} = \frac{1}{5\times 3!}[S_2,[S_2,[S_2,[S_2,H_1]]]] = -\left(\frac{1}{5\times 3!}\right)\underbrace{-2\left(C_{DR}^{(2)}\, G_{1R,B}^{(2)}\right)}_{G_{DR,B}^{(2)}}\left\{\left(\Phi_1^2 T^{(2)2}\right)_{+2} + \left(\Phi_1^{-2} T^{(2)-2}\right)_{-2}\right\}$	$G_{2R,5}^{(2)}\left\{\left(\Phi_1^2 T^{(2)2}\right)_{+2} + \left(\Phi_1^{-2} T^{(2)-2}\right)_{-2}\right\}$
VI order (λ^6)	$H_6^{(2)} = \frac{i}{6\times 4!}[S_2,[S_2,[S_2,[S_2,[S_2,H_1]]]]] = +\left(\frac{1}{6\times 4!}\right)\underbrace{\left(-2i\, C_{DR}^{(2)}\, G_{DR,B}^{(2)}\right)}_{G_{1R,C}^{(2)}}(I_z)_0$	$G_{1R,6}^{(2)}(I_z)_0$
VII order (λ^7)	$H_7^{(2)} = -\frac{1}{7\times 5!}[S_2,[S_2,[S_2,[S_2,[S_2,[S_2,H_1]]]]]] = +\left(\frac{1}{7\times 5!}\right)\underbrace{-2\left(C_{DR}^{(2)}\, G_{1R,C}^{(2)}\right)}_{G_{DR,C}^{(2)}}\left\{\left(\Phi_1^2 T^{(2)2}\right)_{+2} + \left(\Phi_1^{-2} T^{(2)-2}\right)_{-2}\right\}$	$G_{2R,7}^{(2)}\left\{\left(\Phi_1^2 T^{(2)2}\right)_{+2} + \left(\Phi_1^{-2} T^{(2)-2}\right)_{-2}\right\}$

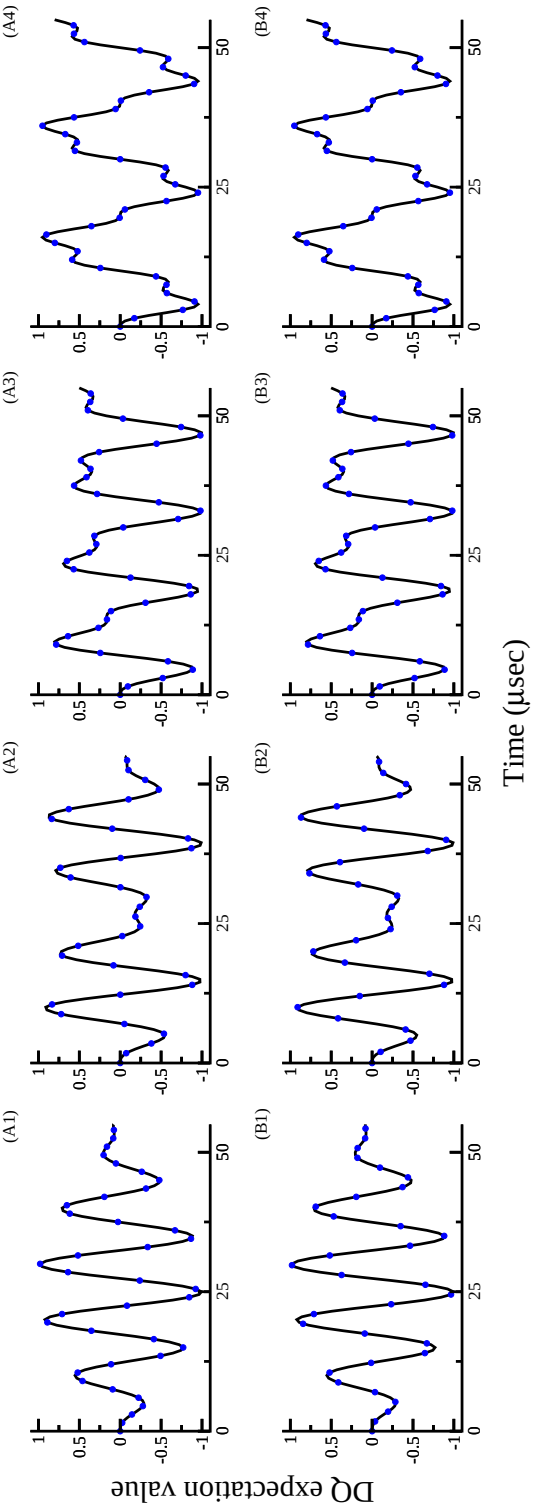

Figure 2.19: Comparison of numerical (black thick line) and analytic simulations (blue dots) based on effective Hamiltonians derived from the second transformation. The off-diagonal contributions to order λ^n from the first transformation ($N_1 > 2$) and diagonal corrections to order λ^2 from the second transformation ($N_2 = 2$) are included in row-1 (Panels A1 $\rightarrow$ A4) and diagonal corrections to order λ^n from the second transformation ($N_2 > 2$) were included in row-2 (Panels B1 $\rightarrow$ B4). In the simulations depicted, the quadrupole coupling constant ($C_Q = {}^{\omega_Q}/_{3\pi}$) is varied A1, B1) $C_Q = 25$ kHz, A2, B2) $C_Q = 50$ kHz, A3,B3) $C_Q = 100$ kHz, A4,B4) $C_Q = 200$ kHz, employing an excitation pulse of constant RF amplitude, $({}^{\omega_1}/_{2\pi}) = 100$ kHz. The simulations correspond to a single crystal.

Hence, depending on the relative magnitudes of the quadrupolar frequency (ω_Q) and the amplitude of the pulse (ω_1), the choice of appropriate interaction frame plays an important role in the convergence of the perturbation corrections in the proposed effective Hamiltonians. Below, we present a summary of the results obtained.

Regime-I

$$H_0 = \frac{\omega_Q}{2} I_F + \hbar\Delta \left(T^{(2)0}\right)_0$$

$$H_{eff} = \frac{\omega_Q}{2} I_F + G^{(n)}_{ZQ} \left(T^{(2)0}\right)_0 + \; G^{(n)}_{DQ} \left(\hat{D}_S\right)_0 \tag{D.13}$$

$$\left\langle T^{(2)-2}(t_{p1})\right\rangle = ie^{2i\omega_0 t_2} \; \Phi_1^2 \; \Phi_R \left\{\cos^2(\alpha) \; \sin(\theta_{DQ}) - \sin^2(\alpha)\sin(\beta)\right\} \tag{D.14}$$

Regime-II

$$H_0 = \omega_1 I_F + \left(\frac{\hbar\Omega_Q}{2\sqrt{6}}\right) \left(T^{(2)0}\right)_0$$

$$H_{eff} = \omega_1 I_F + \; G^{(n)}_{1R} \left(I_z\right)_0 + G^{(1)}_{2R} \left(T^{(2)0}\right)_0 \tag{D.15}$$

$$\left\langle T^{(2)-2}(t_{p1})\right\rangle = ie^{2i\omega_0 t_2} \; \Phi_1^2 \; \Phi_R \left\{\sin(\xi_{2R})\cos(\xi_{1R}) + \cos(\xi_{2R})\sin(\xi_{1R})\sin(2\xi_{DR})\right\} \tag{D.16}$$

E Derivation of higher order corrections (Regime-I)

E.1 For first transformation S_1

Table E.1.1: Description of the coefficients employed in the derivation of effective Hamiltonian (Eq. 2.25) based on the first transformation

$G^{(1)}_{DQ}$	$G^{(1)}_{ZQ}$
$G^{(1)}_{DQ,0} = 0$	$G^{(1)}_{ZQ,0} = \Delta$
$G^{(1)}_{DQ,1} = 0$	$G^{(1)}_{ZQ,1} = 0$
$G^{(1)}_{DQ,2} = -\frac{1}{2\times 0!}\left(\frac{\omega_1}{2}\right)(\theta)$	$G^{(1)}_{ZQ,2} = -\frac{\sqrt{6}}{2\times 0!}\left(\frac{\omega_1}{2}\right)(\theta)$
$G^{(1)}_{DQ,3} = 0$	$G^{(1)}_{ZQ,3} = 0$
$G^{(1)}_{DQ,4} = +\frac{1}{4\times 2!}\left(\frac{\omega_1}{2}\right)(\theta)^3$	$G^{(1)}_{ZQ,4} = +\frac{\sqrt{6}}{4\times 2!}\left(\frac{\omega_1}{2}\right)(\theta)^3$
$G^{(1)}_{DQ,5} = 0$	$G^{(1)}_{ZQ,5} = 0$
$G^{(1)}_{DQ,6} = -\frac{1}{6\times 4!}\left(\frac{\omega_1}{2}\right)(\theta)^5$	$G^{(1)}_{ZQ,6} = -\frac{\sqrt{6}}{6\times 4!}\left(\frac{\omega_1}{2}\right)(\theta)^5$
$G^{(1)}_{DQ,7} = 0$	$G^{(1)}_{ZQ,7} = 0$
.	.
.	.
$G^{(1)}_{DQ} = \left(\frac{\omega_1}{2}\right)\left\{-\frac{1}{2\times 0!}(\theta) + \frac{1}{4\times 2!}(\theta)^3 - \frac{1}{6\times 4!}(\theta)^5 + ...\right\}$	$G^{(1)}_{ZQ} = \Delta + \left(\frac{\omega_1}{2}\right)\sqrt{6}\left\{-\frac{1}{2\times 0!}(\theta) + \frac{1}{4\times 2!}(\theta)^3 - \frac{1}{6\times 4!}(\theta)^5 + ...\right\}$
$\theta = \left(\frac{4\omega_1}{\Omega_Q}\right) \quad ; \quad C_{(\theta)} = \cos(\theta)$	

Table E.1.2: Coefficients employed in the derivation of Effective Hamiltonians for Case-I and Case-II

	$G^{(1)}_{DQ}$	$G^{(1)}_{ZQ}$
Case-I $(N_1 = 2)$	$-\frac{1}{2\times 0!}\left(\frac{\omega_1}{2}\right)(\theta)$	$\Delta - \frac{\sqrt{6}}{2\times 0!}\left(\frac{\omega_1}{2}\right)(\theta)$
Case-II $(N_1 > 2)$	$\left(\frac{\omega_1}{2}\right)\left\{-\frac{1}{2\times 0!}(\theta) + \frac{1}{4\times 2!}(\theta)^3 - \frac{1}{6\times 4!}(\theta)^5 + ...\right\}$	$\Delta + \left(\frac{\omega_1}{2}\right)\sqrt{6}\left\{-\frac{1}{2\times 0!}(\theta) + \frac{1}{4\times 2!}(\theta)^3 - \frac{1}{6\times 4!}(\theta)^5 + ...\right\}$
$\theta = \left(\frac{4\omega_1}{\Omega_Q}\right) \quad ; \quad C_{(\theta)} = \cos(\theta)$		

E.2 For second transformation S_2

Table E.2.1: Description of the coefficients employed in the perturbing Hamiltonian (Eq. 2.40)

$G^{(1)}_{SQ}$
$G^{(1)}_{SQ,0} = 0$ $G^{(1)}_{SQ,1} = 0$ $G^{(1)}_{SQ,2} = 0$ $G^{(1)}_{SQ,3} = \frac{1}{3\times 1!}\left(\frac{\omega_1}{2}\right)(\theta)^2$ $G^{(1)}_{SQ,4} = 0$ $G^{(1)}_{SQ,5} = -\frac{1}{5\times 3!}\left(\frac{\omega_1}{2}\right)(\theta)^4$ $G^{(1)}_{SQ,6} = 0$ $G^{(1)}_{SQ,7} = \frac{1}{7\times 5!}\left(\frac{\omega_1}{2}\right)(\theta)^6$.   .
$G^{(1)}_{SQ} = \left(\frac{\omega_1}{2}\right)\left\{\frac{1}{3\times 1!}(\theta)^2 - \frac{1}{5\times 3!}(\theta)^4 + \frac{1}{7\times 5!}(\theta)^6 - ....\right\}$
$\theta = \left(\frac{4\omega_1}{\Omega_Q}\right) \quad ; \quad C_{(\theta)} = \cos(\theta) \quad ; \quad S_{(\theta)} = \sin(\theta)$

Table E.2.2: Description of the coefficients employed in the derivation of effective Hamiltonian (Eq. 2.39) based on the second transformation

$G^{(2)}_{DQ}$	$G^{(2)}_{ZQ}$	$G^{(2)}_{SQ}$
$G^{(2)}_{DQ,0} = G^{(1)}_{DQ}$	$G^{(2)}_{ZQ,0} = G^{(1)}_{ZQ}$	$G^{(2)}_{SQ,0} = 0$
$G^{(2)}_{DQ,1} = 0$	$G^{(2)}_{ZQ,1} = 0$	$G^{(2)}_{SQ,1} = 0$
$G^{(2)}_{DQ,2} = +\frac{1}{2\times 0!}\, G^{(2)}_{DQ,A}$	$G^{(2)}_{ZQ,2} = +\frac{\sqrt{6}}{2\times 0!}\, G^{(2)}_{DQ,A}$	$G^{(2)}_{SQ,2} = 0$
$G^{(2)}_{DQ,3} = 0$	$G^{(2)}_{ZQ,3} = 0$	$G^{(2)}_{SQ,3} = +\frac{1}{3\times 1!}\, G^{(2)}_{SQ,A}$
$G^{(2)}_{DQ,4} = -\frac{1}{4\times 2!}\, G^{(2)}_{DQ,B}$	$G^{(2)}_{ZQ,4} = -\frac{\sqrt{6}}{4\times 2!}\, G^{(2)}_{DQ,B}$	$G^{(2)}_{SQ,4} = 0$
$G^{(2)}_{DQ,5} = 0$	$G^{(2)}_{ZQ,5} = 0$	$G^{(2)}_{SQ,5} = -\frac{1}{5\times 3!}\, G^{(2)}_{SQ,B}$
$G^{(2)}_{DQ,6} = +\frac{1}{6\times 4!}\, G^{(2)}_{DQ,C}$	$G^{(2)}_{ZQ,6} = +\frac{\sqrt{6}}{6\times 4!}\, G^{(2)}_{DQ,C}$	$G^{(2)}_{SQ,6} = 0$
$G^{(2)}_{DQ,7} = 0$	$G^{(2)}_{ZQ,7} = 0$	$G^{(2)}_{SQ,7} = +\frac{1}{7\times 5!}\, G^{(2)}_{SQ,C}$
.	.	.
.	.	.
$G^{(2)}_{DQ} = G^{(1)}_{DQ} + \Big\{\frac{1}{2\times 0!}\, G^{(2)}_{DQ,A}$ $-\frac{1}{4\times 2!}\, G^{(2)}_{DQ,B} + \frac{1}{6\times 4!}\, G^{(2)}_{DQ,C} + ...\Big\}$	$G^{(2)}_{ZQ} = G^{(1)}_{ZQ} + \sqrt{6}\Big\{\frac{1}{2\times 0!}\, G^{(2)}_{DQ,A}$ $-\frac{1}{4\times 2!}\, G^{(2)}_{DQ,B} + \frac{1}{6\times 4!}\, G^{(2)}_{DQ,C} + ...\Big\}$	$G^{(2)}_{SQ} = \Big\{\frac{1}{3\times 1!}\, G^{(2)}_{SQ,A}$ $-\frac{1}{5\times 3!}\, G^{(2)}_{SQ,B} + \frac{1}{7\times 5!}\, G^{(2)}_{SQ,C} + ...\Big\}$
$\theta = \left(\frac{4\omega_1}{\Omega_Q}\right) \quad ; \quad C_{(\theta)} = \cos(\theta)$		

F Derivation of higher order corrections (Regime-II)

F.1 For first transformation S_1

Table F.1.1: Definition of the coefficients employed in the derivation of effective Hamiltonian (Eq. 2.57) based on first transformation

$G_{1R}^{(1)}$	$G_{2R}^{(1)}$
$G_{1R,0}^{(1)} = 0$	$G_{2R,0}^{(1)} = \frac{\Omega_Q}{2\sqrt{6}}$
$G_{1R,1}^{(1)} = 0$	$G_{2R,1}^{(1)} = 0$
$G_{1R,2}^{(1)} = \frac{1}{2\times 0!}\left(\frac{-\Omega_Q}{4}\right)(\xi)$	$G_{2R,2}^{(1)} = 0$
$G_{1R,3}^{(1)} = 0$	$G_{2R,3}^{(1)} = 0$
$G_{1R,4}^{(1)} = \frac{1}{4\times 2!}\left(\frac{\Omega_Q}{4}\right)(\xi)^3$	$G_{2R,4}^{(1)} = 0$
$G_{1R,5}^{(1)} = 0$	$G_{2R,5}^{(1)} = 0$
$G_{1R,6}^{(1)} = \frac{1}{6\times 4!}\left(\frac{-\Omega_Q}{4}\right)(\xi)^5$	$G_{2R,6}^{(1)} = 0$
$G_{1R,7}^{(1)} = 0$	$G_{2R,7}^{(1)} = 0$
.	.
.	.
$G_{1R}^{(1)} = \left(\frac{-\Omega_Q}{4}\right)\left\{+\frac{1}{2\times 0!}(\xi) - \frac{1}{4\times 2!}(\xi)^3 + \frac{1}{6\times 4!}(\xi)^5 + ...\right\}$	$G_{2R}^{(1)} = \frac{\Omega_Q}{2\sqrt{6}}$
$\xi = \left(\frac{\Omega_Q}{4\omega_1}\right) \quad ; \quad C_{(\xi)} = \cos(\xi)$	

Table F.1.2: Coefficients employed in the derivation of Effective Hamiltonians for Case-I and Case-II

	$G_{1R}^{(1)}$	$G_{2R}^{(1)}$
Case-I $(N_1 = 2)$	$-\frac{1}{2\times 0!}\left(\frac{\Omega_Q}{4}\right)(\xi)$	$\frac{\Omega_Q}{2\sqrt{6}}$
Case-II $(N_1 > 2)$	$\left(\frac{-\Omega_Q}{4}\right)\left\{+\frac{1}{2\times 0!}(\xi) - \frac{1}{4\times 2!}(\xi)^3 + \frac{1}{6\times 4!}(\xi)^5 + ...\right\}$	$\frac{\Omega_Q}{2\sqrt{6}}$
$\xi = \left(\frac{\Omega_Q}{4\omega_1}\right) \quad ; \quad C_{(\theta)} = \cos(\theta)$		

F.2 For second transformation S_2

Table F.2.1: Description of the coefficients employed in the perturbing Hamiltonian (Eq. D.2)

$G^{(1)}_{DR}$
$G^{(1)}_{DR,0} = 0$ $G^{(1)}_{DR,1} = 0$ $G^{(1)}_{DR,2} = 0$ $G^{(1)}_{DR,3} = \frac{1}{3\times 1!}\left(\frac{\Omega_Q}{4}\right)(\xi)^2$ $G^{(1)}_{DR,4} = 0$ $G^{(1)}_{DR,5} = -\frac{1}{5\times 3!}\left(\frac{\Omega_Q}{4}\right)(\xi)^4$ $G^{(1)}_{DR,6} = 0$ $G^{(1)}_{DR,7} = \frac{1}{7\times 5!}\left(\frac{\Omega_Q}{4}\right)(\xi)^6$.   .
$G^{(1)}_{DR} = +\left(\frac{\Omega_Q}{4}\right)\left\{\frac{1}{3\times 1!}(\xi)^2 - \frac{1}{5\times 3!}(\xi)^4 + \frac{1}{7\times 5!}(\xi)^6 - ....\right\}$
$\xi = \left(\frac{\Omega_Q}{4\omega_1}\right) \quad ; \quad C_{(\xi)} = \cos(\xi)$

Table F.2.2: Description of the coefficients employed in the derivation of effective Hamiltonian (Eq. D.1) based on the first transformation

$G^{(2)}_{1R}$	$G^{(2)}_{DR}$
$G^{(2)}_{1R,0} = G^{(1)}_{1R}$	$G^{(2)}_{DR,0} = 0$
$G^{(2)}_{1R,1} = 0$	$G^{(2)}_{DR,1} = 0$
$G^{(2)}_{1R,2} = +\frac{1}{2\times 0!}\, G^{(2)}_{1R,A}$	$G^{(2)}_{DR,2} = 0$
$G^{(2)}_{1R,3} = 0$	$G^{(2)}_{SQ,3} = -\frac{1}{3\times 1!}\, G^{(2)}_{DR,A}$
$G^{(2)}_{1R,4} = -\frac{1}{4\times 2!}\, G^{(2)}_{1R,B}$	$G^{(2)}_{DR,4} = 0$
$G^{(2)}_{1R,5} = 0$	$G^{(2)}_{SQ,5} = +\frac{1}{5\times 3!}\, G^{(2)}_{DR,B}$
$G^{(2)}_{1R,6} = +\frac{1}{6\times 4!}\, G^{(2)}_{1R,C}$	$G^{(2)}_{DR,6} = 0$
$G^{(2)}_{1R,7} = 0$	$G^{(2)}_{SQ,7} = -\frac{1}{7\times 5!}\, G^{(2)}_{DR,C}$
.	.
.	.
$G^{(2)}_{DQ} = G^{(1)}_{DQ} + \left\{ \frac{1}{2\times 0!}\, G^{(2)}_{1R,A} - \frac{1}{4\times 2!}\, G^{(2)}_{1R,B} + \frac{1}{6\times 4!}\, G^{(2)}_{1R,C} + ... \right\}$	$G^{(2)}_{DR} = \left\{ -\frac{1}{3\times 1!} G^{(2)}_{DR,A} + \frac{1}{5\times 3!}\, G^{(2)}_{DR,B} - \frac{1}{7\times 5!}\, G^{(2)}_{DR,C} + ... \right\}$
$\xi = \left(\frac{\Omega_Q}{4\omega_1}\right) \quad ; \quad C_{(\theta)} = \cos(\theta)$	

CHAPTER-3

EFFECTIVE HAMILTONIANS FOR TRIPLE−QUANTUM (TQ) EXCITATION IN SPIN $I = {}^{3}/_{2}$

Chapter 3

Effective Hamiltonians forTriple Quantum excitation in spin $I = {}^{3}/_{2}$

3.1 Introduction

To further validate the effective Floquet Hamiltonian approach proposed in Chapter-2, we extend the present study for describing NMR experiments involving half-integral quadrupolar nuclear spins. Specifically, we confine our discussion to spin $I = {}^{3}/_{2}$ systems. Although, '^{7}Li' and '^{23}Na' are the most commonly studied spin '$I = {}^{3}/_{2}$' systems, the disparate order of magnitudes in their quadrupolar coupling constants necessitates different experimental strategies for detecting them. For example, the quadrupolar coupling constant in solids for ^{7}Li nucleus ranges from 1 to 50 kHz, while, for ^{23}Na it ranges from 0.5 to 5 MHz[1]. Since, the amplitude of the RF pulse ranges from $10 - 200$ kHz, the optimum conditions of the excitation may vary and deserves a formal theoretical discussion. Here in this chapter we confine our discussion to the excitation of TQ transitions in spin $I = {}^{3}/_{2}$ systems both in isotropic and anisotropic solids. Specifically, we focus our attention to the single-pulse based excitation of Triple-quantum (TQ) transitions in spin I=$^{3}/_{2}$ nucleus.

As described in Figure. 3.1, in the presence of a static external magnetic field (of strength B_0) the frequencies corresponding to the three Single-Quantum (SQ) transitions (corresponding to $|{}^{3}/_{2}\rangle \rightarrow |{}^{1}/_{2}\rangle, |{}^{1}/_{2}\rangle \rightarrow |{}^{-1}/_{2}\rangle, |{}^{-1}/_{2}\rangle \rightarrow |{}^{-3}/_{2}\rangle$) are de-

generate, resulting in a single peak. In the presence of quadrupolar interactions (to first order only) the degeneracy associated with the three SQ transitions is lifted resulting in three peaks (see Fig. 3.1).

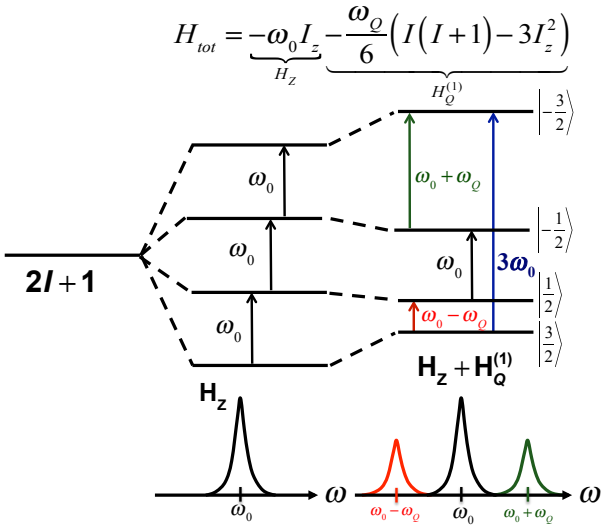

Figure 3.1: Energy level diagram of Spin I=$^3/_2$ depicting the energy shifts due to Zeeman Hamiltonian and the first order quadrupolar Hamiltonian is presented. In the equation of the Hamiltonain ($\hbar = 1$). It is to be noted that the degeneracy of Zeeman NMR signal is lifted due to the presence of electric field gradient due to the quadrupolar Hamiltonian. The Triple Quantum (TQ) transition independent of first order quadrupolar coupling constant is also shown.

As depicted in Figure. 3.1, the SQ transitions corresponding to the states $|^1/_2\rangle \rightarrow |^{-1}/_2\rangle$ is independent of the quadrupolar interaction (first order) and is commonly referred to as the 'Central Transition' (CT) in half-integral quadrupolar spins. The remaining two SQ transitions corresponding to the two pairs of states ($|^3/_2\rangle \rightarrow |^1/_2\rangle$ and $|^{-1}/_2\rangle \rightarrow |^{-3}/_2\rangle$) are referred to as satellite transitions and are dependent on the first-order quadrupolar interactions.

In a powder sample, the quadrupolar interaction is anisotropic resulting in a distribution of quadrupolar coupling constants. Consequently, the NMR peaks corresponding to the two SQ transitions are broadened compromising the spectral resolution. Hence, detection of the central transitions is preferred in NMR studies involving half integral quadrupolar spins. As an alternative, detection of Triple-Quantum (TQ) transitions ($|^3/_2\rangle \rightarrow |^{-3}/_2\rangle$) is also explored in studies involving

spin $^3/_2$ nuclei. Although, both the central and the TQ transitions are independent of the first-order quadrupolar interactions, the higher resolution offered in the MQ domain makes TQ excitation an attractive option for studying systems involving multiple sites. Since TQ transitions are forbidden, a formal understanding of the excitation process is essential for developing new experimental strategies and quantifying experimental data involving spin $I = {}^3/_2$ nuclei.

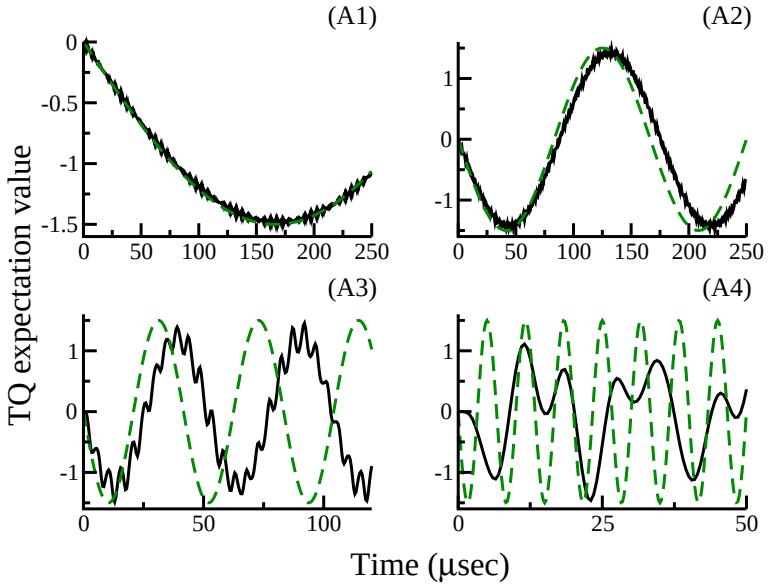

Figure 3.2: Simulations depicting the efficiency of triple quantum (TQ) excitation in spin I=$^3/_2$ (single crystal) derived from analytic[2] (green dotted lines) and numerical (black thick lines) methods.In the simulations depicted, the quadrupole coupling constant ($C_Q = {}^{\omega_Q}/_{\pi}$) is varied A1) C_Q = 2 MHz, A2) C_Q = 1 MHz, A3) C_Q = 500 kHz, A4) C_Q = 200 kHz, employing an excitation pulse of constant RF amplitude, ($^{\omega_1}/_{2\pi}$) = 100 kHz.

To this end, Vega and Naor[2] proposed a theoretical framework for describing MQ transitions in spin I=$^3/_2$ system. Employing the fictitious spin operator algebra[3,4], analytic expression describing the excitation of triple-quantum (TQ) transitions in single crystal was proposed in 1980. A brief illustration of the dependence of the excitation profile on the quadrupolar coupling constants (C_Q) is presented in Figure. 3.2 along with a comparison of their analytic results with exact numerical

simulations emerging from SIMPSON[5–7]. As depicted, the simulations emerging from their analytic results agree only in the strong coupling regime ($C_Q > ({}^{\omega_1}/_{2\pi})$) and deviate when the magnitude of the quadrupolar constant approaches to that of the amplitude of the RF pulse. In contrast to the simulations presented in the spin $I = 1$ studies (Chapter 2), significant derivations are observed even for quadrupolar coupling constants, $C_Q = 500$ kHz (see Panel A3).
To address this discrepancy, the effective Floquet Hamiltonians framework presented in Chapter-2 is employed to explain the TQ excitation in isotropic and anisotropic solids.

3.2 Theory and Simulations

The Hamiltonian in the laboratory frame is transformed into the Zeeman interaction frame ($U_1 = e^{-(i\omega_0 t)I_z}$) ,

$$H_{lab}(t) = \underbrace{-\hbar\omega_0 I_z}_{H_z} \underbrace{-2\hbar\omega_1 \cos(\omega t - \phi_1)\ I_x}_{H_{RF}} \underbrace{-\hbar\Omega_Q T^{(2)0}}_{H_Q} \tag{3.1}$$

$$\begin{aligned}\tilde{H}(t) &= U_1\ H_{lab}(t)\ U_1^{-1} = e^{-(i\omega_0 t)I_z}\ H_{lab}(t)\ e^{(i\omega_0 t)I_z} \\ &= -\hbar\omega_1 \left(i\sqrt{\frac{5}{2}}\right) \left\{ \left(e^{i(\omega-\omega_0)t} + e^{-i(\omega+\omega_0)t}\right) \Phi_1 T^{(1)1} \right. \\ &\qquad \left. - \left(e^{i(\omega+\omega_0)t} + e^{-i(\omega-\omega_0)t}\right) \Phi_1^{-1} T^{(1)-1} \right\} - \hbar\Omega_Q T^{(2)0}\end{aligned} \tag{3.2}$$

Following description in Chapter-2, under secular approximation and the resonance condition $\omega = \omega_0$, the Hamiltonian in the zeeman interaction frame reduces to a much simpler form.

$$\tilde{H} = -\hbar\omega_1 \left(\sqrt{\frac{5}{2}}\right) \left\{ \Phi_1 i T^{(1)1} - \Phi_1^{-1} i T^{(1)-1} \right\} - \hbar\Omega_Q T^{(2)0} \tag{3.3}$$

The definition of the coefficients in the above Hamiltonian is identical to those employed in Chapter-2 ($\Omega_Q = \omega_Q$ for single crystal, and $\Omega_Q = \omega_Q^{(\alpha\beta\gamma)}$ for powder

sample).

3.2.1 TQ excitation in Single Crystal ($\Omega_Q = \omega_Q$)

Regime-I: Strong coupling ($\omega_Q >> \omega_1$)

When the magnitude of the quadrupolar coupling constant exceeds the amplitude of the pulse, 'ω_1', the Hamiltonian in the Zeeman interaction frame[8] (Eq. 3.2) is further transformed into the quadrupolar interaction frame, defined by the transformation operator $U_2 = e^{-\left(i\omega_Q t\right)T^{(2)0}}$.

$$\tilde{\tilde{H}}(t) = U_2\ \tilde{H}(t)\ U_2^{-1} = e^{-\left(i\omega_Q t\right)T^{(2)0}}\ \tilde{H}(t)\ e^{\left(i\omega_Q t\right)T^{(2)0}} \tag{3.4}$$

$$= \tilde{\tilde{H}}_Q + \tilde{\tilde{H}}_{RF}(t) \tag{3.5}$$

Accordingly, the quadrupolar and the RF Hamiltonian get transformed in the Zeeman-Quadrupolar interaction frame.

$$\tilde{\tilde{H}}_Q = \hbar\Delta T^{(2)0} \tag{3.6}$$

$$\begin{aligned}
\tilde{\tilde{H}}_{RF}(t) = &-\hbar\omega_1 \left(\Phi_1 \left(i\sqrt{\frac{2}{5}}\ T^{(1)1} + i\sqrt{\frac{3}{5}}\ T^{(3)1} \right) \right. \\
&\left. +\Phi_1^{-1} \left(-i\sqrt{\frac{2}{5}}\ T^{(1)-1} - i\sqrt{\frac{3}{5}}\ T^{(3)-1} \right) \right) \\
&- \frac{\hbar\omega_1}{2} \left\{ \left(\Phi_1 \left(i\frac{3}{\sqrt{10}}\ T^{(1)1} + \sqrt{\frac{3}{2}}\ T^{(2)1} - i\sqrt{\frac{3}{5}}\ T^{(3)1} \right)\ e^{i\omega_Q t} \right. \right. \\
&\left. +\Phi_1^{-1} \left(-i\frac{3}{\sqrt{10}}\ T^{(1)-1} + \sqrt{\frac{3}{2}}\ T^{(2)-1} + i\sqrt{\frac{3}{5}}\ T^{(3)-1} \right)\ e^{i\omega_Q t} \right) \\
&+ \left(\Phi_1^{-1} \left(-i\frac{3}{\sqrt{10}}\ T^{(1)-1} - \sqrt{\frac{3}{2}}\ T^{(2)-1} + i\sqrt{\frac{3}{5}}\ T^{(3)-1} \right)\ e^{-i\omega_Q t} \right. \\
&\left. \left. +\Phi_1 \left(i\frac{3}{\sqrt{10}}\ T^{(1)1} - \sqrt{\frac{3}{2}}\ T^{(2)1} - i\sqrt{\frac{3}{5}}\ T^{(3)1} \right)\ e^{-i\omega_Q t} \right) \right\}
\end{aligned} \tag{3.7}$$

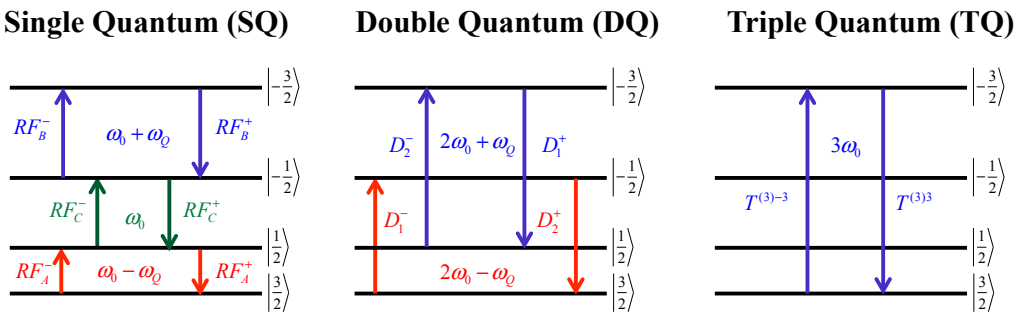

Figure 3.3: Schematic depiction of transitions along with operators for a spin I=$^3/_2$ system

In contrast to the $I = 1$ system, the Hamiltonian depicting the RF pulse in half integral quadrupolar spins comprises of a static term (associated with the central transition) besides the two time-dependent terms (associated with the satellite transitions).

Analogous, to the description in spin $I = 1$ system, the RF Hamiltonian in the Zeeman-Quadrupolar interaction frame is expressed in-terms of operators depicting the possible transitions in the spin $I = {}^3/_2$ systems. A detailed description, of the operators and their relationship with the spherical tensor operators is illustrated in Tables.3.1 and 3.2. Along with the quadrupolar offset term ($\Delta = \omega_Q - \omega_Q^{(\alpha\beta\gamma)}$), the Hamiltonians describing the RF pulse is represented by,

$$H_{pulse}(t) = \tilde{\tilde{H}}_{Q,off} + \tilde{\tilde{H}}_{CT} + \tilde{\tilde{H}}_{ST}(t) \tag{3.8}$$

where,

$$\tilde{\tilde{H}}_{Q,off} = \hbar\Delta T^{(2)0} \tag{3.9}$$

$$\tilde{\tilde{H}}_{CT} = -\hbar\omega_1 \left(\hat{CT}_S\right) \tag{3.10}$$

$$\tilde{\tilde{H}}_{ST}(t) = -\frac{\hbar\omega_1}{2}\left\{\left(\hat{SQ}_S^{(cr)}\right)e^{i\omega_Q t} + \left(\hat{SQ}_S^{(r)}\right)e^{-i\omega_Q t}\right\} \tag{3.11}$$

In the above equation, '$\tilde{\tilde{H}}_{CT}$' represents the Hamiltonian depicting the central transition, while the satellite transitions are represented by '$\tilde{\tilde{H}}_{ST}(t)$'

Table 3.1: Definition of the spin operators corresponding to the possible transitions in a spin $I = {}^3/_2$ system

Operator	Tensoral Operators	Frequency
Zero Coherence Operators		
ZQ_A	$\frac{i}{\sqrt{5}}\left(T^{(1)0} - 2T^{(3)0}\right)$	
ZQ_B	$\frac{i}{\sqrt{5}}\left(2T^{(1)0} + T^{(3)0}\right)$	
ZQ_C	$\frac{i}{\sqrt{5}}\left(T^{(1)0} + 3T^{(3)0}\right)$	
ZQ_D	$\frac{i}{\sqrt{5}}\left(3T^{(1)0} - T^{(3)0}\right)$	
+1 Coherence Operators		
RF_A^+	$i\frac{3}{\sqrt{10}}\,T^{(1)1} + \sqrt{\frac{3}{2}}\,T^{(2)1} - i\sqrt{\frac{3}{5}}\,T^{(3)1}$	$\omega = \omega_0 - \omega_Q$
RF_B^+	$i\frac{3}{\sqrt{10}}\,T^{(1)1} - \sqrt{\frac{3}{2}}\,T^{(2)1} - i\sqrt{\frac{3}{5}}\,T^{(3)1}$	$\omega = \omega_0 + \omega_Q$
RF_C^+	$i\sqrt{\frac{2}{5}}\,T^{(1)1} + i\sqrt{\frac{3}{5}}\,T^{(3)1}$	$\omega = \omega_0$
-1 Coherence Operators		
RF_A^-	$-i\frac{3}{\sqrt{10}}\,T^{(1)-1} - \sqrt{\frac{3}{2}}\,T^{(2)-1} + i\sqrt{\frac{3}{5}}\,T^{(3)-1}$	$\omega = \omega_0 - \omega_Q$
RF_B^-	$-i\frac{3}{\sqrt{10}}\,T^{(1)-1} + \sqrt{\frac{3}{2}}\,T^{(2)-1} + i\sqrt{\frac{3}{5}}\,T^{(3)-1}$	$\omega = \omega_0 + \omega_Q$
RF_C^-	$-i\sqrt{\frac{2}{5}}\,T^{(1)-1} - i\sqrt{\frac{3}{5}}\,T^{(3)-1}$	$\omega = \omega_0$
+2 Coherence Operators		
D_1^+	$T^{(2)2} + i\,T^{(3)2}$	$\omega = 2\omega_0 + \omega_Q$
D_2^+	$T^{(2)2} - i\,T^{(3)2}$	$\omega = 2\omega_0 - \omega_Q$
-2 Coherence Operators		
D_1^-	$T^{(2)-2} - i\,T^{(3)-2}$	$\omega = 2\omega_0 - \omega_Q$
D_2^-	$T^{(2)-2} + i\,T^{(3)-2}$	$\omega = 2\omega_0 + \omega_Q$
+3 Coherence Operators		
T^+	$T^{(3)3}$	$\omega = 3\omega_0$
-3 Coherence Operators		
T^-	$T^{(3)-3}$	$\omega = 3\omega_0$

Table 3.2: Symmetric and Anti-symmetric combination of spin operators employed in spin $I = {}^3/_2$ system

Operator	Combination	Operator	Combination
$\hat{CT}_S$	$\left(\Phi_1 RF_C^+ + \Phi_1^{-1} RF_C^-\right)$	$\hat{CT}_{AS}$	$\left(\Phi_1 RF_C^+ - \Phi_1^{-1} RF_C^-\right)$
$\hat{SQ}_S^{(r)}$	$\left(\Phi_1^{-1} RF_A^- + \Phi_1 RF_B^+\right)$	$\hat{SQ}_{AS}^{(r)}$	$\left(\Phi_1^{-1} RF_A^- - \Phi_1 RF_B^+\right)$
$\hat{SQ}_S^{(cr)}$	$\left(\Phi_1 RF_A^+ + \Phi_1^{-1} RF_B^-\right)$	$\hat{SQ}_{AS}^{(cr)}$	$\left(\Phi_1 RF_A^+ - \Phi_1^{-1} RF_B^-\right)$
$\hat{D}_S^{(r)}$	$\left(\Phi_1^2 D_1^+ + \Phi_1^{-2} D_1^-\right)$	$\hat{D}_{AS}^{(r)}$	$\left(\Phi_1^2 D_1^+ - \Phi_1^{-2} D_1^-\right)$
$\hat{D}_S^{(cr)}$	$\left(\Phi_1^2 D_2^+ + \Phi_1^{-2} D_2^-\right)$	$\hat{D}_{AS}^{(cr)}$	$\left(\Phi_1^2 D_2^+ - \Phi_1^{-2} D_2^-\right)$
$\hat{T}_S$	$\left(\Phi_1^3 T^+ + \Phi_1^{-3} T^-\right)$	$\hat{T}_{AS}$	$\left(\Phi_1^3 T^+ - \Phi_1^{-3} T^-\right)$

Following the procedure described in Chapter-2, the above time-dependent Hamiltonian is transformed into a time-independent Floquet Hamiltonian[8–16].

$$H_F = \omega_Q I_F + \hbar\Delta \left(T^{(2)0}\right)_0 - \hbar\omega_1 \left(\hat{CT}_S\right)_0 - \frac{\hbar\omega_1}{2}\left\{\left(\hat{SQ}_S^{(cr)}\right)_{-1} + \left(\hat{SQ}_S^{(r)}\right)_{+1}\right\} \tag{3.12}$$

In contrast to the spin $I = 1$ description, the modulation frequency in the spin $I = {}^3/_2$ differs (equals to ω_Q) and could be deduced from the energy level diagram depicted in Figure.3.1.

To facilitate the derivation of effective Hamiltonians, the Floquet Hamiltonian (Eq.3.12) is re-expressed interms of zero-order (H_0) and perturbing Hamiltonian (H_1).

$$H_F = H_0 + H_1 \tag{3.13}$$

$$H_0 = \omega_Q I_F + \hbar\Delta \left(T^{(2)0}\right)_0 \tag{3.14}$$

The perturbing Hamiltonian in the present study comprises of both diagonal and

off-diagonal terms.

$$H_1 = H_{1,d} + H_{1,od}$$
$$H_{1,d} = -\omega_1 \left(\hat{CT}_S\right)_0; \quad H_{1,od} = -\frac{\omega_1}{2}\left\{\left(\hat{SQ}_S^{(r)}\right)_{+1} + \left(\hat{SQ}_S^{(cr)}\right)_{-1}\right\} \tag{3.15}$$

Such a choice of grouping of the spin Hamiltonians is problem specific and its validity could only be verified through a comparison with exact numerical simulations. The above classification is equally valid for all half-integral quadrupolar systems. Employing the transformation function 'S_1'[17–20], the original untransformed Floquet Hamiltonian (Eq. 3.12) is transformed through a unitary transformation illustrated below.

$$H_{eff} = e^{i\lambda S_1}\ H_F\ e^{-i\lambda S_1} \tag{3.16}$$
$$S_1 = \ C_{SQ}^{(1)}\left\{\left(\hat{SQ}_S^{(r)}\right)_{+1} - \left(\hat{SQ}_S^{(cr)}\right)_{-1}\right\} \tag{3.17}$$

where,

$$C_{SQ}^{(1)} = -i\left(\frac{\omega_1}{2\Omega_Q}\right) \tag{3.18}$$

To first-order, the effective Hamiltonian comprises of only '$H_{1,d}$'

$$H_1^{(1)} = -\omega_1\left(\hat{CT}_S\right)_0 \tag{3.19}$$

Subsequently, through Baker-Campbell-Hausdorff (BCH) expansion[21], the higher-order corrections to the effective Hamiltonian are derived. In the notation, '$H_n^{(1)}$' represents the n^{th} order corrections obtained from the first transformation, 'S_1'. In the present problem, the higher order corrections mainly arise from commutator expressions involving the transformation function 'S_1' and the perturbing Hamiltonian ('$H_{1,d}$' and '$H_{1,od}$'). The commutator of the transformation function 'S_1'

with '$H_{1,d}$' to various orders could be derived through the expression.

$$H^{(1)}_{n,d} = \sum_{n=1}^{\infty} \frac{(i)^{n-1}}{(n-1)!} \left[\underbrace{[S_1, \ldots\ldots\ldots\ldots [S_1}_{n-1}, H_{1,d}\,] \ldots\ldots\ldots\ldots] \right] \tag{3.20}$$

In a similar vein, the commutator of 'S_1' with '$H_{1,od}$' is derived through the general expression given below

$$H^{(1)}_{n,od} = \sum_{n=2}^{\infty} \frac{(i)^{n-1}}{n \times (n-2)!} \left[\underbrace{[S_1, \ldots\ldots\ldots\ldots [S_1}_{n-1}, H_{1,od}\,] \ldots\ldots\ldots\ldots] \right] \tag{3.21}$$

A detailed description of the commutator relations involving the transformation function 'S_1' and 'H_1' to various orders of 'λ' are tabulated in Table 3.3 and 3.4. To illustrate the importance of the perturbation corrections, a systematic study similar to the one described in Chapter-2 was carried out to understand the role of these terms in the TQ excitation process. As illustrated in Tables. 3.3, 3.4, the higher order contributions mainly arise from the (diagonal arising from ZQ ($T^{(2)0}$), CT $\left(\hat{CT}_S\right)$ and TQ $\left(\hat{T}_{AS}\right)$) and off-diagonal (from SQ $\left(\hat{SQ}^{(r,cr)}_S\right)_{\pm 1}$ and DQ $\left(\hat{D}^{(r,cr)}_S\right)_{\pm 1}$) operators. A pedagogical description illustrating the role of the higher order corrections is discussed in the following sections.

I. Effective Hamiltonians from first transformation, 'S_1'

To begin with, let the general form of the effective Hamiltonian (comprising of diagonal corrections only) resulting from a single transformation be represented by,

$$\begin{aligned} H_{eff} &= e^{i\lambda S_1}\ H_F\ e^{-i\lambda S_1} \\ &= \omega_Q I_F + G^{(1)}_{CT}\left(\hat{CT}_S\right)_0 + i\ G^{(1)}_{TQ}\left(\hat{T}_{AS}\right)_0 + G^{(1)}_{ZQ}\left(T^{(2)0}\right)_0 \end{aligned} \tag{3.22}$$

In the above equation, '$G^{(1)}_{CT}$' denotes the coefficients (obtained from the first transformation, denoted by the superscript) corresponding to the central transition operator. The contributions from the various higher orders (N_1 denotes the desired order, power of λ) are included in $G^{(1)}_{CT}$.

Table 3.3: Description of higher order (diagonal and off-diagonal) contributions to the effective Hamiltonian derived from the first transformation

n^{th} **order**	**Coefficients in the Effective Hamiltonian**	
Correction	$H_{eff} = H_1^{(1)} + H_3^{(1)} + H_5^{(1)} + \cdots = \sum_{j=0}^{N_1} G_{CT,j}^{(1)} \left(\hat{CT}_S\right)_0 + \sum_{j=0}^{N_1} i\ G_{TQ,j}^{(1)} \left(\hat{T}_{AS}\right)_0$	
	Expression from the '$H_{1,d}$' term	**Non-zero 'G' Coefficients**
Zero order (λ^0)	$H_0^{(1)} = 0$	
I order (λ^1)	$H_1^{(1)} = H_{1,d} = -\omega_1 \left(\hat{CT}_S\right)_0$	$G_{CT,1}^{(1)} \left(\hat{CT}_S\right)_0$
II order (λ^2)	$H_2^{(1)} = i\,[S_1, H_{1,d}] = -\frac{\omega_1}{2\sqrt{2}}(\theta)\left\{\left(\hat{D}_S^{(r)}\right)_{+1} + \left(\hat{D}_S^{(cr)}\right)_{-1}\right\}$	$G_{DQ,2}^{(1)} \left\{\left(\hat{D}_S^{(r)}\right)_{+1} + \left(\hat{D}_S^{(cr)}\right)_{-1}\right\}$
III order (λ^3)	$H_3^{(1)} = -\frac{1}{2!}[S_1, [S_1, H_{1,d}]] = \frac{1}{2!}\left(\frac{\omega_1}{2}\right)(\theta)^2 \left\{\left(\hat{CT}_S\right)_0 + i\left(\hat{T}_{AS}\right)_0\right\}$	$G_{CT,3}^{(1)} \left(\hat{CT}_S\right)_0 + iG_{TQ,3}^{(1)} \left(\hat{T}_{AS}\right)_0$
IV order (λ^4)	$H_4^{(1)} = -\frac{i}{3!}[S_1, [S_1, [S_1, H_{1,d}]]] = \frac{1}{3!}\left(\frac{\omega_1}{2\sqrt{2}}\right)(\theta)^3 \left\{\left(\hat{D}_S^{(r)}\right)_{+1} + \left(\hat{D}_S^{(cr)}\right)_{-1}\right\}$	$G_{DQ,4}^{(1)} \left\{\left(\hat{D}_S^{(r)}\right)_{+1} + \left(\hat{D}_S^{(cr)}\right)_{-1}\right\}$
V order (λ^5)	$H_5^{(1)} = \frac{1}{4!}[S_1, [S_1, [S_1, [S_1, H_{1,d}]]]] = -\frac{1}{4!}\left(\frac{\omega_1}{2}\right)(\theta)^4 \left\{\left(\hat{CT}_S\right)_0 + i\left(\hat{T}_{AS}\right)_0\right\}$	$G_{CT,5}^{(1)} \left(\hat{CT}_S\right)_0 + iG_{TQ,5}^{(1)} \left(\hat{T}_{AS}\right)_0$
VI order (λ^6)	$H_6^{(1)} = \frac{i}{5!}[S_1, [S_1, [S_1, [S_1, [S_1, H_{1,d}]]]]] = -\frac{1}{5!}\left(\frac{\omega_1}{2\sqrt{2}}\right)(\theta)^5 \left\{\left(\hat{D}_S^{(r)}\right)_{+1} + \left(\hat{D}_S^{(cr)}\right)_{-1}\right\}$	$G_{DQ,6}^{(1)} \left\{\left(\hat{D}_S^{(r)}\right)_{+1} + \left(\hat{D}_S^{(cr)}\right)_{-1}\right\}$
VII order (λ^7)	$H_7^{(1)} = -\frac{1}{6!}[S_1, [S_1, [S_1, [S_1, [S_1, [S_1, H_{1,d}]]]]]] = \frac{1}{6!}\left(\frac{\omega_1}{2}\right)(\theta)^6 \left\{\left(\hat{CT}_S\right)_0 + i\left(\hat{T}_{AS}\right)_0\right\}$	$G_{CT,7}^{(1)} \left(\hat{CT}_S\right)_0 + iG_{TQ,7}^{(1)} \left(\hat{T}_{AS}\right)_0$
$\theta = \left(\frac{\sqrt{3}\omega_1}{\Omega_Q}\right)$		

Table 3.4: Description of higher order (diagonal and off-diagonal) contributions to the effective Hamiltonian derived from the first transformation

n^{th} **order Correction**	**Coefficients in the Effective Hamiltonian** $H_{eff} = H_0^{(1)} + H_2^{(1)} + H_4^{(1)} + H_6^{(1)} + \cdots = \omega_Q I_F + \sum_{i=0}^{N_1} G_{ZQ,i}^{(1)} \left(T^{(2)0}\right)_0$	
	Expression from the '$H_{1,od}$' term	**Non-zero 'G' Coefficients**
Zero order (λ^0)	$H_0^{(1)} = \omega_Q I_F + (\Delta) \left(T^{(2)0}\right)_0$	$\omega_Q I_F + G_{ZQ,0}^{(1)} \left(T^{(2)0}\right)_0$
I order (λ^1)	$H_1^{(1)} = 0$	
II order (λ^2)	$H_2^{(1)} = \frac{i}{2 \times 0!}[S_1, H_{1,od}] = -\frac{1}{2 \times 0!}\, \Omega_Q \left(\theta\right)^2 \left(T^{(2)0}\right)_0$	$G_{ZQ,2}^{(1)} \left(T^{(2)0}\right)_0$
III order (λ^3)	$H_3^{(1)} = -\frac{1}{3 \times 1!}[S_1, [S_1, H_{1,od}]] = \frac{1}{3 \times 1!} \left(\frac{\omega_1}{2}\right) \left(\theta\right)^2 \left\{ \left(\hat{SQ}_S^{(r)}\right)_{+1} + \left(\hat{SQ}_S^{(cr)}\right)_{-1} \right\}$	$G_{SQ,3}^{(1)} \left\{ \left(\hat{SQ}_S^{(r)}\right)_{+1} + \left(\hat{SQ}_S^{(cr)}\right)_{-1} \right\}$
IV order (λ^4)	$H_4^{(1)} = -\frac{i}{4 \times 2!}[S_1, [S_1, [S_1, H_{1,od}]]] = +\frac{1}{4 \times 2!}\, \Omega_Q \left(\theta\right)^4 \left(T^{(2)0}\right)_0$	$G_{ZQ,4}^{(1)} \left(T^{(2)0}\right)_0$
V order (λ^5)	$H_5^{(1)} = \frac{1}{5 \times 3!}[S_1, [S_1, [S_1, [S_1, H_{1,od}]]]] = -\frac{1}{5 \times 3!} \left(\frac{\omega_1}{2}\right) \left(\theta\right)^4 \left\{ \left(\hat{SQ}_S^{(r)}\right)_{+1} + \left(\hat{SQ}_S^{(cr)}\right)_{-1} \right\}$	$G_{SQ,5}^{(1)} \left\{ \left(\hat{SQ}_S^{(r)}\right)_{+1} + \left(\hat{SQ}_S^{(cr)}\right)_{-1} \right\}$
VI order (λ^6)	$H_6^{(1)} = \frac{i}{6 \times 4!}[S_1, [S_1, [S_1, [S_1, [S_1, H_{1,od}]]]]] = -\frac{1}{6 \times 4!}\, \Omega_Q \left(\theta\right)^6 \left(T^{(2)0}\right)_0$	$G_{ZQ,6}^{(1)} \left(T^{(2)0}\right)_0$
VII order (λ^7)	$H_7^{(1)} = -\frac{1}{7 \times 5!}[S_1, [S_1, [S_1, [S_1, [S_1, [S_1, H_{1,od}]]]]]] = \frac{1}{7 \times 5!} \left(\frac{\omega_1}{2}\right) \left(\theta\right)^6 \left\{ \left(\hat{SQ}_S^{(r)}\right)_{+1} + \left(\hat{SQ}_S^{(cr)}\right)_{-1} \right\}$	$G_{SQ,7}^{(1)} \left\{ \left(\hat{SQ}_S^{(r)}\right)_{+1} + \left(\hat{SQ}_S^{(cr)}\right)_{-1} \right\}$
$\theta = \left(\frac{\sqrt{3}\omega_1}{\Omega_Q}\right)$		

In a similar vein, '$G^{(1)}_{TQ}$' represents the corrections corresponding to the TQ operator, while '$G^{(1)}_{ZQ}$' denotes the corrections to the second rank ZQ operator. A detailed description of the coefficients illustrating the contributions from various orders is listed in Appendix.B.1 (Table.B.1.2)

$$G^{(1)}_{CT} = \sum_{i=0}^{N_1} G^{(1)}_{CT,i} \quad ; \quad G^{(1)}_{TQ} = \sum_{i=0}^{N_1} G^{(1)}_{TQ,i} \quad ; \quad G^{(1)}_{ZQ} = \sum_{i=0}^{N_1} G^{(1)}_{ZQ,i}$$

$$G^{(1)}_{CT} = -\left(\frac{\omega_1}{2}\right)\left\{C_{(\theta)} + 1\right\} \quad ; \tag{3.23}$$

$$G^{(1)}_{TQ} = -\left(\frac{\omega_1}{2}\right)\left\{C_{(\theta)} - 1\right\} \quad ; \tag{3.24}$$

$$G^{(1)}_{ZQ} = \Delta + (\Omega_Q)\left\{-\frac{1}{2\times 0!}(\theta)^2 + \frac{1}{4\times 2!}(\theta)^4 - \frac{1}{6\times 4!}(\theta)^6 + ...\right\} \tag{3.25}$$

To have a consistent description, the initial density operator ($\rho_F(0) = (I_z)_0$) along with the detection operator '$T^{(3)-3}$,' (corresponding to TQ transition) is transformed by the transformation function 'S_1.' The transformed initial density operator and the detection operators are illustrated below.

$$\begin{aligned}\tilde{\rho}_F(0) &= e^{i\lambda S_1}\ \rho_F(0)\ e^{-i\lambda S_1} \\ &= R^{(1)}_{Iz}\ (I_z)_0 + R^{(1)}_{ZQA}\,(ZQ_A)_0 + R^{(1)}_{SQ}\ S_{(\theta)}\left\{\left(\hat{SQ}^{(r)}_{AS}\right)_{+1} + \left(\hat{SQ}^{(cr)}_{AS}\right)_{-1}\right\}\end{aligned} \tag{3.26}$$

$$\begin{aligned}\tilde{T}^{(3)-3}_F &= e^{i\lambda S_1}\ T^{(3)-3}_F\ e^{-i\lambda S_1} \\ &= e^{3i\omega_0 t_2}\ \Phi_R\left\{P^{(1)}_{TQ}\left(T^{(3)-3}\right)_0 + P^{(1)}_{CT}\left(\Phi_1^2 RF^-_C\right)_0\right. \\ &\qquad \left. + P^{(1)}_{DQ}\left\{\left(\Phi_1 D^-_1\right)_{+1} + \left(\Phi_1 D^-_2\right)_{-1}\right\}\right\}\end{aligned} \tag{3.27}$$

A detailed description of the 'R' and 'P' coefficients are illustrated in Table. B.1.1. Subsequently, employing the proposed effective Floquet Hamiltonian (Eq. 3.22), the evolution of the density operator during pulse is evaluated.

$$\tilde{\rho}_F(t_{p1}) = \ exp\left(\frac{-iH_{eff}t_{p1}}{\hbar}\right)\ \tilde{\rho}_F(0)\ exp\left(\frac{iH_{eff}t_{p1}}{\hbar}\right) \tag{3.28}$$

A detailed description of this calculation along with coefficients is illustrated in Appendix.B.1. Based on the above calculations, the TQ signal observed is calculated using the expression given below.

$$\left\langle T^{(3)-3}(t_{p1})\right\rangle = Tr\left[\rho_F(t_{p1}).T_F^{(3)-3}\right] = -\frac{3}{2}\left(\Phi_1^3\Phi_R\right)\sin\left(\frac{3\omega_1^3 t_{p1}}{2\Omega_Q^2}\right) \quad (3.29)$$

As represented in Tables. 3.3, and 3.4, the diagonal corrections to odd-orders result from cross-terms between the SQ (satellite) and DQ transitions operators and are expressed in terms of the central (CT) and triple quantum (TQ) operators. In a similar vein, the diagonal corrections to even order results from cross terms between the SQ satellite transition operators and are represented through the '$T^{(2)0}$' operator.To illustrate the role of the higher order corrections in the exactness of the proposed approach, a systematic study incorporating their contributions is discussed below.

In Figure.3.4, the TQ excitation in spin $I = {}^3/_2$ is depicted for quadrupolar coupling constants ranging from 2 MHz - 200 kHz. Along the first row (panels A1 $\rightarrow$ A4) diagonal corrections to order λ^2 have been incorporated, while, diagonal corrections to n^{th} order have been included in the simulations depicted in the second row (Panels B1 $\rightarrow$ B4).

As depicted, when the magnitude of the quadrupolar frequecy (ω_Q) largely exceeds the amplitude of the RF pulse, the analytic simulations are in excellent agreement with those obtained from SIMPSON. In the extreme strong coupling limit, the TQ signal in Eq. B.1.9 reduces to the familiar form proposed by Vega and Naor[2].

$$\left\langle T^{(3)-3}(t_{p1})\right\rangle = -\frac{3}{2}\sin\left(\frac{3\omega_1^3 t_{p1}}{2\Omega_Q^2}\right) \quad (3.30)$$

However, with decreasing magnitudes of the quadrupolar frequency, the discrepancy between the analytic and numerical simulations increases and is maximum when the magnitude of the quadrupolar frequency is equal to the RF amplitude.

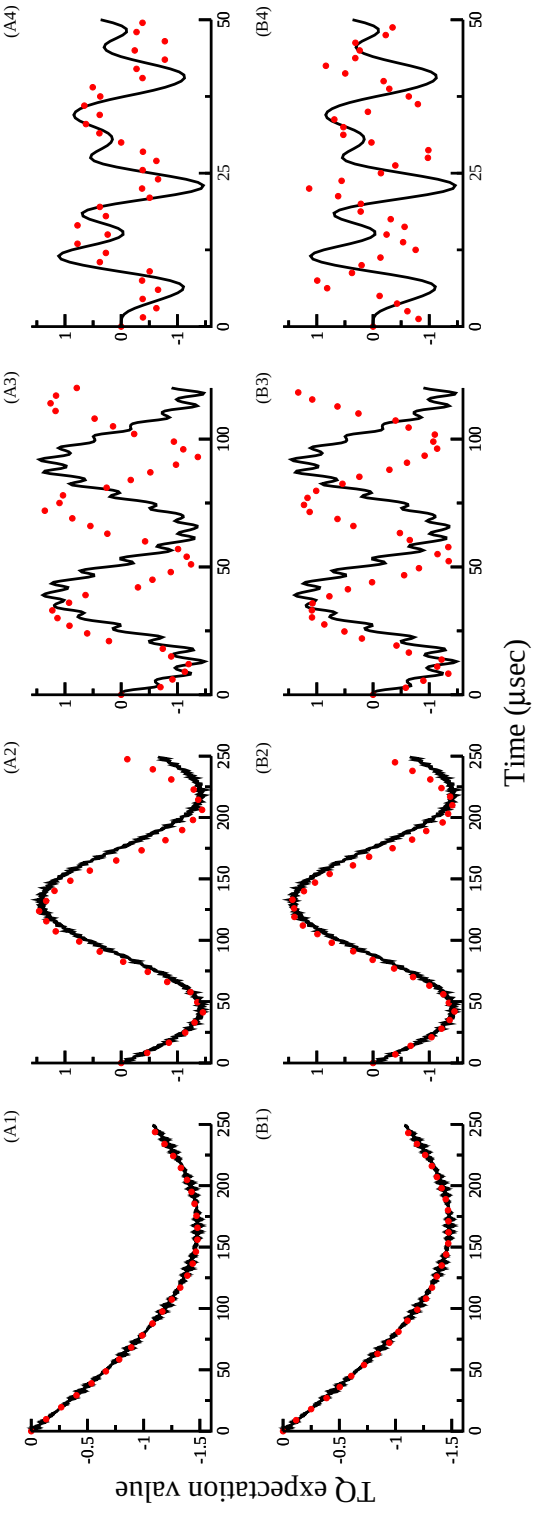

Figure 3.4: Comparison of numerical (black thick line) and analytic simulations (red dots) based on effective Hamiltonians derived from a single transformation comprising of diagonal corrections to order $\lambda^3(N_1 = 3)$ (from Panels A1 $\rightarrow$ A4) and to the order $\lambda^n(N_1 > 3)$ (from Panels B1 $\rightarrow$ B4) . In the simulations depicted, the quadrupole coupling constant ($C_Q = {}^{\omega_Q}/_{\pi}$) is varied A1, B1) $C_Q = 2$ MHz, A2, B2) $C_Q = 1$ MHz, A3, B3) $C_Q = 500$ kHz, A4, B4) $C_Q = 200$ kHz, employing an excitation pulse of constant RF amplitude, $({}^{\omega_1}/_{2\pi}) = 100$ kHz. The simulations correspond to a single crystal.

To address this aspect, effective Hamiltonians comprising of diagonal contributions to (n^{th} order) were employed in the simulations depicted in the second row (Panels B1 $\rightarrow$ B4) Figure. 3.4. As depicted, the discrepancy still prevails in panels A3 and A4, despite the inclusion of higher order diagonal corrections. Hence, the residual off-diagonal terms ignored from the first transformation could play an important role in the excitation process.

II. Effective Hamiltonians from second transformation, 'S_2'

To resolve the discrepancy observed in the analytic simulations, the role of residual off-diagonal terms neglected in the first transformation were considered in the calculations. As depicted in Tables. 3.3 and 3.4, the off-diagonal contributions comprise of the double-quantum (DQ) and single-quantum (SQ) satellite transitions operators. To fold the off-diagonal contributions, a second transformation function 'S_2' is employed. The diagonal corrections from the first transformation are included along 'H_0', while, the off-diagonal operators $\left(\left(\hat{SQ}\right)_{\pm 1} and \left(\hat{D}\right)_{\pm 1}\right)$ forms the perturbation H_1.

$$H_0 = \omega_Q I_F + G^{(1)}_{CT}\left(\hat{CT}_S\right)_0 + i\, G^{(1)}_{TQ}\left(\hat{T}_{AS}\right)_0 + G^{(1)}_{ZQ}\left(T^{(2)0}\right)_0 \tag{3.31}$$

$$H_1 = G^{(1)}_{SQ}\left\{\left(\hat{SQ}^{(r)}_S\right)_{+1} + \left(\hat{SQ}^{(cr)}_S\right)_{-1}\right\} + G^{(1)}_{DQ}\left\{\left(\hat{D}^{(r)}_S\right)_{+1} + \left(\hat{D}^{(cr)}_S\right)_{-1}\right\} \tag{3.32}$$

As depicted in Tables. 3.3 and 3.4, the coefficient of '$G^{(1)}_{SQ}$' corresponding to the operators $\left\{\left(\hat{SQ}^{(r,cr)}_S\right)_{\pm 1}\right\}$ results from 'odd-order' terms depicted in Table. 3.4 (commutator between S_1 and $H_{1,od}$; $[S_1, H_{1,od}]$). In a similar vein, the coefficient of '$G^{(1)}_{DQ}$' corresponding to the $\left\{\left(\hat{D}^{(r,cr)}_S\right)_{\pm 1}\right\}$ operator results from the 'even-order' terms depicted in Table. 3.3 (commutator between S_1 and $H_{1,d}$; $[S_1, H_{1,d}]$).
Depending on the desired level of accuracy, the off-diagonal contributions (denoted by the value of 'N_1') to the above operators cound be incorporated based on

Tables.3.3 and 3.4.

$$G^{(1)}_{SQ} = \sum_{i=0}^{N_1} G^{(1)}_{SQ,i} = + \left(\frac{\omega_1}{2}\right) \left\{ \frac{1}{3 \times 1!} (\theta)^2 - \frac{1}{5 \times 3!} (\theta)^4 + \frac{1}{7 \times 5!} (\theta)^6 - .... \right\} \tag{3.33}$$

$$G^{(1)}_{DQ} = \sum_{i=0}^{N_1} G^{(1)}_{DQ,i} = - \left(\frac{\omega_1}{2\sqrt{2}}\right) S_{(\theta)} \tag{3.34}$$

Employing the transformation function 'S_2', the off-diagonal term in H_1 (Eq. 3.32) are folded

$$S_2 = C^{(2)}_{SQ'} \left\{ \left(\hat{SQ}^{(r)}_S\right)_{+1} - \left(\hat{SQ}^{(cr)}_S\right)_{-1} \right\} + C^{(2)}_{DQ'} \left\{ \left(\hat{D}^{(r)}_S\right)_{+1} - \left(\hat{D}^{(cr)}_S\right)_{-1} \right\} \tag{3.35}$$

$$\begin{aligned} C^{(2)}_{SQ'} &= \frac{i}{\sqrt{3}} \left(\frac{\sqrt{2}\, G^{(1)}_{DQ} \left(G^{(1)}_{CT} + G^{(1)}_{TQ}\right) + \sqrt{3}\, G^{(1)}_{SQ} \left(G^{(1)}_{ZQ} - \omega_Q\right)}{\left(G^{(1)}_{CT} + G^{(1)}_{TQ}\right)^2 - \left(G^{(1)}_{ZQ} - \omega_Q\right)^2} \right) \\ C^{(2)}_{DQ'} &= \frac{i}{\sqrt{2}} \left(\frac{\sqrt{3}\, G^{(1)}_{SQ} \left(G^{(1)}_{CT} + G^{(1)}_{TQ}\right) + \sqrt{2}\, G^{(1)}_{DQ} \left(G^{(1)}_{ZQ} - \omega_Q\right)}{\left(G^{(1)}_{CT} + G^{(1)}_{TQ}\right)^2 - \left(G^{(1)}_{ZQ} - \omega_Q\right)^2} \right) \end{aligned} \tag{3.36}$$

$$C^{(i+1)}_{SQ} = \sum_{i=1}^{n-1} C^{(i+1)}_{SQ'} \quad ; \quad C^{(i+1)}_{DQ} = \sum_{i=1}^{n-1} C^{(i+1)}_{DQ'} \tag{3.37}$$

In Eq. 3.37, 'i' takes values from 1 to '$n-1$', where 'n' is the number of 'S' transformations applied (Here $n = 2$).

A general expression illustrating the various contributions could be derived using the general expression presented below.

$$H^{(2)}_n = \sum_{n=2}^{\infty} \frac{(i)^{n-1}}{n \times (n-2)!} \left[\underbrace{[S_2, ... [S_2}_{n-1}, H_1\,] .....] \right] \tag{3.38}$$

Table 3.5: Description of the higher order (diagonal and off-diagonal) contributions to the effective Hamiltonian (Eq. 3.39) derived from second transformation

n^{th} order	Coefficients in the Effective Hamiltonian	
Correction	$H_{eff} = H_0^{(1)} + H_2^{(1)} + H_4^{(1)} + H_6^{(1)} + \cdots = \omega_Q I_F + G_{CT}^{(1)}\left(\hat{CT}_S\right)_0 + i\, G_{TQ}^{(1)}\left(\hat{T}_{AS}\right)_0 + G_{ZQ}^{(2)}\left(T^{(2)0}\right)_0$	
	Expression from the '$H_{1,od}$' term	**Non-zero 'G' Coefficients**
Zero order (λ^0)	$H_0^{(2)} = \omega_Q I_F + G_{CT}^{(1)}\left(\hat{CT}_S\right)_0 + i\, G_{TQ}^{(1)}\left(\hat{T}_{AS}\right)_0 + G_{ZQ}^{(1)}\left(T^{(2)0}\right)_0$	$\omega_Q I_F + G_{CT}^{(1)}\left(\hat{CT}_S\right)_0 + i\, G_{TQ}^{(1)}\left(\hat{T}_{AS}\right)_0 + G_{ZQ}^{(1)}\left(T^{(2)0}\right)_0$
I order (λ^1)	$H_1^{(2)} = 0$	
II order (λ^2)	$H_2^{(2)} = \frac{i}{2\times 0!}[S_2, H_1] = +\left(\frac{i}{2\times 0!}\right)\underbrace{\left\{\frac{12\, C_{SQ}^{(2)}\, G_{SQ}^{(1)} + 8\, C_{DQ}^{(2)}\, G_{DQ}^{(1)}}{G_{ZQ,A}^{(2)}}\right\}}\left(T^{(2)0}\right)_0 \underbrace{-2\sqrt{6}\left(C_{SQ}^{(2)}\, G_{DQ}^{(1)} + C_{DQ}^{(2)}\, G_{SQ}^{(1)}\right)}_{G_{CTQ,A}^{(2)}}\left\{\left(\hat{CT}_S\right)_0 + i\left(\hat{T}_{AS}\right)_0\right\}$	$G_{ZQ,2}^{(2)}\ \left(T^{(2)0}\right)_0 + G_{CT,2}^{(2)}\left(\hat{CT}_S\right)_0 + i\, G_{TQ,2}^{(2)}\left(\hat{T}_{AS}\right)_0$
III order (λ^3)	$H_3^{(2)} = -\frac{1}{3\times 1!}[S_2, [S_2, H_1]] = +\left(\frac{1}{3\times 1!}\right)\Bigg\{-\underbrace{\left(C_{SQ}^{(2)}\, G_{ZQ,A}^{(2)} - 2\sqrt{\frac{2}{3}}\, C_{DQ}^{(2)}\, G_{CTQ,A}^{(2)}\right)}_{G_{SQ,A}^{(2)}}\left\{\left(\hat{SQ}_S^{(r)}\right)_{+1} + \left(\hat{SQ}_S^{(cr)}\right)_{-1}\right\} - \underbrace{\left(-\sqrt{6}\, C_{SQ}^{(2)}\, G_{CTQ,A}^{(2)} + C_{DQ}^{(2)}\, G_{ZQ,A}^{(2)}\right)}_{G_{DQ,A}^{(2)}}\left\{\left(\hat{D}_S^{(r)}\right)_{+1} + \left(\hat{D}_S^{(cr)}\right)_{-1}\right\}\Bigg\}$	$G_{SQ,3}^{(2)}\left\{\sum\left(\hat{SQ}_S^{(r/cr)}\right)_{\pm 1}\right\} + G_{DQ,3}^{(2)}\left\{\sum\left(\hat{D}_S^{(r/cr)}\right)_{\pm 1}\right\}$
IV order (λ^4)	$H_4^{(2)} = -\frac{i}{4\times 2!}[S_2, [S_2, [S_2, H_1]]] = -\left(\frac{i}{4\times 2!}\right)\Bigg\{\underbrace{\left(12\, C_{SQ}^{(2)}\, G_{SQ,A}^{(2)} + 8\, C_{DQ}^{(2)}\, G_{DQ,A}^{(2)}\right)}_{G_{ZQ,B}^{(2)}}\left(T^{(2)0}\right)_0 \underbrace{-2\sqrt{6}\left(C_{SQ}^{(2)}\, G_{DQ,A}^{(2)} + C_{DQ}^{(2)}\, G_{SQ,A}^{(2)}\right)}_{G_{CTQ,B}^{(2)}}\left\{\left(\hat{CT}_S\right)_0 + i\left(\hat{T}_{AS}\right)_0\right\}\Bigg\}$	$G_{ZQ,4}^{(2)}\ \left(T^{(2)0}\right)_0 + G_{CT,4}^{(2)}\left(\hat{CT}_S\right)_0 + i\, G_{TQ,4}^{(2)}\left(\hat{T}_{AS}\right)_0$
V order (λ^5)	$H_5^{(2)} = \frac{1}{5\times 3!}[S_2, [S_2, [S_2, [S_2, H_1]]]] = -\left(\frac{1}{5\times 3!}\right)$	
	$\Bigg\{-\underbrace{\left(C_{SQ}^{(2)}\, G_{ZQ,B}^{(2)} - 2\sqrt{\frac{2}{3}}\, C_{DQ}^{(2)}\, G_{CTQ,B}^{(2)}\right)}_{G_{SQ,B}^{(2)}}\left\{\left(\hat{SQ}_S^{(r)}\right)_{+1} + \left(\hat{SQ}_S^{(cr)}\right)_{-1}\right\} - \underbrace{\left(-\sqrt{6}\, C_{SQ}^{(2)}\, G_{CTQ,B}^{(2)} + C_{DQ}^{(2)}\, G_{ZQ,B}^{(2)}\right)}_{G_{DQ,B}^{(2)}}\left\{\left(\hat{D}_S^{(r)}\right)_{+1} + \left(\hat{D}_S^{(cr)}\right)_{-1}\right\}\Bigg\}$	$G_{SQ,5}^{(2)}\left\{\sum\left(\hat{SQ}_S^{(r/cr)}\right)_{\pm 1}\right\} + G_{DQ,5}^{(2)}\left\{\sum\left(\hat{D}_S^{(r/cr)}\right)_{\pm 1}\right\}$
VI order (λ^6)	$H_6^{(2)} = \frac{i}{6\times 4!}[S_2, [S_2, [S_2, [S_2, [S_2, H_1]]]]] = +\left(\frac{i}{6\times 4!}\right)$	
	$\Bigg\{\underbrace{\left(12\, C_{SQ}^{(2)}\, G_{SQ,B}^{(2)} + 8\, C_{DQ}^{(2)}\, G_{DQ,B}^{(2)}\right)}_{G_{ZQ,C}^{(2)}}\left(T^{(2)0}\right)_0 \underbrace{-2\sqrt{6}\left(C_{SQ}^{(2)}\, G_{DQ,B}^{(2)} + C_{DQ}^{(2)}\, G_{SQ,B}^{(2)}\right)}_{G_{CTQ,C}^{(2)}}\left\{\left(\hat{CT}_S\right)_0 + i\left(\hat{T}_{AS}\right)_0\right\}\Bigg\}$	$G_{ZQ,6}^{(2)}\ \left(T^{(2)0}\right)_0 + G_{CT,6}^{(2)}\left(\hat{CT}_S\right)_0 + i\, G_{TQ,6}^{(2)}\left(\hat{T}_{AS}\right)_0$
VII order (λ^7)	$H_7^{(2)} = -\frac{1}{7\times 5!}[S_2, [S_2, [S_2, [S_2, [S_2, H_1]]]]] = +\left(\frac{1}{7\times 5!}\right)$	
	$\Bigg\{-\underbrace{\left(C_{SQ}^{(2)}\, G_{ZQ,C}^{(2)} - 2\sqrt{\frac{2}{3}}\, C_{DQ}^{(2)}\, G_{CTQ,C}^{(2)}\right)}_{G_{SQ,C}^{(2)}}\left\{\left(\hat{SQ}_S^{(r)}\right)_{+1} + \left(\hat{SQ}_S^{(cr)}\right)_{-1}\right\} - \underbrace{\left(-\sqrt{6}\, C_{SQ}^{(2)}\, G_{CTQ,C}^{(2)} + C_{DQ}^{(2)}\, G_{ZQ,C}^{(2)}\right)}_{G_{DQ,C}^{(2)}}\left\{\left(\hat{D}_S^{(r)}\right)_{+1} + \left(\hat{D}_S^{(cr)}\right)_{-1}\right\}\Bigg\}$	$G_{SQ,7}^{(2)}\left\{\sum\left(\hat{SQ}_S^{(r/cr)}\right)_{\pm 1}\right\} + G_{DQ,7}^{(2)}\left\{\sum\left(\hat{D}_S^{(r/cr)}\right)_{\pm 1}\right\}$

A detailed description of the diagonal and off-diagonal contributions resulting from the second transformation are tabulated in Table. 3.5. As illustrated in Table. 3.5, the even order terms comprise of diagonal contributions (arising from ZQ ($T^{(2)0}$), CT $\left(\hat{CT}_S\right)$ and TQ $\left(\hat{T}_{AS}\right)$) , while the odd-order terms, represent the off-diagonal contributions (from SQ $\left(\hat{SQ}_S^{(r,cr)}\right)_{\pm 1}$ and DQ $\left(\hat{D}_S^{(r,cr)}\right)_{\pm 1}$).
Following the standard procedure, the effective Hamiltonian after second transformation is derived systematically to the desired level of accuracy.

$$\begin{aligned} H_{eff} &= e^{i\lambda^2 S_2}\ e^{i\lambda S_1}\ H_F\ e^{-i\lambda S_1}\ e^{-i\lambda^2 S_2} \\ &= \omega_Q I_F + G_{CT}^{(2)}\left(\hat{CT}_S\right)_0 + i\ G_{TQ}^{(2)}\left(\hat{T}_{AS}\right)_0 + G_{ZQ}^{(2)}\left(T^{(2)0}\right)_0 \end{aligned} \tag{3.39}$$

In Eq. 3.39, the coefficients '$G_{CT}^{(2)}$', '$G_{TQ}^{(2)}$', '$G_{ZQ}^{(2)}$' represent diagonal contributions resulting from both the first and second transformation.

$$\begin{aligned} G_{CT}^{(2)} &= \sum_{i=0}^{N_1} G_{CT,i}^{(1)} + \sum_{j=0}^{N_2} G_{CT,j}^{(2)} = G_{CT}^{(1)} + \left\{\ G_{CT,1}^{(2)} + G_{CT,2}^{(2)} +\ G_{CT,3}^{(2)} + ...\right\} \\ G_{TQ}^{(2)} &= \sum_{i=0}^{N_1} G_{TQ,i}^{(1)} + \sum_{j=0}^{N_2} G_{TQ,j}^{(2)} = G_{TQ}^{(1)} + \left\{\ G_{TQ,1}^{(2)} +\ G_{TQ,2}^{(2)} +\ G_{TQ,3}^{(2)} + ...\right\} \\ G_{ZQ}^{(2)} &= \sum_{i=0}^{N_1} G_{ZQ,i}^{(1)} + \sum_{j=0}^{N_2} G_{ZQ,j}^{(2)} = G_{ZQ}^{(1)} + \left\{\ G_{ZQ,1}^{(2)} +\ G_{ZQ,2}^{(2)} +\ G_{ZQ,3}^{(2)} + ...\right\} \end{aligned} \tag{3.40}$$

Analogous to the description in the previous section, the initial density operator and the detection operators are transformed by the second transformation function, S_2. A detailed description of the calculations along with the evolution of the density operator employing the effective Hamiltonians derived from the second transformation (Eq.3.39) is described in Appendix.B.2.
On further simplification, an approximate expression for calculating the TQ signal is arrived at as given below.

$$\left\langle T^{(3)-3}(t_{p1})\right\rangle \propto \left\{S_{\left(\theta_{TQ}\right)} + S_{(\theta_{CT})} + C_{(\theta_{RF})}\ S_{(\theta_{ZQ})} + S_{(\theta_{RF})}\ C_{(\theta_{ZQ})}\right\} \tag{3.41}$$

$$\left(where,\ \theta_{TQ} = \frac{3\omega_1^3 t_{p1}}{2\Omega_Q^2} \quad ; \quad \theta_{CT} = -2\omega_1 t_{p1} + \frac{3\omega_1^3 t_{p1}}{2\Omega_Q^2} \quad ; \quad \theta_{RF} = \omega_1 t_{p1} \right.$$
$$\left. \theta_{ZQ} = (\Delta - \omega_Q) t_{p1} - \frac{3\omega_1^2 t_{p1}}{2\ \Omega_Q} \right)$$

To illustrate the role of the off-diagonal contributions from the first transformation, two sets of simulations corresponding to

- Off-diagonal contributions to λ^3 from first transformation i.e. $N_1 = 3$ (see Eq. 3.33, 3.34 and Figure. 3.5)
- Off-diagonal contributions to λ^n from first transformation i.e. $N_1 = n$ (see Eq. 3.33, 3.34 and Figure. 3.6)

were performed.

Table 3.6: Definition of coefficients employed in the perturbing Hamiltonians for Case-III (a,b) and Case-IV (a,b)

	$G_{SQ}^{(1)}$	$G_{DQ}^{(1)}$
Case-III (a) and Case-IV(a) $(N_1 = 3)$	$+\frac{1}{3}\left(\frac{\omega_1}{2}\right)(\theta)^2$	$-\frac{\omega_1}{2\sqrt{2}}(\theta)$
Case-III (b) and Case-IV(b) $(N_1 > 3)$	$+\left(\frac{\omega_1}{2}\right)\left\{\frac{1}{3\times 1!}(\theta)^2 - \frac{1}{5\times 3!}(\theta)^4 + \frac{1}{7\times 5!}(\theta)^6 - ....\right\}$	$-\frac{\omega_1}{2\sqrt{2}} S_{(\theta)}$

	$G_{CT}^{(2)}$	$G_{TQ}^{(2)}$	$G_{ZQ}^{(2)}$
Case-III (a)	$\sum_{i=0}^{3} G_{CT,i}^{(1)} + \sum_{j=1}^{2} G_{CT,j}^{(2)}$	$\sum_{i=0}^{3} G_{TQ,i}^{(1)} + \sum_{j=1}^{2} G_{TQ,j}^{(2)}$	$\sum_{i=0}^{3} G_{ZQ,i}^{(1)} + \sum_{j=1}^{2} G_{ZQ,j}^{(2)}$
Case-III (b)	$\sum_{i=0}^{3} G_{CT,i}^{(1)} + \sum_{j=1}^{N_2} G_{CT,j}^{(2)}$	$\sum_{i=0}^{3} G_{TQ,i}^{(1)} + \sum_{j=1}^{N_2} G_{TQ,j}^{(2)}$	$\sum_{i=0}^{3} G_{ZQ,i}^{(1)} + \sum_{j=1}^{N_2} G_{ZQ,j}^{(2)}$
Case-IV (a)	$\sum_{i=0}^{N_1} G_{CT,i}^{(1)} + \sum_{j=1}^{2} G_{CT,j}^{(2)}$	$\sum_{i=0}^{N_1} G_{TQ,i}^{(1)} + \sum_{j=1}^{2} G_{TQ,j}^{(2)}$	$\sum_{i=0}^{N_1} G_{ZQ,i}^{(1)} + \sum_{j=1}^{2} G_{ZQ,j}^{(2)}$
Case-IV (b)	$\sum_{i=0}^{N_1} G_{CT,i}^{(1)} + \sum_{j=1}^{N_2} G_{CT,j}^{(2)}$	$\sum_{i=0}^{N_1} G_{TQ,i}^{(1)} + \sum_{j=1}^{N_2} G_{TQ,j}^{(2)}$	$\sum_{i=0}^{N_1} G_{ZQ,i}^{(1)} + \sum_{j=1}^{N_2} G_{ZQ,j}^{(2)}$

$$\theta = \left(\frac{\sqrt{3}\omega_1}{\Omega_Q}\right) \quad ; \quad C_{(\theta)} = \cos(\theta) \quad ; \quad S_{(\theta)} = \sin(\theta)$$

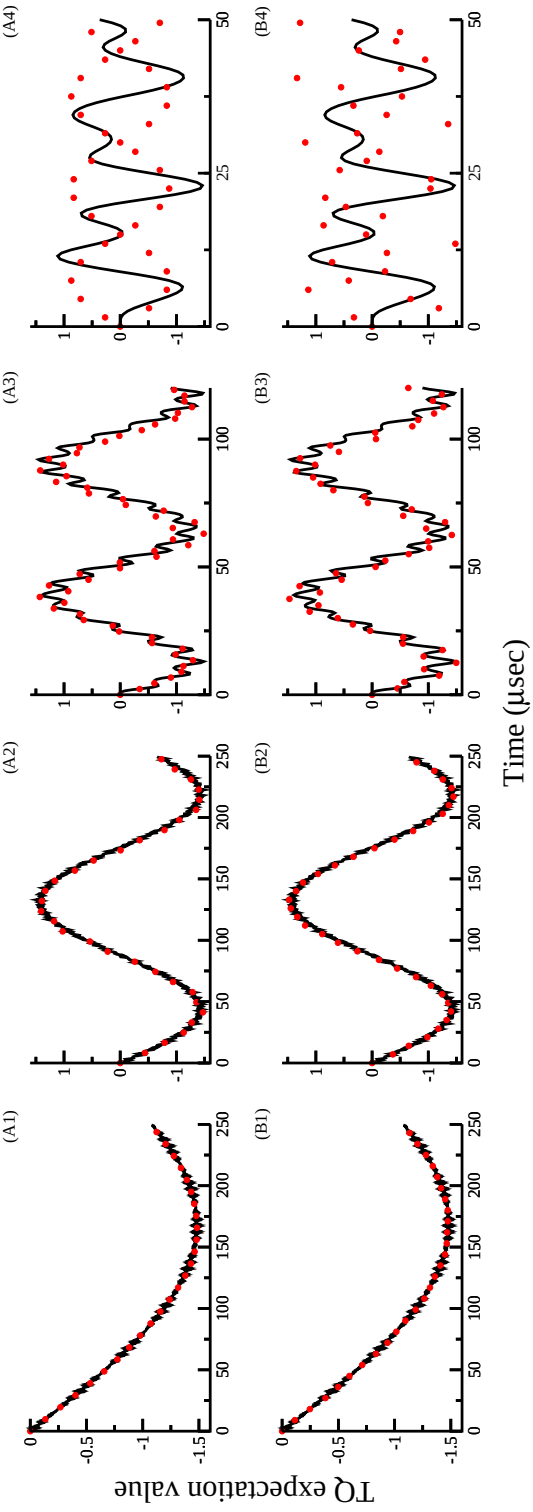

Figure 3.5: Comparison of numerical (black thick line) and analytic simulations (red dots) based on effective Hamiltonians derived from the second transformation. The off-diagonal contributions to order λ^3 from the first transformation ($N_1 = 3$) and diagonal corrections to order λ^2 from the second transformation ($N_2 = 2$) (from Panels A1 $\rightarrow$ A4) and to order λ^n from the second transformation ($N_2 > 2$) (from Panels B1 $\rightarrow$ B4) were included in the derivation of the effective Hamiltonians. In the simulations depicted, the quadrupole coupling constant ($C_Q = {}^{\omega_Q}/_{\pi}$) is varied A1, B1) $C_Q = 2$ MHz, A2, B2) $C_Q = 1$ MHz, A3, B3) $C_Q = 500$ kHz, A4, B4) $C_Q = 200$ kHz, employing an excitation pulse of constant RF amplitude, $({}^{\omega_1}/_{2\pi}) = 100$ kHz. The simulations correspond to a single crystal.

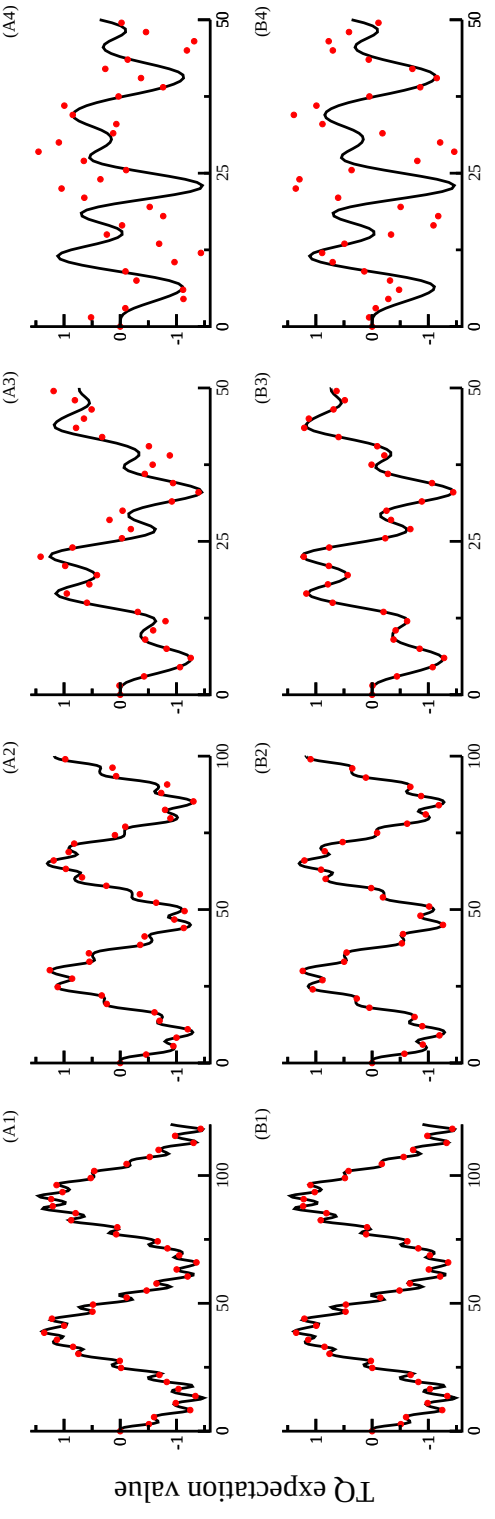

Figure 3.6: Comparison of numerical (black thick line) and analytic simulations (red dots) based on effective Hamiltonians derived from the second transformation. The off-diagonal contributions to order λ^n from the first transformation ($N_1 > 3$) and diagonal corrections to order λ^2 from the second transformation ($N_2 = 2$) (from Panels A1 $\rightarrow$ A4) and to order λ^n from the second transformation ($N_2 > 2$) (from Panels B1 $\rightarrow$ B4) were included in the derivation of the effective Hamiltonians. In the simulations depicted, the quadrupole coupling constant ($C_Q = {}^{\omega_Q}/_{\pi}$) is varied A1, B1) $C_Q = 500$ kHz, A2, B2) $C_Q = 400$ kHz, A3, B3) $C_Q = 300$ kHz, A4, B4) $C_Q = 200$ kHz, employing an excitation pulse of constant RF amplitude, $({}^{\omega_1}/_{2\pi}) = 100$ kHz. The simulations correspond to a single crystal.

In both these sets of simulations, diagonal corrections to second order and n^{th} order resulting from the second transformation, S_2, were incorporated. The panels (A1 $\rightarrow$ A4) in Figures. 3.5 and 3.6 are based on diagonal corrections to second order, while, panels (B1 $\rightarrow$ B4) depict the effect of diagonal corrections to the n^{th} order.

As depicted in Figures. 3.5 and 3.6, inclusion of the off-diagonal terms from the first transformation and the subsequent folding through the second transformation, S_2, play an important role in improving the exactness of the derived effective Floquet Hamiltonians. Nevertheless, when the magnitude of the quadrupolar coupling constant is very similar to the amplitude of the pulse, significant deviations are still present in accord with the calculations (spin $I = 1$) presented in Chapter-2.

Regime-II: Weak coupling ($\omega_Q \approx \omega_1$)

To address the discrepancy observed in the analytic simulations (for systems with smaller quadrupolar coupling constants), the Hamiltonian in the Zeeman-interaction frame is transformed such that the RF field is quantized along z-direction using the transformation function 'U_2' ($U_2 = e^{i\pi/2 I_y}$).

$$\tilde{H} = -\hbar\omega_1 I_x - \hbar\Omega_Q T^{(2)0} \tag{3.42}$$

$$\begin{aligned}\tilde{\tilde{H}} =& U_2\ \tilde{H}\ U_2^{-1} \\ =& -\hbar\omega_1 I_z + \left(\frac{\hbar\Omega_Q}{2}\right) T^{(2)0} - \sqrt{\frac{3}{2}}\left(\frac{\hbar\Omega_Q}{2}\right)\left(\Phi_1^2 T^{(2)2} + \Phi_1^{-2} T^{(2)-2}\right)\end{aligned} \tag{3.43}$$

To further simplify the description, the above Hamiltonian is transformed into the RF interaction frame defined by the transformation function, 'U_3' ($U_3 = exp\,(-i\omega_1 t I_z)$)

$$\begin{aligned}\tilde{\tilde{H}}(t) =& U_3\ \tilde{\tilde{H}}\ U_3^{-1} \\ =& \left(\frac{\hbar\Omega_Q}{2}\right) T^{(2)0} - \sqrt{\frac{3}{2}}\left(\frac{\hbar\Omega_Q}{2}\right)\left(\Phi_1^2 T^{(2)2} e^{-2i\omega_1 t} + \Phi_1^{-2} T^{(2)-2} e^{2i\omega_1 t}\right)\end{aligned} \tag{3.44}$$

In accord with the description presented in the previous section, the above time-dependent Hamiltonian is transformed into a time-independent Floquet Hamiltonian.

$$H_F = \omega_1 I_F + \left(\frac{\hbar\Omega_Q}{2}\right)\left(T^{(2)0}\right)_0 - \sqrt{\frac{3}{2}}\left(\frac{\hbar\Omega_Q}{2}\right)\left\{\left(\Phi_1^2 T^{(2)2}\right)_2 + \left(\Phi_1^{-2} T^{(2)-2}\right)_{-2}\right\} \tag{3.45}$$

To facilitate analytic description in terms of effective Hamiltonians, the above Floquet Hamiltonian is re-expressed in-terms of zero-order and perturbing Hamiltonian. The perturbing Hamiltonian (H_1) comprises of both diagonal ($H_{1,d}$) and off-diagonal terms ($H_{1,od}$).

$$\begin{gathered} H_0 = \omega_1 I_F H_1 = H_{1,d} + H_{1,od} \\ H_{1,d} = +\left(\frac{\Omega_Q}{2}\right)\left(T^{(2)0}\right)_0; \quad H_{1,od} = -\sqrt{\frac{3}{2}}\left(\frac{\Omega_Q}{2}\right)\left\{\left(\Phi_1^2 T^{(2)2}\right)_2 + \left(\Phi_1^{-2} T^{(2)-2}\right)_{-2}\right\} \end{gathered} \tag{3.46}$$

In contrast to the analytic description present in Regime-I, the quadrupolar interaction acts like a perturbation and plays an important role in the excitation of TQ transitions in Regime-II. Employing the transformation function, 'S_1'.

$$H_{eff} = e^{i\lambda S_1}\ H_F\ e^{-i\lambda S_1}$$

$$S_1 = C_{DR}^{(1)}\left\{\left(\Phi_1^2 T^{(2)2}\right)_2 - \left(\Phi_1^{-2} T^{(2)-2}\right)_{-2}\right\} \tag{3.47}$$

$$C_{DR}^{(1)} = -i\sqrt{\frac{3}{2}}\left(\frac{\Omega_Q}{4\omega_1}\right) \tag{3.48}$$

the off-diagonal contributions in H_1 (i.e. $H_{1,od}$) are folded and the higher order corrections to the effective Floquet Hamiltonian are derived using the relations described in previous chapter. To first-order, the effective Hamiltonian comprises of '$H_{1,d}$'.

$$H_1^{(1)} = \left(\frac{\hbar\Omega_Q}{2}\right)\left(T^{(2)0}\right)_0 \tag{3.49}$$

Table 3.7: Description of higher order (diagonal and off-diagonal) contributions to the effective Hamiltonians derived in Regime-II based on the first transformation

n^{th} **order Correction**	**Coefficients in the Effective Hamiltonian** $H_{eff} = H_1^{(1)} + H_3^{(1)} + H_5^{(1)} + \cdots = \sum_{i=0}^{N_1} G_{2R,i}^{(1)} \left(T^{(2)0}\right)_0$	
	Expression from the '$H_{1,d}$' term	**Non-zero 'G' Coefficients**
Zero order (λ^0)	$H_0^{(1)} = 0$	
I order (λ^1)	$H_1^{(1)} = H_{1,d} = +\left(\frac{\Omega_Q}{2}\right)\left(T^{(2)0}\right)_0$	$G_{2R,1}^{(1)}\left(T^{(2)0}\right)_0$
II order (λ^2)	$H_2^{(1)} = i[S_1, H_{1,d}] = -\left(\frac{\Omega_Q}{2\sqrt{2}}\right)(\xi)\left\{\left(i\Phi_1^2 T^{(3)2}\right)_2 + \left(i\Phi_1^{-2}T^{(3)-2}\right)_{-2}\right\}$	$G_{TR,2}^{(1)}\left\{\left(i\Phi_1^2 T^{(3)2}\right)_2 + \left(i\Phi_1^{-2}T^{(3)-2}\right)_{-2}\right\}$
III order (λ^3)	$H_3^{(1)} = -\frac{1}{2!}[S_1,[S_1,H_{1,d}]] = -\frac{1}{2!}\left(\frac{\Omega_Q}{2}\right)(\xi)^2\left(T^{(2)0}\right)_0$	$G_{2R,3}^{(1)}\left(T^{(2)0}\right)_0$
IV order (λ^4)	$H_4^{(1)} = -\frac{i}{3!}[S_1,[S_1,[S_1,H_{1,d}]]] = +\frac{1}{3!}\left\{\left(\frac{\Omega_Q}{2\sqrt{2}}\right)(\xi)^3\right\}\left\{\left(i\Phi_1^2 T^{(3)2}\right)_2 + \left(i\Phi_1^{-2}T^{(3)-2}\right)_{-2}\right\}$	$G_{TR,4}^{(1)}\left\{\left(i\Phi_1^2 T^{(3)2}\right)_2 + \left(i\Phi_1^{-2}T^{(3)-2}\right)_{-2}\right\}$
V order (λ^5)	$H_5^{(1)} = \frac{1}{4!}[S_1,[S_1,[S_1,[S_1,H_{1,d}]]]] = +\frac{1}{4!}\left(\frac{\Omega_Q}{2}\right)(\xi)^4\left(T^{(2)0}\right)_0$	$G_{2R,5}^{(1)}\left(T^{(2)0}\right)_0$
VI order (λ^6)	$H_6^{(1)} = \frac{i}{5!}[S_1,[S_1,[S_1,[S_1,[S_1,H_{1,d}]]]]] = -\frac{1}{5!}\left\{\left(\frac{\Omega_Q}{2\sqrt{2}}\right)(\xi)^5\right\}\left\{\left(i\Phi_1^2 T^{(3)2}\right)_2 + \left(i\Phi_1^{-2}T^{(3)-2}\right)_{-2}\right\}$	$G_{TR,6}^{(1)}\left\{\left(i\Phi_1^2 T^{(3)2}\right)_2 + \left(i\Phi_1^{-2}T^{(3)-2}\right)_{-2}\right\}$
VII order (λ^7)	$H_7^{(1)} = -\frac{1}{6!}[S_1,[S_1,[S_1,[S_1,[S_1,[S_1,H_{1,d}]]]]]] = -\frac{1}{6!}\left(\frac{\Omega_Q}{2}\right)(\xi)^6\left(T^{(2)0}\right)_0$	$G_{2R,7}^{(1)}\left(T^{(2)0}\right)_0$
$\xi = \left(\frac{\sqrt{3}\Omega_Q}{4\omega_1}\right)$		

Table 3.8: Description of higher order (diagonal and off-diagonal) contributions to the effective Hamiltonians derived in Regime-II based on the first transformation

n^{th} **order**	**Coefficients in the Effective Hamiltonian**	
Correction	$H_{eff} = H_0^{(1)} + H_2^{(1)} + H_4^{(1)} + H_6^{(1)} + \cdots = \omega_1 I_F + \left(\frac{i}{\sqrt{5}}\right) \sum_{j=0}^{N_1} G_{1R,j}^{(1)} \left(T^{(1)0}\right)_0 + \left(\frac{i}{\sqrt{5}}\right) \sum_{j=0}^{N_1} G_{3R,j}^{(1)} \left(T^{(3)0}\right)_0$	
	Expression from the '$H_{1,od}$' term	**Non-zero 'G' Coefficients**
Zero order (λ^0)	$H_0^{(1)} = \omega_1 I_F$	$\omega_1 I_F$
I order (λ^1)	$H_1^{(1)} = 0$	
II order (λ^2)	$H_2^{(1)} = \frac{i}{2 \times 0!}[S_1, H_{1,od}] = +\frac{1}{2 \times 0!} \left\{ \left(\frac{\sqrt{3}\Omega_Q}{2} \right) (\xi) \right\} \left\{ \left(\frac{i}{\sqrt{5}} \right) \left(2T^{(1)0} + T^{(3)0} \right)_0 \right\}$	$\left(\frac{i}{\sqrt{5}} \right) \left(G_{1R,2}^{(1)} \left(T^{(1)0} \right)_0 + G_{3R,2}^{(1)} \left(T^{(3)0} \right)_0 \right)$
III order (λ^3)	$H_3^{(1)} = -\frac{1}{3 \times 1!}[S_1, [S_1, H_{1,od}]] = +\frac{1}{3 \times 1!} \left\{ \left(\frac{\sqrt{3}\Omega_Q}{2\sqrt{2}} \right) (\xi)^2 \right\} \left\{ \left(\Phi_1^2 T^{(2)2} \right)_2 + \left(\Phi_1^{-2} T^{(2)-2} \right)_{-2} \right\}$	$G_{DR,3}^{(1)} \left\{ \left(\Phi_1^2 T^{(2)2} \right)_2 + \left(\Phi_1^{-2} T^{(2)-2} \right)_{-2} \right\}$
IV order (λ^4)	$H_4^{(1)} = -\frac{i}{4 \times 2!}[S_1, [S_1, [S_1, H_{1,od}]]] = -\frac{1}{4 \times 2!} \left\{ \left(\frac{\sqrt{3}\Omega_Q}{2} \right) (\xi)^3 \right\} \left\{ \left(\frac{i}{\sqrt{5}} \right) \left(2T^{(1)0} + T^{(3)0} \right)_0 \right\}$	$\left(\frac{i}{\sqrt{5}} \right) \left(G_{1R,4}^{(1)} \left(T^{(1)0} \right)_0 + G_{3R,4}^{(1)} \left(T^{(3)0} \right)_0 \right)$
V order (λ^5)	$H_5^{(1)} = \frac{1}{5 \times 3!}[S_1, [S_1, [S_1, [S_1, H_{1,od}]]]] = -\frac{1}{5 \times 3!} \left\{ \left(\frac{\sqrt{3}\Omega_Q}{2\sqrt{2}} \right) (\xi)^4 \right\} \left\{ \left(\Phi_1^2 T^{(2)2} \right)_2 + \left(\Phi_1^{-2} T^{(2)-2} \right)_{-2} \right\}$	$G_{DR,5}^{(1)} \left\{ \left(\Phi_1^2 T^{(2)2} \right)_2 + \left(\Phi_1^{-2} T^{(2)-2} \right)_{-2} \right\}$
VI order (λ^6)	$H_6^{(1)} = \frac{i}{6 \times 4!}[S_1, [S_1, [S_1, [S_1, [S_1, H_{1,od}]]]]] = +\frac{1}{6 \times 4!} \left\{ \left(\frac{\sqrt{3}\Omega_Q}{2} \right) (\xi)^5 \right\} \left\{ \left(\frac{i}{\sqrt{5}} \right) \left(2T^{(1)0} + T^{(3)0} \right)_0 \right\}$	$\left(\frac{i}{\sqrt{5}} \right) \left(G_{1R,6}^{(1)} \left(T^{(1)0} \right)_0 + G_{3R,6}^{(1)} \left(T^{(3)0} \right)_0 \right)$
VII order (λ^7)	$H_7^{(1)} = -\frac{1}{7 \times 5!}[S_1, [S_1, [S_1, [S_1, [S_1, [S_1, H_{1,od}]]]]]] = +\frac{1}{7 \times 5!} \left\{ \left(\frac{\sqrt{3}\Omega_Q}{2\sqrt{2}} \right) (\xi)^6 \right\} \left\{ \left(\Phi_1^2 T^{(2)2} \right)_2 + \left(\Phi_1^{-2} T^{(2)-2} \right)_{-2} \right\}$	$G_{DR,7}^{(1)} \left\{ \left(\Phi_1^2 T^{(2)2} \right)_2 + \left(\Phi_1^{-2} T^{(2)-2} \right)_{-2} \right\}$
$\xi = \left(\frac{\sqrt{3}\Omega_Q}{4\omega_1} \right)$		

A detailed derivation of the commutator relations involving the transformation 'S_1' and 'H_1' to various orders of 'λ' is tabulated in Table. 3.7, and 3.8. As illustrated (in Table.3.7, 3.8), the diagonal corrections mainly comprise of ZQ operators $\left(\left(T^{(k)0}\right)_0; k = 1, 2, 3\right)$, while the off-diagonal contributions are represented through the DQ operators $\left(\left(T^{(2)\pm 2}\right)_{\pm 2}\right)$. Below, a pedagogical description analogous to Regime-I is presented to explicate the role of the higher-order contributions in the excitation process.

I. Effective Hamiltonians from first transformation, 'S_1'

To begin with, let the effective Hamiltonian (comprising of diagonal corrections only) describing the excitation process (in Regime-II) be represented by,

$$\begin{aligned} H_{eff} &= e^{i\lambda S_1}\ H_F\ e^{-i\lambda S_1} \\ &= \omega_1 I_F + \frac{i}{\sqrt{5}}\ G^{(1)}_{1R}\left(T^{(1)0}\right)_0 + \ G^{(1)}_{2R}\left(T^{(2)0}\right)_0 + \frac{i}{\sqrt{5}}\ G^{(1)}_{3R}\left(T^{(3)0}\right)_0 \end{aligned} \tag{3.50}$$

The 'G' coefficients deduced from Tables.3.7 and 3.8 are expanded below.

$$G^{(1)}_{1R} = \sum_{i=1}^{N_1} G^{(1)}_{1R,i} \quad ; \quad G^{(1)}_{2R} = \sum_{i=1}^{N_1} G^{(1)}_{2R,i} \quad ; \quad G^{(1)}_{3R} = \sum_{i=1}^{N_1} G^{(1)}_{3R,i}$$

$$G^{(1)}_{1R} = \left(\sqrt{3}\Omega_Q\right)\left\{+\frac{1}{2\times 0!}(\xi) - \frac{1}{4\times 2!}(\xi)^3 + \frac{1}{6\times 4!}(\xi)^5 + ...\right\} \tag{3.51}$$

$$G^{(1)}_{2R} = \left(\frac{\Omega_Q}{2}\right) C_{(\xi)} \tag{3.52}$$

$$G^{(1)}_{3R} = \left(\frac{\sqrt{3}\Omega_Q}{2}\right)\left\{+\frac{1}{2\times 0!}(\xi) - \frac{1}{4\times 2!}(\xi)^3 + \frac{1}{6\times 4!}(\xi)^5 + ...\right\} \tag{3.53}$$

and (N_1 represents the order of the correction from the first transformation).
In accord with the descriptions presented in this thesis, the initial density operator and detection operator are transformed using the transformation function, S_1. A detailed description of the density matrix calculations is presented in Appendix. C.1. Based on the calculations, the TQ signal in Regime-II is evaluated.
Analogous to the description in Regime-I (refer Eq. 3.29), the TQ signal expression comprises of four terms. To illustrate the exactness of the proposed effective Floquet Hamiltonians in Regime-II, simulations incorporating diagonal corrections

to second order (Panels A1 → A3) and n^{th} (Panels B1 → B3)order resulting from the first transformation are depicted in Figure. 3.7. In the simulations depicted in Fig. 3.7, the quadrupolar coupling constant was varied from 50 kHz to 200 kHz.

$$\begin{aligned}\left\langle T^{(3)-3}(t_{p1})\right\rangle = \left(\Phi_1^3\ \Phi_R\right)\Bigg\{ & -\frac{1}{8}\ S_{(\theta_{TQ})}\left\{\left\{C_{(\xi)}-1\right\}\left\{2\ C_{(\xi)}-1\right\}\right\} \\ & +\frac{1}{8}\ S_{(\theta_{CT})}\left\{\left\{C_{(\xi)}+1\right\}\left\{2\ C_{(\xi)}+1\right\}\right\} \\ & -\frac{3}{8}\ S_{(\theta_{STA})}\left\{\left\{\frac{1}{\sqrt{3}}\ S_{(\xi)}-1\right\}\left\{\frac{2}{\sqrt{3}}\ S_{(\xi)}-1\right\}\right\} \\ & -\frac{3}{8}\ S_{(\theta_{STB})}\left\{\left\{\frac{1}{\sqrt{3}}\ S_{(\xi)}+1\right\}\left\{\frac{2}{\sqrt{3}}\ S_{(\xi)}+1\right\}\right\}\Bigg\}\end{aligned} \tag{3.54}$$

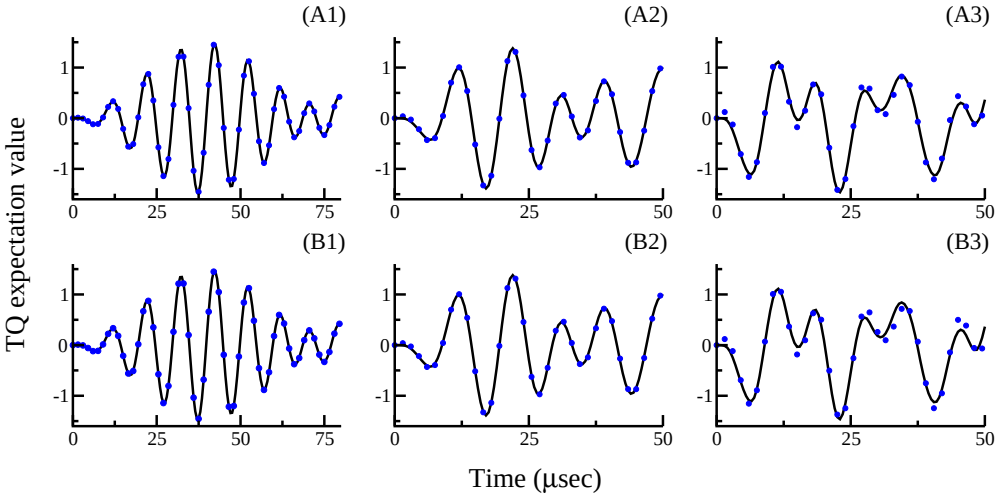

Figure 3.7: Comparison of numerical (black thick line) and analytic simulations (blue dots) based on effective Hamiltonians derived from a single transformation comprising of diagonal corrections to order $\lambda^3(N_1 = 3)$ (from Panels A1 → A3) and to the order $\lambda^n(N_1 > 3)$ (from Panels B1 → B3). In the simulations depicted, the quadrupole coupling constant ($C_Q = {}^{\omega_Q}/_{\pi}$) is varied A1, B1) $C_Q = 50$ kHz, A2, B2) $C_Q = 100$ kHz, A3, B3) $C_Q = 200$ kHz, employing an excitation pulse of constant RF amplitude, $({}^{\omega_1}/_{2\pi}) = 100$ kHz. The simulations correspond to a single crystal.

As depicted in Figure. 3.7, (see Panels A3 and B3), the deviations reported in Regime-I calculations are resolved through the effective Hamiltonians derived from Regime-II. The minimum variations observed in the simulations could further be improved with a second transformation, S_2. A detailed description of the same is presented in Appendix. C.2.

3.2.2 TQ excitation in Powder Sample

To test the validity of the proposed effective Floquet Hamiltonians in the description of anisotropic solids, the above calculations were extended to study the excitation in powder samples. In Figures. 3.8 - 3.10, TQ excitation in powder samples is calculated based on the effective Hamiltonians derived from Regime-I.

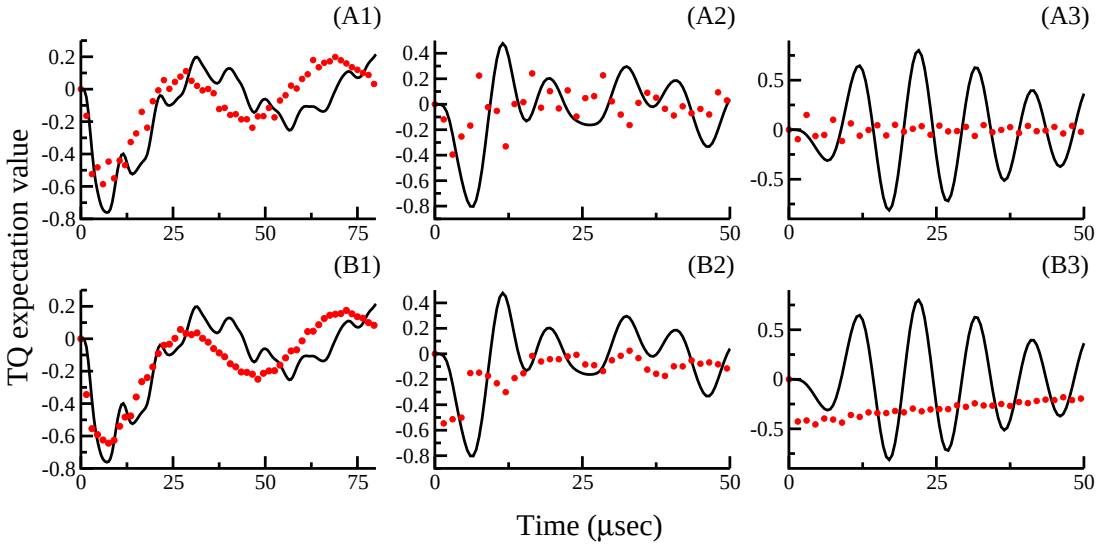

Figure 3.8: Comparison of numerical (black thick line) and analytic simulations (red dots) based on effective Hamiltonians derived from a single transformation comprising of diagonal corrections to order $\lambda^3(N_1 = 3)$ (from Panels A1 $\rightarrow$ A3) and to the order $\lambda^n(N_1 > 3)$ (from Panels B1 $\rightarrow$ B3). In the simulations depicted, the quadrupole coupling constant ($C_Q = {}^{\omega_Q}/_{\pi}$) is varied A1, B1) $C_Q = 1$ MHz, A2, B2) $C_Q = 500$ kHz, A3, B3) $C_Q = 200$ kHz, employing an excitation pulse of constant RF amplitude, $({}^{\omega_1}/_{2\pi}) = 100$ kHz. The powder simulations were performed using a crystal file having 28656 orientations (α, β).

In the simulations presented, diagonal corrections to II-order (panels A1 $\rightarrow$ A3) and n^{th} order (panels B1 $\rightarrow$ B3) resulting from the first transformation were employed. As depicted, significant deviations are observed in the analytical simulations even at $C_Q = 1$ MHz. To address this, the off-diagonal corrections ignored in the first transformations were incorporated systematically in the simulations.

- To order λ^3 i.e. $N_1 = 3$ in Figure. 3.9
- To orderλ^n i.e. $N_1 = n$ in Figure. 3.10

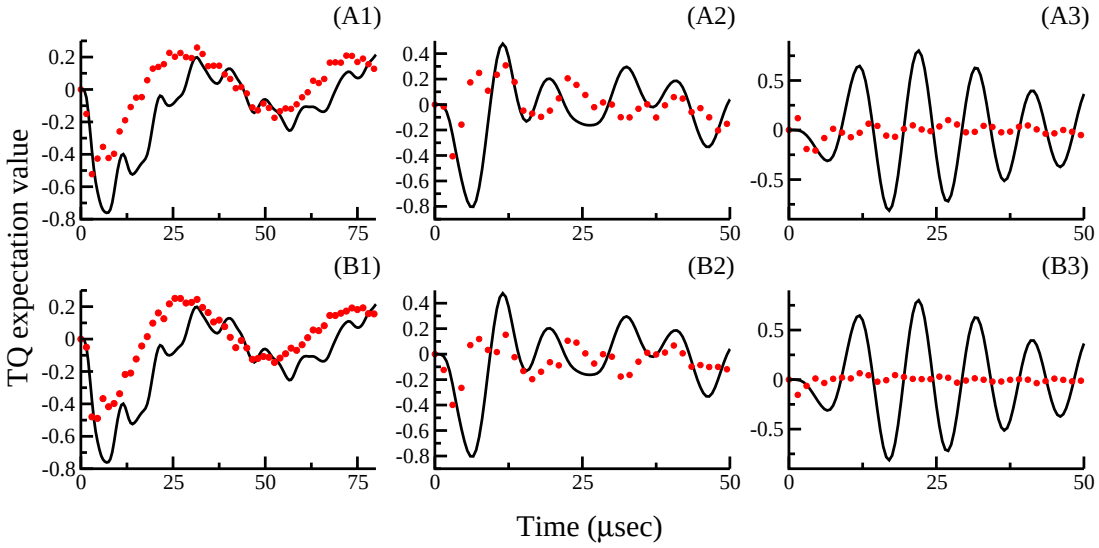

Figure 3.9: Comparison of numerical (black thick line) and analytic simulations (red dots) based on effective Hamiltonians derived from the second transformation. The off-diagonal contributions to order λ^3 from the first transformation ($N_1 = 3$) and diagonal corrections to order λ^2 from the second transformation ($N_2 = 2$) (from Panels A1 $\rightarrow$ A3) and to order λ^n from the second transformation ($N_2 > 2$) (from Panels B1 $\rightarrow$ B3) were included in the derivation of the effective Hamiltonians. In the simulations depicted, the quadrupole coupling constant ($C_Q = {}^{\omega_Q}/_{\pi}$) is varied A1, B1) $C_Q = 1$ MHz, A2, B2) $C_Q = 500$ kHz, A3, B3) $C_Q = 200$ kHz, employing an excitation pulse of constant RF amplitude, $({}^{\omega_1}/_{2\pi}) = 100$ kHz. The powder simulations were performed using a crystal file having 28656 orientations (α, β).

Nevertheless, significant deviations are still observed in the analytic simulations irrespective of the inclusion of the higher order corrections (both diagonal and

off-diagonal contributions from Regime-I only).

To address this issue, the hybrid method[22] proposed in chapter-2 was employed to describe the TQ excitation in powder samples. For crystallite orientations with '$\left|\omega_Q^{(\alpha\beta\gamma)}\right| < |\omega_1|$', the effective Hamiltonians based on Regime-II were employed(Eq. C.2.9, C.2.12), while for '$\left|\omega_Q^{(\alpha\beta\gamma)}\right| > |\omega_1|$', effective Hamiltonians based in Regime-I were employed (Eq. 3.39, B.2.10) in simulating the excitation profile in powder samples.

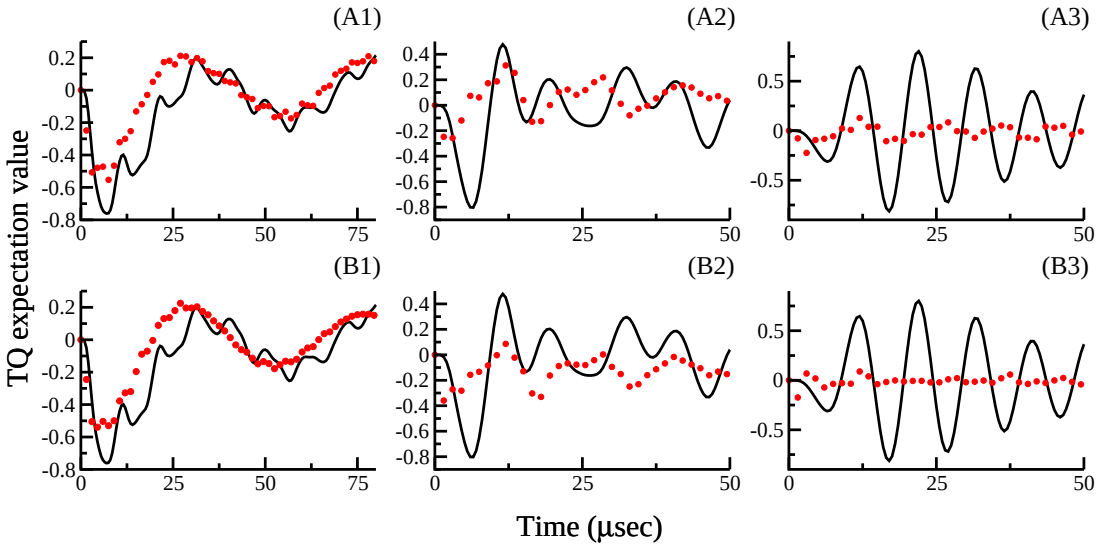

Figure 3.10: Comparison of numerical (black thick line) and analytic simulations (red dots) based on effective Hamiltonians derived from the second transformation. The off-diagonal contributions to order λ^n from the first transformation ($N_1 > 3$) and diagonal corrections to order λ^2 from the second transformation ($N_2 = 2$) (from Panels A1 $\rightarrow$ A3) and to order λ^n from the second transformation ($N_2 > 2$) (from Panels B1 $\rightarrow$ B3) were included in the derivation of the effective Hamiltonians. In the simulations depicted, the quadrupole coupling constant ($C_Q = {}^{\omega_Q}/_{\pi}$) is varied A1, B1) $C_Q = 1$ MHz, A2, B2) $C_Q = 500$ kHz, A3, B3) $C_Q = 200$ kHz, employing an excitation pulse of constant RF amplitude, $({}^{\omega_1}/_{2\pi}) = 100$ kHz. The powder simulations were performed using a crystal file having 28656 orientations (α, β).

A schematic depiction of the simulations based on the hybrid method illustrating the extent of the contributions of the two regimes is presented in Figure. 3.12

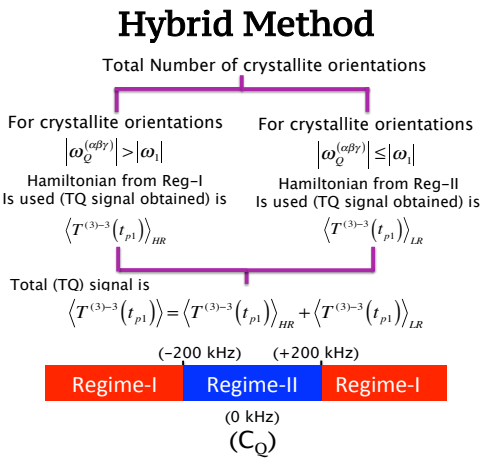

Figure 3.11: A schematic diagram depicting the hybrid method employed in obtaining TQ signal in spin $I = {}^3/_2$ powder samples.

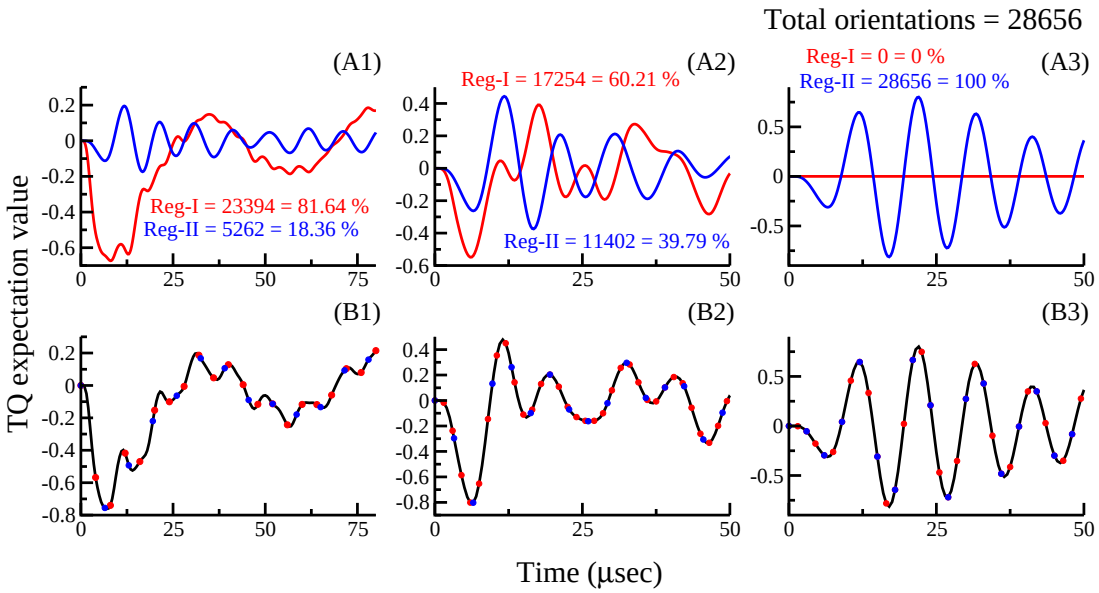

Figure 3.12: The analytic simulations emerging from the effective Hamiltonians derived from Regime-I (red thick line) and Regime-II (blue thick line), are depicted along the row-I (see Panels A1 $\rightarrow$ A3). In row -II (Panels B1 $\rightarrow$ B3), comparison of numerical (black thick line) and analytic simulations (red and blue dots) based on effective Hamiltonians derived from both regimes (using Hybrid method) is presented. In the simulations depicted, the quadrupole coupling constant ($C_Q = {}^{\omega_Q}/_{\pi}$) is varied A1, B1) $C_Q = 1$ MHz, A2, B2) $C_Q = 500$ kHz, A3, B3) $C_Q = 200$ kHz, employing an excitation pulse of constant RF amplitude, $({}^{\omega_1}/_{2\pi}) = 100$ kHz. The choice of Regime-I and Regime-II is purely dependent on the magnitude of $\omega_Q^{(\alpha\beta\gamma)}$ relative to the RF amplitude. When $\left|\omega_Q^{(\alpha\beta\gamma)}\right| < |\omega_1|$, Regime-II is employed, $\left|\omega_Q^{(\alpha\beta\gamma)}\right| > |\omega_1|$, Regime-I is employed. The powder simulations were performed using a crystal file having 28656 orientations (α, β).

In the panels (A1 $\rightarrow$ A3), the fraction of crystallites in regime-I and regime-II are identified for a crystal file comprising of 28656 orientations. As depicted, with decreasing quadrupolar coupling constants, the fraction of crystallites governed by effective Hamiltonian from Regime-II increases and is in accord with the results presented in chapter-2. As indicated, the analytic simulations based on the hybrid method are in excellent agreement (panels, B1 $\rightarrow$ B3) with SIMPSON simulations justifying our strategy.

References

[1] A. J. Vega, in *Quadrupolar Nuclei in Solids, eMagRes (eds R. K. Harris and R. L. Wasylishen)*, Am. Can. Soc., 2010.

[2] S. Vega and Y. Naor, *J. Chem. Phys.*, 1981, **75**, 75–86.

[3] S. Vega, *J. Chem. Phys.*, 1978, **68**, 5518–5527.

[4] A. Abragam, *The Principles of Nuclear Magnetism*, Clarendon Press, 1961.

[5] M. Bak, J. T. Rasmussen and N. C. Nielsen, *J. Magn. Reson.*, 2000, **147**, 296 – 330.

[6] M. Bak, J. T. Rasmussen and N. C. Nielsen, *J. Magn. Reson.*, 2011, **213**, 366 – 400.

[7] Z. Tosner, R. Andersen, B. Stevensson, M. Edén, N. C. Nielsen and T. Vosegaard, *J. Magn. Reson.*, 2014, **246**, 79 – 93.

[8] R. Venkata SubbaRao, D. Srivastava and R. Ramachandran, *Phys. Chem. Chem. Phys.*, 2013, **15**, 2081–2104.

[9] R. Ramesh and M. S. Krishnan, *J. Chem. Phys.*, 2001, **114**, 5967–5973.

[10] D. Srivastava and R. Ramachandran, *RSC Adv.*, 2013, **3**, 25231–25236.

[11] D. Srivastava, R. Venkata SubbaRao and R. Ramachandran, *Phys. Chem. Chem. Phys.*, 2013, **15**, 6699–6713.

[12] G. Floquet, *Ann. Sci. Ecole Norm. Sup.*, 1883, **12**, 47–88.

[13] J. H. Shirley, *Phys. Rev.*, 1965, **138**, B979–B987.

[14] I. Scholz, J. D. van Beek and M. Ernst, *Solid State Nucl. Magn. Reson.*, 2010, **37**, 39 – 59.

[15] R. Ramachandran and R. G. Griffin, *J. Chem. Phys.*, 2005, **122**, 164502.

[16] M. Leskes, P. Madhu and S. Vega, *Prog. Nucl. Magn. Reson. Spectrosc.*, 2010, **57**, 345380.

[17] V. Aliev, M.R. Aleksanyan, *Optika Spectroscopia*, 1968, **24**, 520.

[18] V. Aliev, M.R. Aleksanyan, *Optika Spectroscopia*, 1968, **24**, 695.

[19] D. Papousek and M. Aliev, *Molecular Vibrational-rotational Spectra: Theory and Applications of High Resolution Infrared*, Elsevier, 1982.

[20] J. H. Van Vleck, *Phys. Rev.*, 1929, **33**, 467–506.

[21] C. P. Slichter, *Principles of Magnetic Resonance*, Springer Science & Business Media, 2013, vol. 1.

[22] V. Ganapathy and R. Ramachandran, *J. Chem. Phys.*, 2017, **147**, 144202.

Appendix

A Matrix Representation of Operators and Commutator Relations

A.1 Definition of Tensor Operators for Spin $I = {}^3/_2$

Table A.1.1: **The Basis Tensors for spin I=3/2**

Zero Coherence Tensors	
$T^{(0)0} = \frac{1}{2}\begin{bmatrix} 1 & 0 & 0 & 0 \\ 0 & 1 & 0 & 0 \\ 0 & 0 & 1 & 0 \\ 0 & 0 & 0 & 1 \end{bmatrix}$	$T^{(1)0} = \frac{i}{2\sqrt{5}}\begin{bmatrix} 3 & 0 & 0 & 0 \\ 0 & 1 & 0 & 0 \\ 0 & 0 & -1 & 0 \\ 0 & 0 & 0 & -3 \end{bmatrix}$
$T^{(2)0} = \frac{1}{2}\begin{bmatrix} -1 & 0 & 0 & 0 \\ 0 & 1 & 0 & 0 \\ 0 & 0 & 1 & 0 \\ 0 & 0 & 0 & -1 \end{bmatrix}$	$T^{(3)0} = \frac{i}{2\sqrt{5}}\begin{bmatrix} -1 & 0 & 0 & 0 \\ 0 & 3 & 0 & 0 \\ 0 & 0 & -3 & 0 \\ 0 & 0 & 0 & 1 \end{bmatrix}$
+1 Coherence Tensors	
$T^{(1)1} = -i\sqrt{\frac{1}{10}}\begin{bmatrix} 0 & \sqrt{3} & 0 & 0 \\ 0 & 0 & 2 & 0 \\ 0 & 0 & 0 & \sqrt{3} \\ 0 & 0 & 0 & 0 \end{bmatrix}$	$T^{(2)1} = \sqrt{\frac{1}{2}}\begin{bmatrix} 0 & 1 & 0 & 0 \\ 0 & 0 & 0 & 0 \\ 0 & 0 & 0 & -1 \\ 0 & 0 & 0 & 0 \end{bmatrix}$
$T^{(3)1} = i\sqrt{\frac{1}{5}}\begin{bmatrix} 0 & 1 & 0 & 0 \\ 0 & 0 & -\sqrt{3} & 0 \\ 0 & 0 & 0 & 1 \\ 0 & 0 & 0 & 0 \end{bmatrix}$	$RF_A^+ = \begin{bmatrix} 0 & \sqrt{3} & 0 & 0 \\ 0 & 0 & 0 & 0 \\ 0 & 0 & 0 & 0 \\ 0 & 0 & 0 & 0 \end{bmatrix}$
$RF_B^+ = \begin{bmatrix} 0 & 0 & 0 & 0 \\ 0 & 0 & 0 & 0 \\ 0 & 0 & 0 & \sqrt{3} \\ 0 & 0 & 0 & 0 \end{bmatrix}$	$RF_C^+ = \begin{bmatrix} 0 & 0 & 0 & 0 \\ 0 & 0 & 1 & 0 \\ 0 & 0 & 0 & 0 \\ 0 & 0 & 0 & 0 \end{bmatrix}$
−1 Coherence Tensors	
$T^{(1)-1} = i\sqrt{\frac{1}{10}}\begin{bmatrix} 0 & 0 & 0 & 0 \\ \sqrt{3} & 0 & 0 & 0 \\ 0 & 2 & 0 & 0 \\ 0 & 0 & \sqrt{3} & 0 \end{bmatrix}$	$T^{(2)-1} = \sqrt{\frac{1}{2}}\begin{bmatrix} 0 & 0 & 0 & 0 \\ -1 & 0 & 0 & 0 \\ 0 & 0 & 0 & 0 \\ 0 & 0 & 1 & 0 \end{bmatrix}$
$T^{(3)-1} = -i\sqrt{\frac{1}{5}}\begin{bmatrix} 0 & 0 & 0 & 0 \\ 1 & 0 & 0 & 0 \\ 0 & -\sqrt{3} & 0 & 0 \\ 0 & 0 & 1 & 0 \end{bmatrix}$	$RF_A^- = \begin{bmatrix} 0 & 0 & 0 & 0 \\ \sqrt{3} & 0 & 0 & 0 \\ 0 & 0 & 0 & 0 \\ 0 & 0 & 0 & 0 \end{bmatrix}$

The Basis Tensors for spin I=3/2 (*contd.*)

$RF_B^- = \begin{bmatrix} 0 & 0 & 0 & 0 \\ 0 & 0 & 0 & 0 \\ 0 & 0 & 0 & 0 \\ 0 & 0 & \sqrt{3} & 0 \end{bmatrix}$	$RF_C^- = \begin{bmatrix} 0 & 0 & 0 & 0 \\ 0 & 0 & 0 & 0 \\ 0 & 1 & 0 & 0 \\ 0 & 0 & 0 & 0 \end{bmatrix}$
+2 Coherence Tensors	
$T^{(2)2} = -\sqrt{\frac{1}{2}} \begin{bmatrix} 0 & 0 & 1 & 0 \\ 0 & 0 & 0 & 1 \\ 0 & 0 & 0 & 0 \\ 0 & 0 & 0 & 0 \end{bmatrix}$	$T^{(3)2} = i\sqrt{\frac{1}{2}} \begin{bmatrix} 0 & 0 & -1 & 0 \\ 0 & 0 & 0 & 1 \\ 0 & 0 & 0 & 0 \\ 0 & 0 & 0 & 0 \end{bmatrix}$
$D_1^+ = \begin{bmatrix} 0 & 0 & 0 & 0 \\ 0 & 0 & 0 & -\sqrt{2} \\ 0 & 0 & 0 & 0 \\ 0 & 0 & 0 & 0 \end{bmatrix}$	$D_2^+ = \begin{bmatrix} 0 & 0 & -\sqrt{2} & 0 \\ 0 & 0 & 0 & 0 \\ 0 & 0 & 0 & 0 \\ 0 & 0 & 0 & 0 \end{bmatrix}$
−2 Coherence Tensors	
$T^{(2)-2} = -\sqrt{\frac{1}{2}} \begin{bmatrix} 0 & 0 & 0 & 0 \\ 0 & 0 & 0 & 0 \\ 1 & 0 & 0 & 0 \\ 0 & 1 & 0 & 0 \end{bmatrix}$	$T^{(3)-2} = i\sqrt{\frac{1}{2}} \begin{bmatrix} 0 & 0 & 0 & 0 \\ 0 & 0 & 0 & 0 \\ -1 & 0 & 0 & 0 \\ 0 & 1 & 0 & 0 \end{bmatrix}$
$D_1^- = \begin{bmatrix} 0 & 0 & 0 & 0 \\ 0 & 0 & 0 & 0 \\ -\sqrt{2} & 0 & 0 & 0 \\ 0 & 0 & 0 & 0 \end{bmatrix}$	$D_2^- = \begin{bmatrix} 0 & 0 & 0 & 0 \\ 0 & 0 & 0 & 0 \\ 0 & 0 & 0 & 0 \\ 0 & -\sqrt{2} & 0 & 0 \end{bmatrix}$
±3 Coherence Tensors	
$T^{(3)3} = T^+ = i \begin{bmatrix} 0 & 0 & 0 & 1 \\ 0 & 0 & 0 & 0 \\ 0 & 0 & 0 & 0 \\ 0 & 0 & 0 & 0 \end{bmatrix}$	$T^{(3)-3} = T^- = -i \begin{bmatrix} 0 & 0 & 0 & 0 \\ 0 & 0 & 0 & 0 \\ 0 & 0 & 0 & 0 \\ 1 & 0 & 0 & 0 \end{bmatrix}$

A.2 Commutation Relations for Spin $I = {}^3/_2$

1. $\left[(\Phi RF_A^+ + \Phi^{-1} RF_B^-), I_z\right] = -\left(\Phi RF_A^+ - \Phi^{-1} RF_B^-\right)$
2. $\left[(\Phi RF_A^+ - \Phi^{-1} RF_B^-), I_z\right] = -\left(\Phi RF_A^+ + \Phi^{-1} RF_B^-\right)$
3. $\left[(\Phi^{-1} RF_A^- + \Phi RF_B^+), I_z\right] = \Phi^{-1} RF_A^- - \Phi RF_B^+$
4. $\left[(\Phi^{-1} RF_A^- - \Phi RF_B^+), I_z\right] = \Phi^{-1} RF_A^- + \Phi RF_B^+$
5. $\left[(\Phi RF_C^+ + \Phi^{-1} RF_C^-), I_z\right] = -\left(\Phi RF_C^+ - \Phi^{-1} RF_C^-\right)$

6. $\left[(\Phi RF_C^+ - \Phi^{-1}RF_C^-), I_z\right] = -\left(\Phi RF_C^+ + \Phi^{-1}RF_C^-\right)$

7. $\left[((\Phi RF_A^+ + \Phi^{-1}RF_B^-), T^{(2)0}\right] = (\Phi RF_A^+ + \Phi^{-1}RF_B^-)$
8. $\left[(\Phi RF_A^+ - \Phi^{-1}RF_B^-), T^{(2)0}\right] = (\Phi RF_A^+ - \Phi^{-1}RF_B^-)$
9. $\left[(\Phi^{-1}RF_A^- + \Phi RF_B^+), T^{(2)0}\right] = -(\Phi^{-1}RF_A^- + \Phi RF_B^+)$
10. $\left[(\Phi^{-1}RF_A^- - \Phi RF_B^+), T^{(2)0}\right] = -(\Phi^{-1}RF_A^- - \Phi RF_B^+)$
11. $\left[(\Phi RF_C^+ + \Phi^{-1}RF_C^-), T^{(2)0}\right] = 0$
12. $\left[(\Phi RF_C^+ - \Phi^{-1}RF_C^-), T^{(2)0}\right] = 0$
13. $\left[\left(\Phi^2 D_1^+ + \Phi^{-2}D_1^-\right), T^{(2)0}\right] = -\left(\Phi^2 D_1^+ + \Phi^{-2}D_1^-\right)$
14. $\left[\left(\Phi^2 D_1^+ - \Phi^{-2}D_1^-\right), T^{(2)0}\right] = -\left(\Phi^2 D_1^+ - \Phi^{-2}D_1^-\right)$
15. $\left[\left(\Phi^2 D_2^+ + \Phi^{-2}D_2^-\right), T^{(2)0}\right] = \left(\Phi^2 D_2^+ + \Phi^{-2}D_2^-\right)$
16. $\left[\left(\Phi^2 D_2^+ - \Phi^{-2}D_2^-\right), T^{(2)0}\right] = \left(\Phi^2 D_2^+ - \Phi^{-2}D_2^-\right)$

17. $\left[(\Phi RF_A^+ + \Phi^{-1}RF_B^-), T^{(3)0}\right] = \frac{2i}{\sqrt{5}}\left(\Phi RF_A^+ - \Phi^{-1}RF_B^-\right)$
18. $\left[(\Phi RF_A^+ - \Phi^{-1}RF_B^-), T^{(3)0}\right] = \frac{2i}{\sqrt{5}}\left(\Phi RF_A^+ + \Phi^{-1}RF_B^-\right)$
19. $\left[(\Phi^{-1}RF_A^- + \Phi RF_B^+), T^{(3)0}\right] = -\frac{2i}{\sqrt{5}}\left(\Phi^{-1}RF_A^- - \Phi RF_B^+\right)$
20. $\left[(\Phi^{-1}RF_A^- - \Phi RF_B^+), T^{(3)0}\right] = -\frac{2i}{\sqrt{5}}\left(\Phi^{-1}RF_A^- + \Phi RF_B^+\right)$
21. $\left[(\Phi RF_C^+ + \Phi^{-1}RF_C^-), T^{(3)0}\right] = -\frac{3i}{\sqrt{5}}\left(\Phi RF_C^+ - \Phi^{-1}RF_C^-\right)$
22. $\left[(\Phi RF_C^+ - \Phi^{-1}RF_C^-), T^{(3)0}\right] = -\frac{3i}{\sqrt{5}}\left(\Phi RF_C^+ + \Phi^{-1}RF_C^-\right)$

23. $\left[(\Phi RF_A^+ + \Phi^{-1}RF_B^-), (\Phi RF_A^+ + \Phi^{-1}RF_B^-)\right] = 0$

24. $\left[(\Phi RF_A^+ + \Phi^{-1}RF_B^-), (\Phi RF_A^+ - \Phi^{-1}RF_B^-)\right] = 0$

25. $\left[(\Phi RF_A^+ + \Phi^{-1}RF_B^-), (\Phi^{-1}RF_A^- + \Phi RF_B^+)\right] = -6\ T^{(2)0}$

26. $\left[(\Phi RF_A^+ + \Phi^{-1}RF_B^-), (\Phi^{-1}RF_A^- - \Phi RF_B^+)\right] = -\frac{6i}{\sqrt{5}}\left(T^{(1)0} - 2\ T^{(3)0}\right)$

27. $\left[(\Phi RF_A^+ + \Phi^{-1}RF_B^-), (\Phi RF_C^+ + \Phi^{-1}RF_C^-)\right] = -\sqrt{\frac{3}{2}}\left(\Phi^2 D_2^+ + \Phi^{-2}D_2^-\right)$

28. $\left[(\Phi RF_A^+ + \Phi^{-1}RF_B^-), (\Phi RF_C^+ - \Phi^{-1}RF_C^-)\right] = -\sqrt{\frac{3}{2}}\left(\Phi^2 D_2^+ - \Phi^{-2}D_2^-\right)$

29. $\left[(\Phi RF_A^+ + \Phi^{-1}RF_B^-), (\Phi^2 D_1^+ + \Phi^{-2}D_1^-)\right] = \sqrt{6}\left((\hat{CT}_S) + i(\hat{T}_{AS}))\right)$

30. $\left[(\Phi RF_A^+ + \Phi^{-1}RF_B^-), (\Phi^2 D_1^+ - \Phi^{-2}D_1^-)\right] = \sqrt{6}\left((\hat{CT}_{AS}) + i(\hat{T}_S))\right)$

31. $\left[(\Phi RF_A^+ + \Phi^{-1}RF_B^-), (\Phi^2 D_2^+ + \Phi^{-2}D_2^-)\right] = 0$

32. $\left[(\Phi RF_A^+ + \Phi^{-1}RF_B^-), (\Phi^2 D_2^+ - \Phi^{-2}D_2^-)\right] = 0$

33. $\left[(\Phi RF_A^+ + \Phi^{-1}RF_B^-), \left((\hat{CT}_S) + i(\hat{T}_{AS}))\right)\right] = -\sqrt{6}\ (\Phi^2 D_2^+ + \Phi^{-2}D_2^-)$

34. $\left[(\Phi RF_A^+ - \Phi^{-1}RF_B^-), (\Phi RF_A^+ - \Phi^{-1}RF_B^-)\right] = 0$

35. $\left[(\Phi RF_A^+ - \Phi^{-1}RF_B^-), (\Phi^{-1}RF_A^- + \Phi RF_B^+)\right] = -\frac{6i}{\sqrt{5}}\left(T^{(1)0} - 2\ T^{(3)0}\right)$

36. $\left[(\Phi RF_A^+ - \Phi^{-1}RF_B^-), (\Phi^{-1}RF_A^- - \Phi RF_B^+)\right] = -6\ T^{(2)0}$

37. $\left[(\Phi RF_A^+ - \Phi^{-1}RF_B^-), (\Phi RF_C^+ + \Phi^{-1}RF_C^-)\right] = -\sqrt{\frac{3}{2}}\left(\Phi^2 D_2^+ - \Phi^{-2}D_2^-\right)$

38. $\left[(\Phi RF_A^+ - \Phi^{-1}RF_B^-), (\Phi RF_C^+ - \Phi^{-1}RF_C^-)\right] = -\sqrt{\frac{3}{2}}\left(\Phi^2 D_2^+ + \Phi^{-2}D_2^-\right)$

39. $\left[(\Phi^{-1}RF_A^- + \Phi RF_B^+), (\Phi RF_A^+ + \Phi^{-1}RF_B^-)\right] = 6\ T^{(2)0}$

40. $\left[(\Phi^{-1}RF_A^- + \Phi RF_B^+), (\Phi RF_A^+ - \Phi^{-1}RF_B^-)\right] = \frac{6i}{\sqrt{5}}\left(T^{(1)0} - 2\ T^{(3)0}\right)$

41. $\left[(\Phi^{-1}RF_A^- + \Phi RF_B^+), (\Phi^{-1}RF_A^- + \Phi RF_B^+)\right] = 0$

42. $\left[(\Phi^{-1}RF_A^- + \Phi RF_B^+), (\Phi^{-1}RF_A^- - \Phi RF_B^+)\right] = 0$

43. $\left[(\Phi^{-1}RF_A^- + \Phi RF_B^+), (\Phi RF_C^+ + \Phi^{-1}RF_C^-)\right] = \sqrt{\frac{3}{2}}\left(\Phi^2 D_1^+ + \Phi^{-2}D_1^-\right)$

44. $\left[(\Phi^{-1}RF_A^- + \Phi RF_B^+), (\Phi RF_C^+ - \Phi^{-1}RF_C^-)\right] = \sqrt{\frac{3}{2}}\left(\Phi^2 D_1^+ - \Phi^{-2}D_1^-\right)$

45. $\left[(\Phi^{-1}RF_A^- + \Phi RF_B^+), \left(\Phi^2 D_1^+ + \Phi^{-2}D_1^-\right)\right] = 0$

46. $\left[(\Phi^{-1}RF_A^- + \Phi RF_B^+), \left(\Phi^2 D_1^+ - \Phi^{-2}D_1^-\right)\right] = 0$

47. $\left[(\Phi^{-1}RF_A^- + \Phi RF_B^+), \left(\Phi^2 D_2^+ + \Phi^{-2}D_2^-\right)\right] = -\sqrt{6}\left((\hat{CT}_S) + i(\hat{T}_{AS}))\right)$

48. $\left[(\Phi^{-1}RF_A^- + \Phi RF_B^+), \left((\hat{CT}_S) + i(\hat{T}_{AS}))\right)\right] = \sqrt{6}\left(\Phi^2 D_1^+ + \Phi^{-2}D_1^-\right)$

49. $\left[(\Phi^{-1}RF_A^- - \Phi RF_B^+), (\Phi RF_A^+ + \Phi^{-1}RF_B^-)\right] = \frac{6i}{\sqrt{5}}\left(T^{(1)0} - 2\ T^{(3)0}\right)$

50. $\left[(\Phi^{-1}RF_A^- - \Phi RF_B^+), (\Phi RF_A^+ - \Phi^{-1}RF_B^-)\right] = 6\ T^{(2)0}$

51. $\left[(\Phi^{-1}RF_A^- - \Phi RF_B^+), (\Phi^{-1}RF_A^- + \Phi RF_B^+)\right] = 0$

52. $\left[(\Phi^{-1}RF_A^- - \Phi RF_B^+), (\Phi^{-1}RF_A^- - \Phi RF_B^+)\right] = 0$

53. $\left[(\Phi^{-1}RF_A^- - \Phi RF_B^+), (\Phi RF_C^+ + \Phi^{-1}RF_C^-)\right] = -\sqrt{\frac{3}{2}}\left(\Phi^2 D_1^+ - \Phi^{-2}D_1^-\right)$

54. $\left[(\Phi^{-1}RF_A^- - \Phi RF_B^+), (\Phi RF_C^+ - \Phi^{-1}RF_C^-)\right] = -\sqrt{\frac{3}{2}}\left(\Phi^2 D_1^+ + \Phi^{-2}D_1^-\right)$

55. $\left[(\Phi RF_C^+ + \Phi^{-1}RF_C^-), (\Phi RF_C^+ - \Phi^{-1}RF_C^-)\right] = \frac{2i}{\sqrt{5}}\left(T^{(1)0} + 3\ T^{(3)0}\right)$

56. $\left[\left(\Phi^2 D_1^+ + \Phi^{-2} D_1^-\right), (\Phi R F_C^+ + \Phi^{-1} R F_C^-)\right] = \sqrt{\frac{2}{3}}\ (\Phi^{-1} R F_A^- + \Phi R F_B^+)$

57. $\left[\left(\Phi^2 D_2^+ + \Phi^{-2} D_2^-\right), (\Phi R F_C^+ + \Phi^{-1} R F_C^-)\right] = -\sqrt{\frac{2}{3}}\ (\Phi R F_A^+ + \Phi^{-1} R F_B^-)$

58. $\left[(\Phi R F_A^+ + \Phi^{-1} R F_B^-), T^{(3)-3}\right] = -i\sqrt{\frac{3}{2}}\ (\Phi\ D_2^-)$

59. $\left[(\Phi R F_A^+ - \Phi^{-1} R F_B^-), T^{(3)-3}\right] = -i\sqrt{\frac{3}{2}}\ (\Phi\ D_2^-)$

60. $\left[(\Phi^{-1} R F_A^- + \Phi R F_B^+), T^{(3)-3}\right] = i\sqrt{\frac{3}{2}}\ (\Phi\ D_1^-)$

61. $\left[(\Phi^{-1} R F_A^- - \Phi R F_B^+), T^{(3)-3}\right] = -i\sqrt{\frac{3}{2}}\ (\Phi\ D_1^-)$

62. $\left[\left(\Phi^2 D_1^+ + \Phi^{-2} D_1^-\right), T^{(3)-3}\right] = i\sqrt{\frac{2}{3}}\ (\Phi^2\ R F_A^-)$

63. $\left[\left(\Phi^2 D_2^+ + \Phi^{-2} D_2^-\right), T^{(3)-3}\right] = -i\sqrt{\frac{2}{3}}\ (\Phi^2\ R F_B^-)$

64. $\left[(\Phi R F_A^+ + \Phi^{-1} R F_B^-), (\Phi\ D_1^-)\right] = \sqrt{6}\ (\Phi^2 R F_c^- - i\ T^{(3)-3})$

65. $\left[(\Phi R F_A^+ + \Phi^{-1} R F_B^-), (\Phi\ D_2^-)\right] = 0$

66. $\left[(\Phi R F_A^+ + \Phi^{-1} R F_B^-), (\Phi^2 R F_c^- - i\ T^{(3)-3})\right] = -\sqrt{6}\ (\Phi\ D_2^-)$

67. $\left[(\Phi^{-1} R F_A^- + \Phi R F_B^+), (\Phi\ D_1^-)\right] = 0$

68. $\left[(\Phi^{-1} R F_A^- + \Phi R F_B^+), (\Phi\ D_2^-)\right] = -\sqrt{6}\ (\Phi^2 R F_c^- - i\ T^{(3)-3})$

69. $\left[(\Phi^{-1} R F_A^- + \Phi R F_B^+), (\Phi^2 R F_c^- - i\ T^{(3)-3})\right] = \sqrt{6}\ (\Phi\ D_1^-)$

70. $\left[\left(\Phi^2 D_1^+ + \Phi^{-2} D_1^-\right), (\Phi^2 R F_c^- - i\ T^{(3)-3})\right] = \sqrt{\frac{2}{3}}\ (\Phi^2\ R F_A^- + \Phi^4\ R F_B^+)$

71. $\left[\left(\Phi^2 D_2^+ + \Phi^{-2} D_2^-\right), (\Phi^2 RF_c^- - i\ T^{(3)-3})\right] = -\sqrt{\frac{2}{3}}\ (\Phi^2\ RF_B^- + \Phi^4\ RF_A^+)$

B Calculations involving effective Hamiltonians from Regime-I

B.1 From first transformation S_1

Subsequently, to induce TQ transitions, the initial density operator (Eq. 3.26) is transformed by the effective pulse Hamiltonians (Eq. 3.22). Accordingly, the density operator during the pulse is evaluated,

$$\tilde{\rho}_F(t_{p1}) = \ exp\left(\frac{-iH_{eff}t_{p1}}{\hbar}\right)\ \tilde{\rho}_F(0)\ exp\left(\frac{iH_{eff}t_{p1}}{\hbar}\right) \tag{B.1.1}$$

where, 't_{p1}' is the duration of the pulse. To simplify the description and illustrate the development of coherences, the density operator is re-expressed in terms of the different coherences present in the system.

$$\tilde{\rho}_F(t_{p1}) = \tilde{\rho}_F(t_{p1})_{ZQ} + \tilde{\rho}_F(t_{p1})_{SQ} + \tilde{\rho}_F(t_{p1})_{DQ} + \tilde{\rho}_F(t_{p1})_{TQ} \tag{B.1.2}$$

The Zero-Quantum (ZQ) coherence or the populations is represented by,

$$\begin{aligned}\tilde{\rho}_F(t_{p1})_{ZQ} =& R_{Iz}^{(1)}\ (I_z)_0 + R_{ZQA}^{(1)}\,(ZQ_A)_0 + R_{ZQC}^{(1)}\left\{C_{(\theta_{CT})} - 1\right\}(ZQ_C)_0 \\ &+ R_{ZQD}^{(1)}\left\{C_{(\theta_{TQ})} - 1\right\}(ZQ_D)_0\end{aligned} \tag{B.1.3}$$

The Single-Quantum (SQ) coherence comprises of both the central (CT) and non-central (NCT) transitions.

$$\tilde{\rho}_F(t_{p1})_{SQ} = \tilde{\rho}_F(t_{p1})_{SQ,CT} + \tilde{\rho}_F(t_{p1})_{SQ,NCT}$$

It is important to realize here that the 'SQ' coherence corresponding to the central transitions is represented through diagonal operators $\left(\left(\hat{CT}\right)_0\right)$, while the non-

central transitions are represented by off-diagonal operators $\left(\left(\hat{SQ}\right)_{\pm 1}\right)$ in the Floquet space.

$$\tilde{\rho}_F(t_{p1})_{SQ,CT} = R^{(1)}_{CT}\ S_{(\theta_{CT})}\left(\hat{CT}_{AS}\right)_0 \tag{B.1.4}$$

$$\tilde{\rho}_F(t_{p1})_{SQ,NCT} = R^{(1)}_{SQ}\ C_{(\theta_{RF})}\left\{\left(\hat{SQ}^{(cr)}_{AS}\right)_{-1} e^{i(\theta_{ZQ})} + \left(\hat{SQ}^{(r)}_{AS}\right)_{+1} e^{-i(\theta_{ZQ})}\right\} \tag{B.1.5}$$

where,

$$\theta_{RF} = \omega_1 t_{p1} \quad ; \quad \theta_{ZQ} = \left(G^{(1)}_{ZQ} - \omega_Q\right) t_{p1}$$

The coherence corresponding to the two sets of Double-Quantum (DQ) transitions (see Figure. 3.3) are represented through off-diagonal operators $\left(\left(\hat{D}\right)_{\pm 1}\right)$

$$\tilde{\rho}_F(t_{p1})_{DQ} = R^{(1)}_{DQ}\ S_{(\theta_{RF})}\left\{\left(\hat{D}^{(cr)}_{AS}\right)_{-1} e^{i(\theta_{ZQ})} + \left(\hat{D}^{(r)}_{AS}\right)_{+1} e^{-i(\theta_{ZQ})}\right\} \tag{B.1.6}$$

In a similar vein, the Triple-Quantum (TQ) coherences are represented by,

$$\tilde{\rho}_F(t_{p1})_{TQ} = R^{(1)}_{TQ}\ S_{(\theta_{TQ})}\left(\hat{T}_S\right)_0 \tag{B.1.7}$$

As represented above, the coherences corresponding to the ZQ,SQ(CT) and TQ transitions are expressed in terms of diagonal operators, while the coherences corresponding to the SQ(NCT) and DQ transitions are represented in terms of off-diagonal operators in the Floquet framework. Although, from an experimental perspective, TQ transitions cannot be detected through direct means (they need to be reconverted back to detectable SQ(-1) transitions), the TQ excitation effi-

ciency is evaluated through the standard procedure illustrated below.

$$\begin{aligned}\left\langle T^{(3)-3}(t_{p1})\right\rangle &= Tr\left[\tilde{\rho}_F(t_{p1}).\tilde{T}_F^{(3)-3}\right] \\ &= R_{CT}^{(1)}.P_{CT}^{(1)}\ S_{(\theta_{CT})} + 2\ R_{DQ}^{(1)}.P_{DQ}^{(1)}\ S_{(\theta_{RF})}\left(e^{i(\theta_{ZQ})} + e^{-i(\theta_{ZQ})}\right) \\ &+ R_{TQ}^{(1)}.P_{TQ}^{(1)}\ S_{(\theta_{TQ})} \end{aligned} \tag{B.1.8}$$

On further simplification, the 'TQ' efficiency observed in experiments is calculated using the expression given below

$$\left\langle T^{(3)-3}(t_{p1})\right\rangle = \left(\Phi_1^3\Phi_R\right)\left\{-\frac{1}{4}\ J_1^{(\theta)}\ J_2^{(\theta)}\ S_{(\theta_{TQ})} + \frac{1}{4}\ J_{-1}^{(\theta)}\ J_{-2}^{(\theta)}\ S_{(\theta_{CT})} - \frac{1}{2}\left(S_{(\theta)}\right)^2 S_{(\theta_{RF})}\ C_{(\theta_{ZQ})}\right\} \tag{B.1.9}$$

In Eq. B.1.9, the notation $J_{\pm n}^{(\theta)} = \cos(\theta) \pm n$ with $\theta = \left(\frac{\sqrt{3}\omega_1}{\Omega_Q}\right)$ (where $(\Omega_Q = \omega_Q)$) has been employed.

When the initial density matrix and the detection operator are untransformed (i.e., $\rho_F(0) = (I_z)_0 \quad ; \quad T_F^{(3)-3} = e^{3i\omega_0 t_2}\ \Phi_R\left\{\left(T^{(3)-3}\right)_0\right\}$), the density operator after the pulse is evaluated using the standard procedure.

$$\begin{aligned}\rho_F(t_{p1}) &= (I_z)_0 - \frac{1}{2}\ \left\{C_{(\theta_{CT})} - 1\right\}(ZQ_C)_0 - \frac{3}{2}\ \left\{C_{(\theta_{TQ})} - 1\right\}(ZQ_D)_0 \\ &+ \frac{i}{2}\ S_{(\theta_{CT})}\left(\hat{CT}_{AS}\right)_0 - \frac{3}{2}\ S_{(\theta_{TQ})}\left(\hat{T}_S\right)_0 \end{aligned} \tag{B.1.10}$$

Subsequently, the expression for TQ signal reduces to a much simpler form.

$$\left\langle T^{(3)-3}(t_{p1})\right\rangle = Tr\left[\rho_F(t_{p1}).T_F^{(3)-3}\right] = \left(\Phi_1^3\ \Phi_R\right)\left\{-\frac{3}{2}\ S_{(\theta_{TQ})}\right\} \tag{B.1.11}$$

The above equation partially resembles to those proposed by Vega and Naor[2] (it is opposite in sign and twice in magnitude to their TQ expression).

Table B.1.1: Coefficients employed in the description of the density operator (Eqs. 3.26 and B.1.2) and the detection operator Eq. 3.27

Operator	0 **coherence**	± 1 **coherence**
density matrix	$R^{(1)}_{Iz} = 1$ $R^{(1)}_{ZQA} = -J^{(\theta)}_{-1}$ $R^{(1)}_{ZQC} = +\frac{1}{2}\ J^{(\theta)}_{-2}$ $R^{(1)}_{ZQD} = -\frac{1}{2}\ J^{(\theta)}_{2}$	$R^{(1)}_{CT} = -\frac{i}{2}\ J^{(\theta)}_{-2}$ $R^{(1)}_{SQ} = \frac{1}{2\sqrt{3}}\ S_{(\theta)}$
	± 2 **coherence**	± 3 **coherence**
	$R^{(1)}_{DQ} = +\frac{i}{2\sqrt{2}}\ S_{(\theta)}$	$R^{(1)}_{TQ} = -\frac{1}{2}\ J^{(\theta)}_{2}$
Operator	0 **coherence**	± 1 **coherence**
detection operator	0	$P^{(1)}_{CT} = \frac{i}{2}\ J^{(\theta)}_{-1}$
	± 2 **coherence**	± 3 **coherence**
	$P^{(1)}_{DQ} = +\frac{i}{2\sqrt{2}}\ S_{(\theta)}$	$P^{(1)}_{TQ} = \frac{1}{2}\ J^{(\theta)}_{+1}$

$$\theta_{CT} = 2G^{(1)}_{CT}t_{p1} \quad ; \quad \theta_{ZQ} = \left(G^{(1)}_{ZQ} - \omega_Q\right)t_{p1} \quad ; \quad \theta_{RF} = \omega_1 t_{p1}$$

$$\theta_{TQ} = 2G^{(1)}_{TQ}t_{p1} \quad ; \quad C_{(\theta)} = \cos(\theta) \quad ; \quad S_{(\theta)} = \sin(\theta)$$

$$J^{(\theta)}_{\pm n} = \cos(\theta) \pm n \quad ; \quad \theta = \left(\frac{\sqrt{3}\omega_1}{\Omega_Q}\right) \quad ; \quad \Phi^n_1 = e^{-in\phi}$$

Table B.1.2: Description of the coefficients employed in the derivation of effective Hamiltonian (Eq. 3.22) based on the first transformation

$G^{(1)}_{CT}$	$G^{(1)}_{TQ}$	$G^{(1)}_{ZQ}$
$G^{(1)}_{CT,0} = 0$	$G^{(1)}_{TQ,0} = 0$	$G^{(1)}_{ZQ,0} = \Delta$
$G^{(1)}_{CT,1} = -\omega_1$	$G^{(1)}_{TQ,1} = 0$	$G^{(1)}_{ZQ,1} = 0$
$G^{(1)}_{CT,2} = 0$	$G^{(1)}_{TQ,2} = 0$	$G^{(1)}_{ZQ,2} = -\left(\frac{\Omega_Q}{2}\right)(\theta)^2$
$G^{(1)}_{CT,3} = \frac{1}{2!}\left(\frac{\omega_1}{2}\right)(\theta)^2$	$G^{(1)}_{TQ,3} = \frac{1}{2!}\left(\frac{\omega_1}{2}\right)(\theta)^2$	$G^{(1)}_{ZQ,3} = 0$
$G^{(1)}_{CT,4} = 0$	$G^{(1)}_{TQ,4} = 0$	$G^{(1)}_{ZQ,4} = \left(\frac{\Omega_Q}{4\times 2!}\right)(\theta)^4$
$G^{(1)}_{CT,5} = -\frac{1}{4!}\left(\frac{\omega_1}{2}\right)(\theta)^4$	$G^{(1)}_{TQ,5} = -\frac{1}{4!}\left(\frac{\omega_1}{2}\right)(\theta)^4$	$G^{(1)}_{ZQ,5} = 0$
$G^{(1)}_{CT,6} = 0$	$G^{(1)}_{TQ,6} = 0$	$G^{(1)}_{ZQ,6} = -\left(\frac{\Omega_Q}{6\times 4!}\right)(\theta)^6$
$G^{(1)}_{CT,7} = \frac{1}{6!}\left(\frac{\omega_1}{2}\right)(\theta)^6$	$G^{(1)}_{TQ,7} = \frac{1}{6!}\left(\frac{\omega_1}{2}\right)(\theta)^6$	$G^{(1)}_{ZQ,7} = 0$
.	.	.
.	.	.
$G^{(1)}_{CT} = -\left(\frac{\omega_1}{2}\right)\{C_{(\theta)}+1\}$	$G^{(1)}_{TQ} = -\left(\frac{\omega_1}{2}\right)\{C_{(\theta)}-1\}$	$G^{(1)}_{ZQ} = \Delta + (\Omega_Q)\left\{-\frac{1}{2\times 0!}(\theta)^2 + \frac{1}{4\times 2!}(\theta)^4 - \frac{1}{6\times 4!}(\theta)^6 + ...\right\}$
$\theta = \left(\frac{\sqrt{3}\omega_1}{\Omega_Q}\right) \quad ; \quad C_{(\theta)} = \cos(\theta)$		

Table B.1.3: Coefficients employed in the derivation of Effective Hamiltonians for Case-I and Case-II

	$G^{(1)}_{CT}$	$G^{(1)}_{TQ}$	$G^{(1)}_{ZQ}$
Case-I $(N_1 = 3)$	$-\omega_1 + \frac{1}{2!}\left(\frac{\omega_1}{2}\right)(\theta)^2$	$+\frac{1}{2!}\left(\frac{\omega_1}{2}\right)(\theta)^2$	$\Delta - \frac{\Omega_Q}{2}(\theta)^2$
Case-II $(N_1 > 3)$	$-\frac{\omega_1}{2}\{C_{(\theta)}+1\}$	$-\frac{\omega_1}{2}\{C_{(\theta)}-1\}$	$\Delta + (\Omega_Q)\left\{-\frac{1}{2\times 0!}(\theta)^2 + \frac{1}{4\times 2!}(\theta)^4 - \frac{1}{6\times 4!}(\theta)^6 + ...\right\}$
$\theta = \left(\frac{\sqrt{3}\omega_1}{\Omega_Q}\right) \quad ; \quad C_{(\theta)} = \cos(\theta)$			

B.2 From second transformation S_2

The effective initial density matrix and the detector operators are given by,

$$\begin{aligned}\tilde{\tilde{\rho}}_F(0) &= e^{i\lambda^2 S_2}\ e^{i\lambda S_1}\ \rho_F(0)\ e^{-i\lambda S_1}\ e^{-i\lambda^2 S_2} \\ &= R^{(2)}_{Iz}\ \left(I_z\right)_0 + R^{(2)}_{ZQA}\left(ZQ_A\right)_0 + R^{(2)}_{ZQB}\left(ZQ_B\right)_0 \\ &+ R^{(2)}_{SQ1}\left\{\left(\hat{SQ}^{(r)}_{AS}\right)_{+1} + \left(\hat{SQ}^{(cr)}_{AS}\right)_{-1}\right\} - R^{(2)}_{DQ2}\left\{\left(\hat{D}^{(r)}_{AS}\right)_{+1} - \left(\hat{D}^{(cr)}_{AS}\right)_{-1}\right\}\end{aligned} \tag{B.2.1}$$

$$\begin{aligned}\tilde{\tilde{T}}^{(3)-3}_F &= e^{i\lambda^2 S_2}\ e^{i\lambda S_1}\ T^{(3)-3}_F\ e^{-i\lambda S_1}\ e^{-i\lambda^2 S_2} \\ \tilde{\tilde{T}}^{(3)-3}_F &= e^{3i\omega_0 t_2}\ \Phi_R\left\{P^{(2)}_{TQ-}\left(T^{(3)-3}\right)_0 + P^{(2)}_{CT-}\left(\Phi_1^2 RF^-_C\right)_0 + P^{(2)}_{CT+}\left(\Phi_1^4 RF^+_C\right)_0\right. \\ &\quad + P^{(2)}_{TQ+}\left(\Phi_1^6 T^{(3)3}\right)_0 + P^{(2)}_{SQ+}\left\{\left(\Phi_1^2 RF^-_A\right)_{+1} + \left(\Phi_1^2 RF^-_B\right)_{-1}\right\} \\ &\quad + P^{(2)}_{SQ-}\left\{\left(\Phi_1^4 RF^+_B\right)_{+1} + \left(\Phi_1^4 RF^+_A\right)_{-1}\right\} \\ &\quad \left. + P^{(2)}_{DQ}\left\{\left(\Phi_1 D^-_1\right)_{+1} + \left(\Phi_1 D^-_2\right)_{-1}\right\}\right\}\end{aligned} \tag{B.2.2}$$

A detailed description of the coefficients employed in Eqs. B.2.1 and B.2.2 are tabulated in Table.B.2.1.

Employing the effective Hamiltonian (Eq. 3.39) obtained from the second transformation 'S_2', the density matrix during the pulse is evaluated and re-expressed in terms of the coherences and populations.

$$\tilde{\tilde{\rho}}_F(t_{p1}) = \tilde{\tilde{\rho}}_F(t_{p1})_{ZQ} + \tilde{\tilde{\rho}}_F(t_{p1})_{SQ} + \tilde{\tilde{\rho}}_F(t_{p1})_{DQ} + \tilde{\tilde{\rho}}_F(t_{p1})_{TQ} \tag{B.2.3}$$

$$\begin{aligned}\tilde{\tilde{\rho}}_F(t_{p1})_{ZQ} =& R^{(2)}_{Iz}\ \left(I_z\right)_0 + R^{(ZQA)}_{Iz}\left(ZQ_A\right)_0 + R^{(2)}_{ZQB}\left(ZQ_B\right)_0 \\ &+ R^{(2)}_{ZQC}\left\{C_{(\theta_{CT})} - 1\right\}\left(ZQ_C\right)_0 + R^{(2)}_{ZQD}\left\{C_{(\theta_{TQ})} - 1\right\}\left(ZQ_D\right)_0\end{aligned} \tag{B.2.4}$$

$$\begin{aligned}\tilde{\tilde{\rho}}_F(t_{p1})_{SQ} &= \tilde{\tilde{\rho}}_F(t_{p1})_{SQ,CT} + \tilde{\tilde{\rho}}_F(t_{p1})_{SQ,NCT} \\ \tilde{\tilde{\rho}}_F(t_{p1})_{SQ,CT} &= R^{(2)}_{CT}\ S_{(\theta_{CT})}\left(\hat{CT}_{AS}\right)_0\end{aligned} \tag{B.2.5}$$

$$\tilde{\tilde{\rho}}_F(t_{p1})_{SQ,NCT} = \left(R^{(2)}_{SQ1}\ C_{(\theta_{RF})} - R^{(2)}_{SQ2}\ S_{(\theta_{RF})}\right)\left\{\left(\hat{SQ}^{(r)}_{AS}\right)_{+1} e^{-i(\theta_{ZQ})}\right\} + \left(R^{(2)}_{SQ1}\ C_{(\theta_{RF})} + R^{(2)}_{SQ2}\ S_{(\theta_{RF})}\right)\left\{\left(\hat{SQ}^{(cr)}_{AS}\right)_{-1} e^{i(\theta_{ZQ})}\right\} \quad \text{(B.2.6)}$$

$$\tilde{\tilde{\rho}}_F(t_{p1})_{DQ} = \left(R^{(2)}_{DQ1}\ S_{(\theta_{RF})} - R^{(2)}_{DQ2}\ C_{(\theta_{RF})}\right)\left\{\left(\hat{D}^{(r)}_{AS}\right)_{+1} e^{-i(\theta_{ZQ})}\right\} + \left(R^{(2)}_{DQ1}\ S_{(\theta_{RF})} + R^{(2)}_{DQ2}\ C_{(\theta_{RF})}\right)\left\{\left(\hat{D}^{(cr)}_{AS}\right)_{-1} e^{i(\theta_{ZQ})}\right\} \quad \text{(B.2.7)}$$

$$\tilde{\tilde{\rho}}_F(t_{p1})_{TQ} = R^{(2)}_{TQ}\ S_{(\theta_{TQ})}\left(\hat{T}_S\right)_0 \quad \text{(B.2.8)}$$

A detailed description of the coefficients is represented in Table. B.2.1. Subsequently, the TQ signal after two transformations is derived and represented by,

$$\begin{aligned}\left\langle T^{(3)-3}(t_{p1})\right\rangle = &\left(R^{(2)}_{TQ}.P^{(2)}_{TQ+} + R^{(2)}_{TQ}.P^{(2)}_{TQ-}\right)\ S_{(\theta_{TQ})} \\ &+ \left(R^{(2)}_{CT}.P^{(2)}_{CT-} - R^{(2)}_{CT}.P^{(2)}_{CT+}\right)\ S_{(\theta_{CT})} \\ &+ \Big\{2\ \left(R^{(2)}_{DQ1}\ S_{(\theta_{RF})} + R^{(2)}_{DQ2}\ C_{(\theta_{RF})}\right).P^{(2)}_{DQ} \\ &\quad +3\ \left(R^{(2)}_{SQ1}\ C_{(\theta_{RF})} + R^{(2)}_{SQ2}\ S_{(\theta_{RF})}\right).P^{(2)}_{SQ+} \\ &\quad -3\ \left(R^{(2)}_{SQ1}\ C_{(\theta_{RF})} + R^{(2)}_{SQ2}\ S_{(\theta_{RF})}\right).P^{(2)}_{SQ-}\Big\}.e^{i(\theta_{ZQ})} \\ &+ \Big\{2\ \left(R^{(2)}_{DQ1}\ S_{(\theta_{RF})} - R^{(2)}_{DQ2}\ C_{(\theta_{RF})}\right).P^{(2)}_{DQ} \\ &\quad -3\ \left(R^{(2)}_{SQ1}\ C_{(\theta_{RF})} - R^{(2)}_{SQ2}\ S_{(\theta_{RF})}\right).P^{(2)}_{SQ+} \\ &\quad +3\ \left(R^{(2)}_{SQ1}\ C_{(\theta_{RF})} - R^{(2)}_{SQ2}\ S_{(\theta_{RF})}\right).P^{(2)}_{SQ-}\Big\}.e^{-i(\theta_{ZQ})}\end{aligned} \quad \text{(B.2.9)}$$

$$\begin{aligned}\left\langle T^{(3)-3}\right\rangle = \left(\Phi_1^3\ \Phi_R\right)\Big\{&-\frac{1}{4}\ K^{(\theta_1,\theta_2)}_{+1}\ K^{(\theta_1,\theta_2)}_{+2}\ S_{(\theta_{TQ})} + \frac{1}{4}\ K^{(\theta_1,\theta_2)}_{-1}\ K^{(\theta_1,\theta_2)}_{-2}\ S_{(\theta_{CT})} \\ &-\frac{3}{2}\ S_{(\theta_1)}\ S_{(\theta_2)}\ C_{(\theta_{RF})}\ S_{(\theta_{ZQ})} \\ &-\left\{\frac{1}{2}\ \left(S_{(\theta_1)}\right)^2 + \left(S_{(\theta_2)}\right)^2\right\}\ S_{(\theta_{RF})}\ C_{(\theta_{ZQ})}\Big\}\end{aligned} \quad \text{(B.2.10)}$$

Table B.2.1: Coefficients employed in the derivation of the density operator (Eqs. B.2.1 and B.2.3) and the detection operator (Eq. B.2.2) after the second transformation

Operator	0 **coherence**	± 1 **coherence**
density matrix	$R^{(2)}_{Iz} = 1$ $R^{(2)}_{ZQA} = -J^{(\theta_1)}_{-1}$ $R^{(2)}_{ZQB} = -2J^{(\theta_2)}_{-1}$ $R^{(2)}_{ZQC} = +\frac{1}{2}\, K^{(\theta_1,\theta_2)}_{-2}$ $R^{(2)}_{ZQD} = -\frac{1}{2}\, K^{(\theta_1,\theta_2)}_{+2}$	$R^{(2)}_{CT} = -\frac{i}{2}\, K^{(\theta_1,\theta_2)}_{-2}$ $R^{(2)}_{SQ1} = \frac{1}{2\sqrt{3}}\, S_{(\theta_1)}$ $R^{(2)}_{SQ2} = \frac{i}{\sqrt{3}}\, S_{(\theta_2)}$
	± 2 **coherence**	± 3 **coherence**
	$R^{(2)}_{DQ1} = \frac{i}{2\sqrt{2}}\, S_{(\theta_1)}$ $R^{(2)}_{DQ2} = \frac{1}{\sqrt{2}}\, S_{(\theta_2)}$	$R^{(2)}_{TQ} = -\frac{1}{2}\, K^{(\theta_1,\theta_2)}_{+2}$

Operator	0 **coherence**	± 1 **coherence**
detection operator	0	$P^{(2)}_{CT-} = \frac{i}{2}\, C_{(\theta_1)} + \frac{i}{4}\, J^{(\theta)}_{-1}\, C_{(\theta_2)} - \frac{i}{4}\, J^{(\theta)}_{+1}$ $P^{(2)}_{CT+} = +\frac{i}{4}\, J^{(\theta)}_{+1}\, J^{(\theta_2)}_{-1}$ $P^{(2)}_{SQ+} = +\frac{i}{4\sqrt{3}}\, J^{(\theta)}_{+1}\, S_{(\theta_2)}$ $P^{(2)}_{SQ-} = +\frac{i}{4\sqrt{3}}\, J^{(\theta)}_{-1}\, S_{(\theta_2)}$
	± 2 **coherence**	± 3 **coherence**
	$P^{(2)}_{DQ} = +\frac{i}{2\sqrt{2}}\, S_{(\theta_1)}$	$P^{(2)}_{TQ-} = \frac{1}{2}\, C_{(\theta_1)} + \frac{1}{4}\, J^{(\theta)}_{+1}\, C_{(\theta_2)} - \frac{1}{4}\, J^{(\theta)}_{-1}$ $P^{(2)}_{TQ+} - \frac{1}{4}\, J^{(\theta)}_{-1}\, J^{(\theta_2)}_{-1}$

$$\theta_1 = \theta + 2\sqrt{3}\left(i\ C^{(2)}_{SQ}\right) \quad ; \quad \theta_2 = 2\sqrt{2}\left(i\ C^{(2)}_{DQ}\right) \quad ; \quad \theta_{ZQ} = \left(G^{(2)}_{ZQ} - \omega_Q\right) t_{p1}$$

$$\theta_{RF} = \omega_1 t_{p1} \quad ; \quad \theta_{CT} = 2G^{(2)}_{CT} t_{p1} \quad ; \quad \theta_{TQ} = 2G^{(2)}_{TQ} t_{p1} \quad ;$$

$$\theta = \left(\frac{\sqrt{3}\omega_1}{\Omega_Q}\right) \quad ; \quad J^{(\theta)}_{\pm n} = \cos(\theta) \pm n \quad ; \quad K^{(\theta_1,\theta_2)}_{\pm n} = \cos(\theta_1) \pm n\cos(\theta_2)$$

$$C_{(\theta)} = \cos(\theta) \quad ; \quad S_{(\theta)} = \sin(\theta)$$

Table B.2.2: Description of the coefficients employed in the perturbing Hamiltonian (Eq. 3.32)

$G^{(1)}_{SQ}$	$G^{(1)}_{DQ}$
$G^{(1)}_{SQ,0} = 0$	$G^{(1)}_{DQ,0} = 0$
$G^{(1)}_{SQ,1} = 0$	$G^{(1)}_{DQ,1} = 0$
$G^{(1)}_{SQ,2} = 0$	$G^{(1)}_{DQ,2} = -\frac{\omega_1}{2\sqrt{2}}(\theta)$
$G^{(1)}_{SQ,3} = \frac{1}{3\times 1!}\left(\frac{\omega_1}{2}\right)(\theta)^2$	$G^{(1)}_{DQ,3} = 0$
$G^{(1)}_{SQ,4} = 0$	$G^{(1)}_{DQ,4} = \frac{1}{3!}\left(\frac{\omega_1}{2\sqrt{2}}\right)(\theta)^3$
$G^{(1)}_{SQ,5} = -\frac{1}{5\times 3!}\left(\frac{\omega_1}{2}\right)(\theta)^4$	$G^{(1)}_{DQ,5} = 0$
$G^{(1)}_{SQ,6} = 0$	$G^{(1)}_{DQ,6} = -\frac{1}{5!}\left(\frac{\omega_1}{2\sqrt{2}}\right)(\theta)^5$
$G^{(1)}_{SQ,7} = \frac{1}{7\times 5!}\left(\frac{\omega_1}{2}\right)(\theta)^6$	$G^{(1)}_{DQ,7} = 0$
.	.
.	.
$G^{(1)}_{SQ} = +\left(\frac{\omega_1}{2}\right)\left\{\frac{1}{3\times 1!}(\theta)^2 - \frac{1}{5\times 3!}(\theta)^4 + \frac{1}{7\times 5!}(\theta)^6 - ....\right\}$	$G^{(1)}_{DQ} = -\left(\frac{\omega_1}{2\sqrt{2}}\right)S_{(\theta)}$
$\theta = \left(\frac{\sqrt{3}\omega_1}{\Omega_Q}\right) \quad ; \quad C_{(\theta)} = \cos(\theta) \quad ; \quad S_{(\theta)} = \sin(\theta)$	

Table B.2.3: Coefficients employed in the description of the Effective Hamiltonian (Eq. 3.39) derived from second transformation

$G^{(2)}_{CT}$	$G^{(2)}_{TQ}$	$G^{(2)}_{ZQ}$
$G^{(2)}_{CT,0} = G^{(1)}_{CT}$	$G^{(2)}_{TQ,0} = G^{(1)}_{TQ}$	$G^{(2)}_{ZQ,0} = G^{(1)}_{ZQ}$
$G^{(2)}_{CT,1} = 0$	$G^{(2)}_{TQ,1} = 0$	$G^{(2)}_{ZQ,1} = 0$
$G^{(2)}_{CT,2} = \frac{i}{2}\, G^{(2)}_{CTQ,A}$	$G^{(2)}_{TQ,2} = \frac{i}{2}\, G^{(2)}_{CTQ,A}$	$G^{(2)}_{ZQ,2} = \frac{i}{2}\, G^{(2)}_{ZQ,A}$
$G^{(2)}_{CT,3} = 0$	$G^{(2)}_{TQ,3} = 0$	$G^{(1)}_{ZQ,3} = 0$
$G^{(2)}_{CT,4} = -\frac{i}{4\times 2!}\, G^{(2)}_{CTQ,B}$	$G^{(2)}_{TQ,4} = -\frac{i}{4\times 2!}\, G^{(2)}_{CTQ,B}$	$G^{(2)}_{ZQ,4} = -\frac{i}{4\times 2!}\, G^{(2)}_{ZQ,B}$
$G^{(2)}_{CT,5} = 0$	$G^{(2)}_{TQ,5} = 0$	$G^{(2)}_{ZQ,5} = 0$
$G^{(2)}_{CT,6} = \frac{i}{6\times 4!}\, G^{(2)}_{CTQ,C}$	$G^{(2)}_{TQ,6} = \frac{i}{6\times 4!}\, G^{(2)}_{CTQ,C}$	$G^{(2)}_{ZQ,6} = \frac{i}{6\times 4!}\, G^{(2)}_{ZQ,C}$
$G^{(2)}_{CT,7} = 0$	$G^{(2)}_{TQ,7} = 0$	$G^{(2)}_{ZQ,7} = 0$
.	.	.
.	.	.
$G^{(2)}_{CT} = G^{(1)}_{CT} + \Big\{\, G^{(2)}_{CT,1}$ $+G^{(2)}_{CT,2} + \; G^{(2)}_{CT,3} + ...\Big\}$	$G^{(2)}_{TQ} = G^{(1)}_{TQ} + \Big\{\, G^{(2)}_{TQ,1}$ $+\; G^{(2)}_{TQ,2} + \; G^{(2)}_{TQ,3} + ...\Big\}$	$G^{(2)}_{ZQ} = G^{(1)}_{ZQ} + \Big\{\, G^{(2)}_{ZQ,1}$ $+\; G^{(2)}_{ZQ,2} + \; G^{(2)}_{ZQ,3} + ...\Big\}$
$\theta = \left(\frac{\sqrt{3}\omega_1}{\Omega_Q}\right) \quad ; \quad C_{(\theta)} = \cos(\theta)$		

C Calculations involving effective Hamiltonians from Regime-II

C.1 From first transformation S_1

To have a consistent description, the initial density operator ($\rho_F(0) = (I_z)_0$) along with the detection operator '$T^{(3)-3}$', is transformed by the transformation function 'S_1.' The transformed initial density operator and the detection operators are

illustrated below.

$$\begin{aligned}\tilde{\rho}_F(0) =& e^{i\lambda S_1}\ \rho_F(0)\ e^{-i\lambda S_1}\\ &= R^{(1)}_{STA}\left\{\left(\Phi_1 RF^{+}_{A}\right)_{+1} + \left(\Phi_1^{-1} RF^{-}_{A}\right)_{-1}\right\} + R^{(1)}_{STB}\left\{\left(\Phi_1 RF^{+}_{B}\right)_{+1} + \left(\Phi_1^{-1} RF^{-}_{B}\right)_{-1}\right\}\\ &+ R^{(1)}_{CT}\left\{\left(\Phi_1 RF^{+}_{C}\right)_{+1} + \left(\Phi_1^{-1} RF^{-}_{C}\right)_{-1}\right\} + R^{(1)}_{TQ}\left\{\left(i\Phi_1^{3} T^{(3)3}\right)_{+3} - \left(i\Phi_1^{-3} T^{(3)-3}\right)_{-3}\right\}\end{aligned} \tag{C.1.1}$$

$$\begin{aligned}\tilde{T}^{(3)-3}_{F} &= e^{i\lambda S_1}\ T^{(3)-3}_{F}\ e^{-i\lambda S_1}\\ &= e^{3i\omega_0 t_2}\ \Phi_R\left\{P^{(1)}_{TQ-}\left(T^{(3)-3}\right)_{-3} + P^{(1)}_{TQ+}\left(\Phi_1^{6} T^{(3)3}\right)_{+3}\right.\\ &\qquad + P^{(1)}_{CT-}\left(\Phi_1^{2} RF^{-}_{C}\right)_{-1} + P^{(1)}_{CT+}\left(\Phi_1^{4} RF^{+}_{C}\right)_{+1}\\ &\qquad + P^{(1)}_{STA-}\left(\Phi_1^{2} RF^{-}_{A}\right)_{-1} + P^{(1)}_{STA+}\left(\Phi_1^{4} RF^{+}_{A}\right)_{+1}\\ &\qquad \left. + P^{(1)}_{STB-}\left(\Phi_1^{2} RF^{-}_{B}\right)_{-1} + P^{(1)}_{STB+}\left(\Phi_1^{4} RF^{+}_{B}\right)_{+1}\right\}\end{aligned} \tag{C.1.2}$$

Subsequently, employing the effective Hamiltonian (Eq. 3.50), the evolution of the initial density operator in Regime-II is calculated. In contrast to the description in Regime-I, only SQ and TQ coherences are created by the pulse in Regime-II.

$$\tilde{\rho}_F(t_{p1}) = \tilde{\rho}_F(t_{p1})_{SQ} + \tilde{\rho}_F(t_{p1})_{TQ} \tag{C.1.3}$$

A detailed description of the coherences is illustrated below.

$$\tilde{\rho}_F(t_{p1})_{SQ} = \tilde{\rho}_F(t_{p1})_{SQ,CT} + \tilde{\rho}_F(t_{p1})_{SQ,ST}$$

The SQ central coherence corresponding to the central transition (SQ,CT) is represented by,

$$\tilde{\rho}_F(t_{p1})_{SQ,CT} = R^{(1)}_{CT}\left\{e^{i(\theta_{CT})}\left(\Phi_1 RF^{+}_{C}\right)_{+1} + e^{-i(\theta_{CT})}\left(\Phi_1^{-1} RF^{-}_{C}\right)_{-1}\right\} \tag{C.1.4}$$

while, the satellite transitions (SQ,ST) are represented by,

$$\begin{aligned}\tilde{\rho}_F(t_{p1})_{SQ,ST} &= R^{(1)}_{STA}\left\{e^{i(\theta_{STA})}\left(\Phi_1 RF^{+}_{A}\right)_{+1} + e^{-i(\theta_{STA})}\left(\Phi_1^{-1} RF^{-}_{STA}\right)_{-1}\right\}\\ &+ R^{(1)}_{STB}\left\{e^{i(\theta_{STB})}\left(\Phi_1 RF^{+}_{B}\right)_{+1} + e^{-i(\theta_{STB})}\left(\Phi_1^{-1} RF^{-}_{STB}\right)_{-1}\right\}\end{aligned} \tag{C.1.5}$$

In a similar vein, the TQ coherences are represented by

$$\tilde{\rho}_F(t_{p1})_{TQ} = R^{(1)}_{TQ}\left\{e^{i\left(\theta_{TQ}\right)}\left(i\Phi_1^3 T^{(3)3}\right)_{+3} + e^{-i\left(\theta_{TQ}\right)}\left(i\Phi_1^{-3}T^{(3)-3}\right)_{-3}\right\} \tag{C.1.6}$$

It is important to realize here that in Regime-II, both the SQ and TQ coherences are represented by off-diagonal operators. Subsequently, the TQ signal in Regime-II is calculated by the expression given below.

$$\begin{aligned}
\left\langle T^{(3)-3}(t_{p1})\right\rangle &= Tr\left[\tilde{\rho}_F(t_{p1}).\tilde{T}_F^{(3)-3}\right] \\
&= \left(iR^{(1)}_{TQ}\right).\left\{\left(P^{(1)}_{TQ-}\right)e^{\left(i\theta_{TQ}\right)} - \left(P^{(1)}_{TQ+}\right)e^{\left(-i\theta_{TQ}\right)}\right\} \\
&= \left(R^{(1)}_{CT}\right).\left\{\left(P^{(1)}_{CT-}\right)e^{(i\theta_{CT})} + \left(P^{(1)}_{CT+}\right)e^{(-i\theta_{CT})}\right\} \\
&= \left(R^{(1)}_{STA}\right).\left\{\left(P^{(1)}_{STA-}\right)e^{(i\theta_{STA})} + \left(P^{(1)}_{STA+}\right)e^{(-i\theta_{STA})}\right\} \\
&= \left(R^{(1)}_{STB}\right).\left\{\left(P^{(1)}_{STB-}\right)e^{(i\theta_{STB})} + \left(P^{(1)}_{STB+}\right)e^{(-i\theta_{STB})}\right\}
\end{aligned} \tag{C.1.7}$$

On further simplification, Eq. C.1.7 reduces to a much simpler form

$$\begin{aligned}
\left\langle T^{(3)-3}(t_{p1})\right\rangle = \left(\Phi_1^3\ \Phi_R\right)\Bigg\{ & -\frac{1}{8}\,S_{\left(\theta_{TQ}\right)}\left\{\left\{C_{(\xi)}-1\right\}\left\{2\,C_{(\xi)}-1\right\}\right\} \\
& +\frac{1}{8}\,S_{(\theta_{CT})}\left\{\left\{C_{(\xi)}+1\right\}\left\{2\,C_{(\xi)}+1\right\}\right\} \\
& -\frac{3}{8}\,S_{(\theta_{STA})}\left\{\left\{\frac{1}{\sqrt{3}}\,S_{(\xi)}-1\right\}\left\{\frac{2}{\sqrt{3}}\,S_{(\xi)}-1\right\}\right\} \\
& -\frac{3}{8}\,S_{(\theta_{STB})}\left\{\left\{\frac{1}{\sqrt{3}}\,S_{(\xi)}+1\right\}\left\{\frac{2}{\sqrt{3}}\,S_{(\xi)}+1\right\}\right\}\Bigg\}
\end{aligned} \tag{C.1.8}$$

Table C.1.1: Coefficients employed in the description of density operator (Eqs. C.1.1 and C.1.3) and detection operator Eq. C.1.2 in Regime-II based on first transformation

Operator	± 1 **coherence**	± 3 **coherence**
density matrix	$R^{(1)}_{STA} = +\frac{1}{2}\left\{\frac{1}{\sqrt{3}}\ S_{(\xi)} - 1\right\}$ $R^{(1)}_{STB} = -\frac{1}{2}\left\{\frac{1}{\sqrt{3}}\ S_{(\xi)} + 1\right\}$ $R^{(1)=}_{CT} - \frac{1}{2}\left\{\frac{1}{\sqrt{3}}\ C_{(\xi)} + 1\right\}$	$R^{(1)}_{TQ} = +\frac{1}{2}\left\{\frac{1}{\sqrt{3}}\ C_{(\xi)} - 1\right\}$
Detection operator	$P^{(1)}_{STA-} = +\left\{\frac{i}{8\sqrt{3}}\ S_{(\xi)} - \frac{i}{4}\right\}$ $P^{(1)}_{STA+} = -\left\{\frac{i\sqrt{3}}{8}\ S_{(\xi)}\right\}$ $P^{(1)}_{STB-} = +\left\{-\frac{i}{8\sqrt{3}}\ S_{(\xi)} - \frac{i}{4}\right\}$ $P^{(1)}_{STB+} = +\left\{\frac{i\sqrt{3}}{8}\ S_{(\xi)}\right\}$ $P^{(1)}_{CT-} = -\frac{i}{8}\left\{\ C_{(\xi)} + 1\right\}$ $P^{(1)}_{CT+} = \frac{3i}{8}\left\{\ C_{(\xi)} - 1\right\}$	$P^{(1)}_{TQ-} = \frac{1}{8}\left\{\ C_{(\xi)} + 1\right\}$ $P^{(1)}_{TQ+} = +\frac{3}{8}\left\{C_{(\xi)} - 1\right\}$

$$\xi = \left(\frac{\sqrt{3}\Omega_Q}{4\omega_1}\right) \quad ; \quad C_{(\xi)} = \cos(\xi) \quad ; \quad S_{(\xi)} = \sin(\xi)$$

$$\theta_{TQ} = 3\omega_1 t_{p1} + \frac{\left(3\ G^{(1)}_{1R} - G^{(1)}_{3R}\right) t_{p1}}{5} \quad ; \quad \theta_{CT} = \omega_1 t_{p1} + \frac{\left(G^{(1)}_{1R} + 3\ G^{(1)}_{3R}\right) t_{p1}}{5} \quad ;$$

$$\theta_{STA} = \omega_1 t_{p1} + \frac{\left(G^{(1)}_{1R} + 5\ G^{(1)}_{2R} - 2\ G^{(1)}_{3R}\right) t_{p1}}{5} \quad ; \quad \theta_{STB} = \omega_1 t_{p1} + \frac{\left(G^{(1)}_{1R} - 5\ G^{(1)}_{2R} - 2\ G^{(1)}_{3R}\right) t_{p1}}{5}$$

Table C.1.2: Definition of the coefficients employed in the derivation of effective Hamiltonian (Eq. 3.50) based on first transformation

$G_{1R}^{(1)}$	$G_{2R}^{(1)}$	$G_{3R}^{(1)}$
$G_{1R,1}^{(1)}=0$	$G_{2R,1}^{(1)}=\frac{\Omega_Q}{2}$	$G_{3R,1}^{(1)}=0$
$G_{1R,2}^{(1)}=\frac{1}{2\times 0!}\left(\sqrt{3}\Omega_Q\right)(\xi)$	$G_{2R,2}^{(1)}=0$	$G_{3R,2}^{(1)}=\frac{1}{2\times 0!}\left(\frac{\sqrt{3}\Omega_Q}{2}\right)(\xi)$
$G_{1R,3}^{(1)}=0$	$G_{2R,3}^{(1)}=-\frac{1}{2!}\frac{\Omega_Q}{2}(\xi)^2$	$G_{3R,3}^{(1)}=0$
$G_{1R,4}^{(1)}=-\frac{1}{4\times 2!}\left(\sqrt{3}\Omega_Q\right)(\xi)^3$	$G_{2R,4}^{(1)}=0$	$G_{3R,4}^{(1)}=-\frac{1}{4\times 2!}\left(\frac{\sqrt{3}\Omega_Q}{2}\right)(\xi)^3$
$G_{1R,5}^{(1)}=0$	$G_{2R,5}^{(1)}=\frac{1}{4!}\frac{\Omega_Q}{2}(\xi)^4$	$G_{3R,5}^{(1)}=0$
$G_{1R,6}^{(1)}=\frac{1}{6\times 4!}\left(\sqrt{3}\Omega_Q\right)(\xi)^5$	$G_{2R,6}^{(1)}=0$	$G_{3R,6}^{(1)}=\frac{1}{6\times 4!}\left(\frac{\sqrt{3}\Omega_Q}{2}\right)(\xi)^5$
$G_{1R,7}^{(1)}=0$	$G_{2R,7}^{(1)}=-\frac{1}{6!}\frac{\Omega_Q}{2}(\xi)^6$	$G_{3R,7}^{(1)}=0$
.	.	.
.	.	.
$G_{1R}^{(1)}=\left(\sqrt{3}\Omega_Q\right)\left\{+\frac{1}{2\times 0!}(\xi)\right.$ $\left.-\frac{1}{4\times 2!}(\xi)^3+\frac{1}{6\times 4!}(\xi)^5+....\right\}$	$G_{2R}^{(1)}=\left(\frac{\Omega_Q}{2}\right)C_{(\xi)}$	$G_{3R}^{(1)}=\left(\frac{\sqrt{3}\Omega_Q}{2}\right)\left\{+\frac{1}{2\times 0!}(\xi)\right.$ $\left.-\frac{1}{4\times 2!}(\xi)^3+\frac{1}{6\times 4!}(\xi)^5+....\right\}$
$\xi=\left(\frac{\sqrt{3}\Omega_Q}{4\omega_1}\right)\quad;\quad C_{(\xi)}=\cos(\xi)$		

Table C.1.3: Coefficients employed in the derivation of Effective Hamiltonians for Case-I and Case-II in Regime-II based on first transformation

	$G_{1R}^{(1)}$	$G_{2R}^{(1)}$	$G_{3R}^{(1)}$
Case-I	$\left\{\left(\frac{\sqrt{3}\Omega_Q}{2}\right)(\xi)\right\}$	$+\left(\frac{\Omega_Q}{2}\right)-\frac{1}{2!}\left(\frac{\Omega_Q}{2}\right)(\xi)^2$	$\frac{1}{2}\left\{\left(\frac{\sqrt{3}\Omega_Q}{2}\right)(\xi)\right\}$
Case-II	$\left(\sqrt{3}\Omega_Q\right)\left\{+\frac{1}{2\times 0!}(\xi)\right.$ $\left.-\frac{1}{4\times 2!}(\xi)^3+\frac{1}{6\times 4!}(\xi)^5+....\right\}$	$\left(\frac{\Omega_Q}{2}\right)C_{(\xi)}$	$\left(\frac{\sqrt{3}\Omega_Q}{2}\right)\left\{+\frac{1}{2\times 0!}(\xi)\right.$ $\left.-\frac{1}{4\times 2!}(\xi)^3+\frac{1}{6\times 4!}(\xi)^5+....\right\}$
$\xi=\left(\frac{\sqrt{3}\Omega_Q}{4\omega_1}\right)\quad;\quad C_{(\xi)}=\cos(\xi)$			

C.2 From second transformation S_2

To further improve the accuracy of the analytic simulations, the residual off-diagonal terms neglected in the first transformation were further considered in the calculations. As illustrated in Table.3.7, 3.8the off-diagonal contributions in Regime-II mainly comprise of the DQ transitions operators. To fold the above off-diagonal contributions, a second transformation 'S_2' was employed. The diagonal corrections from the first transformation were included along 'H_0' and the off-diagonal operators $\left(\left(\hat{D}\right)_{\pm 1}\right)$ were included as perturbations. A brief description of the procedure employed in the derivation of effective Floquet Hamiltonian from the second transformation 'S_2' is outlined below.

$$H_0 = \omega_1 I_F + \frac{i}{\sqrt{5}}\, G_{1R}^{(1)} \left(T^{(1)0}\right)_0 + \; G_{2R}^{(1)} \left(T^{(2)0}\right)_0 + \frac{i}{\sqrt{5}}\, G_{3R}^{(1)} \left(T^{(3)0}\right)_0 \tag{C.2.1}$$

$$H_1 = G_{DR}^{(1)} \left\{ \left(\Phi_1^2 T^{(2)2}\right)_{+2} + \left(\Phi_1^{-2} T^{(2)-2}\right)_{-2} \right\} + G_{TR}^{(1)} \left\{ \left(i\Phi_1^2 T^{(3)2}\right)_{+2} + \left(i\Phi_1^{-2} T^{(3)-2}\right)_{-2} \right\} \tag{C.2.2}$$

$$G_{DR}^{(1)} = \sum_{i=1}^{N_1} G_{DR,i}^{(1)} = + \left(\frac{\sqrt{3}\Omega_Q}{2\sqrt{2}}\right) \left\{ \frac{1}{3 \times 1!} (\xi)^2 - \frac{1}{5 \times 3!} (\xi)^4 + \frac{1}{7 \times 5!} (\xi)^6 - .... \right\} \tag{C.2.3}$$

$$G_{TR}^{(1)} = \sum_{i=1}^{N_1} G_{TR,i}^{(1)} = - \left(\frac{\Omega_Q}{2\sqrt{2}}\right) S_{(\xi)} \tag{C.2.4}$$

where, '$G_{DR}^{(1)} = \sum_{i=1}^{N_1} G_{DR,i}^{(1)}$', '$G_{TR}^{(1)} = \sum_{i=1}^{N_1} G_{TR,i}^{(1)}$' and '$N_1$' represents the order of the corrections from the first transformation. Employing the transformation function 'S_2',

$$S_2 = C_{DR'}^{(2)} \left\{ \left(\Phi_1^2 T^{(2)2}\right)_{+2} - \left(\Phi_1^{-2} T^{(2)-2}\right)_{-2} \right\} + C_{TR'}^{(2)} \left\{ \left(i\Phi_1^2 T^{(3)2}\right)_{+2} - \left(i\Phi_1^{-2} T^{(3)-2}\right)_{-2} \right\} \tag{C.2.5}$$

$$C^{(2)}_{DR'} = \frac{-5i\left\{5\ G^{(1)}_{DR}\ G^{(1)}_{2R} + G^{(1)}_{TR}\left(2\ G^{(1)}_{1R} + G^{(1)}_{3R} + 10\ \omega_1\right)\right\}}{\left\{\left(5\ G^{(1)}_{2R}\right)^2 - \left(2\ G^{(1)}_{1R} + G^{(1)}_{3R} + 10\ \omega_1\right)^2\right\}}$$
$$C^{(2)}_{TR'} = \frac{-5i\left\{5\ G^{(1)}_{TR}\ G^{(1)}_{2R} + G^{(1)}_{DR}\left(2\ G^{(1)}_{1R} + G^{(1)}_{3R} + 10\ \omega_1\right)\right\}}{\left\{\left(5\ G^{(1)}_{2R}\right)^2 - \left(2\ G^{(1)}_{1R} + G^{(1)}_{3R} + 10\ \omega_1\right)^2\right\}} \tag{C.2.6}$$

$$C^{(i+1)}_{DR} = \sum_{i=1}^{n-1} C^{(i+1)}_{DR'} \quad ; \quad C^{(i+1)}_{TR} = \sum_{i=1}^{n-1} C^{(i+1)}_{TR'} \tag{C.2.7}$$

where 'i' takes values from 1 to '$n-1$', where 'n' is the number of 'S' transformations applied (Here $n = 2$).

the off-diagonal contributions to 'H_1' are completely folded. In contrast to the previous description involving single transformation, the higher order contributions in the present case are evaluated using the commutator between S_2 and H_1. Analogous to the description in Regime-I, the general expression illustrating the various contributions are presented below.

$$H^{(2)}_n = \sum_{n=2}^{\infty} \frac{(i)^{n-1}}{n \times (n-2)!} \left[\underbrace{[S_2, \ldots\ldots\ldots\ldots [S_2}_{n-1}, H_1\,] \ldots\ldots\ldots\ldots\right] \tag{C.2.8}$$

The diagonal and off-diagonal contributions resulting from the second transformation are tabulated in Table. C.2.1.

As illustrated in Table. C.2.1, the even order terms comprise of diagonal contributions (from ZQ operators $(T^{(1)0}, T^{(2)0}, T^{(3)0})$), while the odd-order terms represent off-diagonal contributions from $(DQ)_{\pm 1}$. Following the standard procedure, the effective Hamiltonian after second transformation is derived and represented below,

$$\begin{aligned} H_{eff} &= e^{i\lambda^2 S_2}\ e^{i\lambda S_1}\ H_F\ e^{-i\lambda S_1}\ e^{-i\lambda^2 S_2} \\ &= \omega_1 I_F + \frac{i}{\sqrt{5}}\ G^{(2)}_{1R}\left(T^{(1)0}\right)_0 + \ G^{(2)}_{2R}\left(T^{(2)0}\right)_0 + \frac{i}{\sqrt{5}}\ G^{(2)}_{3R}\left(T^{(3)0}\right)_0 \end{aligned} \tag{C.2.9}$$

Table C.2.1: Description of the higher order (diagonal and off-diagonal) contributions to the effective Hamiltonian (Eq. C.2.9) derived from second transformation in Regime-II

n^{th} **order Correction**	**Coefficients in the Effective Hamiltonian** $H_{eff} = H_0^{(1)} + H_2^{(1)} + H_4^{(1)} + H_6^{(1)} + \cdots = \omega_1 I_F + \frac{i}{\sqrt{5}}\, G_{1R}^{(2)} \left(T^{(1)0}\right)_0 + \; G_{2R}^{(2)} \left(T^{(2)0}\right)_0 + \frac{i}{\sqrt{5}}\, G_{3R}^{(2)} \left(T^{(3)0}\right)_0$	
	Expression from the '$H_{1,od}$' term	**Non-zero 'G' Coefficients**
Zero order (λ^0)	$H_0^{(2)} = \omega_1 I_F + \frac{i}{\sqrt{5}}\, G_{1R}^{(1)} \left(T^{(1)0}\right)_0 + \; G_{2R}^{(1)} \left(T^{(2)0}\right)_0 + \frac{i}{\sqrt{5}}\, G_{3R}^{(1)} \left(T^{(3)0}\right)_0$	$\omega_1 I_F + \frac{i}{\sqrt{5}}\, G_{1R}^{(1)} \left(T^{(1)0}\right)_0 + \; G_{2R}^{(1)} \left(T^{(2)0}\right)_0 + \frac{i}{\sqrt{5}}\, G_{3R}^{(1)} \left(T^{(3)0}\right)_0$
I order (λ^1)	$H_1^{(2)} = 0$	
II order (λ^2)	$H_2^{(2)} = \frac{i}{2\times 0!}[S_2, H_1] = + \left(\frac{i}{2\times 0!}\right) \left\{ \underbrace{2\left(C_{DR}^{(2)}\, G_{DR}^{(1)} + C_{TR}^{(2)}\, G_{TR}^{(1)}\right)}_{G_{13R,A}^{(2)}} \left\{ \left(\frac{-i}{\sqrt{5}}\right) \left(2T^{(1)0} + T^{(3)0}\right)_0 \right\} + \underbrace{2\left(C_{DR}^{(2)}\, G_{TR}^{(1)} + C_{TR}^{(2)}\, G_{DR}^{(1)}\right)}_{G_{2R,A}^{(2)}} \left(T^{(2)0}\right)_0 \right\}$	$\frac{i}{\sqrt{5}} \left(G_{1R,2}^{(2)} \left(T^{(1)0}\right)_0 + G_{3R,2}^{(2)} \left(T^{(3)0}\right)_0\right) + G_{2R,2}^{(2)} \left(T^{(2)0}\right)_0$
III order (λ^3)	$H_3^{(2)} = -\frac{1}{3\times 1!}[S_2, [S_2, H_1]] = + \left(\frac{1}{3\times 1!}\right) \left\{ - \underbrace{\left(C_{DR}^{(2)}\, G_{13R,A}^{(2)} + C_{TR}^{(2)}\, G_{2R,A}^{(2)}\right)}_{G_{DR,A}^{(2)}} \left\{ \left(\Phi_1^2 T^{(2)2}\right)_{+2} + \left(\Phi_1^{-2} T^{(2)-2}\right)_{-2} \right\} - \underbrace{\left(C_{DR}^{(2)}\, G_{2R,A}^{(2)} + C_{TR}^{(2)}\, G_{13R,A}^{(2)}\right)}_{G_{TR,A}^{(2)}} \left\{ \left(i\Phi_1^2 T^{(3)2}\right)_{+2} + \left(i\Phi_1^{-2} T^{(3)-2}\right)_{-2} \right\} \right\}$	$G_{DR,3}^{(2)} \left\{ \sum \left(\Phi_1^{\pm 2}\; T^{(2)\pm 2}\right)_{\pm 2} \right\} + G_{TR,3}^{(2)} \left\{ \sum i \left(\Phi_1^{\pm 2}\; T^{(3)\pm 2}\right)_{\pm 2} \right\}$
IV order (λ^4)	$H_4^{(2)} = -\frac{i}{4\times 2!}[S_2, [S_2, [S_2, H_1]]] = - \left(\frac{i}{4\times 2!}\right) \left\{ \underbrace{2\left(C_{DR}^{(2)}\, G_{DR,A}^{(2)} + C_{TR}^{(2)}\, G_{TR,A}^{(2)}\right)}_{G_{13R,B}^{(2)}} \left\{ \left(\frac{-i}{\sqrt{5}}\right) \left(2T^{(1)0} + T^{(3)0}\right)_0 \right\} + \underbrace{2\left(C_{DR}^{(2)}\; G_{TR,A}^{(2)} + C_{TR}^{(2)}\; G_{DR,A}^{(2)}\right)}_{G_{2R,B}^{(2)}} \left(T^{(2)0}\right)_0 \right\}$	$\frac{i}{\sqrt{5}} \left(G_{1R,4}^{(2)} \left(T^{(1)0}\right)_0 + G_{3R,4}^{(2)} \left(T^{(3)0}\right)_0\right) + G_{2R,4}^{(2)} \left(T^{(2)0}\right)_0$
V order (λ^5)	$H_5^{(2)} = \frac{1}{5\times 3!}[S_2, [S_2, [S_2, [S_2, H_1]]]] = - \left(\frac{1}{5\times 3!}\right) \left\{ - \underbrace{\left(C_{DR}^{(2)}\, G_{13R,B}^{(2)} + C_{TR}^{(2)}\, G_{2R,B}^{(2)}\right)}_{G_{DR,B}^{(2)}} \left\{ \left(\Phi_1^2 T^{(2)2}\right)_{+2} + \left(\Phi_1^{-2} T^{(2)-2}\right)_{-2} \right\} - \underbrace{\left(C_{DR}^{(2)}\, G_{2R,B}^{(2)} + C_{TR}^{(2)}\, G_{13R,B}^{(2)}\right)}_{G_{TR,B}^{(2)}} \left\{ \left(i\Phi_1^2 T^{(3)2}\right)_{+2} + \left(i\Phi_1^{-2} T^{(3)-2}\right)_{-2} \right\} \right\}$	$G_{DR,5}^{(2)} \left\{ \sum \left(\Phi_1^{\pm 2}\; T^{(2)\pm 2}\right)_{\pm 2} \right\} + G_{TR,5}^{(2)} \left\{ \sum i \left(\Phi_1^{\pm 2}\; T^{(3)\pm 2}\right)_{\pm 2} \right\}$
VI order (λ^6)	$H_6^{(2)} = \frac{i}{6\times 4!}[S_2, [S_2, [S_2, [S_2, [S_2, H_1]]]]] = + \left(\frac{i}{6\times 4!}\right) \left\{ \underbrace{2\left(C_{DR}^{(2)}\, G_{DR,B}^{(2)} + C_{TR}^{(2)}\, G_{TR,B}^{(2)}\right)}_{G_{13R,C}^{(2)}} \left\{ \left(\frac{-i}{\sqrt{5}}\right) \left(2T^{(1)0} + T^{(3)0}\right)_0 \right\} + \underbrace{2\left(C_{DR}^{(2)}\; G_{TR,B}^{(2)} + C_{TR}^{(2)}\; G_{DR,B}^{(2)}\right)}_{G_{2R,C}^{(2)}} \left(T^{(2)0}\right)_0 \right\}$	$\frac{i}{\sqrt{5}} \left(G_{1R,6}^{(2)} \left(T^{(1)0}\right)_0 + G_{3R,6}^{(2)} \left(T^{(3)0}\right)_0\right) + G_{2R,6}^{(2)} \left(T^{(2)0}\right)_0$
VII order (λ^7)	$H_7^{(2)} = -\frac{1}{7\times 5!}[S_2, [S_2, [S_2, [S_2, [S_2, H_1]]]]] = + \left(\frac{1}{7\times 5!}\right) \left\{ - \underbrace{\left(C_{DR}^{(2)}\, G_{13R,C}^{(2)} + C_{TR}^{(2)}\, G_{2R,C}^{(2)}\right)}_{G_{DR,C}^{(2)}} \left\{ \left(\Phi_1^2 T^{(2)2}\right)_{+2} + \left(\Phi_1^{-2} T^{(2)-2}\right)_{-2} \right\} - \underbrace{\left(C_{DR}^{(2)}\, G_{2R,C}^{(2)} + C_{TR}^{(2)}\, G_{13R,C}^{(2)}\right)}_{G_{TR,C}^{(2)}} \left\{ \left(i\Phi_1^2 T^{(3)2}\right)_{+2} + \left(i\Phi_1^{-2} T^{(3)-2}\right)_{-2} \right\} \right\}$	$G_{DR,7}^{(2)} \left\{ \sum \left(\Phi_1^{\pm 2}\; T^{(2)\pm 2}\right)_{\pm 2} \right\} + G_{TR,7}^{(2)} \left\{ \sum i \left(\Phi_1^{\pm 2}\; T^{(3)\pm 2}\right)_{\pm 2} \right\}$

In Eq. C.2.9, the coefficients '$G^{(2)}_{1R}$', '$G^{(2)}_{2R}$', '$G^{(2)}_{3R}$' comprises of diagonal contributions from both the first and second transformation.

$$\begin{aligned}
G^{(2)}_{1R} &= \sum_{i=1}^{N_1} G^{(1)}_{1R,i} + \sum_{j=1}^{N_2} G^{(2)}_{1R,j} \\
&= G^{(1)}_{1R} + \left\{ \frac{i}{2\times 0!}\, G^{(2)}_{13R,A} - \frac{i}{4\times 2!}\, G^{(2)}_{13R,B} + \frac{i}{6\times 4!}\, G^{(2)}_{13R,C} + \dots \right\} \\
G^{(2)}_{2R} &= \sum_{i=1}^{N_1} G^{(1)}_{2R,i} + \sum_{j=1}^{N_2} G^{(2)}_{2R,j} \\
&= G^{(1)}_{2R} + \left\{ \frac{i}{2\times 0!}\, G^{(2)}_{2R,A} - \frac{i}{4\times 2!}\, G^{(2)}_{2R,B} + \frac{i}{6\times 4!}\, G^{(2)}_{2R,C} + \dots \right\} \\
G^{(2)}_{3R} &= \sum_{i=1}^{N_1} G^{(1)}_{3R,i} + \sum_{j=1}^{N_2} G^{(2)}_{3R,j} \\
&= G^{(1)}_{3R} + \left\{ \frac{i}{2\times 0!}\, G^{(2)}_{13R,A}. - \frac{i}{4\times 2!}\, G^{(2)}_{13R,B} + \frac{i}{6\times 4!}\, G^{(2)}_{13R,C} + \dots \right\}
\end{aligned} \tag{C.2.10}$$

The operator form of the transformed initial density operator and the detection operator are identical to those derived in Eq. C.1.2. A detailed description of the coefficients is illustrated in Table. C.2.2

Subsequently, the TQ signal after the second transformation is calculated.

$$\begin{aligned}
\left\langle T^{(3)-3}(t_{p1}) \right\rangle &= Tr\left[\tilde{\rho}_F(t_{p1}).\tilde{T}^{(3)-3}_F \right] \\
&= \left(iR^{(2)}_{TQ} \right) . \left\{ \left(P^{(2)}_{TQ-} \right) e^{\left(i\theta_{TQ} \right)} - \left(P^{(2)}_{TQ+} \right) e^{\left(-i\theta_{TQ} \right)} \right\} \\
&= \left(R^{(2)}_{CT} \right) . \left\{ \left(P^{(2)}_{CT-} \right) e^{(i\theta_{CT})} + \left(P^{(2)}_{CT+} \right) e^{(-i\theta_{CT})} \right\} \\
&= \left(R^{(2)}_{STA} \right) . \left\{ \left(P^{(2)}_{STA-} \right) e^{(i\theta_{STA})} + \left(P^{(2)}_{STA+} \right) e^{(-i\theta_{STA})} \right\} \\
&= \left(R^{(2)}_{STB} \right) . \left\{ \left(P^{(2)}_{STB-} \right) e^{(i\theta_{STB})} + \left(P^{(2)}_{STB+} \right) e^{(-i\theta_{STB})} \right\}
\end{aligned} \tag{C.2.11}$$

Table C.2.2: Coefficients employed in the description of the density operator and the detection operator after the second transformation in Regime-II

Operator	± 1 **coherence**	± 3 **coherence**
density matrix	$R^{(2)}_{STA} = \left\{ \frac{1}{2\sqrt{3}} \left\{ S_{(\xi_1)} - S_{(\xi_2)} \right\} - \frac{1}{2}\, C_{(\xi_2)} \right\}$ $R^{(2)}_{STB} = \left\{ -\frac{1}{2\sqrt{3}} \left\{ S_{(\xi_1)} + S_{(\xi_2)} \right\} - \frac{1}{2}\, C_{(\xi_2)} \right\}$ $R^{(2)}_{CT} = \left\{ -\frac{1}{2} \left\{ C_{(\xi_1)} + C_{(\xi_2)} \right\} + \frac{\sqrt{3}}{2}\, S_{(\xi_2)} \right\}$	$R^{(2)}_{TQ} = \left\{ \frac{1}{2} \left\{ C_{(\xi_1)} - C_{(\xi_2)} \right\} + \frac{\sqrt{3}}{2}\, S_{(\xi_2)} \right\}$
Detection operator	$P^{(2)}_{STA-} = \left\{ \frac{i}{8\sqrt{3}} \left\{ S_{(\xi_1)} + S_{(\xi_2)} \right\} - \frac{i}{4}\, C_{(\xi_2)} \right\}$ $P^{(2)}_{STA+} = \left\{ -\frac{\sqrt{3}i}{8} \left\{ S_{(\xi_1)} - S_{(\xi_2)} \right\} \right\}$ $P^{(2)}_{STB-} = \left\{ \frac{-i}{8\sqrt{3}} \left\{ S_{(\xi_1)} - S_{(\xi_2)} \right\} - \frac{i}{4}\, C_{(\xi_2)} \right\}$ $P^{(2)}_{STB+} = \left\{ \frac{\sqrt{3}i}{8} \left\{ S_{(\xi_1)} + S_{(\xi_2)} \right\} \right\}$ $P^{(2)}_{CT-} = \left\{ \frac{3i}{8} \left\{ C_{(\xi_1)} + C_{(\xi_2)} \right\} \right\}$ $P^{(2)}_{CT+} = \left\{ \frac{-i}{8} \left\{ C_{(\xi_1)} - C_{(\xi_2)} \right\} + \frac{i\sqrt{3}}{4}\, S_{(\xi_2)} \right\}$	$P^{(2)}_{TQ-} = \left\{ \frac{1}{8} \left\{ C_{(\xi_1)} + C_{(\xi_2)} \right\} + \frac{\sqrt{3}}{4}\, S_{(\xi_2)} \right\}$ $P^{(2)}_{TQ+} = \left\{ \frac{3}{8} \left\{ C_{(\xi_1)} - C_{(\xi_2)} \right\} \right\}$
$\xi_1 = \xi + \sqrt{2}\left(iC^{(2)}_{DR}\right) \quad ; \quad \xi_2 = \sqrt{2}\left(iC^{(2)}_{TR}\right) \quad ; \quad C_{(\xi)} = \cos(\xi) \quad ; \quad S_{(\xi)} = \sin(\xi)$ $\theta_{TQ} = 3\omega_1 t_{p1} + \frac{\left(3\ G^{(2)}_{1R} - G^{(2)}_{3R}\right) t_{p1}}{5} \quad ; \quad \theta_{CT} = \omega_1 t_{p1} + \frac{\left(G^{(2)}_{1R} + 3\ G^{(2)}_{3R}\right) t_{p1}}{5} \quad ;$ $\theta_{STA} = \omega_1 t_{p1} + \frac{\left(G^{(2)}_{1R} + 5\ G^{(2)}_{2R} - 2\ G^{(2)}_{3R}\right) t_{p1}}{5} \quad ; \quad \theta_{STB} = \omega_1 t_{p1} + \frac{\left(G^{(2)}_{1R} - 5\ G^{(2)}_{2R} - 2\ G^{(2)}_{3R}\right) t_{p1}}{5}$		

On further simplification, Eq. C.2.11 reduces to a much simpler form

$$\begin{aligned}\left\langle T^{(3)-3}(t_{p1})\right\rangle = \left(\Phi_1^3\ \Phi_R\right)\Bigg\{ & -\frac{1}{8}\ S_{\left(\theta_{TQ}\right)}\left\{\left\{\left\{C_{(\xi_1)}-C_{(\xi_2)}\right\}+\sqrt{3}\ S_{(\xi_2)}\right\}\right. \\ & \left.\cdot\left\{\left\{2\ C_{(\xi_1)}-C_{(\xi_2)}\right\}+\sqrt{3}\ S_{(\xi_2)}\right\}\right\} \\ & +\frac{1}{8}\ S_{(\theta_{CT})}\left\{\left\{\left\{C_{(\xi_1)}+C_{(\xi_2)}\right\}-\sqrt{3}\ S_{(\xi_2)}\right\}\right. \\ & \left.\cdot\left\{\left\{2\ C_{(\xi_1)}+C_{(\xi_2)}\right\}-\sqrt{3}\ S_{(\xi_2)}\right\}\right\} \\ & -\frac{3}{8}\ S_{(\theta_{STA})}\left\{\left\{\frac{1}{\sqrt{3}}\left\{S_{(\xi_1)}-S_{(\xi_2)}\right\}-C_{(\xi_2)}\right\}\right. \\ & \left.\cdot\left\{\frac{1}{\sqrt{3}}\left\{2\ S_{(\xi_1)}-S_{(\xi_2)}\right\}-C_{(\xi_2)}\right\}\right\} \\ & -\frac{3}{8}\ S_{(\theta_{STB})}\left\{\left\{\frac{1}{\sqrt{3}}\left\{S_{(\xi_1)}+S_{(\xi_2)}\right\}+C_{(\xi_2)}\right\}\right. \\ & \left.\cdot\left\{\frac{1}{\sqrt{3}}\left\{2\ S_{(\xi_1)}+S_{(\xi_2)}\right\}+C_{(\xi_2)}\right\}\right\}\Bigg\}\end{aligned} \tag{C.2.12}$$

Based on the coefficients described in Table. C.2.2 and considering the leading terms, a simplified form of the above equation is derived. $\Bigg(\theta_{TQ} = 3\omega_1 t_{p1} + \dfrac{3\Omega_Q^2\ t_{p1}}{16\ \omega_1}$

$\theta_{CT} = \omega_1 t_{p1} + \dfrac{3\Omega_Q^2\ t_{p1}}{16\ \omega_1}$; $\theta_{STA} = \omega_1 t_{p1} + \dfrac{\Omega_Q}{2}\left(1 - \dfrac{3\Omega_Q^2}{32\ \omega_1^2}\right) t_{p1}$;

$\theta_{STB} = \omega_1 t_{p1} - \dfrac{\Omega_Q}{2}\left(1 - \dfrac{3\Omega_Q^2}{32\ \omega_1^2}\right) t_{p1}\Bigg)$

$$\left\langle T^{(3)-3}(t_{p1})\right\rangle \propto \left\{S_{\left(\theta_{TQ}\right)} + S_{(\theta_{CT})} + S_{(\theta_{STA})} + S_{(\theta_{STB})}\right\} \tag{C.2.13}$$

Table C.2.3: Description of the coefficients employed in the perturbing Hamiltonian (Eq. C.2.2)

$G^{(1)}_{DR}$	$G^{(1)}_{TR}$
$G^{(1)}_{DR,1} = 0$	$G^{(1)}_{TR,1} = 0$
$G^{(1)}_{DR,2} = 0$	$G^{(1)}_{TR,2} = -\frac{\Omega_Q}{2\sqrt{2}}(\xi)$
$G^{(1)}_{DR,3} = \frac{1}{3\times 1!}\left(\frac{\sqrt{3}\Omega_Q}{2\sqrt{2}}\right)(\xi)^2$	$G^{(1)}_{TR,3} = 0$
$G^{(1)}_{DR,4} = 0$	$G^{(1)}_{TR,4} = \frac{1}{3!}\left(\frac{\Omega_Q}{2\sqrt{2}}\right)(\xi)^3$
$G^{(1)}_{DR,5} = -\frac{1}{5\times 3!}\left(\frac{\sqrt{3}\Omega_Q}{2\sqrt{2}}\right)(\xi)^4$	$G^{(1)}_{TR,5} = 0$
$G^{(1)}_{DR,6} = 0$	$G^{(1)}_{TR,6} = -\frac{1}{5!}\left(\frac{\Omega_Q}{2\sqrt{2}}\right)(\xi)^5$
$G^{(1)}_{DR,7} = \frac{1}{7\times 5!}\left(\frac{\sqrt{3}\Omega_Q}{2\sqrt{2}}\right)(\xi)^6$	$G^{(1)}_{TR,7} = 0$
.	.
.	.
$G^{(1)}_{DR} = +\left(\frac{\sqrt{3}\Omega_Q}{2\sqrt{2}}\right)\left\{\frac{1}{3\times 1!}(\xi)^2 - \frac{1}{5\times 3!}(\xi)^4 + \frac{1}{7\times 5!}(\xi)^6 - ....\right\}$	$G^{(1)}_{TR} = -\left(\frac{\Omega_Q}{2\sqrt{2}}\right) S_{(\xi)}$
$\xi = \left(\frac{\sqrt{3}\Omega_Q}{4\omega_1}\right) \quad ; \quad C_{(\xi)} = \cos(\xi) \quad ; \quad S_{(\xi)} = \sin(\xi)$	

Table C.2.4: Coefficients employed in the description of the Effective Hamiltonian (Eq. C.2.9) derived from second transformation in Regime-II

$G^{(2)}_{1R}$	$G^{(2)}_{2R}$	$G^{(2)}_{3R}$
$G^{(2)}_{1R,1} = 0$	$G^{(2)}_{2R,1} = 0$	$G^{(2)}_{3R,1} = 0$
$G^{(2)}_{1R,2} = \frac{i}{2}\, G^{(2)}_{13R,A}$	$G^{(2)}_{2R,2} = \frac{i}{2}\, G^{(2)}_{2R,A}$	$G^{(2)}_{3R,2} = \frac{i}{2}\, G^{(2)}_{13R,A}$
$G^{(2)}_{1R,3} = 0$	$G^{(2)}_{2R,3} = 0$	$G^{(1)}_{3R,3} = 0$
$G^{(2)}_{1R,4} = -\frac{i}{4\times 2!}\, G^{(2)}_{13R,B}$	$G^{(2)}_{2R,4} = -\frac{i}{4\times 2!}\, G^{(2)}_{2R,B}$	$G^{(2)}_{3R,4} = -\frac{i}{4\times 2!}\, G^{(2)}_{13R,B}$
$G^{(2)}_{1R,5} = 0$	$G^{(2)}_{2R,5} = 0$	$G^{(2)}_{3R,5} = 0$
$G^{(2)}_{1R,6} = \frac{i}{6\times 4!}\, G^{(2)}_{13R,C}$	$G^{(2)}_{2R,6} = \frac{i}{6\times 4!}\, G^{(2)}_{2R,C}$	$G^{(2)}_{3R,6} = \frac{i}{6\times 4!}\, G^{(2)}_{13R,C}$
$G^{(2)}_{1R,7} = 0$	$G^{(2)}_{2R,7} = 0$	$G^{(2)}_{3R,7} = 0$
.	.	.
$G^{(2)}_{1R} = G^{(1)}_{1R} + \Big\{ \frac{i}{2\times 0!}\, G^{(2)}_{13R,A}$ $-\frac{i}{4\times 2!}\, G^{(2)}_{13R,B} + \frac{i}{6\times 4!}\, G^{(2)}_{13R,C} + \dots \Big\}$	$G^{(2)}_{2R} = G^{(1)}_{2R} + \Big\{ \frac{i}{2\times 0!}\, G^{(2)}_{2R,A}$ $-\frac{i}{4\times 2!}\, G^{(2)}_{2R,B} + \frac{i}{6\times 4!}\, G^{(2)}_{2R,C} + \dots \Big\}$	$G^{(2)}_{3R} = G^{(1)}_{3R} + \Big\{ \frac{i}{2\times 0!}\, G^{(2)}_{13R,A}$ $-\frac{i}{4\times 2!}\, G^{(2)}_{13R,B} + \frac{i}{6\times 4!}\, G^{(2)}_{13R,C} + \dots \Big\}$
$\theta = \left(\frac{\sqrt{3}\omega_1}{\Omega_Q}\right) \quad ; \quad C_{(\theta)} = \cos(\theta)$		

CHAPTER-4

CONCLUSION

Chapter 4

Conclusions and Perspectives

In summary, the effective Floquet Hamiltonian approach proposed in this thesis offers an attractive option for describing multiple-quantum excitation in both isotropic and anisotropic solids. Depending on the relative magnitudes of the quadrupolar coupling constant with respect to the amplitude of the RF pulse, the choice of the interaction frame plays an important role in the convergence of the perturbation corrections to the effective Floquet Hamiltonians. When the magnitude of the quadrupolar frequency (Ω_Q) largely exceeds the RF amplitude (ω_1), the effective Hamiltonians derived from the quadrupolar interaction frame (Regime-I) provide an accurate description of the excitation process. Alternatively, when the quadrupolar frequency (Ω_Q) is lower than the amplitude of the excitation pulse (ω_1), description in the RF interaction frame (Regime-II) is necessary. In both these cases, the convergence of the perturbation corrections/series is faster and the number of transformations required in the derivation of the effective Floquet Hamiltonian is limited to a single unitary transformation. Below, we summarise the results obtained for the DQ excitation in spin $I = 1$ and TQ excitation in spin $I = {}^3/_2$ system. In the strong coupling regime, the DQ excitation is described by Eq. 4.1, while, in the weak-coupling regime (Eq. 4.2) describes the excitation. In a similar vein, the TQ excitation (in $I = {}^3/_2$) in the strong and weak-coupling regimes are described by Eqs. 4.3 and 4.4, respectively.

$$\left\langle T^{(2)-2}(t_{p1})\right\rangle = -i\left(\Phi_1^2\Phi_R\right)\left\{\sin\left(\frac{2\ \omega_1^2\ t_{p1}}{\Omega_Q}\right)\right\} \tag{4.1}$$

$$\left\langle T^{(2)-2}(t_{p1})\right\rangle = i\left(\Phi_1^2\Phi_R\right)\left\{\sin\left(\frac{\Omega_Q t_{p1}}{4}\right) exp\left(i\left(\omega_1 t_{p1} + \frac{\Omega_Q^2 t_{p1}}{32\omega_1}\right)\right)\right\} \tag{4.2}$$

$$\left\langle T^{(3)-3}(t_{p1})\right\rangle = -\left(\Phi_1^3\Phi_R\right)\left\{\frac{3}{2}\sin\left(\frac{3\ \omega_1^3\ t_{p1}}{2\ \Omega_Q^2}\right)\right\} \tag{4.3}$$

$$\left\langle T^{(3)-3}(t_{p1})\right\rangle = \left(\Phi_1^3\Phi_R\right)\left\{\frac{3}{2}\ \sin\left(\omega_1\ t_{p1}\right)\sin^2\left(\frac{\Omega_Q\ t_{p1}}{4}\right)\right\} \tag{4.4}$$

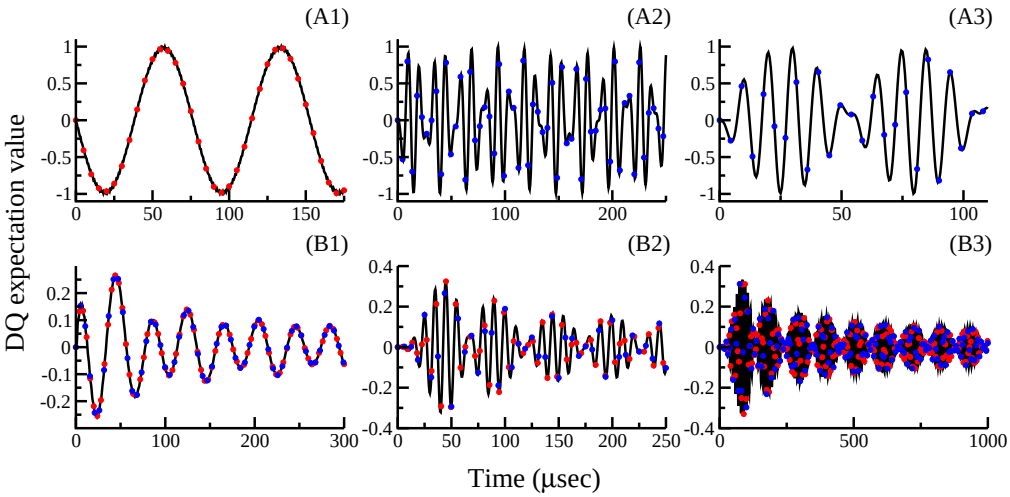

Figure 4.1: Comparison of DQ excitation in a single crystal (panel A) and powder sample (panel B) corresponding to the strong and weak coupling regimes respectively. In contrast to the single crystal, the DQ signal in powder sample (panel B) decays with time, clearly illustrating the interference effects between the different crystallite orientations. The following parameters were employed in the simulations: A1) $C_Q = 1$ MHz, $({}^{\omega_1}/_{2\pi}) = 100$ kHz, A2) $C_Q = 50$ kHz, $({}^{\omega_1}/_{2\pi}) = 100$ kHz, A3) $C_Q = 25$ kHz, $({}^{\omega_1}/_{2\pi}) = 100$ kHz, B1) $C_Q = 1$ MHz, $({}^{\omega_1}/_{2\pi}) = 100$ kHz, B2) $C_Q = 50$ kHz, $({}^{\omega_1}/_{2\pi}) = 100$ kHz and B3) $C_Q = 25$ kHz, $({}^{\omega_1}/_{2\pi}) = 100$ kHz.

As discussed in this thesis, the above expressions are equally valid for describing the excitation in both isotropic (single crystal, $\Omega_Q = \omega_Q$) and anisotropic (powder samples, $\Omega_Q = \omega_Q^{(\alpha\beta\gamma)}$) solids. In contrast to the AHT formalism, the effective Floquet Hamiltonian framework proposed in this thesis presents an unified description for all the crystallites in a powder sample. For comparative purposes, the multiple-quantum excitation (Figure. 4.1, DQ excitation in spin $I = 1$ and Figure. 4.2, TQ excitation in spin $I = {}^3/_2$) observed in single crystal is compared below with those obtained from a powder sample.

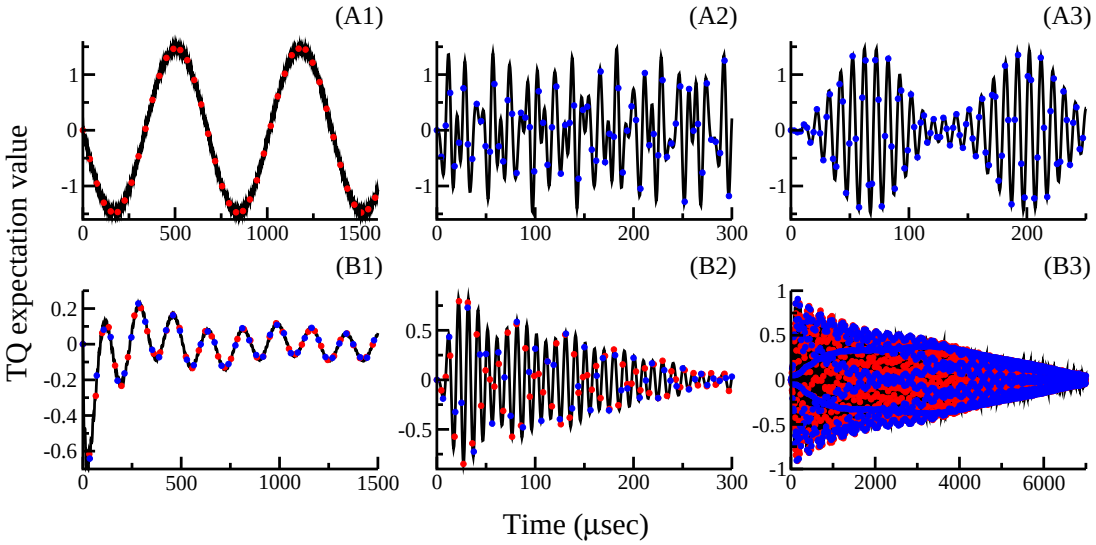

Figure 4.2: Comparison of TQ excitation in a single crystal (panel A) and powder sample (panel B) corresponding to the strong and weak coupling regimes respectively. In contrast to the single crystal, the TQ signal in powder sample (panel B) decays with time, clearly illustrating the interference effects between the different crystallite orientations. The following parameters were employed in the simulations: A1) $C_Q = 2$ MHz, $({}^{\omega_1}/_{2\pi}) = 100$ kHz, A2) $C_Q = 150$ kHz, $({}^{\omega_1}/_{2\pi}) = 100$ kHz, A3) $C_Q = 30$ kHz, $({}^{\omega_1}/_{2\pi}) = 100$ kHz, B1) $C_Q = 2$ MHz, $({}^{\omega_1}/_{2\pi}) = 100$ kHz, B2) $C_Q = 150$ kHz, $({}^{\omega_1}/_{2\pi}) = 100$ kHz and B3) $C_Q = 30$ kHz, $({}^{\omega_1}/_{2\pi}) = 100$ kHz.

As depicted, in the case of a single crystal (panels A1, A3 in Figures. 4.1 and 4.2), the excitation profiles both in the strong and weak-coupling regimes are oscillatory (periodic) and resemble to the Rabi oscillations[1]. Interestingly, in the case of a

powder sample, (panels B1, B3 in Figures. 4.1 and 4.2) the oscillations decrease in intensity with time and are no longer periodic. This dissipation of the signal in the time-domain could be explained through the analytic expressions described above. In the case of a single crystal (both in strong and weak-coupling regimes), the excitation profile is described by a single trigonometric function. On the contrary, in a powder sample, the signal in the time domain (at each time point) is an ensemble average over all possible orientations. Hence, the time-domain signal in a powder sample has contributions from a distribution of quadrupolar frequencies associated with individual crystallites leading to interference between the different trigonometric terms. Consequently, the signal intensity decreases with time (or gets damped) in a powder sample and was also reported recently in a theoretical study involving spin $I = {}^1/_2$ nuclei[2].

Based on the above equations, in the strong coupling regime, the efficiency of DQ and TQ transitions is (a) proportional to the amplitude of the pulse (b) inversely proportional to the quadrupolar coupling constant.

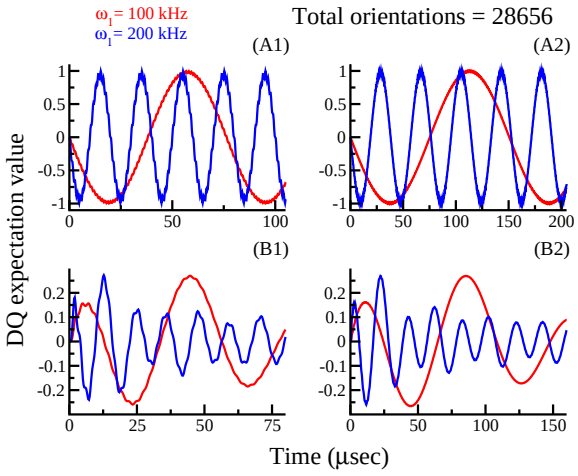

Figure 4.3: Comparison of DQ excitation in a single crystal (panel A) and powder sample (panel B) corresponding to the high coupling regime (Regime-I). In contrast to the single crystal, the DQ signal in powder sample (panel B) decays with time, clearly illustrating the interference effects between the different crystallite orientations. The following parameters were employed in the simulations: A1) $C_Q = 1$ MHz, $({}^{\omega_1}/_{2\pi}) = 100, 200$ kHz, A2) $C_Q = 2$ MHz, $({}^{\omega_1}/_{2\pi}) = 100, 200$ kHz, B1) $C_Q = 1$ MHz, $({}^{\omega_1}/_{2\pi}) = 100, 200$ kHz, and B2) $C_Q = 2$ MHz, $({}^{\omega_1}/_{2\pi}) = 100, 200$ kHz.

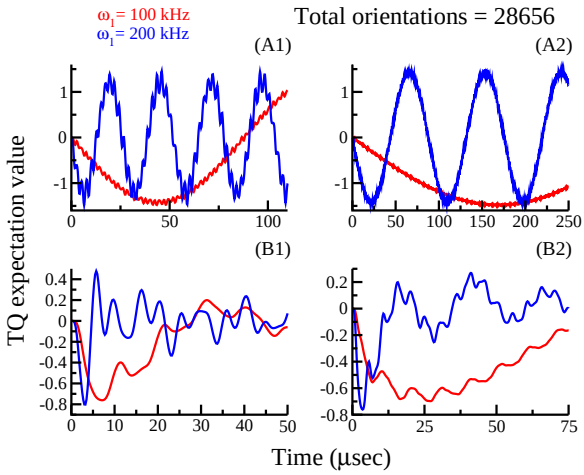

Figure 4.4: Comparison of TQ excitation in a single crystal (panel A) and powder sample (panel B) corresponding to the high coupling regime (Regime-I). In contrast to the single crystal, the TQ signal in powder sample (panel B) decays with time, clearly illustrating the interference effects between the different crystallite orientations. The following parameters were employed in the simulations: A1) $C_Q = 1$ MHz, $(^{\omega_1}/_{2\pi}) = 100, 200$ kHz, A2) $C_Q = 2$ MHz, $(^{\omega_1}/_{2\pi}) = 100, 200$ kHz, B1) $C_Q = 1$ MHz, $(^{\omega_1}/_{2\pi}) = 100, 200$ kHz, and B2) $C_Q = 2$ MHz, $(^{\omega_1}/_{2\pi}) = 100, 200$ kHz.

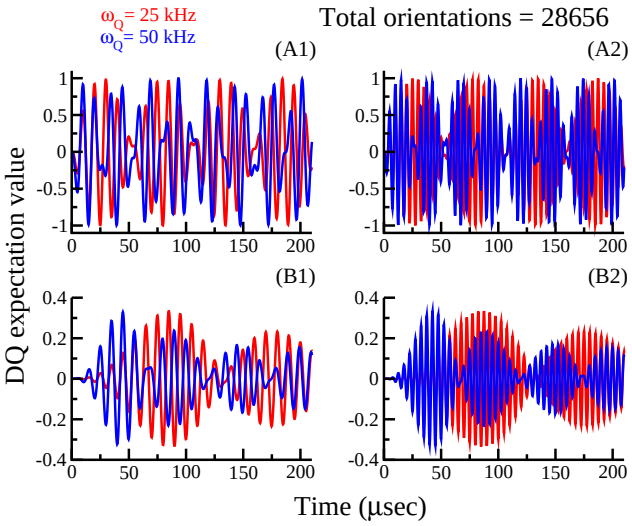

Figure 4.5: Comparison of DQ excitation in a single crystal (panel A) and powder sample (panel B) corresponding to the weak coupling regime (Regime-II). In contrast to the single crystal, the DQ signal in powder sample (panel B) decays with time, clearly illustrating the interference effects between the different crystallite orientations. The following parameters were employed in the simulations: A1) $C_Q = 25, 50$ kHz, $(^{\omega_1}/_{2\pi}) = 100$ kHz, A2) $C_Q = 25, 50$ kHz, $(^{\omega_1}/_{2\pi}) = 200$ kHz, B1) $C_Q = 25, 50$ kHz, $(^{\omega_1}/_{2\pi}) = 100$ kHz, and B2) $C_Q = 25, 50$ kHz, $(^{\omega_1}/_{2\pi}) = 200$ kHz.

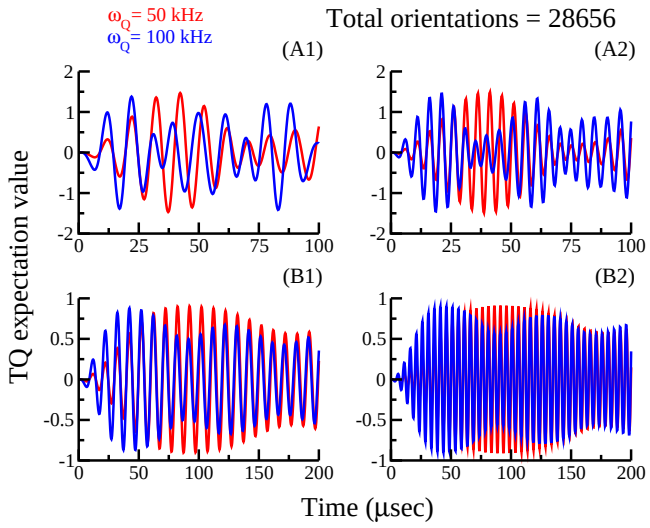

Figure 4.6: Comparison of TQ excitation in a single crystal (panel A) and powder sample (panel B) corresponding to the weak coupling regime (Regime-II). In contrast to the single crystal, the TQ signal in powder sample (panel B) decays with time, clearly illustrating the interference effects between the different crystallite orientations. The following parameters were employed in the simulations: A1) $C_Q = 50, 100$ kHz, $(\omega_1/2\pi) = 100$ kHz, A2) $C_Q = 50, 100$ kHz, $(\omega_1/2\pi) = 200$ kHz, B1) $C_Q = 50, 100$ kHz, $(\omega_1/2\pi) = 100$ kHz, and B2) $C_Q = 50, 100$ kHz, $(\omega_1/2\pi) = 200$ kHz.

By contrast, in the weak-coupling limit, the efficiency of DQ and TQ transitions is (a) proportional to the quadrupolar coupling constant (b) inversely proportional to the amplitude of the pulse.

In the case of the intermediate ($2 \leq \omega_Q/\omega_1 \leq 10$) regime (panels A2, B2 in Figures. 4.1 and 4.2) the MQ oscillations are aperiodic both in the single crystal and powder samples. The non-periodicity in the case of single crystal arises mainly due to the interference effects between the trigonometric expressions present in the signal expression (see Eqs. 4.5, 4.6 and 4.7, 4.8.

Spin $I = 1$ (Intermediate)

Regime-I

$$\left\langle T^{(2)-2}(t_{p1}) \right\rangle = ie^{2i\omega_0 t_2}\ \Phi_1^2\ \Phi_R \left\{ \cos^2(\alpha)\ \sin(\theta_{DQ}) - \sin^2(\alpha) \sin(\beta) \right\} \qquad (4.5)$$

Regime-II

$$\left\langle T^{(2)-2}(t_{p1})\right\rangle = ie^{2i\omega_0 t_2}\ \Phi_1^2\ \Phi_R\left\{\sin\left(\xi_{2R}\right)\cos\left(\xi_{1R}\right)+\cos\left(\xi_{2R}\right)\sin\left(\xi_{1R}\right)\sin\left(2\xi_{DR}\right)\right\} \tag{4.6}$$

Spin $I = {}^3/_2$ (Intermediate)

Regime-I

$$\begin{aligned}\left\langle T^{(3)-3}(t_{p1})\right\rangle \propto \{&\sin\left(\theta_{TQ}\right)+\sin\left(\theta_{CT}\right)+\cos\left(\theta_{RF}\right)\ \sin\left(\theta_{ZQ}\right)\\ &+\sin\left(\theta_{RF}\right)\ \cos\left(\theta_{ZQ}\right)\}\end{aligned} \tag{4.7}$$

Regime-II

$$\left\langle T^{(3)-3}(t_{p1})\right\rangle \propto \{\sin\left(\theta_{TQ}\right)+\sin\left(\theta_{CT}\right)+\sin\left(\theta_{STA}\right)+\sin\left(\theta_{STB}\right)\} \tag{4.8}$$

As discussed in chapters. 2 and 3, in the intermediate regime (whether Regime-I or Regime-II), multiple transformations are required to improve the accuracy of the derived effective Hamiltonians. Consequently, the MQ signal expression has a complicated dependence on the RF amplitude and the quadrupolar frequency. In analytic simulations involving powder samples, the calculations in the intermediate regime could become influential in improving the accuracy of the derived effective Floquet Hamiltonians. As described in this thesis, the hybrid method provides an accurate description in powder samples. Depending on the relative magnitudes of the quadrupolar frequency with respect to the RF amplitude, the percentage of contributions from regime-I and II differ and is illustrated in Tables. 4.1 and 4.2 for spin $I = 1$ and $I = {}^3/_2$, respectively. In the case of MAS experiments, the dominant quadrupolar interaction is time-dependent. Consequently, analytic descriptions based on perturbation theory are ill-suited for describing the spin dynamics.

In cases where the properties of materials under investigation get altered due to repeated bombardment of RF irradiation/pulses, real time analyses of the process in the form of *In- situ or operando* experiments are preferred[3,4]. The in-situ

experiments provide us the real time tracking of dynamic processes and short lived states enabling to extract site- specific data.

Table 4.1: Classification of crystallite orientations of spin $I = 1$ into Regime-I and Regime-II based on the relative magnitude of the anisotropic quadruple coupling constant '$\omega_Q/2\pi$' to the amplitude of the exciting pulse '$\omega_1/2\pi$' when RF amplitude is always at $\omega_1/2\pi = 100$ kHz

$\omega_1 : \omega_Q$	**No. of crystallite orientations in Regime-I**	**No. of crystallite orientations in Regime-II**	**Total No. of crystallite orientations**
1 : 20	26324 (91.86%)	2322 (8.14%)	28656
1 : 10	23934 (83.52%)	4722 (16.48%)	28656
1 : 5	18528 (64.66%)	10128 (35.34%)	28656
1 : 3	9898 (34.54%)	18758 (65.46%)	28656
1 : 2	4708 (16.43%)	23948 (83.57%)	28656
1 : 1	0	28656 (100.00%)	28656

Table 4.2: Classification of crystallite orientations of spin $I = {}^3/_2$ into Regime-I and Regime-II based on the relative magnitude of the anisotropic quadruple coupling constant '$\omega_Q/2\pi$' to the amplitude of the exciting pulse '$\omega_1/2\pi$' when RF amplitude is always at $\omega_1/2\pi = 100$ kHz

$\omega_1 : \omega_Q$	**No. of crystallite orientations in Regime-I**	**No. of crystallite orientations in Regime-II**	**Total No. of crystallite orientations**
1 : 20	27364 (95.50%)	1292 (4.50%)	28656
1 : 10	26064 (90.95%)	2592 (9.05%)	28656
1 : 5	23394 (81.64%)	5262 (18.36%)	28656
1 : 3	19512 (68.09%)	9144 (31.91%)	28656
1 : 2	11228 (39.18%)	17428 (60.82%)	28656
1 : 1	0	28656 (100.00%)	28656

Several ex-situ experiments are combined with in-situ experiments to cross-check the validity of the results[5]. These in-situ experiments are mostly performed under

static conditions[5]. We believe that the present study offers an alternate framework for describing the effects of RF pulses on quadrupolar spins and would be beneficial in the design/quantifying more sophisticated experiments in anisotropic solids.

References

[1] I. I. Rabi, *Phys. Rev.*, 1936, **49**, 324–328.

[2] U. SivaRanjan and R. Ramachandran, *J. Chem. Phys.*, 2014, **140**, 054101.

[3] P. Harks, F. Mulder and P. Notten, *J. Pow. Sour.*, 2015, **288**, 92 – 105.

[4] F. Blanc, M. Leskes and C. P. Grey, *Acc. Chem. Research*, 2013, **46**, 1952–1963.

[5] O. Pecher, J. Carretero-González, K. J. Griffith and C. P. Grey, *Chem. Mat.*, 2017, **29**, 213–242.

Publications

1. Analytic Theory of Multiple-Quantum NMR of Quadrupolar Nuclei. **Vinay Ganapathy** and Ramesh Ramachandran, *Annu. Rep. NMR Spectrosc.* **89**. 123 (2016).

2. Effective Floquet Hamiltonian theory of multiple-quantum NMR in anisotropic solids involving quadrupolar spins: Challenges and Perspectives. **Vinay Ganapathy** and Ramesh Ramachandran, *J. Chem. Phys.* **147**. 144202 (2017).